Design, Synthesis, and Biological Evaluation of Selective Estrogen Receptor Modulator/Histone Deacetylase Inhibitor Hybrid Molecules

Anthony Francesco Palermo

Dr. James Gleason

Department of Chemistry, McGill University

Montréal, Québec, Canada

December 2016

A thesis submitted to McGill University in partial fulfillment of the requirements of the degree of Master of Science

Abstract

Therapeutic options for the treatment of breast cancer have long been limited to invasive surgical procedures, or chemo- and radiotherapies that are plagued with detrimental side-effects. Selective estrogen receptor modulators (SERMs), such as tamoxifen and raloxifene, are a large subclass of molecules that have been used in adjuvant therapies and have provided substantial clinical benefits as preventative and long-term treatment options. Despite their success, endocrine therapies face several challenges including the development of endocrine resistance and, in the case of tamoxifen, the increased risk of endometrial cancer. Recent studies have shown that dual administration of SERMS and histone deacetylase inhibitors (HDACis) in vitro have led to cooperative effects such as increased drug potency, the resensitization of endocrine resistant cell lines, and an overall decrease in the risk of endometrial cancer development. In an effort to combine the cooperative effects of SERMs and HDACis, this project focuses on the design, synthesis, and biological evaluation of a series of hybrid SERM/HDACi molecules that combine the pharmacophores of both drug classes.

The design of the hybrids was based on previous research projects investigating hybrid antiestrogens within the Gleason group. This project expanded on a promising subset of 4-OHT based hybrids and began with *in silico* screening of a virtual library using the *FORECASTOR* docking platform. Seven compounds were chosen for synthesis and a previously devised route was unsuccessfully attempted using a McMurry cross-coupling as the key step. An alternate route to the triphenylethylene scaffold is hinged on a highly convergent and modular three-component coupling reaction was designed and successfully carried out. Four hybrids were synthesized and purified by preparatory HPLC prior to biological evaluation.

Fluorogenic HDACi assays to determine the hybrid affinities of HDACs 3 and 6 were carried out by the author within the Gleason lab. Three of the four hybrids showed low micromolar HDAC 3 potencies (IC_{50}) and the fourth showed submicromolar potency, and

suggested that increased chain-lengths led to a higher degree of HDAC inhibition. HDAC 6 inhibition results trended similar to those of HDAC 3 and three of the four hybrids showed submicromolar potencies. Cell-based bioluminescence resonance energy transfer (BRET) and luciferase transactivation assays were conducted by the Mader lab at Université de Montréal to evaluate the ER affinity and antagonism profile of the hybrids. Each hybrid exhibited full antagonism against the ER and three of the hybrids showed submicromolar IC_{50} values with regards to their ER affinity. MCF-7 breast cancer cell growth curves were carried out and a single hybrid outperformed 4-hydroxytamoxifen (4-OHT), tamoxifen, and endoxifen. The ER data alongside the HDACi results are suggestive of a hybrid SERM/HDACi that was capable of eliciting a cooperative antiproliferative effect against the breast cancer cell line.

The final chapter of this thesis presents a brief project regarding the design of a 3-acyl-1,5-diene substrate for the organocatalytic Cope rearrangement. A novel diazepane carboxylate organocatalyst capable of catalyzing the Cope rearrangement of hindered aldehydes via iminium catalysis was recently reported by the Gleason group. DFT calculations suggested that iminium ion formation of 3-acyl-1,5-dienes would accelerate the Cope rearrangement. The final 3-acyl-1,5-diene substrate was shown to be capable of undergoing the Cope rearrangement under simple thermal conditions and future work will investigate the potential for organocatalytic rate acceleration.

Resumé

Les options thérapeutiques pour le traitement du cancer du sein se limitent depuis longtemps aux interventions chirurgicales invasives ou aux chimiothérapies et radiothérapies qui sont affectées par des effets secondaires. Les modulateurs sélectifs des récepteurs aux œstrogènes (SERM), comme le tamoxifène et le raloxifène, sont une grande sous-classe de molécules qui ont été utilisées dans les thérapies adjuvantes et ont fourni des avantages cliniques substantiels en tant qu'opérations de traitement préventives et à long terme. Malgré leur succès, les thérapies endocriniennes font face à plusieurs défis, y compris le développement de la résistance endocrine et, dans le cas du tamoxifène, le risque accru de cancer de l'endomètre. Des études récentes ont montré que la double administration de SERMs et d'inhibiteurs de l'histone désacétylase (HDACis) *in vitro* a mené à des effets coopératifs telles que l'augmentation de la puissance du médicament, la resensibilisation des lignées cellulaires résistantes aux endocrines et une diminution globale du risque de développement du cancer de l'endomètre. Dans le but combiner les effets coopératifs des SERM et HDACis, ce projet se concentre sur la conception, la synthèse et l'évaluation biologique d'une série de molécules SERM/HDACi hybrides qui combinent les pharmacophores des deux classes de médicaments.

La conception des hybrides était basée sur des projets de recherche antérieurs portant sur des anti-œstrogènes hybrides au sein du groupe Gleason. Ce projet s'est développé sur un sous-ensemble prometteur d'hybrides basés sur 4-OHT et a commencé avec le criblage in silico d'une bibliothèque virtuelle en utilisant la plate-forme d'amarrage de FORECASTOR. Sept composés ont été choisis pour la synthèse et une voie préalablement conçue a été tentée sans succès en utilisant un couplage croisé de McMurry comme étape clé. Un autre itinéraire vers l'échafaudage de triphényléthylène est articulé sur une réaction de couplage à trois composants très convergente et modulaire a été conçu et réalisé avec succès. Quatre hybrides ont été synthétisés et purifiés par HPLC préparatoire avant l'évaluation biologique.

Des analyses HDACi fluorogènes pour déterminer les affinités hybrides des HDAC 3 et 6 ont été réalisées par l'auteur dans le laboratoire Gleason. Trois des quatre hybrides

ont montré des faibles potencies micromolaires HDAC 3 (IC_{50}) et le quatrième a montré une potence submicromolaire, et a suggéré que l'augmentation des longueurs de chaîne conduit à un plus haut degré d'inhibition HDAC. Les résultats d'inhibition de HDAC 6 ont été semblables à ceux de HDAC 3 et trois des quatre hybrides ont montré des potences submicromolaires. Le transfert d'énergie par résonance bioluminescente à cellules (BRET) et les essais de transactivation de luciférase ont été réalisés par le laboratoire Mader de l'Université de Montréal pour évaluer le profil d'affinité et d'antagonisme ER des hybrides. Chaque hybride présentait un antagonisme complet contre l'ER et trois des hybrides présentaient des valeurs IC_{50} submicromolaires en ce qui concerne leur affinité ER. Des courbes de croissance de cellules de cancer du sein MCF-7 ont été réalisées et un seul hybride a surpassé le 4-hydroxytamoxifène (4-OHT), le tamoxifène et l'endoxifène. Les données ER conjointement avec les résultats HDACi suggèrent un hybride SERM / HDACi qui était capable d'induire un effet antiprolifératif coopératif contre la lignée cellulaire de cancer du sein.

Le dernier chapitre de cette thèse présente un bref projet concernant la conception d'un substrat 3-acyl-1,5-diène pour le réarrangement organocatalytique de Cope. Un nouvel organocatalyseur carboxylate de diazépane capable de catalyser le réarrangement de Cope d'aldéhydes encombrés via la catalyse d'iminium abaissant LUMO a été récemment rapporté par le groupe de Gleason. Les calculs de DFT ont suggéré que la formation d'ions iminium de 3-acyl-1,5-diènes accélérerait le réarrangement de Cope. On a montré que le substrat final de 3-acyl-1,5-diène était capable de subir le réarrangement de Cope dans des conditions thermiques simples et des travaux futurs examineront si le catalyseur de carboxylate de diazépane est capable d'induire une accélération du réarrangement.

Acknowledgements

I would like to first thank Prof. Jim Gleason for the opportunity to be a part of his research group, and for his patience and guidance he provided throughout the course of my studies at McGill. His training has allowed me to feel well equipped to tackle any problem, synthetic or not, that I will face throughout my career. The final steps of my project would not have been possible without Dr. Youla Tsantrizos and the instruments that she made available to me. Cyrus Lacbay and Dimitrios Xanthopoulos, thank you for taking the time to help me with the separation of my isomers on the prep-HPLC, your advice and expertise on the system was very much appreciated.

Drs. Nadim Saade and Alex Wahba, your prompt return of my HRMS results was always appreciated. Dr. Robin Stein, thank you for your help within the NMR facility. Chantal Marotte, thank you for all of the administrative help and for the timely reminders that kept my student registration in check.

Jon, I couldn't have asked for a better labmate. You're chemistry advice was invaluable and I always walked away from our conversations having learned something new. You're a great friend and a great chemist, but terrible at fantasy football. Adam, it was a pleasure working with you. The HDAC assays would have been disastrous if we didn't tackle them together and I'm grateful we were able to team up for that challenge. I hope you're never without fridge space for your yogourt. Nick, I admired your militant stance on coffee and cleanliness. If not for that, the lab would have been in ruins and its students unproductive. Your brie-steak will forever be the greatest work lunch I have ever witnessed. Sam, I heard you took a page out of the book of Nick and melted the cheese on top of your peanuts. You're going to achieve great things. Josie, although we only worked together for a few short months it was great to get to know you. The lab finally got to see what a true GTA-er was like and you lived up to the hype, good luck in the Gleason lab. Chris, Shuo, Marx, Daniel, Florent, and Ryan, it was great working with all of you.

Finally, I'd like to thank my parents Tony and Lydia, and my sister Stefanie for always being there to keep me grounded and providing me with everything I needed to succeed.

Table of Contents

List of Abbreviations

1,25D	1α,25-dihydroxyvitamin D
4-OHT	4-hydroxytamoxifen
5-aza-dC	5-aza-2'-deoxycitidine
Å	Ångstrom
p-Ns	*para*-nitrotoluenesulfonate
AF-1	activation factor 1
AF-2	activation factor 2
AIB1	amplified in breast 1
AMEM	alpha minimal essential medium
anyd.	anhydrous
AP-1	activator protein 1
aq.	aqueous
Arg	arginine
Asp	aspartic acid
Bn	benzyl
BRET	bioluminescence resonance energy transfer
cat.	catalytic
CBR	clinical benefit rate
cDNA	complimentary deoxyribonucleic acid
CoREST	Co-RE1-silencing transcription factor
DBD	DNA binding domain
DES	diethylstilbestrol
DFT	density functional theory
DIAD	diisopropyl azodicarboxylate
DIBAL-H	diisobutylaluminum hydride
DIPEA	diisopropylethylamine
DMA	dimethylacetamide
DMAP	dimethylaminopyridine

DMF	dimethylformamide
DMP	Dess-Martin periodinane
DMSO	dimethyl sulfoxide
DNA	deoxyribonucleic acid
dppf	1-1'-bis(diphenylphosphino)ferrocene
dppp	1,3-bis(diphenylphosphino)propane
E2	17β-estradiol
EDC	1-ethyl-3-(3-dimethylaminopropyl)carbodiimide
EDG	electron donating group
EGFR	epidermal growth factor receptor
ER	estrogen receptor
ERE	estrogen response element
EtOAc	ethyl acetate
EWG	electron withdrawing group
FBS	fetal bovine serum
FDA	food and drug administration
FITTED	Flexibility Induced Through Targeted Evolutionary Description
Gen.	generation
Glu	glutamic acid
Gly	glycine
H12	helix 12
HAT	histone acetyl transferase
HDAC	histone deacetylase
HDACi	histone deacetylase inhibitor
HER2	human epidermal growth factor receptor 2
His	histidine
HMPA	hexamethylphosphoramide
HOBt	hydroxybenzotriazole
HOMO	highest occupied molecular orbital
HPLC	high performance liquid chromatography

Hsp70	heat shock protein 70
Hsp90	heat shock protein 90
IC_{50}	half maximal inhibitory concentration
IGF1-R	insulin-like growth factor receptor
imid.	imidazole
K_i	inhibitor dissociation constant
LAH	lithium aluminum hydride
LBD	ligand binding domain
LDA	lithium diisopropylamine
LUMO	lowest unoccupied molecular orbital
MAPK	mitogen-activated protein kinase
MeCN	acetonitrile
MEF-2	mytocyte enhancer factor-2
MeOH	methanol
Mes	mesityl
MMP	matrix metalloproteinases
N-CoRSMRT	nuclear receptor co-repressor 2/thyroid hormone receptor complex
NHC	N-heterocyclic carbene
NMR	nuclear magnetic resonance
NuRD	nucleosome remodeling deacetylase
OBHS	exo-5,6-bis(4-hydroxyphenyl)-7-oxabicyclo[2.2.1]hept-5-ene-2sulfonic acid phenyl ester
P(*o*-tolyl)$_3$	tri(*o*-tolyl)phosphine
p53	transformation-related protein 53
PDB	protein database
PhMe	toluene
Piv	pivaloyl
Pr	propyl
PRC2	polycomb repressive complex 2
PTSA	*para*-toluenesulfonic acid

py.	pyridine
RID	receptor interacting domain
rt	room temperature
S_N2	substitution nucleophilic bimolecular
SAHA	suberoylanilide hydroxamic acid
SERM	selective estrogen receptor modulator
SM	starting material
SP-1	specificity protein 1
SRC1	steroid receptor coactivator 1
SRC3	steroid receptor coactivator 2
STAR	study of tamoxifen and raloxifene
T3P	propylphosphonic anhydride
TBAF	tetrabutylammonium fluoride
TBS	tert-butyldimethylsilyl
TFA	trifluoroacetic acid
TfOH	triflic acid
THF	tetrahydrofuran
THP	tetrahydropyran
TMS	trimethylsilyl
TSA	trichostatin A
VDR	vitamin D receptor
VPA	valproic acid

List of Schemes

List of Figures

List of Tables

Chapter 1: Introduction

1.1 Breast Cancer and the Estrogen Receptor

Breast cancer remains one of the most prevalent forms of cancer diagnosed in women throughout the Western world, second only to lung cancer.[1] A recent Cancer Statistics publication predicts that in Canada, one in nine women will develop breast cancer while 1 in 30 will die from the disease overall. Increased awareness of breast cancer and the organization of provincial mammography screening programs have led to an increase in early breast cancer diagnoses over the past several decades and, as a result, mortality rates have dropped 44% since 1986. The drop can be undoubtedly attributed to improvements in breast cancer treatment options, as surgical intervention and broad-scope chemotherapy are continuously being replaced with effective and lower risk endocrine therapies.[1]

Throughout the past century our understanding of breast cancer has largely been shaped by discoveries pertaining to ovarian hormones and the estrogen receptor (ER). The discovery of ovarian hormones and their proliferative effects on breast tissues and breast tumour growth paved the way for the development of synthetic estrogen antagonists as therapeutics.[2,3] Tamoxifen was identified as a potent inhibitor of the ER in breast tissues, and became FDA approved in 1977 for the treatment of post-menopausal women diagnosed with ER+ breast cancer in both the early and advanced stages. It would later become the gold standard adjuvant treatment for breast cancer in the 1980s, and currently remains the standard for the treatment of both pre- and post-menopausal women with ER+ tumours.[4] Since the introduction of tamoxifen in the late 1970s, a 30% decrease in breast cancer mortality rates has been reported and is largely attributed to the widespread administration of the drug.[5] Despite the improvements in ER+ breast cancer treatment, adjuvant therapies face several challenges. Resistance is known to develop in many cases, in which the tumour becomes hormone-independent and is no longer responsive to endocrine treatment. Moreover, tamoxifen is known to increase the chances of endometrial cancer development due to agonism of the ER in uterine tissues which requires regular screenings to be incorporated into treat-

ment plans.[6] This thesis will briefly discuss the currently accepted mechanism of breast cancer and its ability to acquire resistance to endocrine treatments, the challenges of breast cancer treatment and the proposal, synthesis, and biological evaluation of hybrid selective estrogen receptor modulator (SERM)/histone deacetylase inhibitor (HDACi) analogues that are hypothesized to combine the cooperative behaviour of these two distinct drug classes.

1.1.1 Estrogen Receptor α

The positive effects of oophorectomy on breast tumour regression in female patients provided the first connection between ovarian hormones and breast cancer. Beatson performed the operation on six of his patients and observed a 33% recovery rate in his patients over a 5 year period.[7] Later, several investigations focusing on ovarian tissues and the isolation of biologically active extracts suggested there existed hormones capable of inducing breast cell proliferation.[8,9] The estrogen receptor was isolated by Toft *et al.* in 1966 as a result of developing a cell-free method for studying the proliferative effects of estrogens.[10] The same group also observed tritium labelled 17β-estradiol (E2) to be largely localized in the nuclear extracts of rat uteri after *in vivo* E2 uptake experiments.[11] With this evidence, they suspected that the ER was strongly associated with cellular nuclei and that E2 was inherently associated with the protein, but there was still a significant lack of knowledge regarding the function of E2 binding to the ER and its systemic biological relevance.

The ER was sequenced and successfully cloned by Green *et al.* in 1986. This achievement and easy access to ER samples would accelerate investigations in the field as previous methods required laborious ER extractions from tissue samples. Green's group sequenced the complimentary DNA (cDNA) of the ER from the MCF-7 breast cancer cell line, and used the same cDNA in HeLa cells to express the cloned ER, which was indistinguishable from the ER isolated directly from MCF-7 cell lines.[12] The crystal structure of the ligand binding domain (LBD) of the ERα was solved by Brzozowski *et al.* in 1996 and the agonist and antagonist bound ER conformations provided a molecular understanding regarding the mechanisms of activation and deactivation, respectively.

A second isoform of the ER, ERβ was identified in 1996.[13] ERβ has introduced a new level of complexity to our understanding of ER signalling. Structurally, ERβ possesses a LBD and DNA binding domain (DBD) which are similar to those of ERα and can bind to E2. The role of ERβ is not yet completely clear, however a working model suggests that unbound ERβ acts to regulate ERα mediated gene transcription in the presence of E2 and varying isoform ratios may predict the effects of agonists and antagonists. ERβ will not be discussed in great detail in this thesis, but reviews by Kuiper, Hall, and Koeler may serve as excellent resources regarding our current understanding of its function.[13–15] Any references to the ER in this work will refer to the ERα isoform unless otherwise specified.

1.1.2 Structure of the Estrogen Receptor

The ER is a 595 amino-acid residue nuclear receptor protein that consists of 6 domains (Figure 1.1). The amino terminal domain, known as A/B, contains the Activation Function 1 (AF-1) which plays a role in regulating gene transcription via phosphorylation by coupled biochemical pathways including epidermal growth factor receptor (EGFR), HER2, and insulin-like growth factor receptor (IGF1-R)[16] . Domain C contains a highly conserved DBD and houses two zinc-fingers that are responsible for recognizing the promoter gene sequence known as the estrogen response element (ERE) upon ER activation.[17] Domain D contains heat shock protein 90 (Hsp90) binding sites, the protein surface upon which dimerization occurs, and a hinge region. The carboxy terminus, domains E and F, houses the LBD and Activation Factor 2 (AF-2) which are directly involved in ligand-induced activation and transcription regulation.[17]

The LBD of the ER was first crystallized by Brzozowski *et al.* with the agonist E2 and the antagonist raloxifene with 3.1 and 2.6 Å resolution, respectively.[19] The LBD is a three-layered antiparallel α-helical sandwich and contains a core layer of three helices (H5/6, H9, and H10 (yellow)), flanked by two layers of helices (H7, H8, and H11 (red), and H1-4 (blue)). The front and back of the binding pocket are flanked by a two-stranded antiparallel β-sheet (S1/S2(orange)) and H12 (pink) which seals the opening of the cavity (Figure 1.2a).

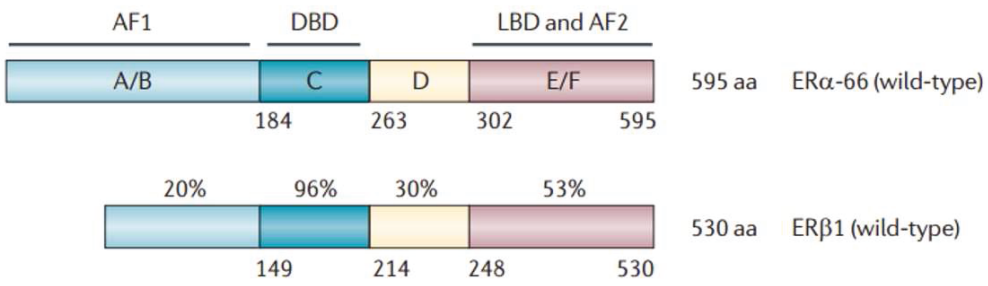

Figure 1.1: Domains of the ERα and ERβ and their sequence homology.[18]

The active ER exists as a dimer; monomer-monomer interactions occur primarily on the H8/H11 face of each monomer (Figure 1.2b). The binding pocket is formed by regions of H3, H6, H8, H11, H12, and the S1/S1 β-sheet.

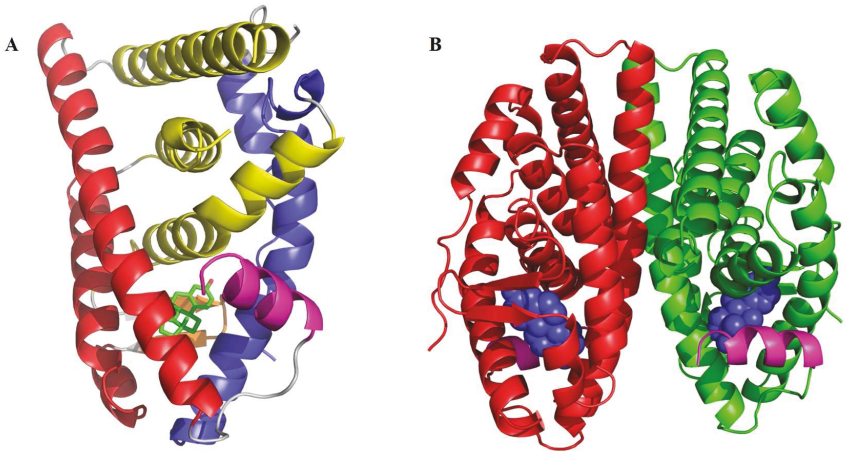

Figure 1.2: a. LBD of ER bound to 17β-estradiol (PDB:1ERE). **b**. Active dimer of ER.

1.1.3 Mechanism of ER Activation

ERα and ERβ are distributed throughout many tissues and regulate several endocrine dependent processes in the female body (Figure 1.3).[20] ERs are found in the hypothalamo-pituitary axis and regulate the release of gonadotropins through positive and negative feedback mechanisms, and gonadotropins regulate the production of endogenous estrogens.[21] Liver cells possess ERs that regulate cholesterol and lipid levels, while the ERs in bone regulate bone density.[22,23] In breast tissues, ER activation occurs by binding to estrogen which

results in gene transcription and cell proliferation.

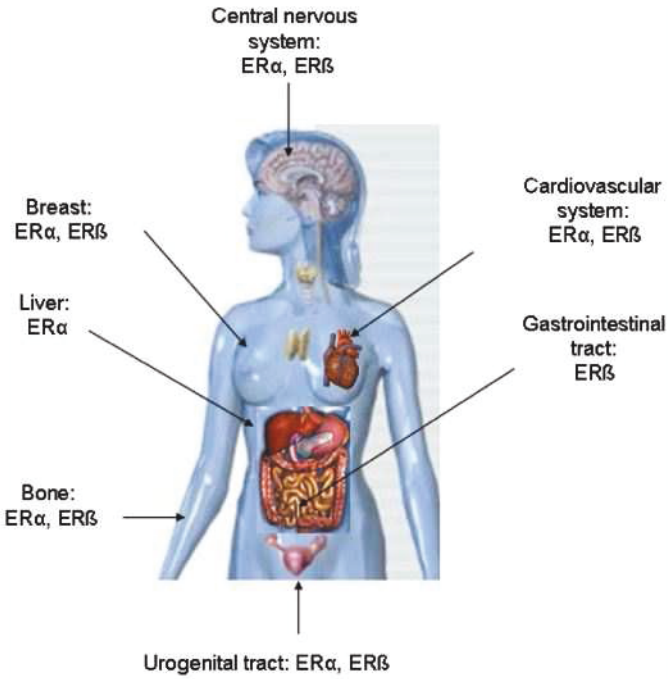

Figure 1.3: Distribution of ERα and ERβ throughout the female body[24]

Activation of the ER involves the recruitment of many transcriptional coregulators, in the form of either coactivators or corepressors, which either induce the activation or silencing of target genes. In the healthy breast cell, endogenous E2 enters the cytosol and binds to the inactive, monomeric ER (Figure 1.4). In its inactive state the ER is bound to and is stabilized by hsp90 and hsp70.[25–27] Agonist binding elicits a conformational change that releases the heat shock proteins and exposes a hydrophobic cleft on the surface of the LBD. The hydrophobic surface facilitates dimerization of the ER which then localizes to the cell nucleus via nuclear localization sites. The cleft can then accommodate the LXXLL motif which is commonly found on the p160 family of coregulators.[19,28] The ER-coregulator complex then recognizes and binds to ERE regions on the DNA, which are 13 bp palindromic inverted repeat sequences (5'-GGTCAnnnTGACC-3'), using a pair of zinc-fingers found within the DBD.[29,30] Once bound to the ERE, coregulators such as SRC1 and SRC3 (steroid receptor coactivators), are then recruited to the ER-complex and can affect chromatin remodelling via the recruitment of histone acetyl transferase (HAT) or histone deacetylase (HDAC) pro-

teins.[31,32] The ER is also known to bind to other coregulators such as activator protein-1 (AP-1) and specificity protein-1 (SP-1), in addition to at least 28 other co-activators, many of which are outlined and thoroughly discussed in the review by Klinge.[33–35] The formation of the ER-coregulator complex is then followed by recruitment of the general transcription machinery to the promoter site and gene transcription is initiated.

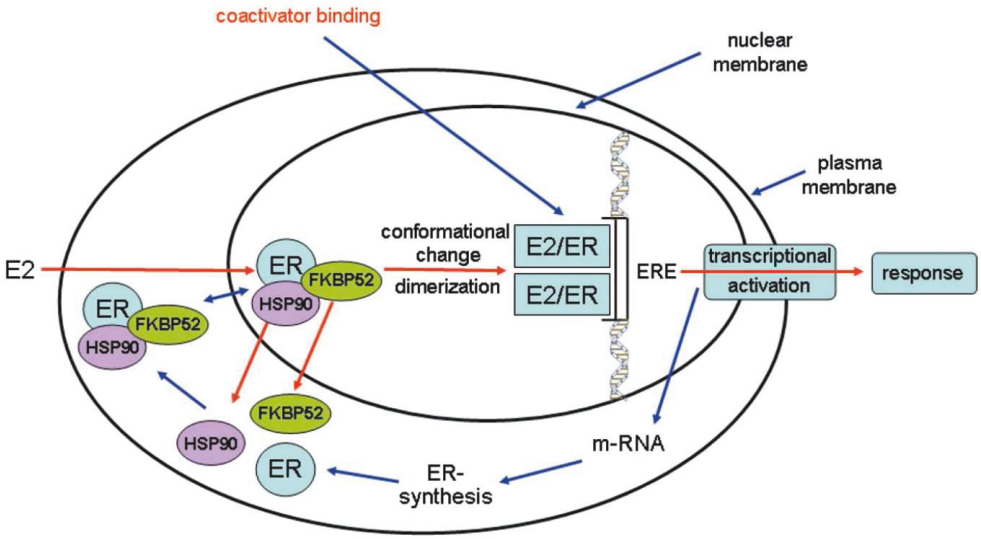

Figure 1.4: Classical model for the activation of ER by E2 and the initiation of transcription.[24]

A second mode of ER activation can arise from the phosphorylation of the receptor's AF-1 domain by membrane receptor tyrosine kinases. Several growth factor dependent pathways such as EGFR, insulin-like growth factor receptor (IGF1-R), and HER2 can intercept and phosphorylate the ER and its coregulators to influence their activity.[36–38] These ligand-independent activation pathways will not be discussed in great detail in this thesis as the focus will be on ligand-dependant activation of the ER, however the references given thus far provide excellent details regarding their importance.

1.2 Agonists and Antagonists of the Estrogen Receptor

1.2.1 Agonists

The most potent natural agonist of the ER is the endogenous estrogen E2, the predominant sex hormone involved in the regulation of several ER mediated processes throughout the female body. The adrenal glands excrete progesterones which are converted by aromatase in the ovaries and adipose tissues into estrogens. In post-menopausal women, ovarian production of E2 halts and adipose tissues become the primary source until death.[39] Other endogenous estrogens include estrone and estriol, however each are 13% as potent as E2.[40] Artificial estrogens such as diethylstilbestrol (DES) can also act as ER agonists, as they possess a similar pharmacophore as E2 and have been used historically as endocrine mimics (Figure 1.5).

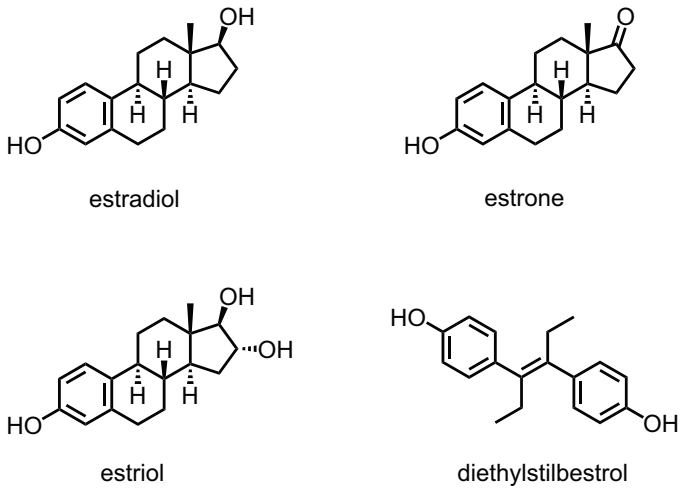

Figure 1.5: E2, estrone, estriol and DES are known agonists of the ER.

The ER recognizes E2 within a hydrophobic pocket in which a specific hydrogen bonding network is engaged. Key interactions involve the hydrogen bonding network of the phenolic moiety of E2, Glu 353, Arg 394 and a molecule of water, and the interaction of the 17β-hydroxyl of E2 with His 524. The core of the hormone is stabilized by hydrophobic interactions throughout the entirety of the binding pocket, and the combined effect leads to a low energy binding event. Once bound to E2, H12 covers the binding pocket completely

and induces a conformational change that exposes the hydrophobic cleft on AF-2 required for coactivator recruitment (Figure 1.6). Similar activation events have been observed in many other human nuclear receptors, including the human retinoid receptor γ, human thyroid receptor, and human nuclear receptor RXR-α.[41–43] The surface features of ligand-bound nuclear receptors are directly associated with the recruitment of the general transcription machinery.[28,44,45] Our understanding of ER activation by agonists has led to several attempts at modulating its effects.

DES was prescribed from the 1940s up until the early 1970s for the treatment of advanced breast cancer in postmenopausal women, adverse pregnancy outcomes such as miscarriages or premature labour, and as an estrogen-replacement therapy drug.[46–48] It was later found to lead to a rare vaginal clear cell carcinoma in females who were exposed to the drug *in utero*, and was then considered a carcinogen, teratogen, and a potent endocrine disruptor due to its estrogenic character.[49,50] Despite the severe consequences of the administration of DES, its ability to act as an ER agonist provides valuable insight into the binding modes of this class of molecules.

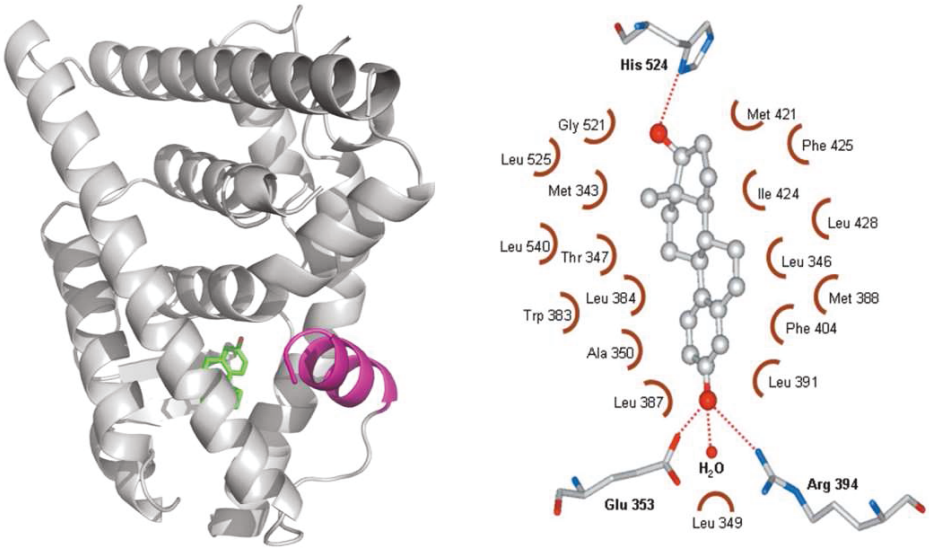

Figure 1.6: LBD of ER bound to agonist E2 and the hydrophobic and hydrogen bonding interactions within the ligand binding cavity.[24] (PDB: 1ERE)

DES is a *trans*-stilbene derivative containing two ethylene groups bound to the tetra-

substituted olefin core. Similar to the hydroxy groups of E2, each of the phenolic moieties are found in hydrogen bonding networks with residues His 524, and with Glu 363, Arg 394, and a molecule of water. The remainder of the molecule is stabilized by hydrophobic interactions by the surrounding residues within the binding pocket (Figure 1.7). DES is held tightly within the LBD and does not protrude from the binding cavity, allowing H12 to reposition itself over the opening, leading to the overall activation of the ER. The ability of DES to act as a potent agonist, while possessing a relatively simple molecular structure relative to a classical steroid, revealed an intriguing chemical space that was later explored.

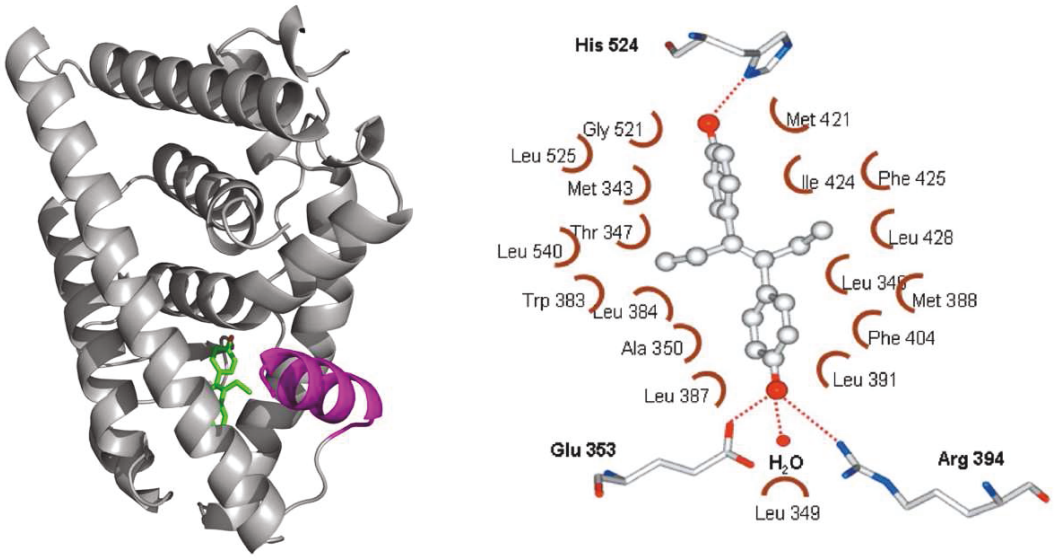

Figure 1.7: LBD of ER bound to agonist DES and the hydrophobic and hydrogen bonding interactions within the ligand binding cavity.[24] (PDB: 4ZN7)

1.2.2 Selective Estrogen Receptor Modulators

Tamoxifen was first discovered by Arthur Walpole in an attempt to invent a novel contraceptive. While it failed to exhibit any significant contraceptive activity, tamoxifen soon became recognized as a potent antiestrogen capable of shutting down the ER in human breast tissues.[51] Interestingly, tamoxifen could also act as an agonist and induce the proliferation of mouse uterine tissues.[52] These contradictory observations regarding the effects

of tamoxifen on the ER were first considered to be a result of species-specific metabolism. However it later became clear that tamoxifen was both estrogenic and antiestrogenic and its behaviour was tissue dependant.[53–55] The mixed agonist/antagonist activity of tamoxifen, and of several other structurally related molecules, led to the class of molecules known as selective estrogen receptor modulators (SERMs) (Figure 1.8).

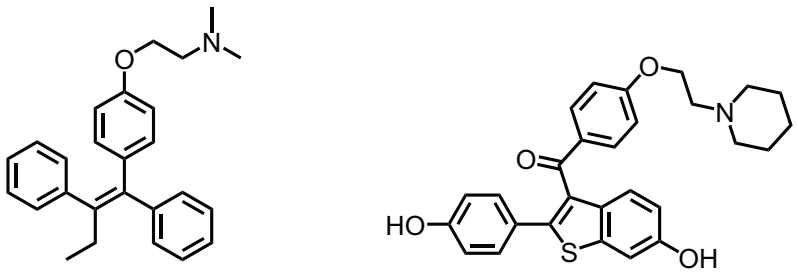

Figure 1.8: Tamoxifen and raloxifene are FDA approved SERMs used in the endocrine treatment of breast cancer.

Tamoxifen is a triphenylethylene-type SERM possessing a tetrasubstituted olefin at its core. Tamoxifen itself has relatively low ER affinity and is a prodrug for 4-hydroxytamoxifen (4-OHT), known to be roughly 100 times more potent than tamoxifen. Tamoxifen is oxidized by cytochrome P450 isoforms CYP3A and CYP2D6 *in vivo* to 4-OHT.[56] Several other metabolites of tamoxifen have been identified, including 4'-hydroxytamoxifen, α-hydroxy tamoxifen, 3-hydroxytamoxifen, and N-desmethyltamoxifen (endoxifen) which has been observed to be as potent as 4-OHT with respect to ER affinity (Figure 1.9).[57] The antiestrogenic activity of 4-OHT is attributed to its *N,N*-dimethylaminoethylene side chain that protrudes from the binding pocket of the ER. The side chain is stabilized by a salt bridge between the tertiary amine and an Asp 351 residue found at the cavity opening. The specific placement of the side chain prevents the closure of H12 over the binding pocket, thus shutting down ER transcriptional activity (Figure 1.10).

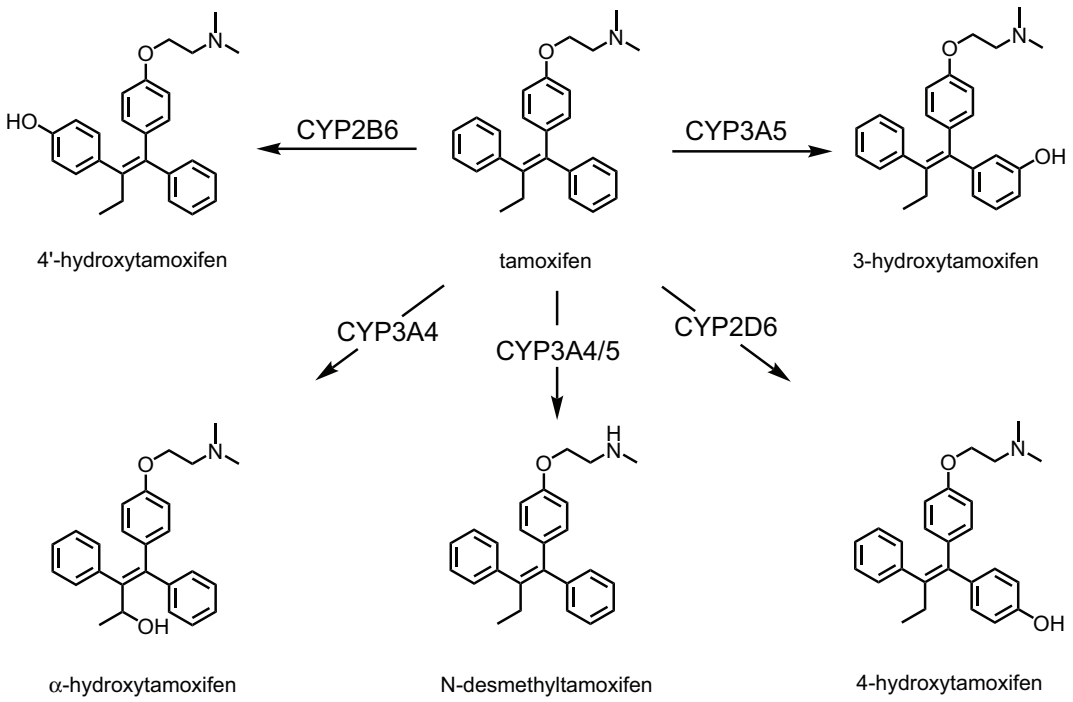

Figure 1.9: Metabolites and cytochrome isoforms associated with tamoxifen metabolism.[57]

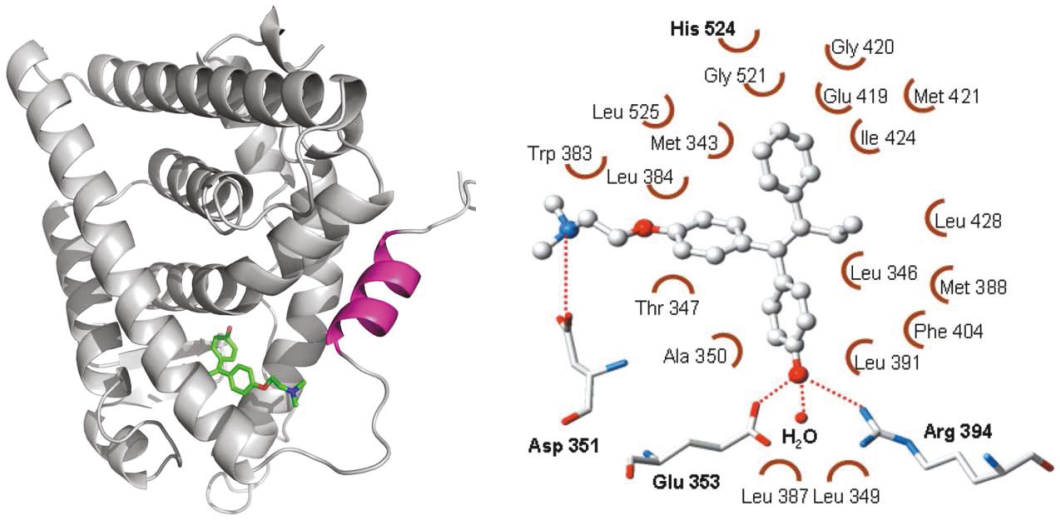

Figure 1.10: LBD of ER bound to SERM 4-OHT and the hydrophobic and hydrogen bonding interactions within the ligand binding cavity.[24] (PDB: 3ERT)

Tamoxifen has been used since the 1970s for the treatment of ER+ advanced breast cancer in post-menopausal women, but its effectiveness as a preventative treatment option was recognized and gained it FDA approval in 1977.[51,58,59] It would later be approved for the treatment of both pre- and post-menopausal women diagnosed with early breast cancer as

an adjuvant therapy option to be used in conjunction with chemotherapy or radiation. The administration of tamoxifen became the standard of care for the treatment of early breast cancer, with a typical treatment plan lasting 5 years.[60] While tamoxifen exhibits antiestrogenic activity in breast tissues, it behaves as an estrogen in the bone and in uterine tissues. Its agonistic activity can be beneficial and it has been used to maintain bone density in mice and in human females.[61,62] However, its agonistic activity in uterine tissues can lead to endometrial cancer, and can increase incidence of the disease by 3-4 times.[6,63] Despite this drawback, tamoxifen still plays a major role as an adjuvant treatment option for advanced breast cancer.

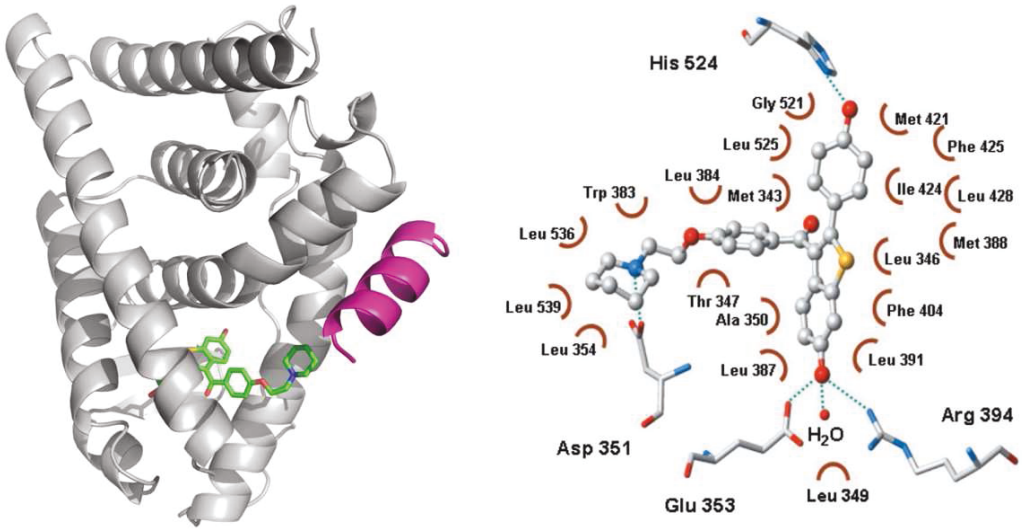

Figure 1.11: LBD of ER bound to SERM raloxifene and the hydrophobic and hydrogen bonding interactions within the ligand binding cavity.[24] (PDB: 1ERR)

Raloxifene is a second generation SERM that exhibits a similar estrogenic profile to tamoxifen. It is a benzothiophene derivative that contains a piperazine side chain and two phenolic moieties. A similar set of hydrophobic and hydrogen bonding interactions take place in the binding of raloxifene as they do with tamoxifen, with an additional hydrogen bonding interaction between the phenol and His 524 (Figure 1.11). This hydrogen bonding event also occurs in the binding of E2, however the imidazole of His 524 is rotated due to the differential positioning of the phenolic -OH of raloxifene compared to the 17β-hydroxyl

group of E2.[19] Antiestrogenic activity is again attributed to the amine-containing side chain which forms a salt bridge with Asp 351 and protrudes from the binding cavity between H3 and H11. The consequence of the protrusion is the inability of H12 to close over top of the cavity and the lack of competent AF-2 region formation necessary for ER activation.

Unlike tamoxifen, raloxifene maintains its antiestrogenic character in uterine tissues and does not increase the risk of endometrial cancer development.[64] The Study of Tamoxifen and Raloxifene (STAR) found that 60 mg/day of raloxifene is as effective as 20 mg/day of tamoxifen, both over 5 year periods, for reducing the risk of invasive breast cancer.[65] Unfortunately, the incidence rate of invasive breast cancer in a group that was administered raloxifene was reduced by only 38%, as opposed to the tamoxifen group whose incidence rate was reduced by 50%, a finding that will likely hinder the administration of raloxifene.[66] The estrogenic activity of raloxifene has been utilized clinically to treat osteoporosis in postmenopausal women due to the agonistic properties it exhibits in bones.[61,67]

The dual nature of SERMs has not yet been fully explained due to the complex nature of the ER and its associated pathways. Some studies have suggested that the different coregulators required for each specific ER mediated pathway are responsible for the differences in activity. For example, the ER in breast tissues require coregulators to bind to the hydrophobic groove defined by a conformational change involving H12, whereas coregulators in other tissues may bind to other sites of the LBD and the disruption of H12 is inconsequential with regards to activation.[68] Another theory suggests that the interplay between ERα and ERβ is tissue-dependent, where activation of either isoform with the same ligand can result in different or opposing responses.[68] Unfortunately, there are currently no definitive molecular explanations for the mixed agonist/antagonistic properties of SERMs. The serendipitous discovery of SERMs and their ability to mitigate the growth of estrogen dependent breast tumours while leaving most other estrogen regulated processes largely untouched is near ideal and demonstrates the power of truly modulating a protein target as opposed to shutting down its activity completely.

1.2.3 Full Antiestrogens

A third class of molecules that have been developed to target the ER are the full antiestrogens. These compounds do not show agonistic properties for the ER in any tissue and are typically reserved for patients who become unresponsive to treatment with SERMs.[2] These pure antiestrogens have higher affinities than SERMs and are capable of inhibiting the ER and completely shutting down its activity. While SERMs shut down AF-2 mediated activity of the ER, full antiestrogens also inhibit AF-1 which mediates activation by ligand-independent phosphorylation.[69,70] Full antiestrogens are typically modelled after E2 with the inclusion of an antiestrogenic side chain at some position within the steroidal scaffold. Notable full antiestrogens include ICI-164,384 and fulvestrant (Figure 1.12).

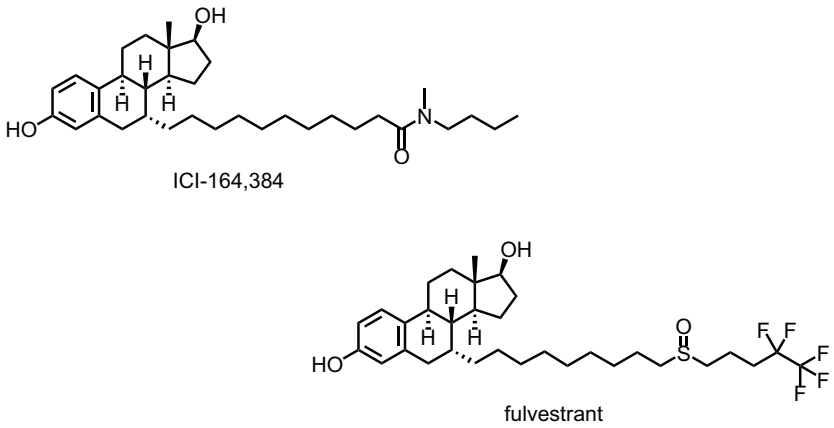

Figure 1.12: Full antiestrogens fulvestrant and ICI-164,384

Fulvestrant is a full antiestrogen derived from ICI-164,384 and was first reported by Wakeling in 1991.[70] It is a competitive inhibitor of the ER, showing a similar affinity to E2 and 100 times the affinity of tamoxifen. Fulvestrant contains a 7α-pentafluoropentylsulfinyl alkyl side chain and was found have an *in vivo* potency an order of magnitude greater than ICI-164,384 in MCF-7 breast cancer cell lines and in mice.[71] Full antiestrogens are also known to downregulate ER activity by mediating protease-mediated degradation of the receptor by both ubiquitination and by sumoylation.[72–75]

The binding mode of full antiestrogens has been observed in the solved crystal struc-

ture of ICI-164,384 and ERβ (Figure 1.13).[76] The complex was resolved as a homodimer with the ligand bound within the binding cavity and surrounded by an analogous set of antiparallel helices as seen in crystal structures of ERα. The most significant difference in the binding of a full antiestrogen compared to a SERM, is the complete destabilization of H12 such that its position could not be identified crystallographically. This highly unstable conformation is a direct consequence of the long 7α-antiestrogenic side chain that completely occupies a hydrophobic pocket that is known to accommodate H12 when the ER is bound to a SERM.[19] Additionally, the steroidal core of ICI-164,384 is flipped 180° with respect to E2 bound to ERα in order to accommodate the 7α-side chain. This orientation results in the engagement of the same hydrogen bonding networks, but the molecule is rotated 180°about its axis relative to E2. The phenol group interacts with Glu 260 and Arg 301 while the 17β-hydroxyl group interacts with His 430, and the core of the molecule is stabilized by hydrophobic residues within the pocket. The side chain extends out of the binding pocket and makes a 90° bend, embedding into a groove between H3 and H5. Remarkably, it is not bound to Asp 258, a crucial binding feature that is observed in the crystal structures of ERα-4-OHT and ERα-raloxifene.[19,45,76]

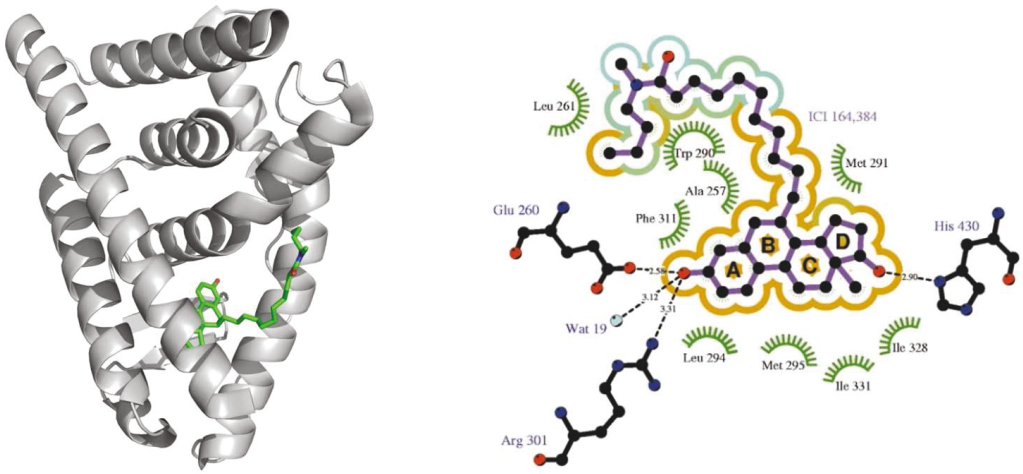

Figure 1.13: ICI-164,384 bound to ERβ and the hydrophobic and hydrogen bonding interactions within the ligand binding cavity.[76] (PDB: 1HJ1)

Full antiestrogens have become clinically relevant in the treatment of metastatic breast

cancer due to their ability to shut down global ER activity. Fulvestrant was FDA approved in 2002 for the treatment of advanced breast cancer in patients who had previously undergone endocrine therapy that proved ineffective.[77] Despite their niche utility, the ability of full antiestrogens to block the systemic activity of estrogen is not a desirable clinical trait. SERMs offer the ability to selectively target breast tumour cells while maintaining estrogenic activity in other areas of the body where ER function is crucial. Unfortunately, a large proportion of endocrine responsive breast tumours develop endocrine resistance and treatment options then become limited to full antiestrogens despite their drawbacks.[78]

1.3 Endocrine Resistant Breast Cancer

1.3.1 Endocrine Resistance

Nearly 75% of breast tumours express the ER and are susceptible to endocrine treatment whereas those who are ER- are typically unresponsive. Multi-gene tests can examine the profiles of patients to assess whether an ER+ tumour would benefit from adjuvant endocrine therapy in conjunction with chemotherapy or radiation, or from endocrine therapy alone.[79,80] Nearly 30% of patients undergoing endocrine therapies will experience tumour regression while an additional 20% of diseases will become stable over a prolonged period of time. The remaining patients' diseases will develop or will have had an inherent resistance to endocrine treatments which can be the result of biochemically related escape pathways. The existence of such pathways suggests that estrogen-mediated proliferation is only one of several potential pathways that tumours utilize for survival.[78]

Although many tumours become endocrine resistant, the ER is still expressed and can be affected using full antiestrogens such as fulvestrant in two-thirds of patients.[81,82] These observations suggest that while SERMs may be inactive against resistant tumours, the ER still plays a regulatory role in tumour growth. Endocrine resistance is thought to be the result of either genetic or epigenetic changes that present alternative survival pathways for tumours. A mutation of the ER is a potential pathway leading to resistance, where one

study observed a Tyr537Asn mutation in the LBD that resulted in an ER that was constitutively active both in the absence of E2 and in the presence of tamoxifen.[83] Additionally, Lys 303 is a target for acetylation by CREB-binding protein and a Lys303Arg mutation can lead to an increase in ER sensitivity to E2, which was observed in 20 of 59 premalignant hyperplastic lesions within a study by Fuqua.[84,85] In addition to adventitious mutations, proliferative pathways that run alongside the ER can also contribute to endocrine resistance.

Coregulators of the ER, and other pathways they associate with, have been heavily implicated as a possible factor that contributes to the development of endocrine resistance. One specific example is the overexpression of coregulator AIB1 which has been directly linked to tamoxifen resistance. High levels of the coactivator and of human epidermal growth factor 2 (HER-2) were associated with a significant decrease in the antiestrogenic activity of tamoxifen in 316 breast cancer tumour samples.[86] Tamoxifen actually became an agonist of the ER in MCF-7 cell lines that overexpressed AIB1 and HER2, leading to tamoxifen induced tumour growth. These findings are explained by the ability of tamoxifen to activate HER2, EGFR, and mitogen-activated protein kinase (MAPK) which can then phosphorylate and activate the ER, even if the ER is bound to tamoxifen.[87] This is one of many examples regarding a mode of endocrine resistance that exemplifies the subtle shifts in protein expression that can lead to a complete reversal of the ability of tamoxifen to act as an antagonist.

These examples regarding either site specific mutations or by the involvement of parallel pathways that regulate proliferation are just two of many similar events that are known to induce endocrine resistance. The 2011 review by Osborne and Schiff and the references therein provide more thorough descriptions and explanations of the many types of mechanisms and pathways that have been associated with endocrine resistance.[78]

1.3.2 Overcoming Endocrine Resistance

Strategies to overcome endocrine resistance have targeted key receptors of associated pathways, namely HER2 and EGFR, that are known to interfere with endocrine sensitiv-

ity. A preliminary trial observed the effects of coadministering tamoxifen with gefitinib, an EGFR inhibitor, which led to a numerical advantage with respect to progression-free survival when compared to a group administered tamoxifen alongside a placebo.[88] Another trial investigated the effects of combining lapatinib, an EGFR inhibitor, with letrozole, an aromatase inhibitor (AI), in an attempt to exploit the apparent cross-talk that occurs between the EGFR pathway and ER mediated proliferation in endocrine resistance breast tumours. The authors found that administration of both classes of drugs led to a 48% clinical benefit rate (CBR) compared to a 29% CBR when patients were given letrozole alone. They suggest that the treatment may be applicable to patients that have relapsed during early adjuvant therapy and have developed tamoxifen-resistant breast cancer, which can be the result of tamoxifen induced upregulation of EGFR. The upregulation and strategic targetting of EGFR would then lead to an increased response rate compared to additional treatment with AIs alone.[87,89,90] However, it was noted that the dual administration treatment failed to prevent or delay endocrine resistance in patients who were initially endocrine sensitive.[90] The complexity of endocrine resistance, whether it be due to cross-talk between parallel signalling pathways or through unknown biomolecular mechanisms, poses a significant challenge but investigations regarding dual administration of different drug classes are promising.

The dual administration of histone deacetylase inhibitors (HDACis) and SERMs has become an area of interest for endocrine resistant tumours, and has introduced the possibility of resensitizing ER- breast tumours to endocrine treatments. One explanation for ER silencing in ER- breast tumours is the result of hypermethylation of the ER gene promotor, a state that can be reversed by treating cells with demethylating agents and HDACis.[91,92] Sharma *et al.* reasoned that HDACis and demethylating agents, trichostatin A and 5-aza-2'-deoxycytidine (5-aza-dC), respectively, could be used to restore function to silenced genes and resensitize ER- cell lines to antiestrogens. Indeed, they achieved resensitization of an ER- MDA-MB-231 breast cancer cell line using their strategy and were able to inhibit proliferation using tamoxifen (Figure 1.14).[93] It should be noted that Jang previously showed that ERβ, not ERα, was upregulated and subsequently inhibited by tamoxifen.[94]

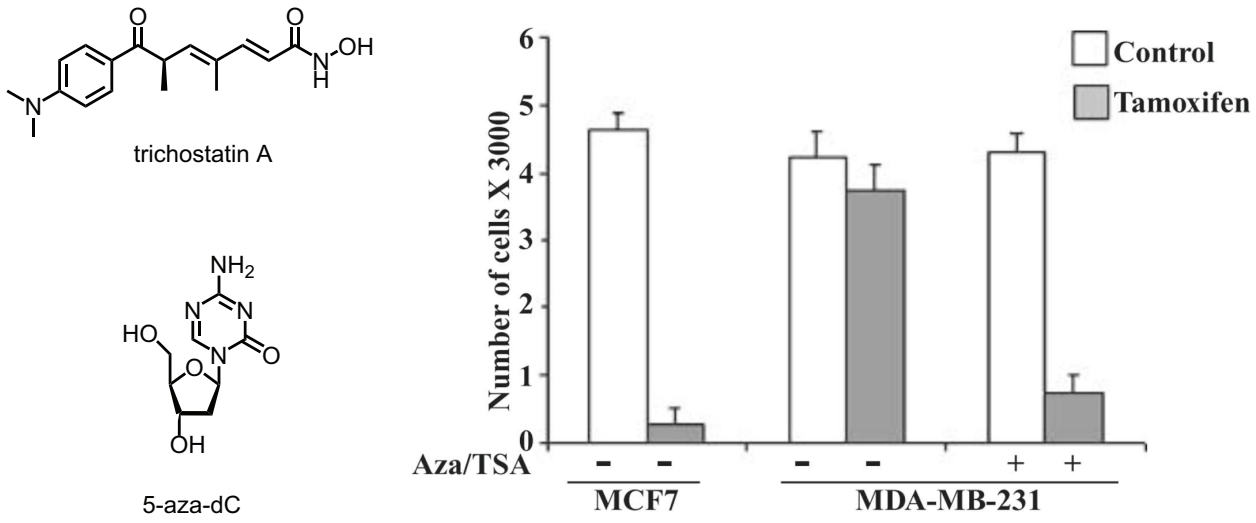

Figure 1.14: Treatment of ER- cells with trichostatin A and 5-aza-dC led to restoration of tamoxifen sensitivity.[93]

The ubiquity of HDACs and the intimate role they play in the regulation of ER mediated gene transcription makes them an interesting target alongside the ER. HDACs and HDAC inhibition have been studied extensively and have recently become clinically relevant in many interesting contexts. Their role in breast cancer and their apparent ability to reinvigorate classical antiestrogen therapies will be discussed in the following section.

1.4 Histone Deacetylase and Breast Cancer

1.4.1 Structure and Function of HDACs

HDACs are best known as epigenetic factors that cooperate in tandem with HATs to acetylate and deacetylate histone proteins to allow or restrict access of the general transcription machinery to DNA. HDACs are often the final set of proteins that are recruited by a variety of coregulators at the conclusion of a signalling pathway, the identities of which can vary greatly depending on the active pathway. HDACs, with the exception of the sirtuins, are metalloproteins that condense chromatin by deacetylating the ϵ-amine of lysine residues via Lewis acid catalysis, exposing a positive charge that attracts the negatively charged phosphate backbone of DNA.[95] The other half of chromatin remodelling requires HATs, which neutralize the positive charge of lysine residues by acetylation which induces chromatin ex-

pansion in preparation for gene transcription.[96] It should be noted that HDACs do not act independently, but rather serve as catalytic subunits that reside in large protein complexes.[97]

HDACs have been organized into four classes, I, IIa, IIb, and IV. There exists a third class of HDACs, class III, known as the Sirtuins, however they are structurally and mechanistically distinct and are covered extensively in a review by Schwer and Verdin.[98] Class I consists of HDACs 1, 2, 3, and 8; Class IIa consists of HDACs 4, 5, 7, and 9; Class IIb consists of HDACs 6 and 10; and Class IV consists only of HDAC 11. Each class of HDACs, with the exception of the Sirtuins, contains a highly conserved zinc-containing deacetylase domain. HDAC classification is dependent on their specific function, structure, and tissue and cellular localization patterns.

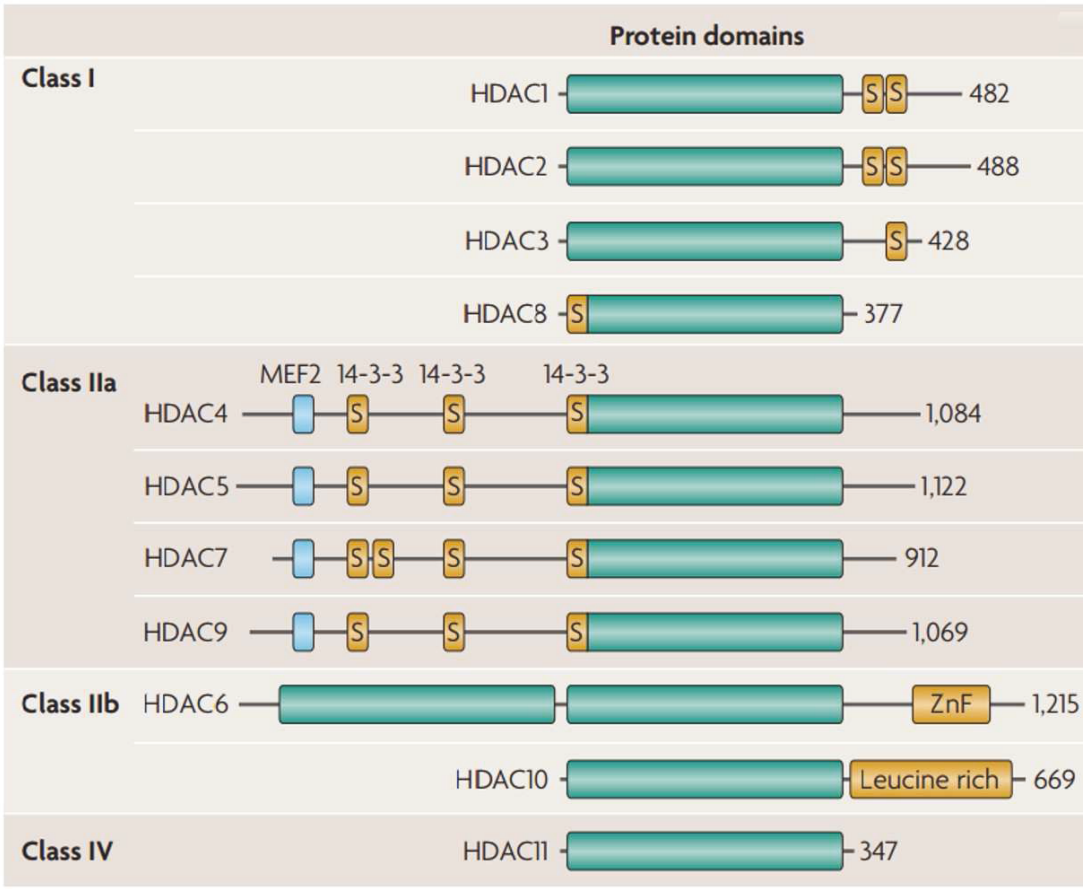

Figure 1.15: Sequence homology of each HDAC and their relevant domains.[99]

Class I HDACs are ubiquitous and are found largely in the cell nucleus. Structurally, they consist of the 390-amino-acid deacetylase region in addition to short carboxy and amino-terminal extensions. HDACs 1 and 2 are known to form Sin3, NuRD, CoREST, and PRC2 repressive complexes, whereas HDAC3 is found in the N-CoR-SMRT complex.[100,101] Class II HDACs are found both in the nucleus and cytoplasm, and are believed to act as signal transducers due to their ability to shuttle between these two subcellular environments depending on their coregulator association, and their ability to deacetylase proteins other than histones.[100] In addition to their deacetylase domain, they contain an N-terminal extension that is capable of binding to the transcription factor myocyte enhancer factor-2 (MEF-2),.[102] Class IIb member HDAC 6 resides largely in the cytoplasm and contains an additional zinc containing deacetylase domain and a C-terminal zinc-finger that can bind ubiquitin, whereas HDAC 10 lacks both a second deacetylase domain and contains a leucine rich C-terminus (Figure 1.15). HDAC 11 shares high sequence homology with other Class I HDACs, however it is phylogenetically distinct and thus resides in a separate class and its specific function is not yet known.[103] Due to their epigenetic role, close association with a wide range of biological functions, and their relatively simple structures, HDACs are interesting therapeutic targets that have become increasingly relevant over the past several years.

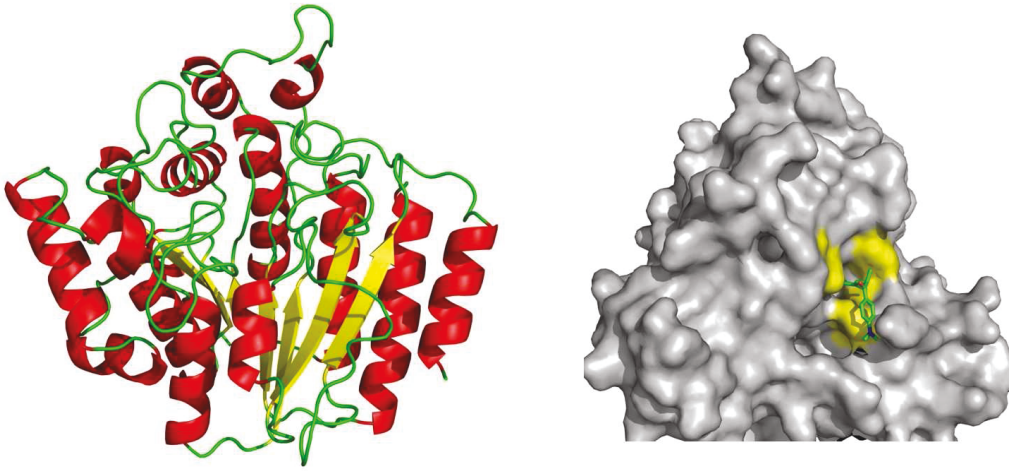

Figure 1.16: Solved crystal structure of HDLP, an HDAC 1 homologue, bound to TSA. (PDB:1C3R)

The crystal structure of an HDAC 1 homologue bound to suberoylanilide hydroxamic acid (SAHA) and trichostatin A (TSA) was solved by Finnin *et al.* in 1999 (Figure 1.16).[95] The protein structure consists of a single-domain containing a central eight-stranded parallel β sheet and sixteen α-helices, four of which are oriented on either side of the β-sheet to form the protein core. The catalytic pocket is defined by extra helices and L1-L7 loops which extend from the core and form a deep, narrow pocket leading to the Zn^{2+}-containing core. The pocket has a depth of 11 Å, is formed by largely hydrophobic and aromatic residues, and is 7.5 Å at its narrowest point which is flanked by two phenylalanine residues. The zinc atom is coordinated at the base of the pocket by Asp 168, His 170, Asp 258, and a molecule of water in a tetrahedral coordination environment. Hydroxamic acid inhibitors SAHA and TSA coordinate zinc similarly via their carbonyl and hydroxyl groups, which displaces a molecule of water, to give a pentacoordinated Zn^{2+}. The aliphatic linkers of each inhibitor reside within the hydrophobic tunnel and are stabilized by Van der Waals interactions, whereas the capping groups reside on the surface of the protein. In the case of TSA, the aromatic group resides snugly in a groove whereas the longer aliphatic linker of SAHA prevents tight positioning of the aromatic group on the protein surface (Figure 1.17).[95]

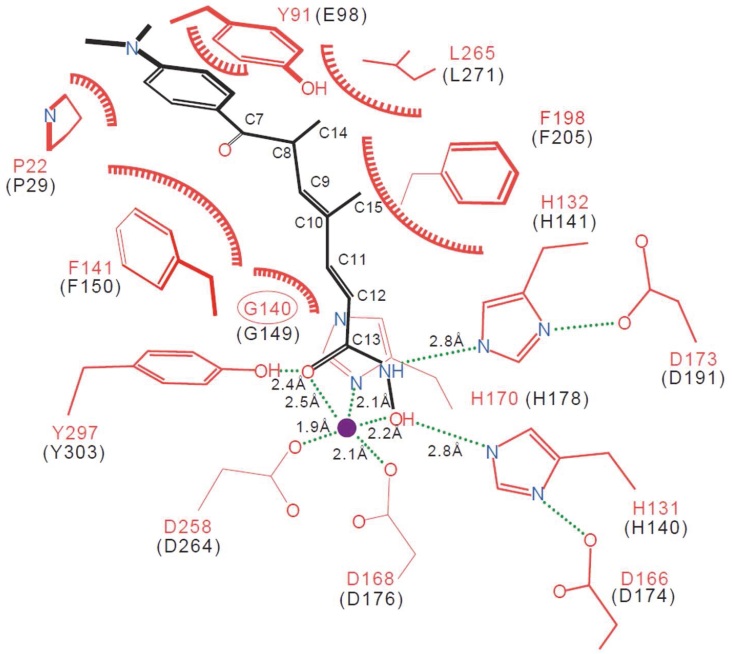

Figure 1.17: Binding mode of TSA within the binding cavity of an HDAC 1 analogue.[95]

1.4.2 HDAC Inhibitiors and Breast Cancer

Several classes of molecules have been identified as HDAC inhibitors including, but not limited to, hydroxamic acids, carboxylic acids, benzamides, thiols, electrophilic ketones and silanediols.[104–107] The molecular structures of HDAC inhibitors tend to follow a characteristic pattern that consists of a terminating aromatic moiety referred to as the capping group, an aliphatic linker, and a bidentate zinc-binding group (Figure 1.18). HDAC inhibitors are competitive inhibitors that shut down the catalytic activity of HDACs by chelating the Zn^{2+} core, which is achieved by the zinc-binding group. The capping group is typically hydrophobic and contains an aromatic moiety, while the aliphatic linker joins the two distal structural features together. The linker can vary in length, stereochemistry, saturation, branching sites, and can contain aromatic groups.[108] A large variety of capping groups and aliphatic linkers are tolerated by HDACs and there are examples of subtle variations in structure that have been used to induce HDAC isoform selectivity.[109]

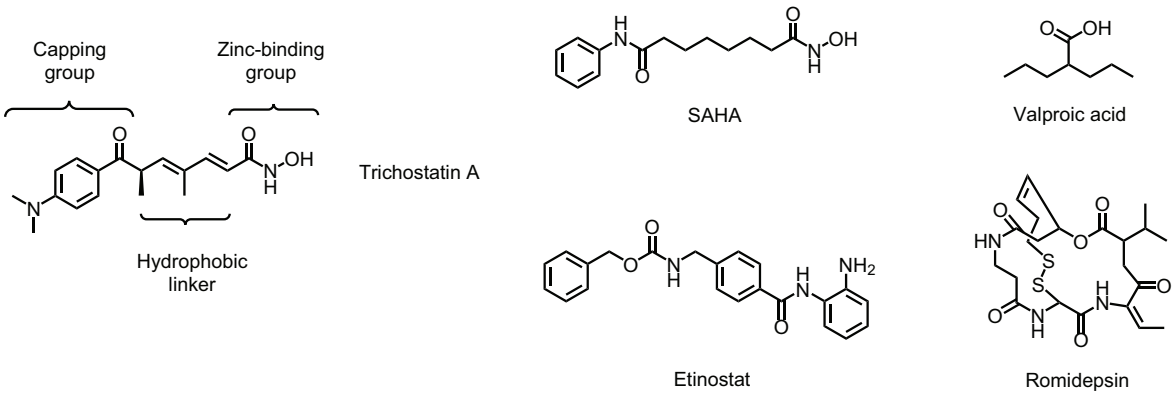

Figure 1.18: Structural features and examples of HDACi.

HDACs have been implicated in many different forms of cancer, including breast cancer, prostate cancer, and acute promyelocytic leukemia. A link between HDAC overexpression and tumorigenesis has not been established, but rather aberrant activity of HDAC is believed to play a role. Low levels of HDACs 1, 2, 3, and 6 have led to apoptosis of tumour cells in breast cancer which suggests that their activity is required for tumour survival. In breast tumours that co-expressed HDAC 1 and ERα, HDAC 1 served as a potential marker for endocrine-responsive patients where higher levels were linked to prolonged, disease free

survival.[110,111] HDAC 3 expression also correlated with ER expression but evaluation of HDAC 1 proved to be a better marker for positive prognoses. Interestingly, MCF-7 cells that overexpressed HDAC 1 also showed a loss of ER and an increase in cell proliferation while MCF-7 cell lines treated with TSA regained ER levels, suggesting HDAC 1 may act to both increase tumour cell proliferation and suppress ER transcription.[112] HDAC 1 and 2 activity has also been linked to deacetylation and, consequently, downregulation of the tumour suppressor gene p53.[113,114] The many links between HDAC activity and tumour cell proliferation have made HDAC a relevant therapeutic target for cancer treatment.

There are currently several HDACis being investigated for the treatment of cancer, inflammation, infection, and neurological and immune disorders.[109] SAHA has been approved for the treatment of cutaneous T cell lymphoma and romidepsin and belinostat have both been approved for the treatment of peripheral T cell lymphoma.[115,116] The treatment protocols for each approved HDACi calls for mono-administration of each drug and, in the SAHA trial, toxicity was an issue that limited the length and intensity of the treatment plan. SAHA has also been reported to induce differentiation and have antiproliferative activity in the ER- breast cancer cell line MDA-468[117] HDAC inhibitors have also been used in combination therapy approaches, specifically in the treatment of breast cancer.

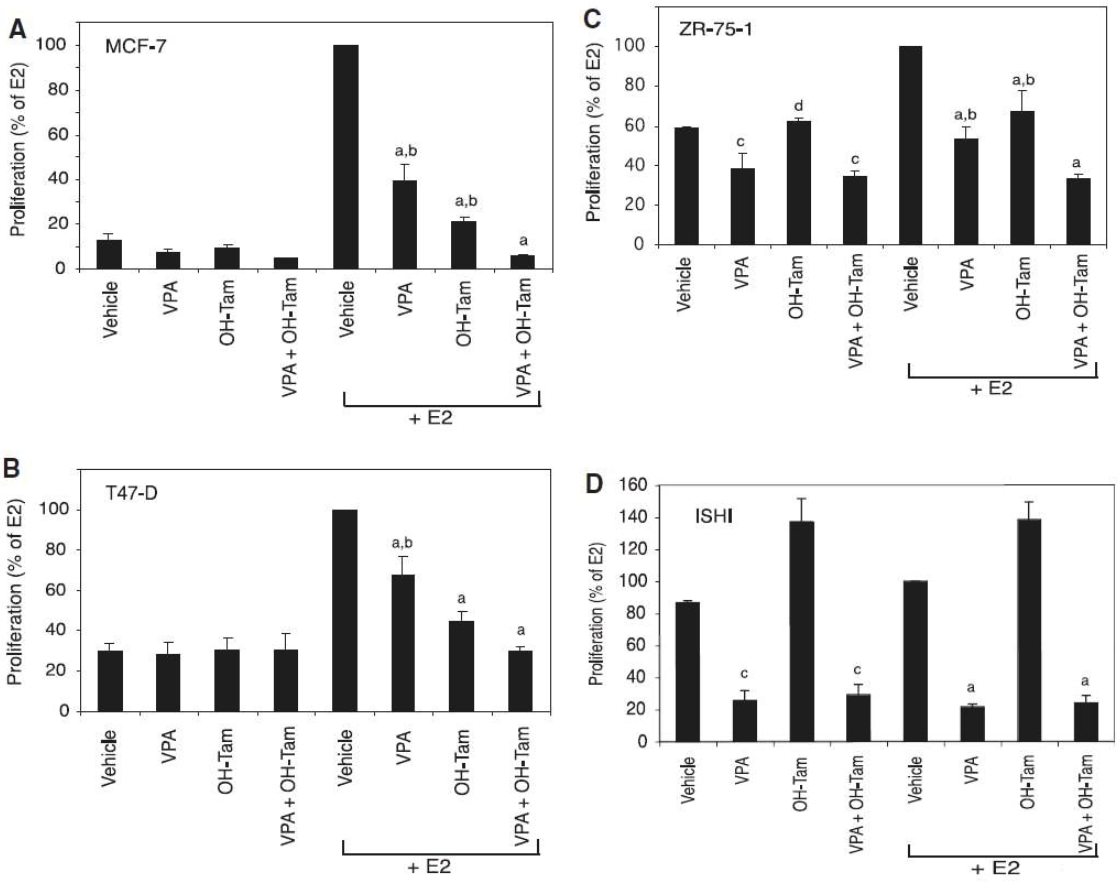

Figure 1.19: Enhanced antiproliferative effects of tamoxifen when combined with valproic acid against breast and endometrial cancer cell lines.[118]

Combination therapies using SERMs and HDACis to treat breast cancer have become an interesting topic of research and early findings have yielded intriguing results. The study by Sharma *et al.*, mentioned in Section 1.3.2 of this thesis, found that ER- breast cancer cells could be resensitized to treatment with tamoxifen after TSA induced ER expression.[93] Further investigation by Hodges-Gallagher *et al.* found that treating MCF-7 cells with valproic acid, SAHA, or TSA and 4-OHT in the presence of E2 led to a greater inhibition of proliferation compared to treatment with any single molecule alone. They reported that tamoxifen lowered the IC_{50} of HDACi by roughly half, suggesting the two classes of molecules can tolerate the other and act cooperatively to induce apoptosis. Enhanced anti-proliferative effects were also observed against T47D and ZR-75-1 cell lines, the latter of which show a higher baseline proliferation rate than MCF-7 cell lines. Co-administration of valproic acid with tamoxifen against Ishikawa adenocarcinoma cells, a model cell line for endocrine cancer,

reversed the agonistic effects of tamoxifen and instead resulted in the inhibition of proliferation (Figure 1.19).[118] Thomas *et al.* also observed cooperativity between valproic acid and tamoxifen, and address the induction of autophagy in a subset of cells and its ability to protect them from cell death as a consequence of triggering apoptosis with the SERM/HDACi drug combination.[119]

A phase two clinical trial investigated the dual administration of SAHA and tamoxifen to ER+ metastatic breast cancer patients. The authors observed that in the presence of an HDACi, tamoxifen induces apoptosis of breast tumour cells and not cell cycle arrest as it does when it is administered alone; the effect is believed to be the result of HDAC 2 inhibition.[120,121] The phase two trial found that 40% of the patients who had already undergone prior hormonal and chemotherapies, experienced tumour regression or prolonged disease stabilization due to the combination SERM/HDACi therapy. The ability for the combination therapy to circumvent tamoxifen resistance was commented on briefly but no formal observations were made regarding this claim.[120] As the potential for combination therapy of HDACis and SERMs become more apparent, the potential for unique implementations of this cooperativity begins to arise.

1.5 Hybrid Molecules

1.5.1 Hybrid Molecules as Drugs

Hybrid molecules that affect two distinct protein targets are an intriguing single-molecule approach to combination therapies. Ideally, the hybrid structure should not rely on a non-functional linker to join the two domains but rather have both distinct domains overlap within a single molecular structure. Many factors must be taken into consideration when designing a hybrid molecule, such as whether both protein targets are able to tolerate the additional pharmacophore, if the synthesis of the hybrid is feasible, and whether the affinity of the hybrid for both targets is within their respective therapeutic ranges. On the other hand, hybrid molecules can potentially combine the effectiveness of combination therapies into a single drug, thereby increasing patient compliance, lowering manufacturing costs,

simplifying formulation and pharmacokinetic and toxicity profiles, and potentially exploiting the inherent uptake capacity of one parent molecule to improve the uptake of the added pharmacophore.[122] The Gleason group has used the hybrid molecule approach to design, synthesize, and evaluate the effectiveness of triciferol, a hybrid vitamin D receptor (VDR) agonist and HDACi (Figure 1.20).[123]

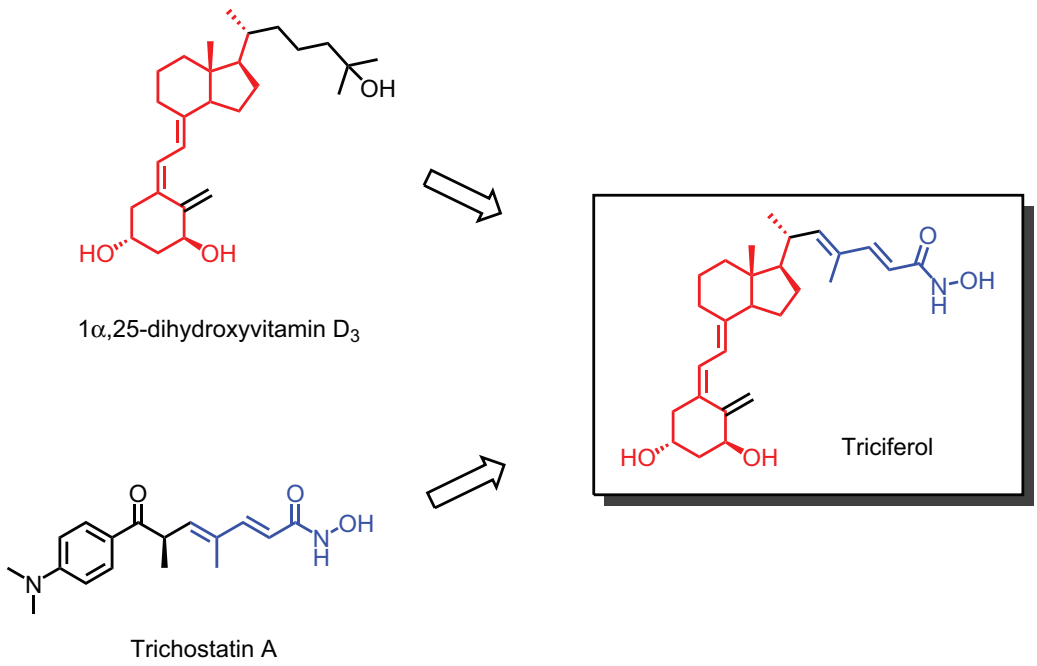

Figure 1.20: Triciferol is a hybrid VDR agonist/HDACi.[123]

Briefly, 1α,25-dihydroxyvitamin D_3 (1,25D) regulates cell differentiation and proliferation by binding the VDR, a nuclear receptor that mediates gene transcription through the upregulation of cell-cycle regulators and differentiation factors. 1,25D and its analogues are of interest for the treatment of cancers due to their ability to attenuate cell proliferation. Previous studies reported that combining TSA and 1,25D showed enhanced antiproliferative effects on 1,25-D resistant cancer cell lines. Based on these data, a hybrid that would bind both the VDR and HDAC was envisioned using rational design principles. The structure of triciferol combined the secosteroidal core of 1,25D and the branched, unsaturated hydroxamic acid sidechain of TSA to give an overlapping structure that contained both pharmacophores. Triciferol showed greater cytotoxicity in poorly differentiated breast and

squamous carcinoma lines as well as in the MCF-7 breast cancer cell line.[123]

A second study examined the effects of substituting various aliphatic chain sizes and zinc-binding groups for the TSA segment of triciferol. They found that not only did a variety of groups lead to strong VDR agonism, but that sterically demanding groups, such as *ortho*-aminoanilides, were tolerated by the VDR. Many of the derivatives showed antiproliferative effects on murine AT84 head and neck squamous carcinoma cells.[124] Both studies are proofs of concept that showed nuclear receptors could tolerate the addition of a functionally distinct pharmacophore within the active structure of their native ligand, and that hybrid molecules of this nature could lead to enhanced cytotoxic effects, even in resistant cell lines.

1.5.2 Hybrid SERM/HDACi Molecules

A hybrid SERM/HDACi molecule could potentially increase the effectiveness of standard endocrine treatments while also addressing the issue of endocrine resistance. It is clear that both the ER and HDAC play a role in breast cancer cell proliferation, as aberrant HDAC activity has been linked to tumour cell proliferation, and ER signalling relies on corepressor complexes that contain HDAC to influence gene transcription.[2,109] The idea of combining SERM and HDACi activity into a single hybrid molecule has been approached recently by several groups.

Patel *et al.* sought to introduce HDACi activity to raloxifene by substituting its antiestrogenic side chain with hydroxamic acids of various chain lengths to elicit HDACi activity. The group successfully generated a series of hybrids, dubbed SERMostats, and one in particular showed 1-3 µM IC_{50} values for HDACs 1-3 and was capable of causing apoptosis in ER- human breast cancer cell lines similar to that of combination HDAC/SERM treatments (Figure 1.21).[125] The group also showed that cytotoxic cargo could be conjugated to a benzothiophene scaffold and localized to the nucleus of ER+ breast cancer cells.[126]

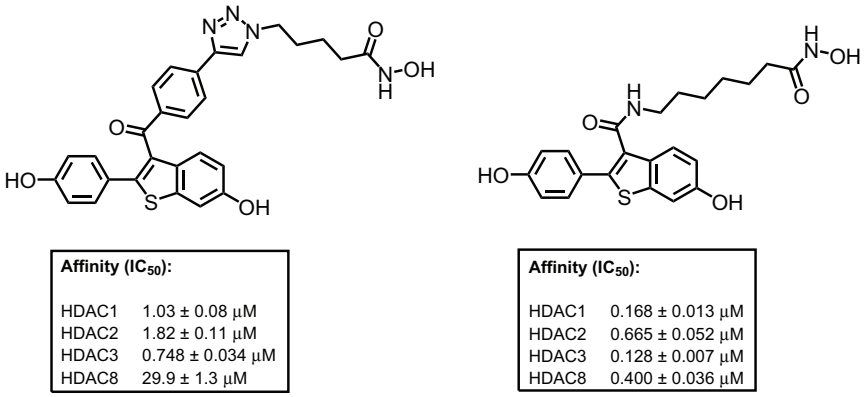

Figure 1.21: Patel *et al.* successfully synthesized biologically active hybrid SERM/HDACi molecules using a benzothiophene scaffold.[125]

A second investigation of hybrid SERM/HDACis by *Tang et al.* constructed a library based on an exo-5,6-bis(4-hydroxyphenyl)-7-oxabicyclo[2.2.1]hept-5-ene-2sulfonic acid phenyl ester (OBHS) scaffold that could be rapidly assembled using a thermal [4+2] Diels-Alder cycloaddition. Similar to the classical SERMs, OBHS is known to antagonize the ER by displacing helix 12.[127] The group employed a highly efficient [4+2] reaction between disubstituted furans and phenyl sulfonate dienophiles as their final synthetic step to quickly build a library of 33 analogues. They reported a K_i of 25 nM and an ERα/β selectivity ratio of 20 for a carboxylate hybrid, however it showed partial antagonist activity in transcription assays (Figure 1.22). The hybrids also displayed potent anti-proliferative activity against MCF-7 and DU-145 cancer cell lines, greater than that of OBHS due to their combined HDACi character. Interestingly, one hybrid showed a much lower binding affinity for both ER isoforms compared to 4-OHT, but was more potent against MCF-7 cell lines, which may suggest that ER affinity is not an absolute parameter when considering antiproliferative potency. Similarly, a separate hybrid showed high affinity for each ER isoform but exhibited poor antiproliferative effects on MCF-7 cell lines. Binding affinities for the majority of the OBHS hybrids for HDAC 1 and 6 were submicromolar, the best being 22 nM for HDAC 1 and 30 nM for HDAC 6 (separate hybrids) (Figure 1.22).[128]

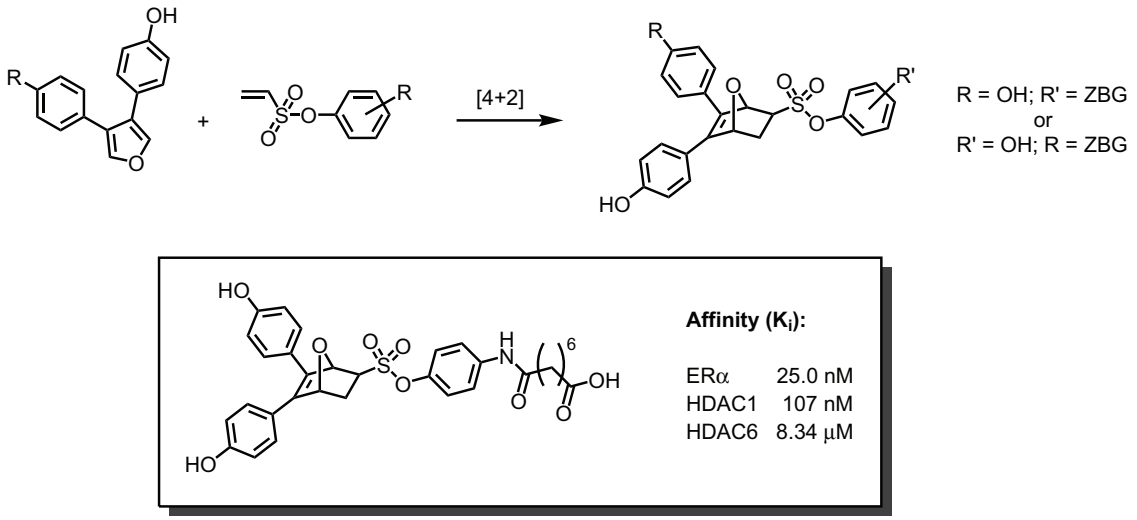

Figure 1.22: Tang *et al.* constructed a hybrid SERM/HDACi library using a Diels-Alder cycloaddition strategy.[128]

Prior work in the Gleason lab by Benjamin Williams and Laurie Lim focused on constructing hybrid SERM/HDACis by introducing an HDACi side chain onto a 4-OHT scaffold (Figure 1.23). The C-ring analogue series was first investigated in which the antiestrogenic side chain of tamoxifen was substituted for an aliphatic side chain, of various chain lengths, bearing a hydroxamic acid. The rationale for introducing C-ring substitution was that perhaps the aliphatic linker would mimic the antiestrogenic character as the *N,N*-dimethylaminoethyl side chain due to the inclusion of polar ether and amide functionalities. Unfortunately, while some hybrids exhibited submicromolar binding of the ER and of HDAC 6, many failed to act as antagonists at all concentrations.[129,130] However, a single C-ring substituted hybrid was found to exhibit antiestrogenicity and an ER IC_{50} of 26 nM, lower than that of 4-OHT (55 nM), but was found to show agonistic properties at higher concentrations relative to 4-OHT at similar concentrations. Next, a series of A-ring substituted analogues were synthesized, but lacked affinity for the ER due to the fact that the phenolic moiety was ablated, which is responsible for a key hydrogen bonding interaction within the ER binding cavity. Finally, a single B-ring substituted analogue was synthesized and showed modest micromolar affinities for both the ER and HDAC 6, while remaining antiestrogenic for the ER at all concentrations.[130] This finding justified the need to further explore the chemical space of the B-ring substituted analogues.

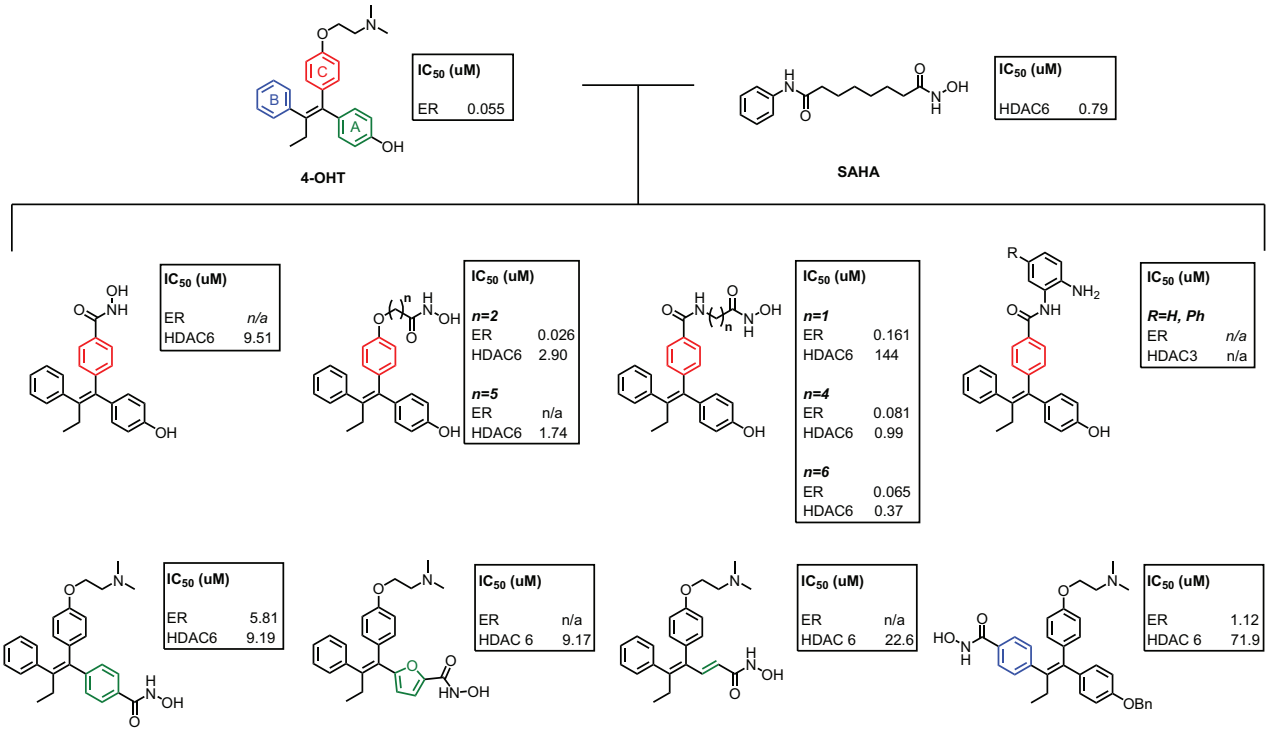

Figure 1.23: Previous work done by Laurie Lim and Benjamin Williams in constructing a hybrid SERM/HDACi library using 4-OHT as a scaffold.[129,130]

This thesis will focus on the expansion of the B-ring substituted analogue chemical space, building on the hybrids that have been constructed and evaluated previously. Prior work shows that poor ER affinity is an issue with the hybrids. However, preservation of the antiestrogenic side chain and phenolic moiety of 4-OHT suggest that the B-ring substituted analogues should exhibit ER antagonism at all concentrations based on the work done by Benjamin Williams. HDAC inhibition has been exhibited by the previous hybrids and improvements on affinity may be achieved by varying the structural characteristics of the linker. The design and molecular docking of a candidate library of analogues using *FITTED*, a molecular docking software program, will be discussed and an improvement on the synthesis of these analogues will be presented. Finally, the biological evaluation of the synthesized hybrids in binding to the ER, determined by BRET assays conducted in collaboration with the Sylvie Mader lab at the Université de Montréal, and HDAC 3 and 6 activity, determined by fluorogenic assays performed in the Gleason lab, will be presented and discussed.

References

1. *Canadian Cancer Society's Advisory Committee on Cancer Statistics. Canadian Cancer Statistics.* **2015**, Toronto, ON: Canadian Cancer Society.
2. Ali, S.; Coombes, R. C. *Nat. Rev. Cancer* **2002**, *2*, 101–112.
3. MacGregor, J.; Jordan, V. *Pharmacol. Rev.* **1998**, *50*, 151–196.
4. Burstein, H. J.; Temin, S.; Anderson, H.; Buchholz, T. A.; Davidson, N. E.; Gelmon, K. E.; Giordano, S. H.; Hudis, C. A.; Rowden, D.; Solky, A. J.; Stearns, V.; Winer, E. P.; Griggs, J. J. *J. Clin. Oncol.* **2014**, *32*, 2255–2269.
5. Wood, A. J.; Osborne, C. K. *N. Engl. J. Med.* **1998**, *339*, 1609–1618.
6. Lavie, O.; Barnett-Griness, O.; Narod, S.; Rennert, G. *Int. J. Gynecol. Cancer* **2008**, *18*, 352–356.
7. Beatson, G. *The Lancet* **1896**, *148*, 162–165.
8. Lathrop, A. E. C.; Loeb, L. *J. Canc. Res.* **1916**, *1*, 1–19.
9. Allen, E.; Doisy, E. A. *JAMA* **1923**, *81*, 819.
10. Toft, D.; Shyamala, G.; Gorski, J. *Proc. Natl. Acad. Sci. U.S.A.* **1967**, *57*, 1740–1743.
11. Gorski, J.; Toft, D.; Shyamala, G.; Smith, D.; Notides, A. *Recent Prog. Horm. Res.* **1968**, *24*, 45–80.
12. Green, S.; Walter, P.; Kumar, V.; Krust, A.; Bornert, J.-M.; Argos, P.; Chambon, P. *Nature* **1986**, *320*, 134–139.
13. Kuiper, G.; Enmark, E.; Pelto-Huikko, M.; Nilsson, S.; Gustafsson, J. *Proc. Natl. Acad. Sci. U.S.A.* **1996**, *93*, 5925–5930.
14. Hall, J.; McDonnell, D. *Endocrinology* **1999**, *140*, 5566–5578.
15. Koehler, K. F.; Helguero, L. A.; Haldosén, L.-A.; Warner, M.; Gustafsson, J.-Å. *Endocrine Reviews* **2005**, *26*, 465–478.
16. Arpino, G.; Wiechmann, L.; Osborne, C. K.; Schiff, R. *Endocr. Rev.* **2008**, *29*, 217–233.
17. Kumar, V.; Green, S.; Stack, G.; Berry, M.; Jin, J.-R.; Chambon, P. *Cell* **1987**, *51*, 941–951.
18. Thomas, C.; Gustafsson, J. *Nat. Rev. Cancer* **2011**, *11*, 597–608.
19. Brzozowski, A.; Pike, A.; Dauter, Z.; Hubbard, R.; Bonn, T.; Engstrom, O.; Ohman, L.; Greene, G.; Gustafsson, J.; Carlquist, M. *Nature* **1997**, *389*, 753–758.
20. Frasor, J.; Stossi, F.; Danes, J. M.; Komm, B.; Lyttle, C. R.; Katzenellenbogen, B. S. *Cancer Res.* **2004**, *64*, 1522–1533.
21. Dorling, A. A.; Todman, M. G.; Korach, K. S.; Herbison, A. E. *Neuroendocrinology* **2003**, *78*, 204–209.
22. Parini, P.; Angelin, B.; Rudling, M. *Arterioscler. Thromb. Vasc. Biol.* **1997**, *17*, 1800–1805.
23. Riggs, B. L. *J. Clin. Invest.* **2000**, *106*, 1203–1204.
24. Bai, Z.; Gust, R. *Arch. Pharm. (Weinheim)* **2009**, *342*, 133–149.
25. Klinge, C.; Brolly, C.; Bambara, R.; Hilf, R. *J. Steroid Biochem. Mol. Biol.* **1997**, *63*, 283–301.
26. Ylikomi, T.; Wurtz, J.-M.; Syvälä, H.; Passinen, S.; Pekki, A.; Haverinen, M.; Bläuer, M.; Tuohimaa, P.; Gronemeyer, H. *Crit. Rev. Biochem. Mol. Biol.* **1998**, *33*, 437–466.

27. Pratt, W.; Toft, D. *Endocr. Rev.* **1997**, *18*, 306–360.
28. Mak, H. Y.; Hoare, S.; Henttu, P. M. A.; Parker, M. G. *Mol. Cell. Biol.* **1999**, *19*, 3895–3903.
29. Klinge, C. M. *Nucleic Acids Res.* **2001**, *29*, 2905–2919.
30. Chen, D.; Pace, P.; Coombes, R.; Ali, S. *Mol. Cell. Biol.* **1999**, *19*, 1002–1015.
31. Kalkhoven, E.; Valentine, J.; Heery, D.; Parker, M. *EMBO J.* **1998**, *17*, 232–243.
32. Voegel, J. J. *The EMBO Journal* **1998**, *17*, 507–519.
33. Kushner, P.; Agard, D.; Greene, G.; Scanlan, T.; Shiau, A.; Uht, R.; Webb, P. *J. Steroid Biochem. Mol. Biol.* **2000**, *74*, 311–317.
34. Klinge, C. *Steroids* **2000**, *65*, 227–251.
35. Klinge, C.; Jernigan, S.; Mattingly, K.; Risinger, K.; Zhang, J. *J. Mol. Endocrinol.* **2004**, *33*, 387–410.
36. Schiff, R.; Massarweh, S.; Shou, J.; Osborne, C. K. *Clin. Cancer Res.* **2003**, *9*, 447S–454S.
37. Schiff, R. *Clin. Cancer Res.* **2004**, *10*, 331S–336.
38. Wu, R.-C.; Smith, C. L.; O'Malley, B. W. *Endocr. Rev.* **2005**, *26*, 393–399.
39. Simpson, E. *J. Steroid Biochem. Mol. Biol.* **2003**, *86*, 225–230.
40. Anstead, G. M.; Carlson, K. E.; Katzenellenbogen, J. A. *Steroids* **1997**, *62*, 268–303.
41. Renaud, J.-P.; Rochel, N.; Ruff, M.; Vivat, V.; Chambon, P.; Gronemeyer, H.; Moras, D. *Nature* **1995**, *378*, 681–689.
42. Bourguet, W.; Ruff, M.; Chambon, P.; Gronemeyer, H.; Moras, D. *Nature* **1995**, *375*, 377–382.
43. Wagner, R. L.; Apriletti, J. W.; McGrath, M. E.; West, B. L.; Baxter, J. D.; Fletterick, R. J. *Nature* **1995**, *378*, 690–697.
44. Feng, W. *Science* **1998**, *280*, 1747–1749.
45. Shiau, A. K.; Barstad, D.; Loria, P. M.; Cheng, L.; Kushner, P. J.; Agard, D. A.; Greene, G. L. *Cell* **1998**, *95*, 927–937.
46. *Subcommittee on Breast and Genital Cancer. JAMA* **1960**, *172*, 1271.
47. *JAMA* **1976**, *236*, 1107–1109.
48. Dieckmann, W.; Davis, M.; Rynkiewicz, L.; Pottinger, R. *Am. J. Obstet. Gynecol.* **1953**, *66*, 1062–1081.
49. Herbst, A.; Ulfelder, H.; Poskanzer, D. *N. Engl. J. Med.* **1971**, *284*, 878–881.
50. Hoover, R. N. *et al. N. Engl. J. Med.* **2011**, *365*, 1304–1314.
51. Cole, M.; Jones, C.; Todd, I. *Br. J. Cancer* **1971**, *25*, 270–275.
52. Jordan, V. C.; Prestwich, G. *J. Endocrinol.* **1978**, *76*, 363–364.
53. Jordan, V.; Robinson, S. *Fed. Proc.* **1987**, *46*, 1870–1874.
54. Gottardis, M.; Robinson, S.; Satyaswaroop, P.; Jordan, V. *Cancer Res.* **1988**, *48*, 812–815.
55. Jordan, V. C. *J. Med. Chem.* **2003**, *46*, 883–908.
56. Borgna, J.; Rochefort, H. *J. Biol. Chem.* **1981**, *256*, 859–868.
57. Desta, Z. *J. Pharmacol. Exp. Ther.* **2004**, *310*, 1062–1075.
58. Ward, H. *Br. Med. J.* **1973**, *1*, 13–14.
59. Ingle, J.; Ahmann, D.; Green, S.; Edmonson, J.; Bisel, H.; Kvols, L.; Nichols, W.; Creagan, E.; Hahn, R.; Rubin, J.; Frytak, S. *N. Engl. J. Med.* **1981**, *304*, 16–21.

60. Stewart, H.; Prescott, R.; Forrest, A. *J. Natl. Cancer Inst.* **2001**, *93*, 456–462.
61. Jordan, V.; Phelps, E.; Lindgren, J. *Breast Cancer Res. Treat.* **1987**, *10*, 31–35.
62. Heaney, R.; Draper, M. *J. Clin. Endocrinol. Metab.* **1997**, *82*, 3425–3429.
63. Cosman, F.; Lindsay, R. *Endocr. Rev.* **1999**, *20*, 418–434.
64. Balfour, J. A.; Goa, K. L. *Drugs & Aging* **1998**, *12*, 335–341.
65. Vogel, V. G. *JAMA* **2006**, *295*, 2727.
66. Vogel, V. G. *et al. Cancer Prev. Res. (Phila)* **2010**, *3*, 696–706.
67. Levenson, A. S.; Wolf, D. M.; Catherino, W. H.; Takei, H.; Jordan, V. C. *Breast Cancer* **1998**, *5*, 99–106.
68. Shao, W.; Brown, M. *Breast Cancer Res.* **2004**, *6*, 39.
69. Bowler, J.; Lilley, T. J.; Pittam, J. D.; Wakeling, A. E. *Steroids* **1989**, *54*, 71–99.
70. Wakeling, A.; Dukes, M.; Bowler, J. *Cancer Res.* **1991**, *51*, 3867–3873.
71. Robertson, J. F.; Cheung, K. L. *Expert Opin. Invest. Drugs* **2002**, *11*, 303–308.
72. Dauvois, S.; Danielian, P.; White, R.; Parker, M. *Proc. Natl. Acad. Sci. U.S.A.* **1992**, *89*, 4037–4041.
73. Long, X.; Nephew, K. P. *J. Biol. Chem.* **2006**, *281*, 9607–9615.
74. Wijayaratne, A.; McDonnell, D. *J. Biol. Chem.* **2001**, *276*, 35684–35692.
75. Hilmi, K.; Hussein, N.; Mendoza-Sanchez, R.; El-Ezzy, M.; Ismail, H.; Durette, C.; Bail, M.; Rozendaal, M. J.; Bouvier, M.; Thibault, P.; Gleason, J. L.; Mader, S. *Mol. Cell. Biol.* **2012**, *32*, 3823–3837.
76. Pike, A.; Brzozowski, A.; Walton, J.; Hubbard, R.; Thorsell, A.; Li, Y.; Gustafsson, J.; Carlquist, M. *Structure* **2001**, *9*, 145–153.
77. Howell, A.; Robertson, J. F. R.; Quaresma Albano, J.; Aschermannova, A.; Mauriac, L.; Kleeberg, U.; Vergote, I.; Erikstein, B.; Webster, A.; Morris, C. *J. Clin. Oncol.* **2002**, *20*, 3396–3403.
78. Osborne, C. K.; Schiff, R. *Annu. Rev. Med.* **2011**, *62*, 233–247.
79. van de Vijver, M. J. *et al. N. Engl. J. Med.* **2002**, *347*, 1999–2009.
80. Paik, S.; Shak, S.; Tang, G.; Kim, C.; Baker, J.; Cronin, M.; Baehner, F. L.; Walker, M. G.; Watson, D.; Park, T.; Hiller, W.; Fisher, E. R.; Wickerham, D. L.; Bryant, J.; Wolmark, N. *N. Engl. J. Med.* **2004**, *351*, 2817–2826.
81. Kuukasjarvi, T.; Kononen, J.; Helin, H.; Holli, K.; Isola, J. *J. Clin. Oncol.* **1996**, *14*, 2584–2589.
82. Howell, A.; DeFriend, D.; Robertson, J.; Blamey, R.; Anderson, L.; Anderson, E.; Sutcliffe, F.; Walton, P. *Br. J. Cancer* **1996**, *74*, 300–308.
83. Zhang, Q.; Borg, A.; Wolf, D.; Oesterreich, S.; Fuqua, S. *Cancer Res.* **1997**, *57*, 1244–1249.
84. Fuqua, S.; Wiltschke, C.; Zhang, Q.; Borg, A.; Castles, C.; Friedrichs, W.; Hopp, T.; Hilsenbeck, S.; Mohsin, S.; O'Connell, P.; Allred, D. *Cancer Res.* **2000**, *60*, 4026–4029.
85. Wang, C.; Fu, M.; Angeletti, R.; Siconolfi-Baez, L.; Reutens, A.; Albanese, C.; Lisanti, M.; Katzenellenbogen, B.; Kato, S.; Hopp, T.; Fuqua, S.; Lopez, G.; Kushner, P.; Pestell, R. *J. Biol. Chem.* **2001**, *276*, 18375–18383.
86. Osborne, C. K.; Bardou, V.; Hopp, T. A.; Chamness, G. C.; Hilsenbeck, S. G.; Fuqua, S. A. W.; Wong, J.; Allred, D. C.; Clark, G. M.; Schiff, R. *J. Natl. Cancer Inst.* **2003**, *95*, 353–361.

87. Shou, J.; Massarweh, S.; Osborne, C. K.; Wakeling, A. E.; Ali, S.; Weiss, H.; Schiff, R. *J. Natl. Cancer Inst.* **2004**, *96*, 926–935.
88. Osborne, C. K.; Neven, P.; Dirix, L. Y.; Mackey, J. R.; Robert, J.; Underhill, C.; Schiff, R.; Gutierrez, C.; Migliaccio, I.; Anagnostou, V. K.; Rimm, D. L.; Magill, P.; Sellers, M. *Clin. Cancer Res.* **2011**, *17*, 1147–1159.
89. Knowlden, J. M.; Hutcheson, I. R.; Jones, H. E.; Madden, T.; Gee, J. M. W.; Harper, M. E.; Barrow, D.; Wakeling, A. E.; Nicholson, R. I. *Endocrinology* **2003**, *144*, 1032–1044.
90. Johnston, S. *et al. J. Clin. Oncol.* **2009**, *27*, 5538–5546.
91. Ottaviano, Y.; Issa, J.; Parl, F.; Smith, H.; Baylin, S.; Davidson, N. *Cancer Res.* **1994**, *54*, 2552–2555.
92. Yang, X.; Phillips, D.; Ferguson, A.; Nelson, W.; Herman, J.; Davidson, N. *Cancer Res.* **2001**, *61*, 7025–7029.
93. Sharma, D.; Saxena, N. K.; Davidson, N. E.; Vertino, P. M. *Cancer Res.* **2006**, *66*, 6370–6378.
94. Jang, E. R.; Lim, S.-J.; Lee, E. S.; Jeong, G.; Kim, T.-Y.; Bang, Y.-J.; Lee, J.-S. *Oncogene* **2004**, *23*, 1724–1736.
95. Finnin, M.; Donigian, J.; Cohen, A.; Richon, V.; Rifkind, R.; Marks, P.; Breslow, R.; Pavletich, N. *Nature* **1999**, *401*, 188–193.
96. Lee, K. K.; Workman, J. L. *Nat. Rev. Mol. Cell Biol.* **2007**, *8*, 284–295.
97. Bantscheff, M. *et al. Nat. Biotechnol.* **2011**, *29*, 255–265.
98. Schwer, B.; Verdin, E. *Cell Metab.* **2008**, *7*, 104–112.
99. Haberland, M.; Montgomery, R. L.; Olson, E. N. *Nat. Rev. Genet.* **2009**, *10*, 32–42.
100. Yang, X.-J.; Seto, E. *Nat. Rev. Mol. Cell Biol.* **2008**, *9*, 206–218.
101. Yang, X.-J.; Seto, E. *Curr. Opin. Genet. Dev.* **2003**, *13*, 143–153.
102. Yang, X.-J.; Gregoire, S. *Mol. Cell. Biol.* **2005**, *25*, 2873–2884.
103. Gregoretti, I. V.; Lee, Y.-M.; Goodson, H. V. *J. Mol. Biol.* **2004**, *338*, 17–31.
104. Yoshida, M.; Horinouchi, S.; Beppu, T. *Bioessays* **1995**, *17*, 423–430.
105. Cousens, L.; Gallwitz, D.; Alberts, B. *J. Biol. Chem.* **1979**, *254*, 1716–1723.
106. Drummond, D. C.; Noble, C. O.; Kirpotin, D. B.; Guo, Z.; Scott, G. K.; Benz, C. C. *Annu. Rev. Pharmacol. Toxicol.* **2005**, *45*, 495–528.
107. Madsen, A. S.; Kristensen, H. M. E.; Lanz, G.; Olsen, C. A. *Chemmedchem* **2014**, *9*, 614–626.
108. Miller, T. A.; Witter, D. J.; Belvedere, S. *J. Med. Chem.* **2003**, *46*, 5097–5116.
109. Falkenberg, K. J.; Johnstone, R. W. *Nat. Rev. Drug Discov.* **2014**, *13*, 673–691.
110. Zhang, Z.; Yamashita, H.; Toyama, T.; Sugiura, H.; Ando, Y.; Mita, K.; Hamaguchi, M.; Hara, Y.; Kobayashi, S.; Iwase, H. *Breast Cancer Res. Treat.* **2005**, *94*, 11–16.
111. Krusche, C. A.; Wulfing, P.; Kersting, C.; Vloet, A.; Bocker, W.; Kiesel, L.; Beier, H. M.; Alfer, J. *Breast Cancer Res. Treat.* **2005**, *90*, 15–23.
112. Kawai, H.; Li, H.; Avraham, S.; Jiang, S.; Avraham, H. K. *Int. J. Cancer* **2003**, *107*, 353–358.
113. Luo, J.; Su, F.; Chen, D.; Shiloh, A.; Gu, W. *Nature* **2000**, *408*, 377–381.
114. Harms, K. L.; Chen, X. *Cancer Res.* **2007**, *67*, 3145–3152.
115. Duvic, M.; Talpur, R.; Ni, X.; Zhang, C.; Hazarika, P.; Kelly, C.; Chiao, J. H.;

Reilly, J. F.; Ricker, J. L.; Richon, V. M.; Frankel, S. R. *Blood* **2007**, *109*, 31–39.
116. VanderMolen, K. M.; McCulloch, W.; Pearce, C. J.; Oberlies, N. H. *J. Antibiot. (Tokyo)* **2011**, *64*, 525–531.
117. Munster, P.; Troso-Sandoval, T.; Rosen, N.; Rifkind, R.; Marks, P.; Richon, V. *Cancer Res.* **2001**, *61*, 8492–8497.
118. Hodges-Gallagher, L.; Valentine, C. D.; Bader, S. E.; Kushner, P. J. *Breast Cancer Res. Treat.* **2007**, *105*, 297–309.
119. Thomas, S.; Thurn, K. T.; Bicaku, E.; Marchion, D. C.; Munster, P. N. *Breast Cancer Res. Treat.* **2011**, *130*, 437–447.
120. Munster, P.; Thurn, K.; Thomas, S.; Raha, P.; Lacevic, M.; Miller, A.; Melisko, M.; Ismail-Khan, R.; Rugo, H.; Moasser, M.; Minton, S. *Br. J. Cancer* **2011**, *104*, 1828–1835.
121. Bicaku, E.; Marchion, D. C.; Schmitt, M. L.; Munster, P. N. *Cancer Res.* **2008**, *68*, 1513–1519.
122. Meunier, B. *Acc. Chem. Res.* **2008**, *41*, 69–77.
123. Tavera-Mendoza, L. E.; Quach, T. D.; Dabbas, B.; Hudon, J.; Liao, X.; Palijan, A.; Gleason, J. L.; White, J. H. *Proc. Natl. Acad. Sci. U.S.A.* **2008**, *105*, 8250–8255.
124. Lamblin, M.; Dabbas, B.; Spingarn, R.; Mendoza-Sanchez, R.; Wang, T.-T.; An, B.-S.; Huang, D. C.; Kremer, R.; White, J. H.; Gleason, J. L. *Bioorg. Med. Chem.* **2010**, *18*, 4119–4137.
125. Patel, H. K.; Siklos, M. I.; Abdelkarim, H.; Mendonca, E. L.; Vaidya, A.; Petukhov, P. A.; Thatcher, G. R. J. *ChemMedChem* **2014**, *9*, 602–613.
126. Dao, K.-L.; Hanson, R. N. *Bioconjug. Chem.* **2012**, *23*, 2139–2158.
127. Zhou, H.-B.; Comninos, J. S.; Stossi, F.; Katzenellenbogen, B. S.; Katzenellenbogen, J. A. *J. Med. Chem.* **2005**, *48*, 7261–7274.
128. Tang, C.; Li, C.; Zhang, S.; Hu, Z.; Wu, J.; Dong, C.; Huang, J.; Zhou, H.-B. *J. Med. Chem.* **2015**, *58*, 4550–4572.
129. Lim, L. Effects Towards the Design and Synthesis of Small Molecule Inhibitors of the Estrogen Receptor. M.Sc. thesis, McGill University, 2011.
130. Williams, B. Design, synthesis and evaluation of selective estrogen receptor modulator/histone deacetylase inhibitor merged bifunctional ligands. M.Sc. thesis, McGill University, 2014.

Chapter 2: Design and Synthesis of SERM/HDACi Hybrids

2.1 Design of SERM/HDACi Hybrids

The incorporation of a dual purpose antiestrogenic/HDACi side-chain onto an E2 scaffold was conducted successfully within the Gleason group by Rodrigo Mendoza-Sanchez in an investigation of hybrid full antiestrogen/HDACis.[1] The E2-based hybrid RMS-575 (**1**) was strongly antiestrogenic and had an IC_{50} of 0.11 µM in luciferase transactivation assays. The hybrid was also strongly antiproliferative in MCF-7 cells (IC_{50} of 0.34 µM) in the presence of E2, and showed an antiproliferative effect on a resistant MDA-MB-231 cancer cell line at 4 µM (Figure 2.1). However, the hybrid showed only a modest affinity for HDAC 6 with an IC_{50} of 44 µM due to the *N*-butyl hydroxamate zinc-binding group. The deliberate inclusion of the *N*-butyl hydroxamate was to improve ER affinity, as the study hypothesized that the polar hydroxamic acids showed an aversion to the coactivator binding pocket on the surface of the receptor that the full antiestrogen side chains tend to occupy.[1] Despite the modest HDAC affinity, the promising ER affinity and antiproliferative characteristics showed that the ER could tolerate antiestrogen/HDACi hybrids.

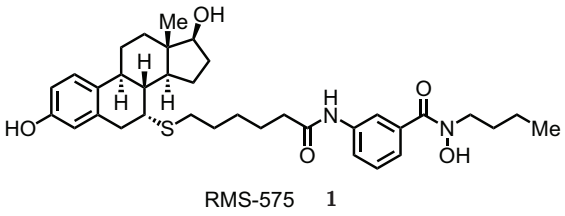

RMS-575 **1**

Affinity IC_{50} (uM)		Antiproliferation IC_{50} (uM)	
HDAC3	1.55	**MCF-7**	0.34
HDAC6	43.7±2.9		
ER (Luc assay)	0.11		

Figure 2.1: Hybrid full antiestrogen/HDACi RMS-575 (**1**) showed ER affinity and antiproliferative effects, but low HDAC affinity due to the N-butyl hydroxamate.

The antiestrogenic activity of SERMs is dependant on a salt-bridge interaction with Asp 351 at the entrance of the binding cavity rather than the coactivator binding pocket. Therefore, a hybrid SERM/HDACi that incorporated a hydroxamic acid may have high affinity for HDAC and retain ER affinity. Based on this notion, the 4-OHT based C-ring substituted analogues were first examined by Laurie Lim and Benjamin Williams (Figure 2.2).[2,3] The most notable hybrid from the C-ring series was BMW-79b, which exhibited antiestrogenic

character at low concentrations and a high affinity for ER with an IC_{50} of 26 nM. However, the hybrid showed estrogenic activity at higher concentrations in BRET assays, likely due to the inability of the side chain to fully mimic the antiestrogenic *N,N*-dimethylaminoethylene side chain of 4-OHT. Importantly, the hybrid had an order of magnitude higher affinity for HDAC 6 than RMS-575 , with an IC_{50} of 2.90 µM.[3] As was mention in Chapter 1, the A-ring analogues were largely unsuccessful due to the lack of a phenol moiety that is known to engage in a hydrogen bonding network within the ER binding pocket. However, BMW-155 did have a modest affinity for the ER (IC_{50} of 5.81 µM) which suggested that the pocket is capable of accommodating the HDACi side chains. The single B-ring analogue BMW-275 showed good affinity for the ER with an IC_{50} of 1.12 µM and remained antagonistic at all concentrations. Unsurprisingly, the short hydroxamic acid side chain gave only modest HDAC 6 affinity, with an IC_{50} of 71.9 µM.

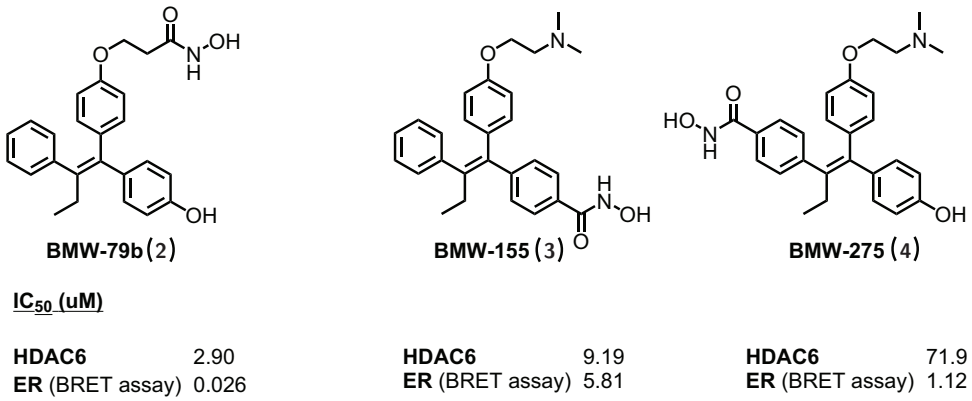

Figure 2.2: C-, A-, and B- ring substituted hybrid SERM/HDACis BMW-79b (**2**), BMW-155 (**2**), and BMW-275 (**2**), respectively.

Further exploration of the B-ring chemical space of the 4-OHT based SERM/HDACi hybrids to improve ER and HDAC affinity would then be the primary focus of this thesis. Based on the previous work, the success of the B-ring analogues is likely due to the persistence of the key phenol and *N,N*-dimethylaminoethylene functionalities found in 4-OHT. We predict that maintaining these units while introducing a more SAHA-like HDACi side chain will increase HDAC affinity and provide a hybrid that shows a favourable antiproliferative profile. The goals of this thesis are to *i)* design a series of B-ring substituted SERM/HDACi

hybrids based on a 4-OHT scaffold that maintain the key structural elements of 4-OHT; *ii)* synthesize the hybrids stereoselectively as the Z-isomer of 4-OHT is known to be biologically active while the E-isomer is not; and *iii)* to evaluate the ER and HDAC affinity for each of the synthesized hybrids and contribute to the SAR developed by the previous projects regarding hybrid antiestrogens/HDACis.

The main concerns of using a modified 4-OHT were whether the ER binding cavity would tolerate the structures due to the added bulk that would be introduced with the HDACi side chains. The binding cavity was shown to be relatively large at 450 $Å^3$, which is twice the volume of E2 (245 $Å^3$), and this observation has been used to explain the ability of the ER to accommodate a wide variety of aromatic and hydrophobic groups.[4,5] Nonetheless, we required more compelling evidence in order to justify the synthesis, characterization, and evaluation of a series of hybrid candidates. A preliminary evaluation of potential hybrids using computational docking methods would provide the support required to make an informed decision in this matter. *In silico* binding techniques using molecular docking programs have been used extensively in medicinal chemistry and have led to the discovery of several inhibitors across many classes of drugs.

The Moitessier group developed the molecular docking software platform *FITTED* (Flexibility Induced Through Targeted Evolutionary Description), which has played a pivotal role in several medicinal chemistry projects, including extensive work done on the development of prolyl oligopeptidase inhibitors.[6–9] *FITTED* outputs a score based on a Lamarckian genetic algorithm that optimizes the binding poses of ligands and subsequently ranks each molecule within a set on a force-field scoring function.[10] Previous work using *FITTED* to assess the binding of full antiestrogens to the ER was carried out by Rodrigo Mendoza-Sanchez in the Gleason lab. The project investigated the validity of the results *FITTED* provided with to docking known ligands to the ER using self-docking and cross-docking experiments with 12 different SERM and protein cocrystallization files. The study concluded that *FITTED* provided accurate and meaningful docking results in the context of the ER, with an accuracy rate of 67% when self-docking and cross-docking.[1]

2.1.1 Docking of Carbon-Linked Hybrids

A virtual library of hybrid SERM/HDACi was first constructed and prepared for virtual docking (Figure 2.3). The library consisted of carbon-linked B-ring substituted analogues bound to an HDACi side chain through a carbon-carbon bond, 4-OHT as a positive control, and BMW-*o*-benzene as a reference as it was evaluated in Ben Williams' thesis.[3] One subset of the hybrids, preserves the phenyl group found in 4-OHT while a second subset, contains a 2,5-disubstituted thiophenyl ring in place of the phenyl in an attempt to probe the effect of bond angles and ring size. An additional hybrid, AFP-5C-US-ACYC, contains an acyclic, flexible diene linker that extends from the tetrasubstituted olefin core. The hybrids within each subset contain hydrophobic linkers that vary with respect to chain length and degree of unsaturation, although branching was not investigated; all hybrid side chains terminate with a hydroxamic acid.

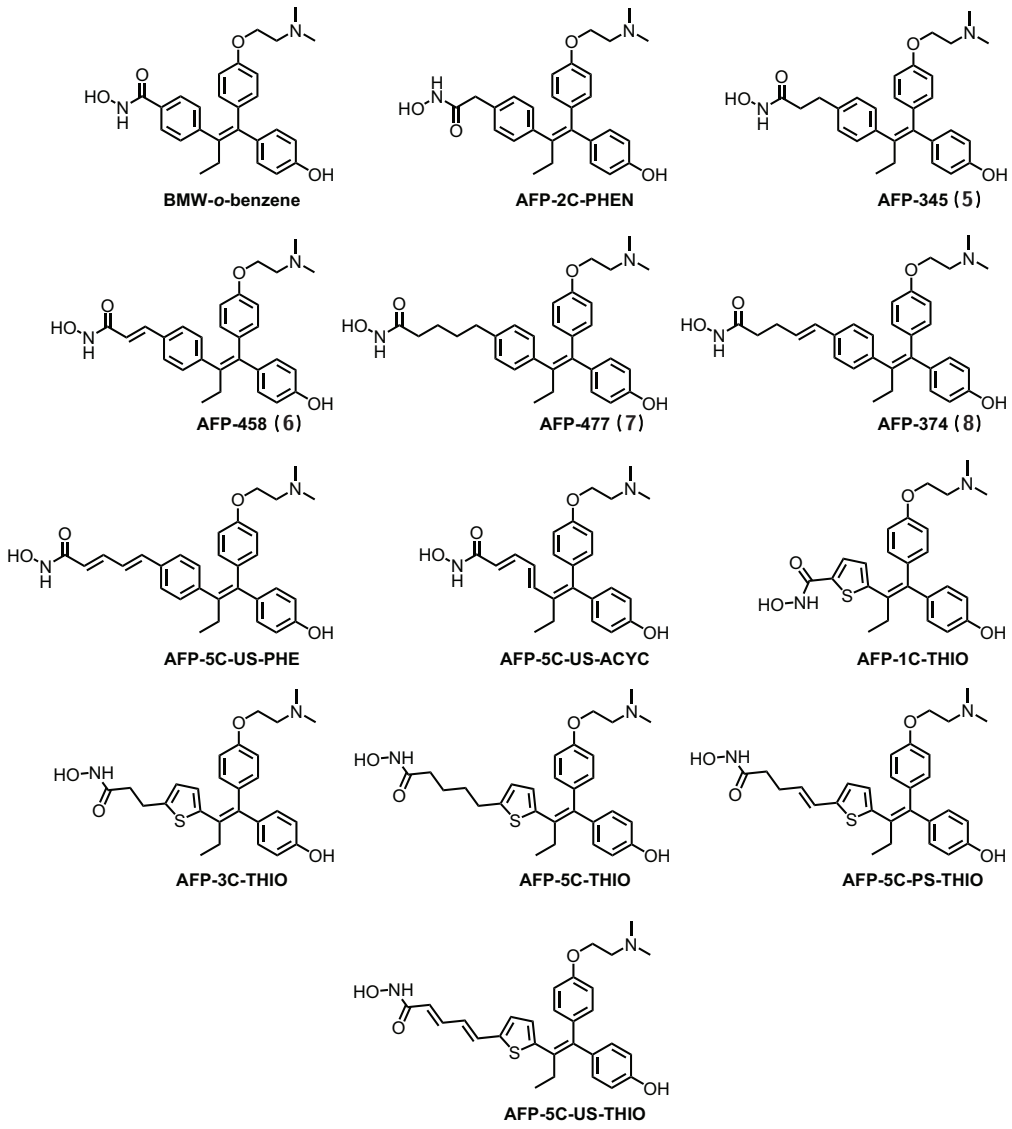

Figure 2.3: Virtual library of 4-OHT based carbon-linked hybrid molecules.

Once uploaded to *FITTED*, the 2D library was automatically converted to a 3D file that was docked and evaluated in conjunction with an appropriate PDB crystal structure file. The PDB file 3ERT, ER bound to 4-OHT was chosen to assess whether the hybrids adopted an antagonistic pose similar to that of 4-OHT within the binding cavity. The results are presented in Figure 2.4 where a more negative score indicates a high affinity ligand-protein interaction. In general, the results suggest that many of the proposed hybrids would adopt a low energy conformation within the ER binding pocket relative to 4-OHT. However, the docked poses would first need to be evaluated to assess the validity of each result. The pose

of AFP-477 suggests that the HDACi side chain would protrude from the binding cavity and form a hydrogen bond with Asp 351, potentially mimicking the antiestrogenic behaviour of the tertiary amine of 4-OHT. Additionally, the phenol is engaged in the classical hydrogen bonding network with Glu 353, Arg 394 and a molecule of water, which is known to confer high ER affinity (Figure 2.5 left). AFP-374 adopted a similar pose to AFP-477, however the lack of flexibility in the side chain prevented it from interacting with Asp 351.

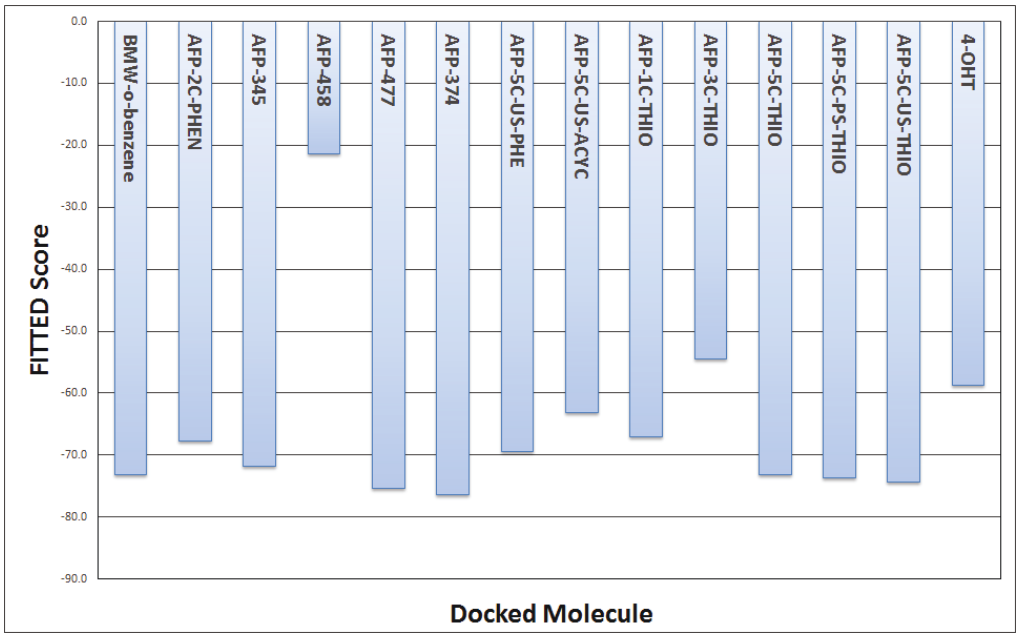

Figure 2.4: *FITTED* scores of carbon-linked hybrids docked to ER (PDB: 3ERT).

The thiophenyl analogues also appeared to have scored well but their docked poses were uncharacteristic of 4-OHT. Thiophenyl hybrids containing five carbon linkers were either docked outside of the binding pocket, forced their hydroxamic acid side chain outside of the pocket while not interacting with Asp 351, or were rotated 90°relative to 4-OHT and satisfied no binding interactions within the pocket. Interestingly, the three carbon linker analogue AFP-5C-THIO scored the poorest of the carbon-linked thiophenyl subset, but possessed a salt bridge interaction between its tertiary amine and Asp 351, a hydrogen bonding interaction with the phenolic moiety and Gly 420 (and likely His 524), as is seen in the binding of raloxifene, and a hydrogen bonding interaction between the hydroxamic acid side and Arg 394. AFP-458 was oriented in a similar manner and satisfied the same bonding

events with the exception of the hydroxamic acid and Arg 394/Glu353 hydrogen bond due to the larger phenyl ring, whereas the thiophenyl ring of AFP-5C-THIO accommodated this interaction (Figure 2.5 right). A lower *FITTED* score suggested that AFP-458 binds more favourably than AFP-5C-THIO despite this difference. The flexible acyclic hybrid AFP-5C-US-ACYC also satisfied each interaction in a similar manner to AFP-5C-THIO and scored relatively well.

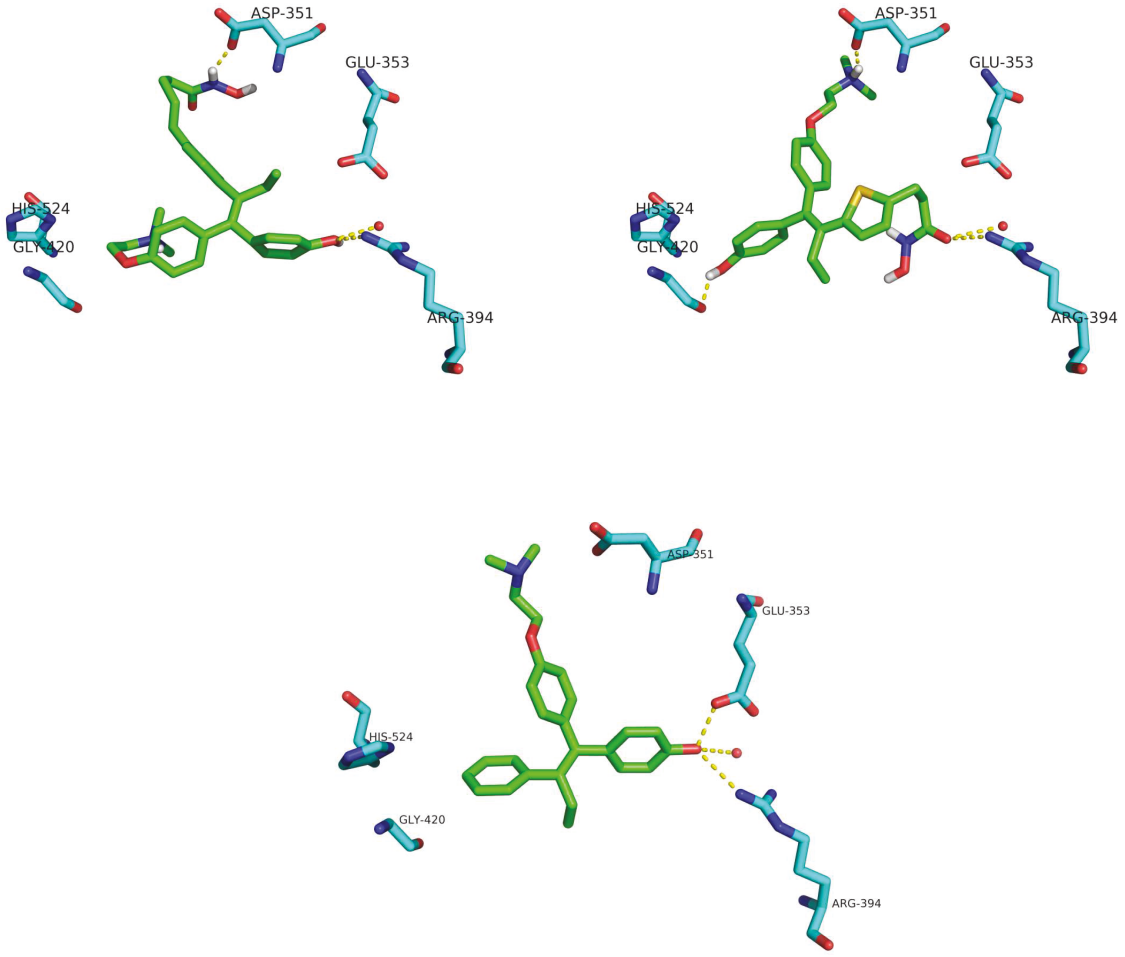

Figure 2.5: Docked poses of hybrids AFP-477 (left), AFP-3C-THIO (right), and 4-OHT (bottom) bound to ER (PDB:3ERT).

2.1.2 Docking of Oxygen-Linked Hybrids

A second hybrid library was constructed and included an oxygen atom rather than carbon to connect the hydroxamic side chain. The inclusion of an additional hydrogen bond acceptor group was thought to invoke an interaction with Arg 394 or, in cases where the hydroxamic acid side chain adopted an antiestrogenic position would be more similar to the *N,N*-dimethylaminoethyl ether side chain found on 4-OHT. Three 4-OHT based hybrid subsets were evaluated, the first had *para*-B-ring substitution of an ether-bridged carbon chain of varying lengths and degrees of unsaturation. The second and third subsets contained 2,5- and 2,4-disubstituted thiophenyl groups, respectively, that connected the ether-bridged side chains. The variation in thiophenyl substitution pattens was introduced to further investigate the effects of bond angles within the binding cavity (Figure 2.7).

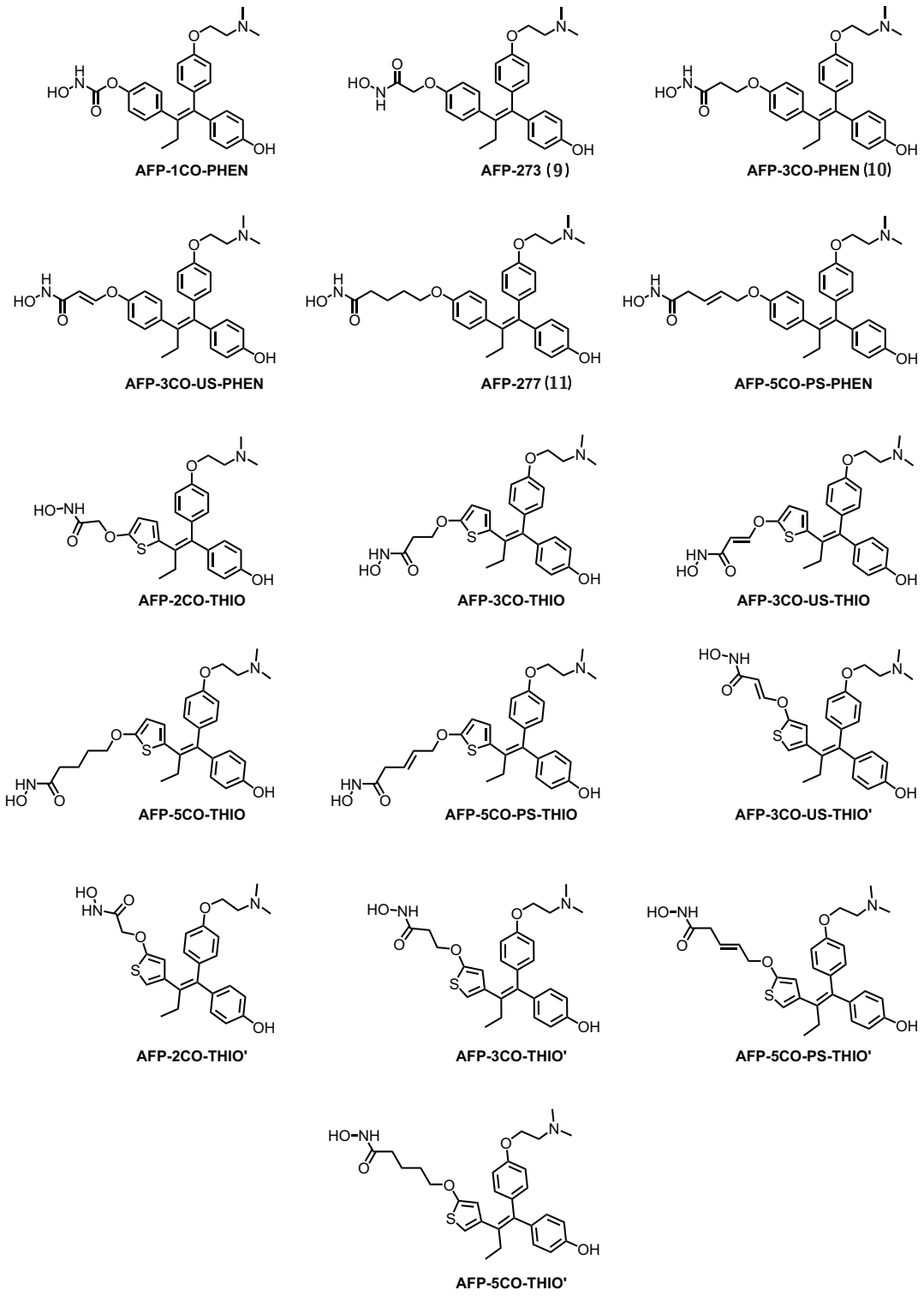

Figure 2.6: Virtual library of 4-OHT based oxygen-linked hybrid molecules.

The *FITTED* results of the oxygen-linked hybrid library indicated that many of the hybrids would have a high affinity for the ER. The thiophenyl analogues AFP-3CO-US-THIO,

-5CO-PS-THIO, and -3CO-THIO' ranked highly however each of their binding poses showed no hydrogen bonding interactions between the hybrids and Glu 353/Arg 394, but rather the space in that region of the cavity houses the hydroxamic acid side chain which is folded on top of the scaffold core. The *N,N*-dimethylaminoethyl side chain and phenol interact with Asp-351 and His 524/Gly 420 in each case, however, it is unlikely the these interactions alone would confer high affinity binding.

The high score of AFP-1CO-PHEN is attributed to the fact that it engages all polar interactions within the binding pocket. Unlike 4-OHT though, the hydroxamic acid side chain invokes hydrogen bonds with Glu 353 and Arg 394 rather than the phenol; in this case the phenol hydrogen bonds to Gly 420/His 524 in a similar manner as raloxifene (Figure 2.8 left).[5] AFP-3CO-PHEN and AFP-2CO-THIO' scored relatively well and invoke all three binding interactions in a pose much like that of AFP-1CO-PHEN. AFP-5CO-PS-PHEN scored well but fails to invoke the Glu353/Arg 394 hydrogen bonding network due to its lack of side chain flexibility, while the saturated analogue AFP-277 engages the hydrogen bonding network with its phenol group and positions its hydroxamic acid side chain outside of the binding pocket much like the *N,N*-dimethylaminoethyl side chain of 4-OHT. Only AFP-273 (**9**) utilized the ether bridge as a hydrogen bond acceptor for Arg 394, while the distal phenol and *N,N*-dimethylaminoethyl side chain interactions remained intact (Figure 2.8 right). In general, both the 2,4- and 2,5-disubstituted thiophenyl analogues bearing five carbon chains, and AFP-3CO-US-THIO', scored poorly due to folding of the side chain within the binding pocket. In contrast, the phenyl variants scored relatively well as a result of the larger ring being positioned at the opening of the cavity which allowed the side chain to extend outward and interact with Asp 351.

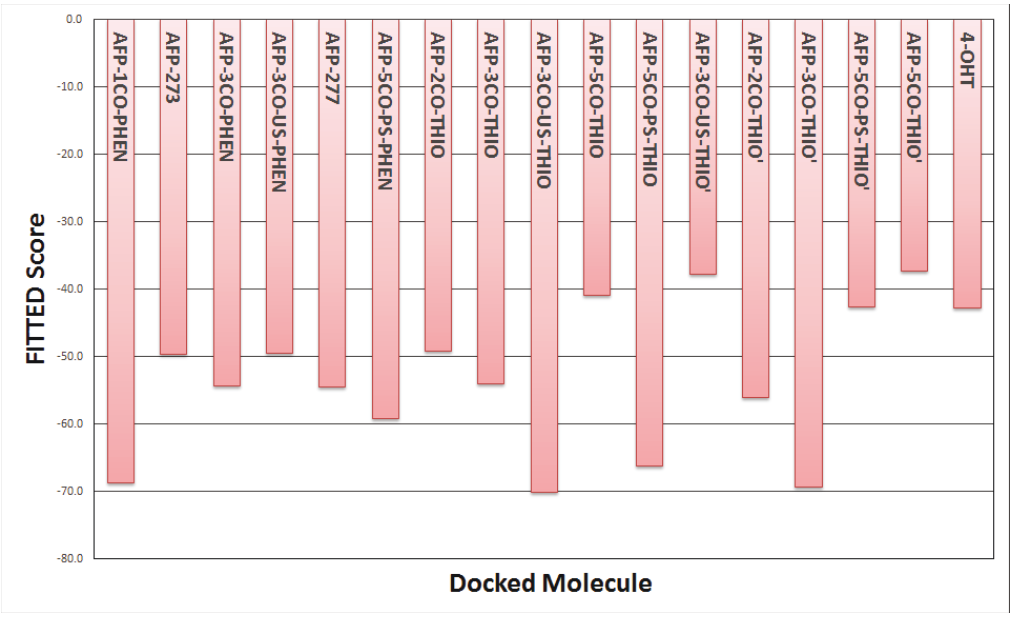

Figure 2.7: *FITTED* scores of oxygen-linked hybrids docked to ER (PDB: 3ERT).

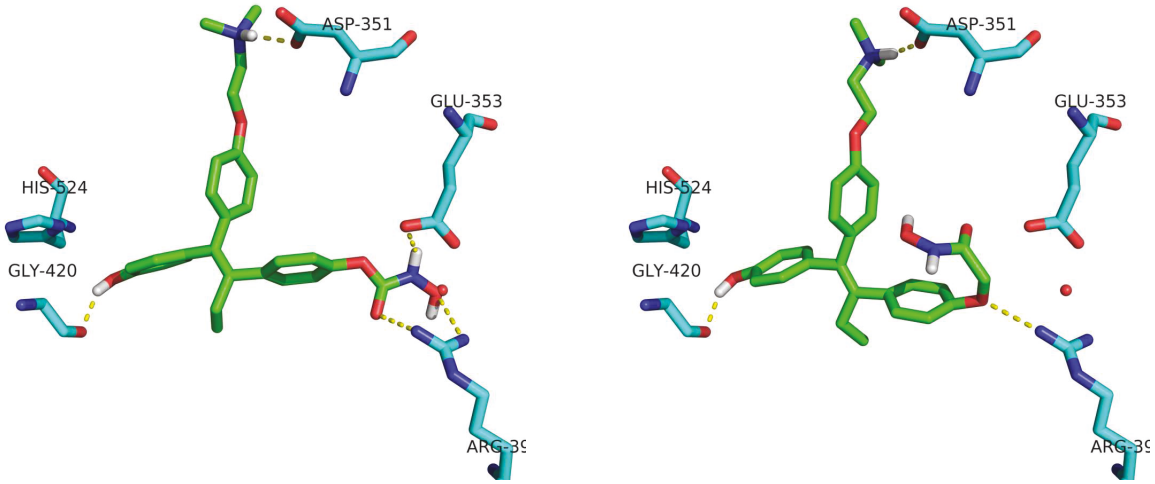

Figure 2.8: Docked poses of hybrids AFP-1CO-PHEN (left) and AFP-273 (**9**) (right) bound to ER (PDB: 3ERT).

While docking is a fast and convenient tool that provides invaluable information that would otherwise take countless hours to acquire, the results were subjected to scrutiny before any conclusions were made. As shown above, many hybrids that scored very well had nonsensical binding poses or poses that contradicted the the known 4-OHT binding mode. As such, the hybrids selected for synthesis were chosen strategically in order to maximize

the potential for discovering a high affinity molecule based on the docking results, and also for their synthetic similarity to other candidates and previously synthesized hybrids in order to maximize the size of the library and streamline synthetic efforts.

The phenyl subsets would take priority due to their structural similarity to hybrids that had been made in previous projects within the Gleason lab since the synthetic strategies would be largely applicable in this case. Within the carbon-linked phenyl subset, hybrids AFP-345 (**5**), -458 (**6**), -477 (**7**), and -374 (**8**) were chosen due to their favourable scores and binding poses, with the exception of AFP-458 which scored poorly but would be easily accessed synthetically due to the similarity to AFP-345 (**5**). Within the oxygen-linked phenyl subset, AFP-273 (**9**), -3CO-PHEN (**10**), and -277 (**11**) were chosen due to their favourable poses and scoring relative to 4-OHT and their structural similarity (Figure 2.9). While AFP-2C-PHEN and -1CO-PHEN both scored very well and exhibited ideal binding poses, its unlikely that the hybrids would bind strongly to HDAC due to their short hydroxamic acid side chains. The ineffectiveness of short-chained hybrids was observed previously by Benjamin Williams.[3] The remainder of this thesis will focus on the synthesis and biological testing of the aforementioned hybrid candidates. Further investigations into the hybrid libraries that have been proposed may be considered in future projects.

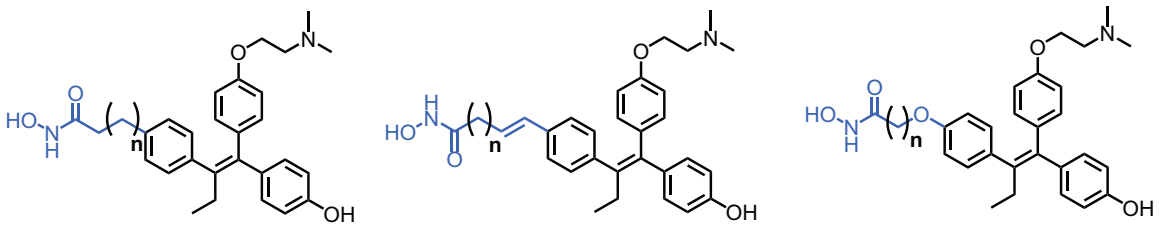

5 AFP-345: n = 1
7 AFP-477: n = 3

6 AFP-458: n = 0
8 AFP-374: n = 2

9 AFP-273: n = 1
10 AFP-3CO-PHEN: n = 3
11 AFP-277: n = 4

Figure 2.9: Synthetic SERM/HDACi targets chosen from docking investigations.

2.2 Synthesis of Hybrid SERM/HDACis

2.2.1 Synthesis of Carbon-Linked B-Ring Substituted Hybrids

A synthetic route to access the first B-ring substituted hybrid, was originally devised by Benjamin Williams and provided the foundation of a first generation synthetic strategy into the hybrid library of this work (Scheme 1).[3] Retrosynthetically, late stage diversification of the library from a common phenol intermediate **12** could be achieved either by direct alkylation or by cross-coupling of the corresponding triflate. Both strategies would accommodate the installation of an aliphatic chain bearing a methyl ester that could be converted into the final hydroxamic acid. Phenol intermediate **12** would be constructed from a McMurry cross-coupling between commercially available 4-hydroxypropiophenone and the appropriately functionalized 4,4'-dihydroxybenzophenone.

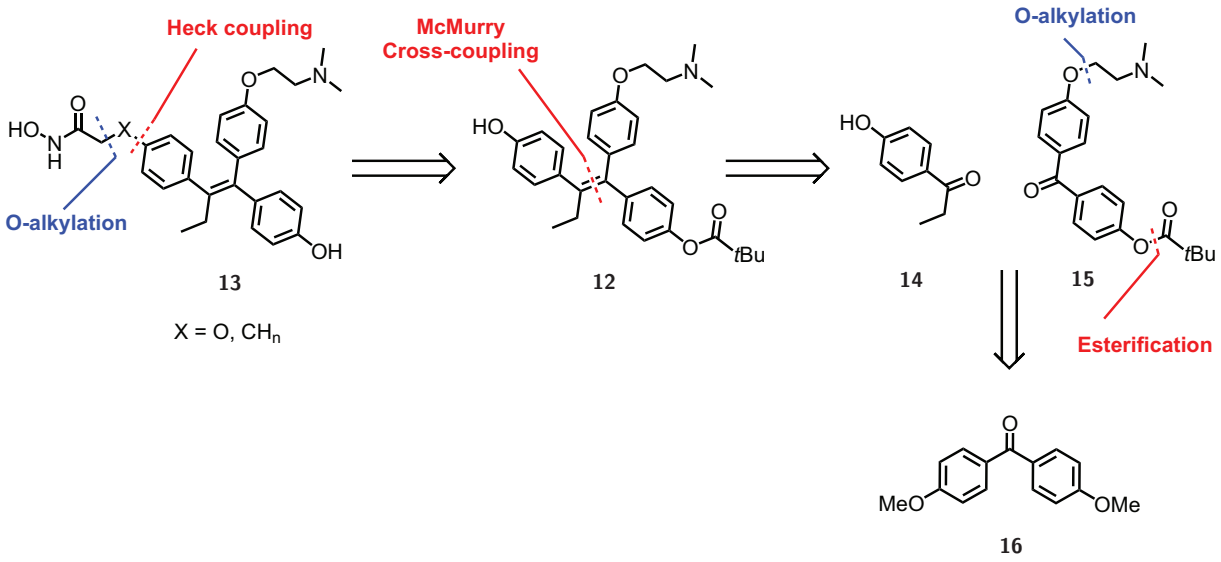

Scheme 1: McMurry cross-coupling strategy to construct the hybrid scaffold **12**.

While the McMurry reaction is typically reserved for homocoupling and intramolecular coupling of ketones or aldehydes, there is precedent for intermolecular cross-coupling specifically in the context of tamoxifen and several of its derivatives.[11,12] Preference for the cross-coupling product over either homocoupled product is suggested to arise from the radical titanium-adduct intermediate derived from benzophenone. The radical species has a

higher reduction potential than that of 4-hydroxypropiophenone and can be further reduced to an anion that can then add to the second ketone in a 1,2 fashion to generate a pinacol type intermediate. The pinacol intermediate is then converted to the tetrasubstituted olefin by elimination of TiO_2 as per the usual McMurry mechanism (Scheme 2).[13] A second argument for cross-coupling considers the steric bulk of the radical benzophenone intermediate in which homocoupling would lead to a highly crowded titanocycle intermediate. The tetrasubstituted olefin within the core of the scaffold also brings *E/Z*-isomer selectivity into consideration, as only the *Z*-isomer of tamoxifen is biologically active.[14] However, others have noted that *E/Z* isomerization tends to be unavoidable within the tamoxifen scaffold, and separation of the isomers is often required.[15–17] Functionalizing 4,4'-dihydroxybenzophenone would require mono-alkylation and a subsequent protection of the remaining phenol.

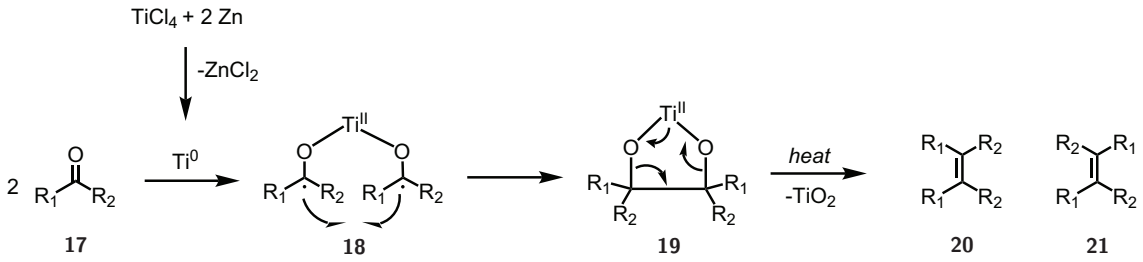

Scheme 2: Classical McMurry homocoupling reaction mechanism with low valent titanium.

The synthesis proceeded in the forward direction beginning with the deprotection of bis ether **16** under standard conditions using BBr_3 to give the free phenol **22** in 90% yield. Although BBr_3 deprotection proceeded smoothly, 3-mercaptopropiophenone (**23**) could also be used as an inexpensive alternative as it yielded similar results. Mono-alkylation of **22** with 2-chloro-*N,N*-dimethylethylamine hydrochloride (**24**) proceeded in poor yield (33%) and severely limited material throughput (Scheme 3). The alkylation was expected to produce a statistical mixture giving **15** in 50% yield based on previous studies.[3,18] Unfortunately, this result could not be reproduced and 33% yield was the highest achieved despite multiple attempts. Pivaloyl ester formation from the phenol then yielded difunctionalized benzophenone **15**.

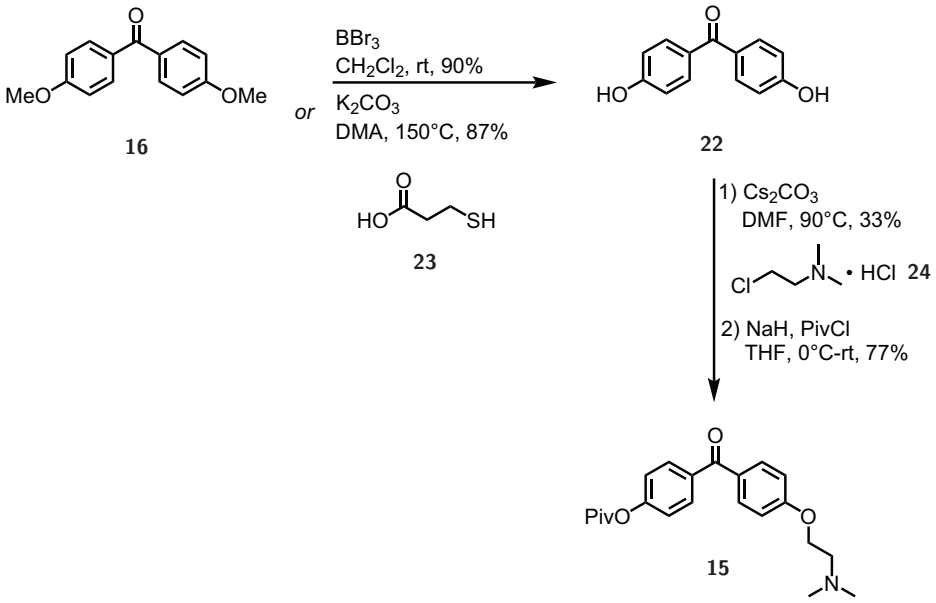

Scheme 3: Synthesis of difunctionalized ketone intermediate **15**.

With the requisite ketone **15** in hand, the McMurry cross-coupling with 4-hydroxypropiophenone proceeded in 29% yield and delivered the phenol intermediate **12** as a mixture of *E/Z* isomers (Scheme 4). The isomeric ratio proved difficult to control and, at best, gave 7:1 *E:Z* mixtures. In addition to low yields and poor isomer selectivity, an unidentified impurity was often generated that proved difficult to remove even after subjecting the product to multiple rounds of flash chromatography. The variation in isomer ratios was due to the generation of HCl in the workup which induced isomerization by protonation of the electron rich olefin, rotation of the transient central σ bond, and subsequent deprotonation. Isomerization of the tetrasubstituted olefins was a persistent problem throughout this project as even mildly acidic conditions would result in 1:1 mixtures of *E:Z* isomers. The preference for *E*- over *Z*-**12** in the McMurry reaction is thought to be the result of a subtle kinetic electronic effect that arises within the forming conjugated system.

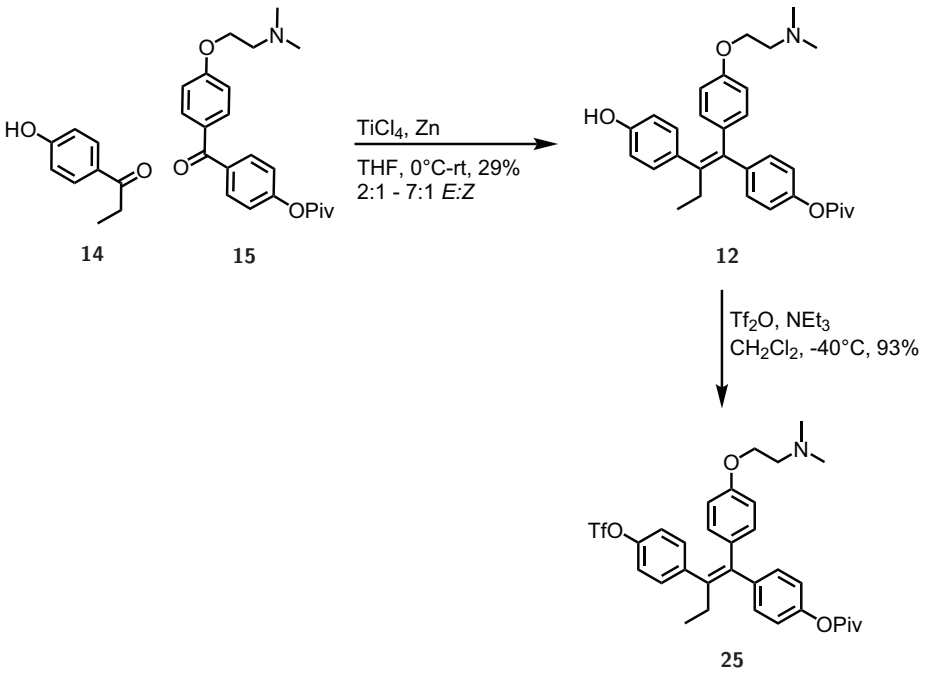

.

Scheme 4: Synthesis of tetrasubstituted olefin scaffold **12** via McMurry cross-coupling followed by triflation to yield **25**

The tetrasubstituted olefin is sterically encumbered to such a degree that at least one phenyl group is likely rotated out of the plane of the central olefin in order to alleviate A-1,2 and A-1,3 strain. The central phenyl group of the *E*-isomer (bearing the *N,N*-dimethylaminoethyl side chain) likely experiences the lowest barrier to rotation, while the remaining two phenyl groups may remain in the plane and conjugated to one another more frequently. If this is the case, the electron donating hydroxyl and inductively withdrawing ester groups would be electronically matched in the *E*-isomer, whereas the *Z*-isomer would possess electronically mismatched electron-donating groups (Figure 2.10).

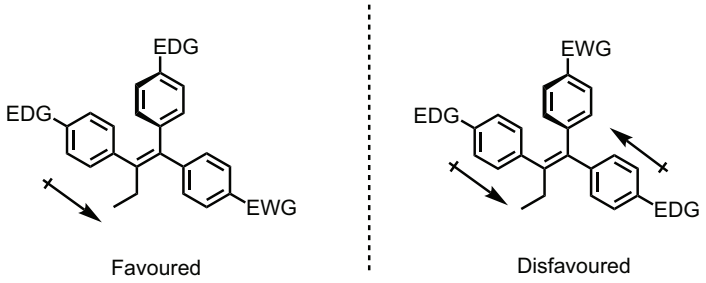

Figure 2.10: Electronic argument to explain McMurry cross-coupling isomer selectivity.

The *E*-isomer preference has been reported in several syntheses of tamoxifen and the phenomenon is known to be functional group dependant. Scriven and Poe reported the McMurry cross-coupling of propiophenone (**26**) and monoalkylated benzophenone (**27**) to yield tamoxifen (**28**) in a 7:1 *Z:E* ratio (Figure 2.11).[12] Gauthier *et al.* reported a reversal of selectivity in the McMurry cross-coupling of mono-alkylated hydroxybenzophenone (**29**) and propiophenone (**26**), and of mono-alkylated hydroxybenzophenone (**29**) and chloropropiophenone (**30**) to yield *E*-isomers as the major products in both cases.[15] The same argument for selectivity can be applied as the ether is slightly less electron donating than phenol and would match more favourably with the electron donating phenyl group than would the phenol with respect to electronics. This basis for stereoselectivity is speculative and no formal investigation has been conducted, but the effects of opposing and cooperative electron donating and accepting groups in such systems would be an interesting concept to explore in an independent study.

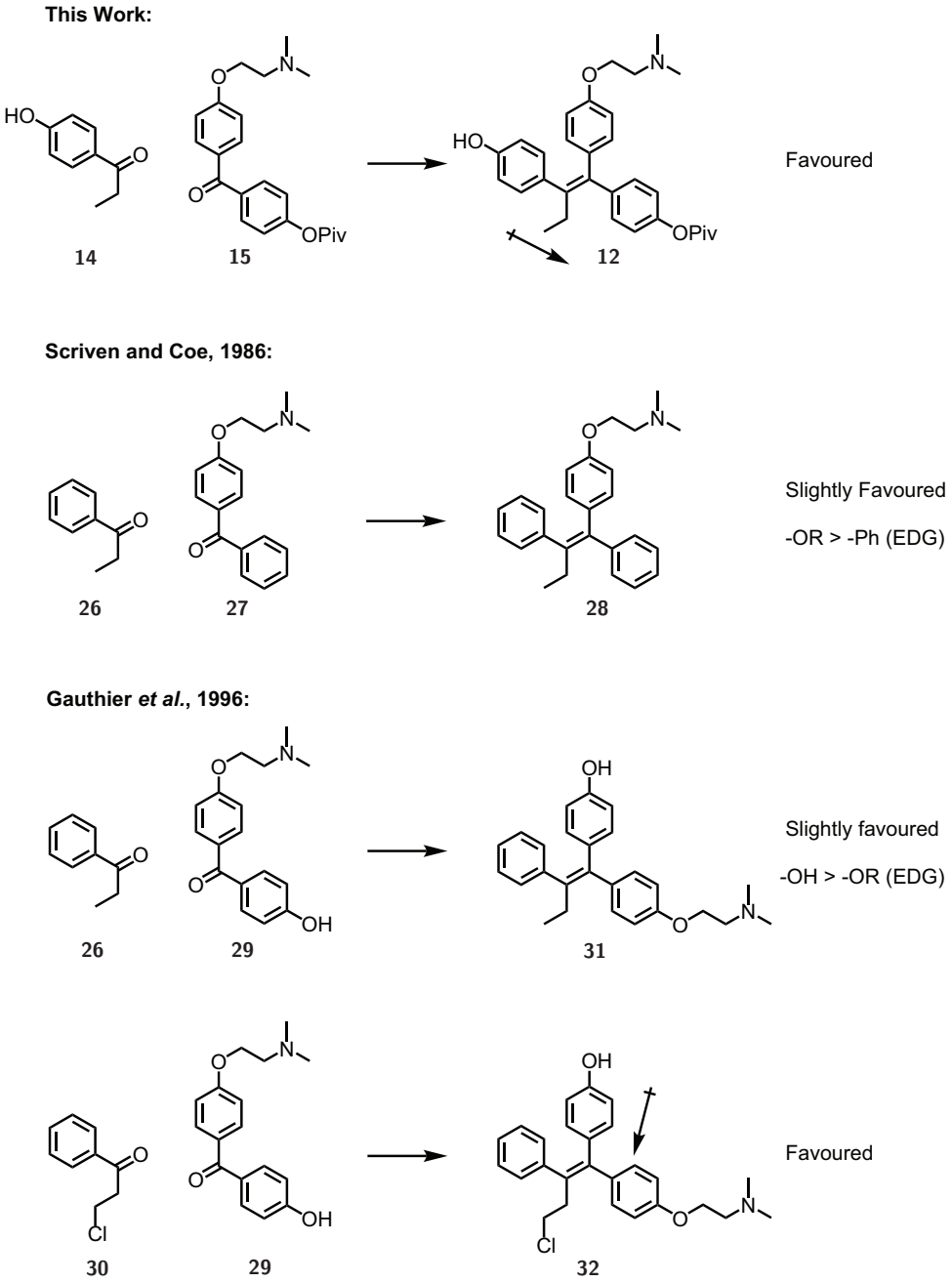

Figure 2.11: Examples of McMurry cross-coupling isomer selectivity.[12,15]

Following triflation of the phenol **12** in 93% yield, the initial strategy for hydroxamic acid side chain installation involved a Heck-coupling to directly install the methyl ester bearing side chain (Table 1). Unfortunately, all Heck cross-couplings of **25** with methyl acrylate failed under a variety of reaction conditions to give methyl ester **33**. In all cases, no conversion of was observed and starting material could be cleanly recovered from the crude reaction

mixture by flash chromatography after workup.

Table 1: Heck cross-coupling conditions screened using aryl triflate **25**.

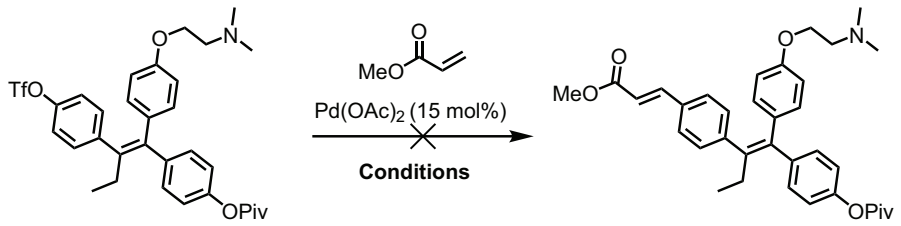

25 33

Entry	Solvent	Base	Ligand (15 mol%)	Temp. (°C)	Time (h)
1*	NEt_3	-	PPh_3	90	16
2*	NEt_3	-	P(*o*-tolyl)$_3$	90	16
3*	DMF	NEt_3	P(*o*-tolyl)$_3$	110	72
4	DMF	NEt_3	P(*o*-tolyl)$_3$	130	48

The failure of the Heck cross-coupling required an alternate strategy in order to access the carbon-linked hybrids. We decided to pursue an olefination strategy which would require an aldehyde handle in place of the triflate. Prior work on these systems showed that the aryl triflate was amenable to palladium catalyzed oxidative carbonylation with $CO_{(g)}$ in 1:1 MeOH:DMF to give a methyl ester, a surprising find in light of the difficulty of the Heck reaction.[3] Rather than form the methyl ester, we were inspired to access the aryl aldehyde directly using a palladium-catalyzed reductive carbonylation. DES was used as a model substrate to test the feasibility of this alternative strategy (Scheme 5).

DES was monoprotected with dihydropyran to give phenol **34** in 45% yield which was then converted to triflate **35** in 63% yield. THP deprotection of **35** occurred *in situ* due to TfOH present in the partially hydrolyzed Tf_2O stock. Triflate **35** was then subjected to reductive carbonylation conditions to give aldehyde **36** in 50% yield.

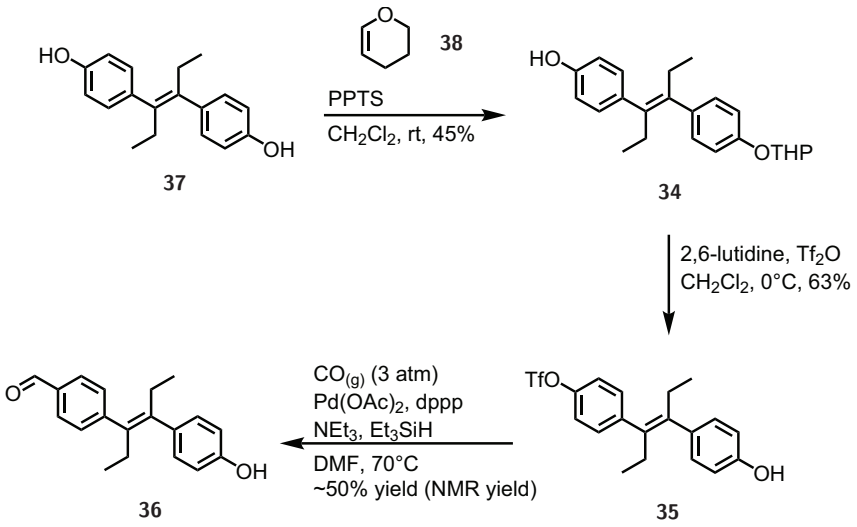

Scheme 5: Synthesis of DES model substrate **35** and reductive carbonylation conditions.

The same reductive carbonylation conditions were applied to triflate **25**. However, no conversion to **39** was observed and 81% of the starting material was recovered alongside a small amount of reduction product (<5%) (Scheme 6). This setback required us to alter our synthetic strategy once again and forego the reductive carbonylation in favour of a three-step oxidative carbonylation-redox sequence. Oxidative carbonylation of **25** proceeded in good yields (64%) to give methyl ester **40** which was then reduced with DIBAL-H to give benzylic alcohol **41** in 49% yield. DMP oxidation then yielded aldehyde **39**, however, purification of the crude proved difficult due to the small quantity of material. Unfortunately, useful quantities of this material could not be accessed despite multiple attempts to increase the scale of the synthetic sequence. Low material throughput severely limited our ability to conduct exploratory chemistry and forced us to address several concerning aspects of our synthetic strategy.

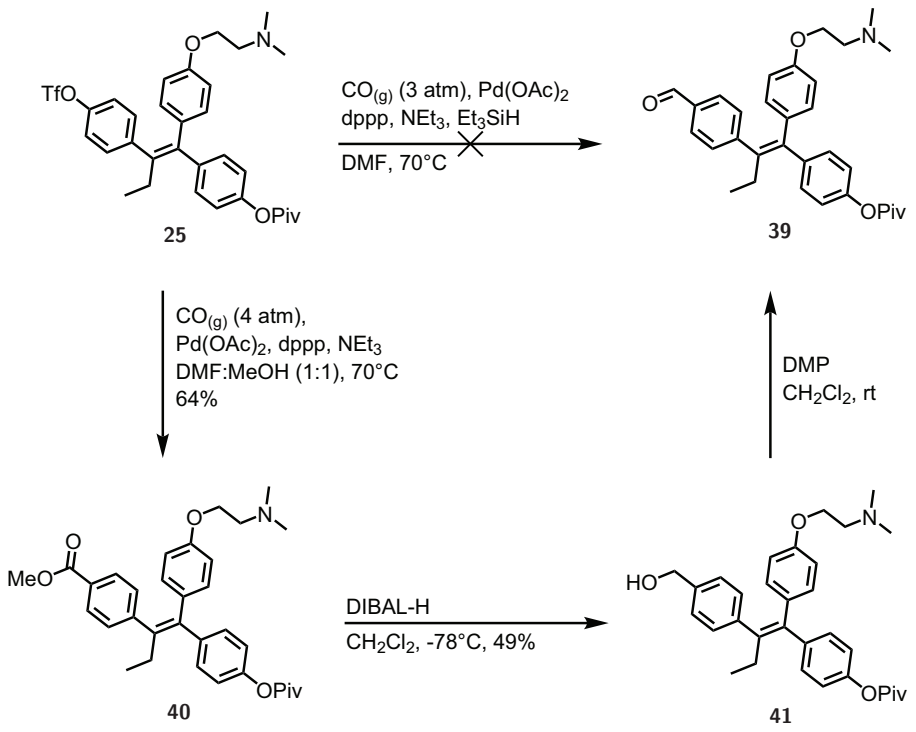

Scheme 6: Synthesis of aldehyde **39** using a three-step workaround.

While the low yields of early stage steps were a major cause of the low material throughput, other factors contributed to the limited success of the first generation synthetic strategy (Scheme 7). Using a McMurry cross-coupling as the key step did indeed allow for a relatively convergent strategy, as the core of the molecule is stitched together from two halves of similar complexity. However, the McMurry cross-coupling is plagued with several limitations including low yields, little to no stereoselectivity between the two isomers, and the reaction often suffered from lengthy workups and persistent impurities. Finally, the late-stage three-step workaround to install an aldehyde was not ideal and would need to be replaced with a more concise solution.

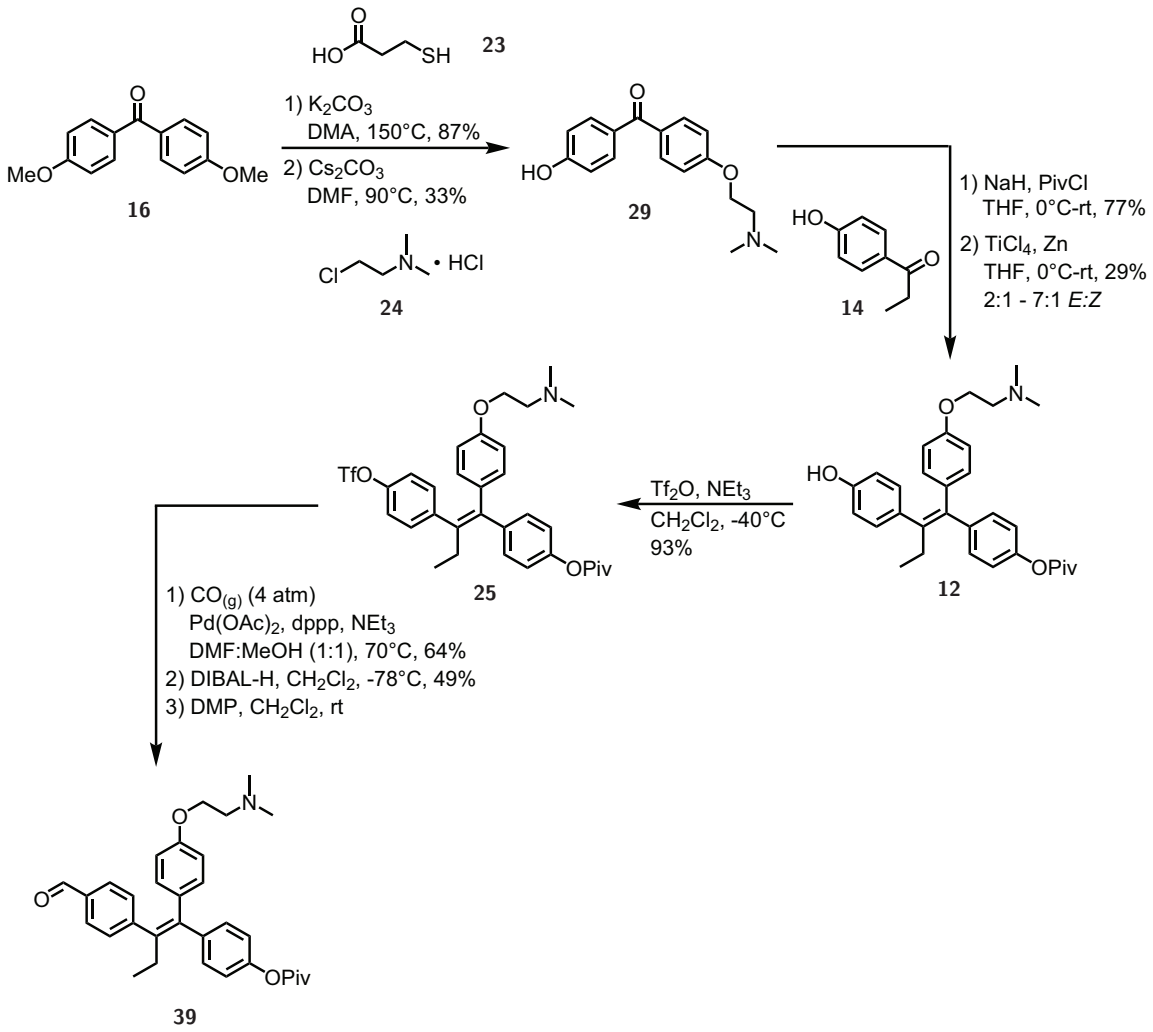

Scheme 7: Overview of first generation synthetic strategy.

We first attempted to remedy the throughput issue by developing an alternate synthetic strategy to access the McMurry precursor **15**. We believed **29** could be accessed using a straightforward Friedel-Crafts strategy (Scheme 8). To this end, 4-hydroxybenzoyl chloride (**42**) was prepared from 4-hydroxybenzoic acid following the standard procedure and *O*-alkylated phenol **43** was prepared in a single step by alkylating phenol (**44**) in quantitative yield. Crude **42** and purified **43** were combined with an excess of $AlCl_3$ but the reaction failed to produce the expected product **29** and instead produced a complex mixture of products. A modified route began with the protection of 4-hydroxybenzoic acid with pivaloyl chloride to give **45**. Next, the corresponding benzoyl chloride **45** was prepared *in situ* and then subjected to Friedel-Crafts conditions with phenol. Unfortunately, the reac-

tion produced two unknown species that did not correspond to the desired benzophenone **46**.

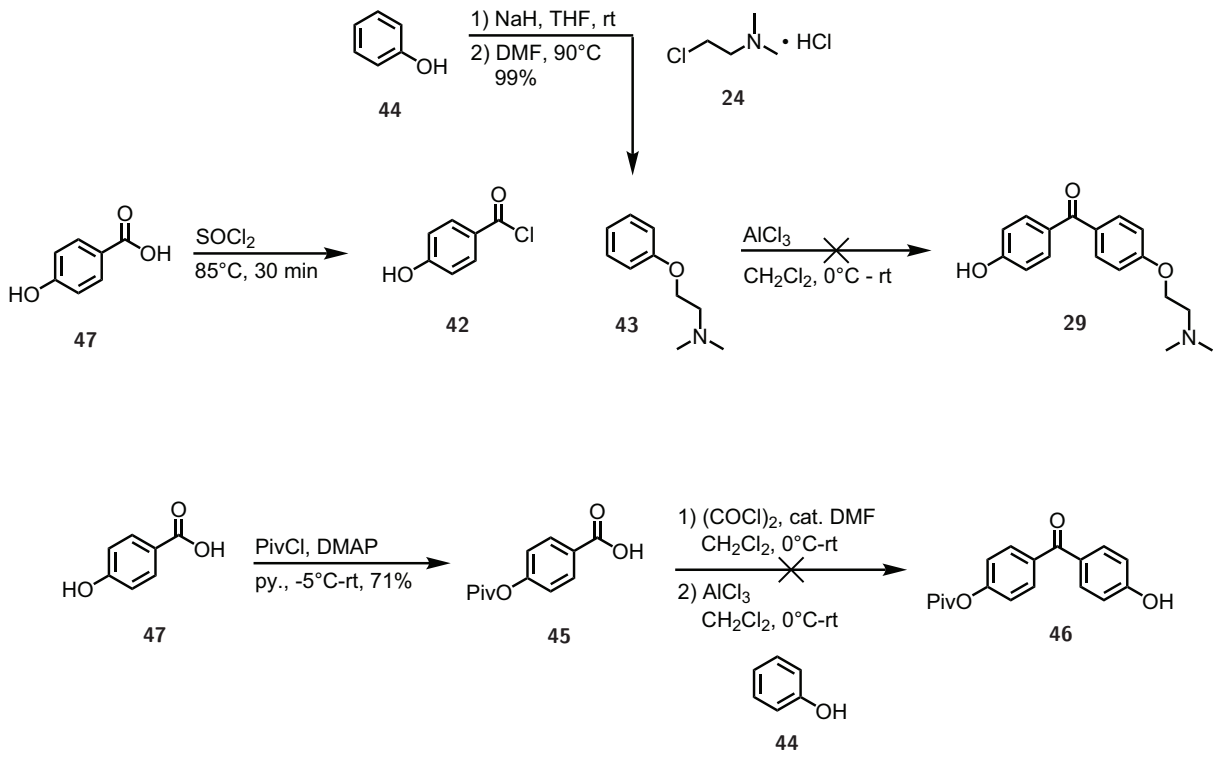

Scheme 8: Friedel-Crafts strategies to access **29** in greater yields.

Our final approach using Friedel-Crafts chemistry was aimed at consolidating the acid chloride formation and phenol protection into a single productive step using *p*-nitrobenzenesulfonyl chloride (*p*-Ns) (Scheme 9). Freidel-Crafts acylations have been carried out using carboxylic acid anhydrides and with mixed anhyrides formed from carboxylic acids and polyphosphoric acid.[19,20] While *p*-Ns is commonly used as a protecting group, we thought that perhaps in this case it could serve a dual purpose as both a carboxylic acid activator and phenolic protecting group. The protection and *in situ* formation of mixed anhydride **48** proceeded smoothly, although attempts to purify the intermediate proved difficult due to its instability on silica. The crude product was then subjected to Friedel-Crafts conditions with phenol but ultimately failed in producing the desired product **49**. We then turned our focus to alternative 1,2-addition strategies in hopes of accessing ketone **15**.

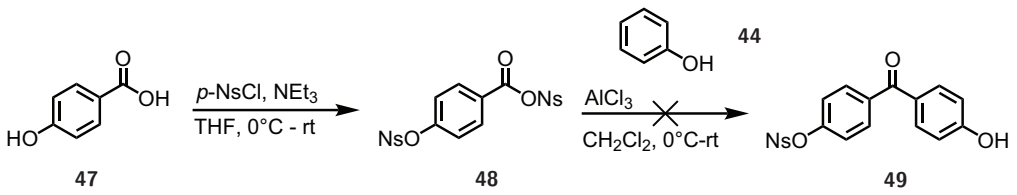

Scheme 9: Friedel-Crafts strategy using a mixed anhydride.

We began by protecting 4-hydroxybenzoic acid to give **45** and then generating the Weinreb amide **50** in 25% yield via addition to the benzoyl chloride which was formed *in situ* using oxalyl chloride and DMF (Scheme 10). Next, the addition of an organolithium derived from aryl halide **51** to the Weinreb amide **50** was attempted, but it failed to deliver the expected product **15** and instead led to pivaloyl ester cleavage.

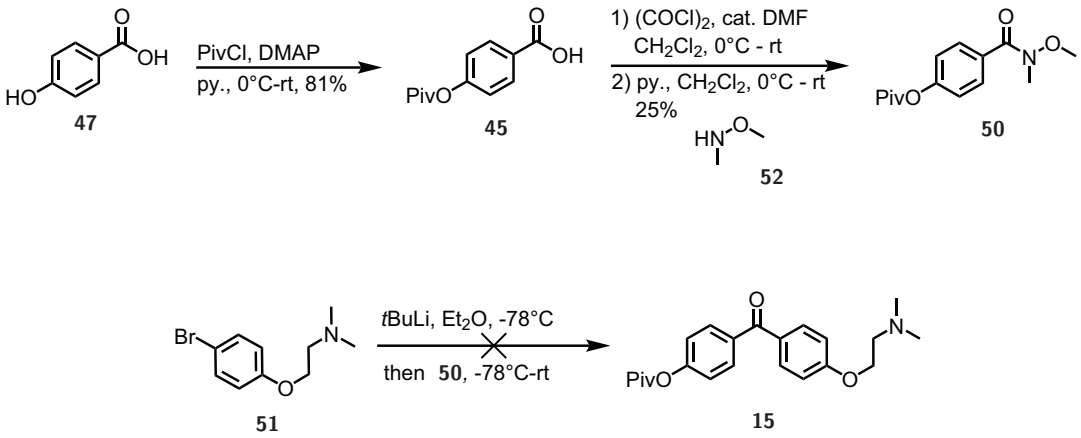

Scheme 10: 1,2-addition strategy using an organolithium addition to Weinreb amide **50**.

Our final attempt to construct the disubstituted ketone **15** was to employ mild organocuprate chemistry that would avoid the cleavage of the pivaloyl ester. Knochel *et al.* have investigated the use of organocuprates derived from Grignard reagents and their ability to selectively form 1,1-disubstituted ketones from acid chlorides directly.[21] With this approach in mind, we began with the alkylation of *p*-bromophenol to generate aryl bromide **53** which was then be converted to the organocuprate *in situ* using CuCN • 2LiCl in THF (Scheme 11). Unfortunately, the organocuprate addition to benzoyl chloride **54** did not lead to the formation of the desired product **15**. The lack of success on all fronts in finding an alternative route to the McMurry precursor **15** was discouraging but inspired us to explore other syn-

thetic strategies to build the tetrasubstituted olefin scaffold.

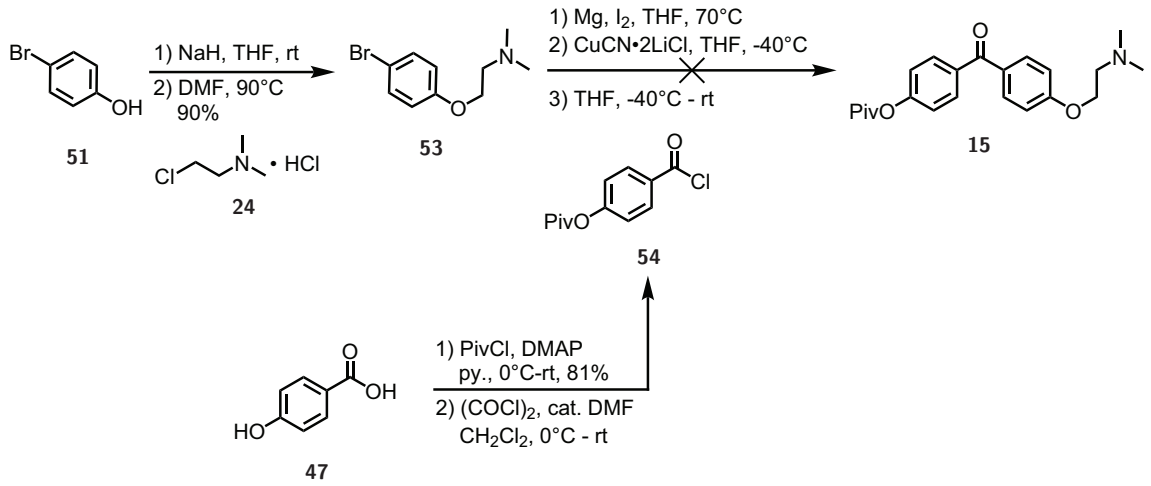

Scheme 11: 1,2-addition strategy using an organocuprate addition to benzoyl chloride **54**.

Xue *et al.* recently published a three-component coupling methodology to construct sterically encumbered tetrasubstituted olefins stereoselectively from an alkyne, using a ligand free Ni catalyst (Scheme 12).[22] The authors suggested that the one-pot reaction proceeds first through a Ni catalyzed carbomagnesiation of the alkyne to produce a vinyl-MgBr intermediate (**55**) which can then undergo a Kumada cross-coupling with the aryl-iodide to generate a tetrasubstituted olefin in good yields. In their model reaction, the authors combined phenylmagnesium bromide (**56**), *p*-iodoanisole (**57**), and diphenylacetylene (**58**) with 1 mol% $NiCl_2 \bullet 6H_2O$ in one-pot to produce tetrasubstituted olefin **59** in 81% yield. The authors conducted a time-based quenching study of the reaction and noted that the initial carbomagnesiation step is fast and leads to an increase in the concentration of the vinyl-MgBr intermediate. The slow Kumada cross-coupling step then becomes the major reactive pathway once the internal alkyne is fully consumed. The group reported that $NiCl_2 \bullet 6H_2O$ and other Ni^{II} catalysts produced the best results while Pd, Fe, and Mn catalysts were unable to replicate this dual mode of reactivity.

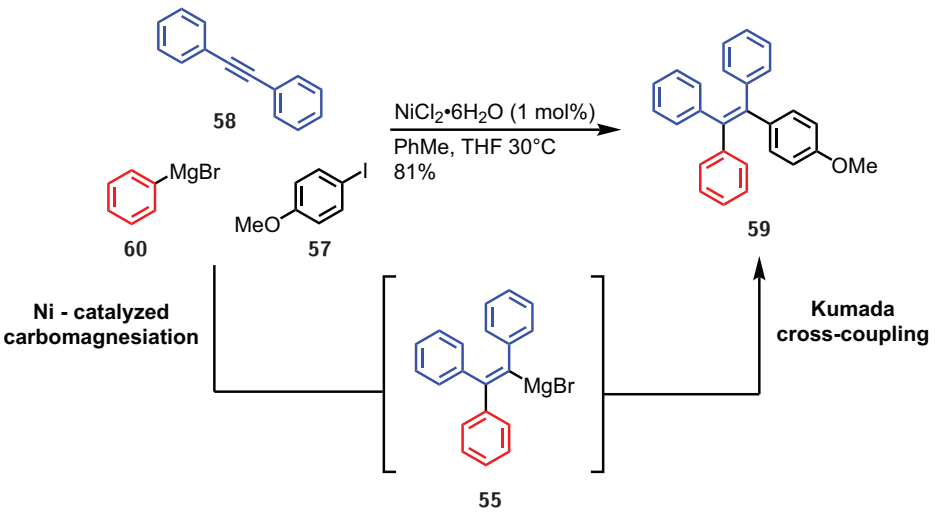

Scheme 12: Model reaction of a nickel catalyzed 3-component coupling published by Xue *et al.*[22]

The tolerance of electron withdrawing and donating groups on both the Grignard reagent and the aryl-iodide were reported, although no investigation into the effects of such groups on phenylacetylene substrates was conducted. Remarkably, the carbomagnesiation of unsymmetric alkyl(aryl)acetylenes were reported to occur stereoselectively to generate the least hindered vinyl-MgBr intermediate. Insertion of the aryl group occurs preferentially onto the least hindered sp carbon so as to avoid unwanted A-1,2 strain, leading to nearly exclusive *Z*-selectivity with respect to the vinyl-MgBr intermediate. The group showcased the simplicity and high degree of selectivity of the reaction with a one-pot synthesis of tamoxifen in 41% yield and 94:6 *Z:E*. Xue's promising methodology appeared to be highly applicable to this project and, coupled with the unsuccessful attempts at efficiently constructing our tetrasubstituted olefin scaffolds, sparked major interest in tailoring the 3-component reaction for the SERM/HDACi hybrids.

Two model reactions were first carried out in order to determine the reproducibility of Xue's methodology. In our hands, diphenylacetylene (**58**), *p*-iodoanisole (**57**), and phenylmagnesium bromide (**60**) reacted easily in toluene with 1 mol% $NiCl_2 \bullet 6H_2O$ as the catalyst to produce the desired tetrasubstituted olefin **59** in 60% yield (Scheme 13). While the successful reproduction was promising, the ability to synthesize tamoxifen with similar con-

ditions would greatly reinforce the notion of incorporating the methodology into the hybrid project. Two simple precursors would first need to be synthesized before tamoxifen could be made. An organolithium addition of lithiated phenylacetylide onto iodoethane provided internal alkyne **61** in 45% yield. Next, *p*-iodophenol (**62**) was alkylated to give aryl iodide **63** in quantitative yield. The components were combined, along with phenylmagnesium bromide in THF, using the same conditions outlined by Xue to give tamoxifen in 23% yield as the pure *Z*-isomer. This exciting result further justified the incorporation of the 3-component coupling reaction into the hybrid synthesis in place of the McMurry cross-coupling.

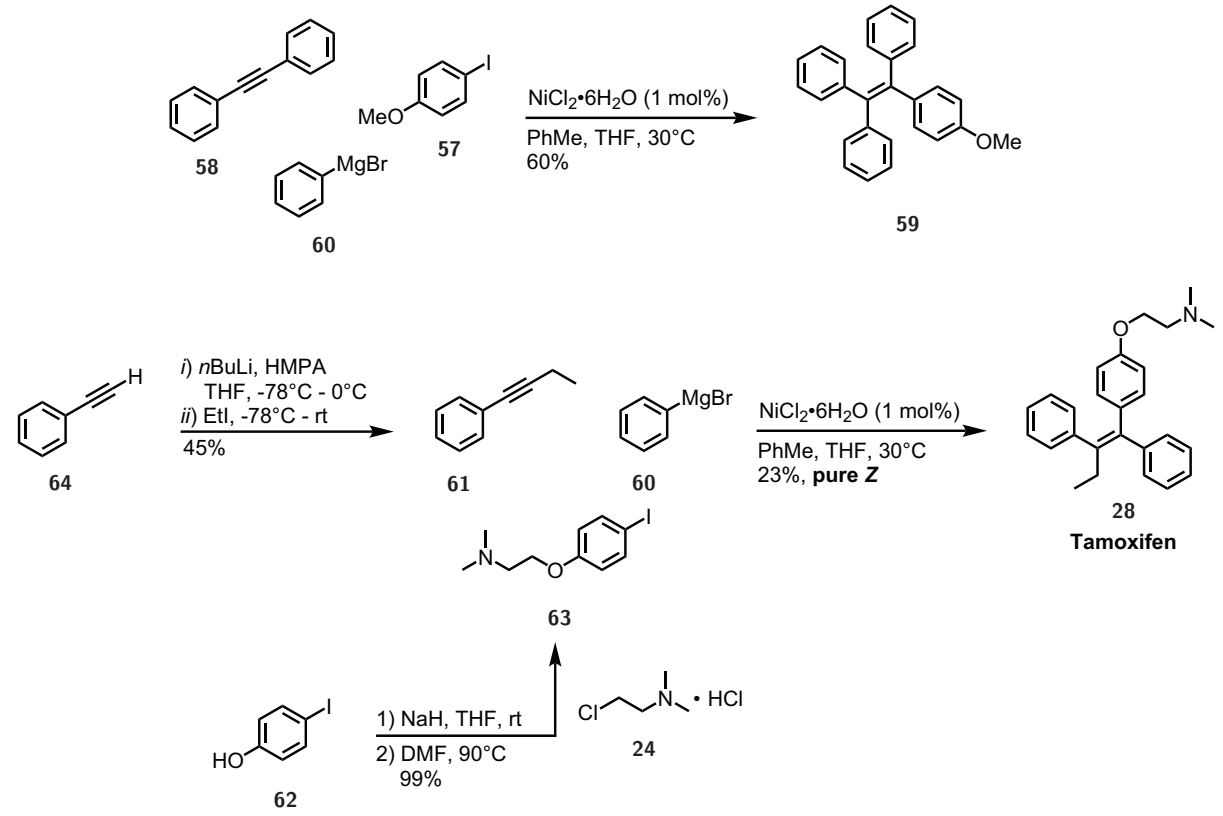

Scheme 13: Reproduction of model reactions carried out by Xue *et al.* using the Ni catalyzed 3-component coupling reaction.

The new strategy would require a vastly different approach and a second generation retrosynthesis was thereby devised (Scheme 14). The late-stage functionalization strategy would remain unchanged and a solution to the three-step work around would later be addressed. The 3-component coupling would construct the tetrasubstituted olefin scaffold **65** in

a single key step from three simple starting materials, one of which had already been accessed for the synthesis of tamoxifen. An organolithium addition of a *p*-substituted phenylacetylene would give the requisite internal alkyne **66** and the terminal alkyne **67** would be the product of a Sonogashira cross-coupling between *p*-iodophenol and TMS acetylene. The revised retrosynthesis improves on several aspects of the initial strategy. As a whole, the strategy is highly convergent, amenable to late stage diversification, and requires very simple starting materials that can be treated as easily modifiable modular components. The 3-component coupling was also expected to be highly stereoselective for the desired isomer, in stark contrast to the mediocre selectivity observed in the McMurry cross coupling.

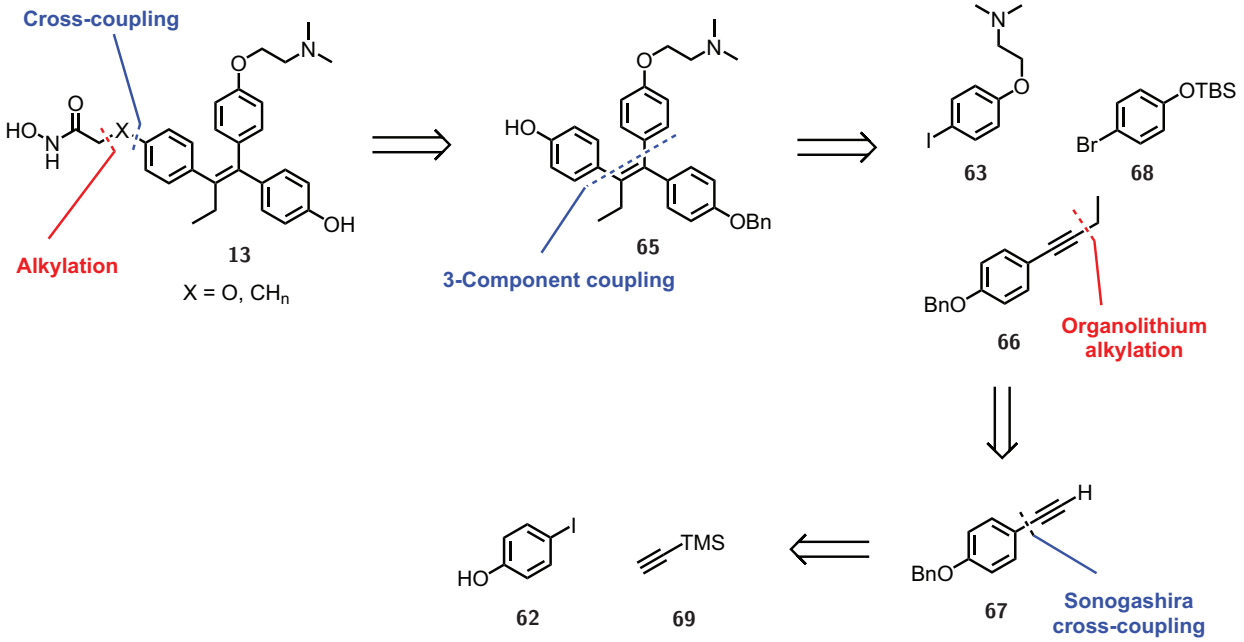

Scheme 14: Revised retrosynthesis of hybrid SERM/HDACi analogues using the 3-component coupling as the key step.

The aryl halide building blocks were each synthesized in single steps from their parent *p*-halophenols. Alkylation of *p*-iodophenol to give **63** and TBS protection of *p*-bromophenol to give **68** proceeded well and could be routinely conducted on 10-15 g scales (Scheme 15). We observed that running the alkylation of *p*-iodophenol in THF or DMF alone led to low yields (40%), whereas a solvent switch from THF to DMF after sodium phenolate formation resulted in quantitative yields. The solvent dependant difference in yields may be due to

several reasons. First, organosodium compounds are highly soluble in THF and conversion to the deprotonated intermediate in THF is likely to proceed to completion. Second, NaH has been observed to act as a source of hydride and can lead to unwanted side products in the presence of DMF.[23] Finally, DMF is capable of completely dissolving 2-chloro-*N,N*-dimethylaminoethyl chloride and is known to facilitate S_N2 reactions.

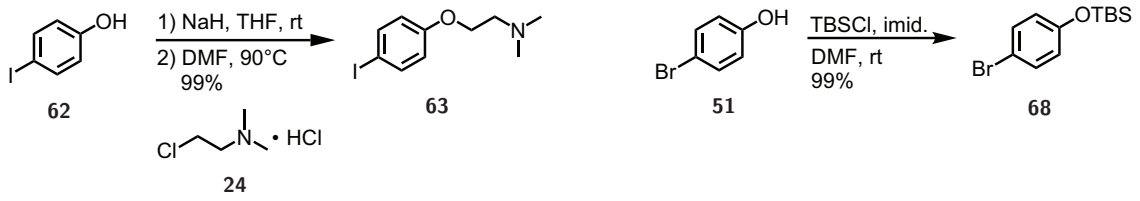

Scheme 15: Single step preparations of aryl halides **63** and **68**.

Synthesis of the internal alkyne began with a Sonogashira cross-coupling of *p*-iodophenol and TMS acetylene (Scheme 16). Initially, the Sonogashira cross-coupling was run in neat NEt_3 and failed to deliver the desired product. Instead, running the reaction in toluene at room temperature using stoichiometric DIPEA lead to near quantitative yields of **70**. Protection of the phenol with benzyl bromide in DMF yielded protected arylacetylene **71** in good yields over two steps (82%). TMS deprotection under mildly basic conditions proceeded smoothly to give terminal acetylene **72** in 80% yield, however alkylation with EtI, using *n*BuLi as base, led to only moderate yields of **66**. Fortunately, conducting the same reaction with LDA provided internal alkyne **66** in excellent yields (93%).

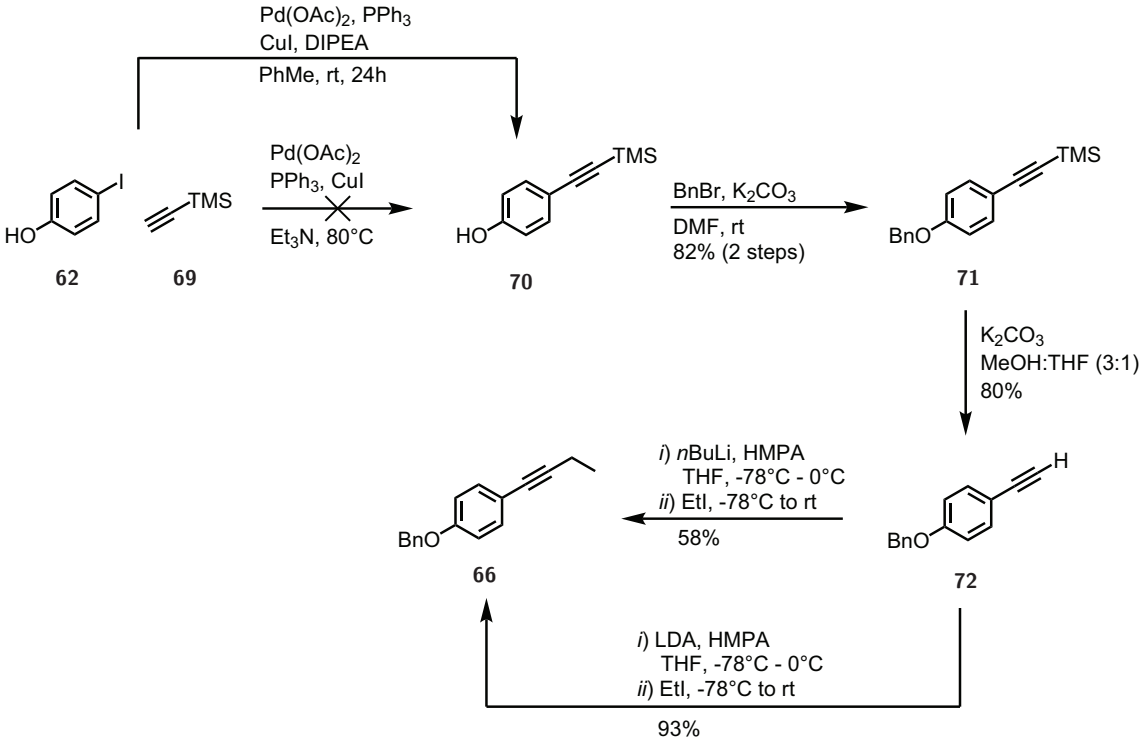

Scheme 16: Four step synthesis of internal alkyne **66**.

While the key step using alkyne **66** had yet to be run, the advantages of the second generation synthetic strategy were already apparent. Material throughput was no longer an issue as the simple, early intermediates of this route could be easily accessed in high yields; a single 10 g scale run through of the first generation route would typically yield 2.8 g (7.6 mmol, 18% over 3 steps) of ketone **15** while a single run through the second generation sequence yielded 6 g (25 mmol, 55% over 4 steps) of alkyne **66**.

Treatment of bromide **51** with Mg turnings and I_2 could be conducted routinely to generate Grignard reagent **73**, which could be titrated against *s*BuOH to determine its concentration immediately prior to use (Scheme 17). Gratifyingly, the 3-component coupling of **73**, **63**, and **66** proceeded well using the same conditions outlined by Xue to give the protected tetrasubstituted olefin **65** exclusively as the *Z* isomer in 33% yield. In an attempt to improve the yield, variations in the order of addition, temperature, time, and catalysts including anhydrous $NiCl_2$, $Ni(OAc)_2$, and $NiCl_2(PPh_3)_2$ were attempted but led to minimal formation of **65**, or to increased yields of a side product formed by the direct Kumada

cross-coupling of **73** and **63**. Despite the low yields, the simplicity of the reaction, ease of synthesis of starting materials and exclusive isomer selectivity encouraged us to maintain the use of this strategy. With the protected 4-OHT scaffold in hand, TBS deprotection was then carried out using TBAF to give free phenol **74** in moderate yields (79%) but as a 2:1 mixture of *Z:E* isomers. The phenol was then triflated to yield aryl triflate **75** in 83% yield.

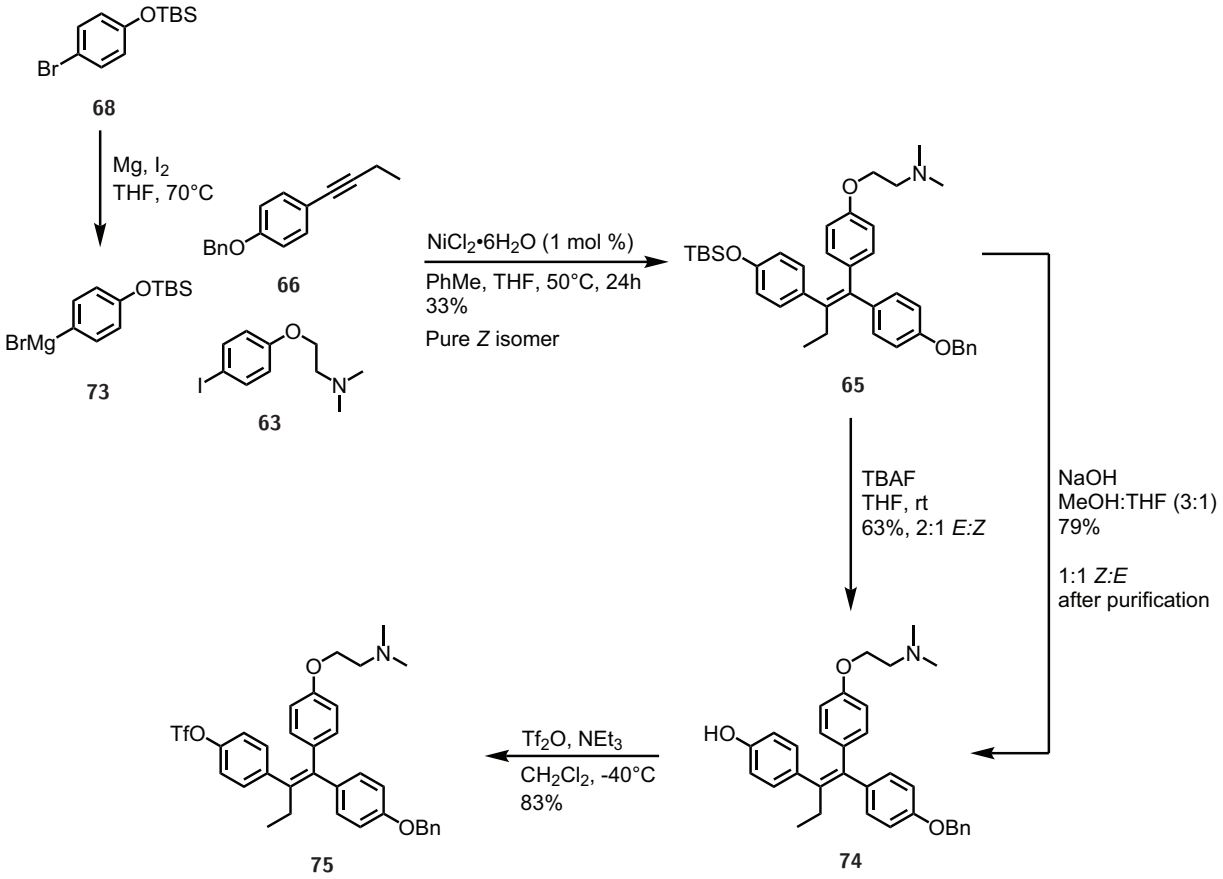

Scheme 17: Three-component coupling of **73**, **76**, and **66** to generate the protected intermediate **65**, followed by TBS deprotection and triflation to yield **75**.

Currently, we do not have an explanation as to why isomerization occurred with TBAF as commercial solutions of the reagent are known to be neutral or mildly basic. However, our knowledge of the acid lability of the olefin scaffold prompted us to attempt a TBS deprotection under strictly basic conditions. The deprotection was carried out smoothly using NaOH in MeOH and the crude product showed no evidence of isomerization. Unfortunately, the product was unstable on silica gel and 1:1 isomerization was observed throughout the

course of purification. Purifying with basic alumina failed to give acceptable resolution and subjecting the crude directly to the next step was often fruitless. Although the 3-component reaction strategy led to the exclusive formation of the desired isomer, the intermediates' proclivity for isomerization forced us to carry the mixture of isomers throughout the remainder of the synthesis and isolate the desired isomers using preparatory HPLC prior to biological testing.

The three-step workaround to access a benzaldehyde type intermediate was abandoned in order to maintain the efficiency of the second generation synthesis. While a Heck cross-coupling of the pivaloyl protected intermediate **25** failed to proceed, we thought that perhaps the altered electronics of the benzyl ether protected intermediate **75** might allow for a productive reaction. However, all attempts to carry out a Heck reaction on substrate **75** led to similar results, the conditions of which are outline in Table 2.

Table 2: Heck cross-coupling conditions screen to functionalize triflate **75**.

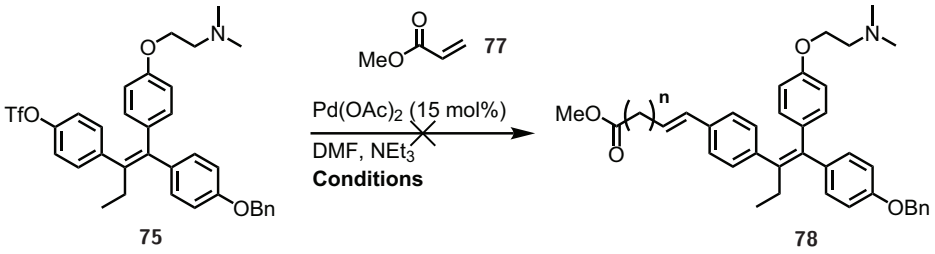

Entry	Additive	Ligand (15 mol%)	Temp. (°C)	Time (h)
1	-	dppf	60	16
2	-	dppp	60	16
3	3 eq. LiCl	PPh3	120	24
4*	-	PPh3	120	24
5	-	dppp	120	24
6	-	dppf	120	24
7**	-	dppf	60	24

*Sealed tube **methyl pent-4-enoate as coupling partner

We then altered our strategy to utilize a Grubbs' cross-metathesis from a styrenyl olefin in order to install the hydroxamic acid side chain. A palladium catalyzed Kumada cross-coupling using vinylmagnesium bromide was carried out, but no conversion of starting

material was detected (Scheme 18). The lack of conversion in all cases suggested that perhaps oxidative insertion into the C-OTf bond was failing to occur on on the electron rich substrates. Working under this assumption, a Kumada cross-coupling was attempted using an electron rich NHC-Ni catalyst system as outlined by Joshi-Pangu *et al.*, but it had also failed to produce the desired styrenyl intermediate **79**.[24] Since attempting to modify the oxidative insertion was unsuccessful, we considered altering the cross-coupling partner in an attempt to effect the transmetallation. A promising investigation by Molander and Rivero into Suzuki cross-couplings using potassium vinyltrifluoroborate outlined specific conditions in which they observed moderate to good yields with electron rich aryl triflates and provided an alternative to introducing a vinyl group into our system.[25] The highly stable potassium vinyltrifluoroborate salt **80** was first prepared using trimethylborate and KHF_2 in 44% yield, and then Molander's Suzuki cross-coupling conditions were employed to successfully transform the recalcitrant triflate **25** to the desired styrenyl intermediate **79** in 81% yield. This single-step conversion of the triflate into an olefin eliminated the need for the lengthy oxidative carbonylation-redox sequence, and provided us with a useful synthetic handle.

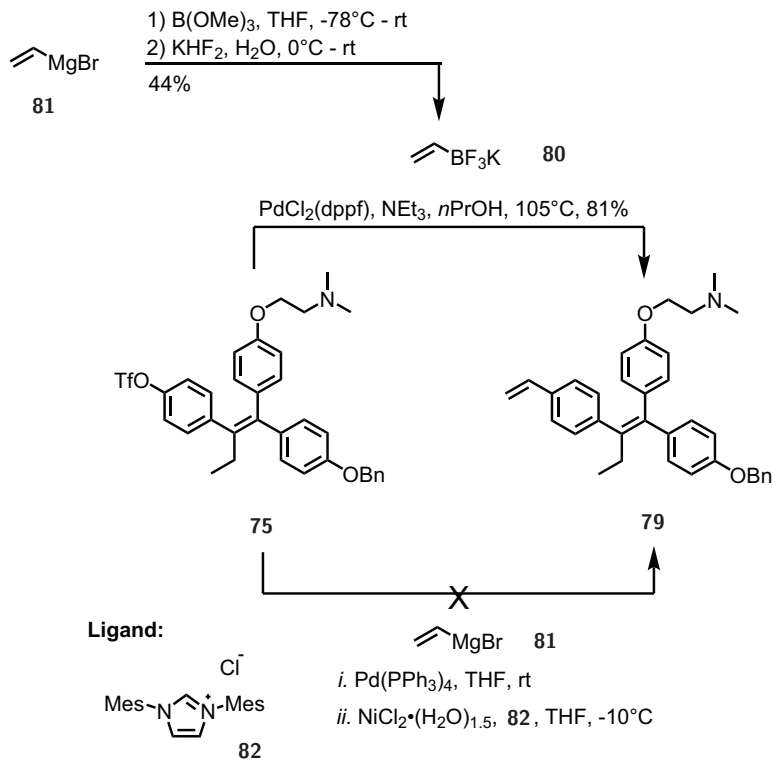

Scheme 18: Suzuki coupling using potassium vinyltrifluoroborate **80** to yield **79**.

Initial attempts at using a Grubbs cross-metathesis to install the remainder of the three-carbon side chain failed with Grubbs generation I and II catalysts, even when using a large excess of the Type I olefin relative to the Type I styrene (Scheme 19). The Lewis basic tertiary amine was quickly determined to be the cause of the problem as Lewis bases are known to occupy empty coordination sites in Ru catalysts and shut down their catalytic activity. Woodward *et al.* demonstrated an elegant solution to this incompatibility by temporarily protecting electron rich amines as stable ammonium salts through the addition of anhydrous *p*-toluenesulfonic acid (PTSA).[26] To test whether this temporary amine-protection strategy would be amenable to our case, a model substrate **83** bearing a similar *N,N*-deimethylaminoethyl side chain was synthesized from a Suzuki cross-coupling of **63** and **80**. A negative control for the Grubbs cross-metathesis was first carried out using the free amine **83** and methyl acrylate (**77**) which led to no conversion of starting material. Following Woodward's protocol, the free amine was protected *in situ* with anhydrous PTSA and subjected to the cross-metathesis conditions to give the methyl cinnamate derivative **84** as the major product following a mildly basic workup (yield not determined).

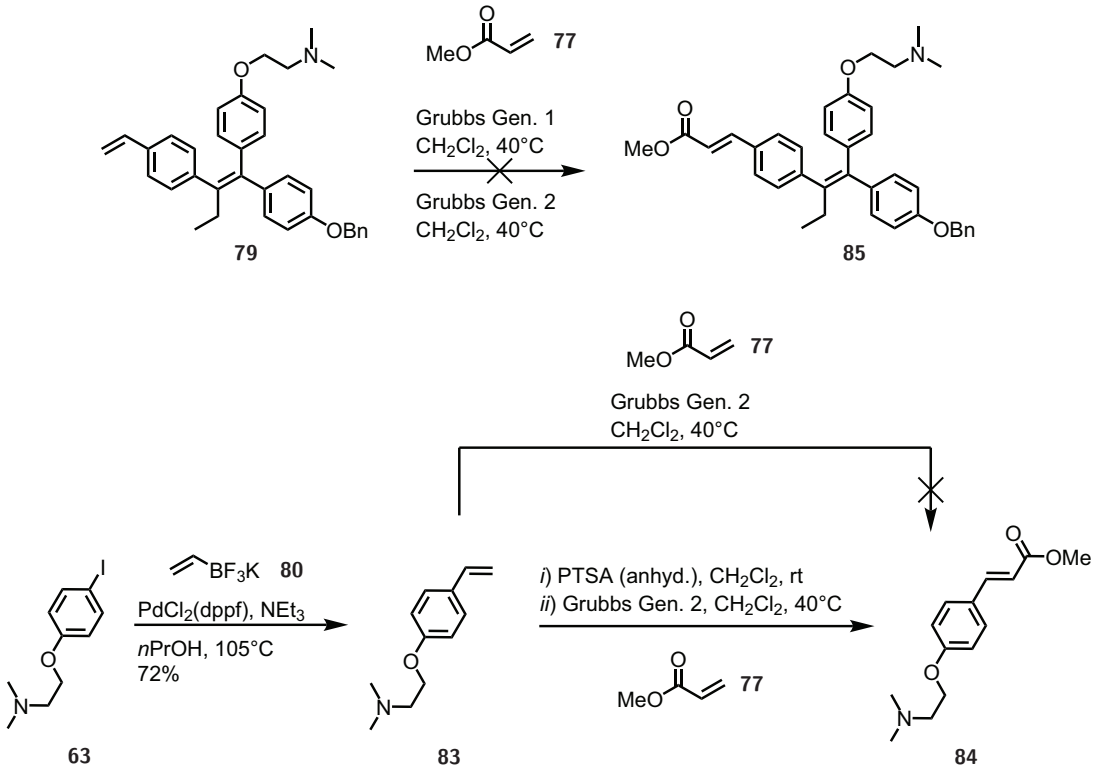

Scheme 19: Grubbs cross-metathesis hindered by nucleophilic tertiary amine of **86**

This simple and effective protocol was then successfully applied to the styrenyl intermediate **79**. The free amine of styrene **79** was protected *in situ* with anhydrous PTSA and then underwent cross–metathesis with methyl acrylate to gratifyingly yield methyl ester **85** (Scheme 20). A second addition of 5 mol% using Grubbs 2nd generation catalyst after 24 hours was found to significantly improve yields from 40% to 70%. The final two steps consisted of a simultaneous benzyl ether deprotection and olefin hydrogenation, followed by base mediated formation of hydroxamic acid **5** (AFP-345) as a 1:1 mixture of *Z:E* isomers using aqueous hydroxylamine in 87% and 57% yield, respectively. Hydrogenation of the internal olefin was not observed, presumably due to the sterically hindered environment. The late stage Grubbs metathesis strategy was then smoothly applied for a second time to yield methyl ester **87** bearing a longer linker in 74% yield, which was then converted in two steps to hydroxamic acid **7** (AFP-477) (29% yield in two steps).

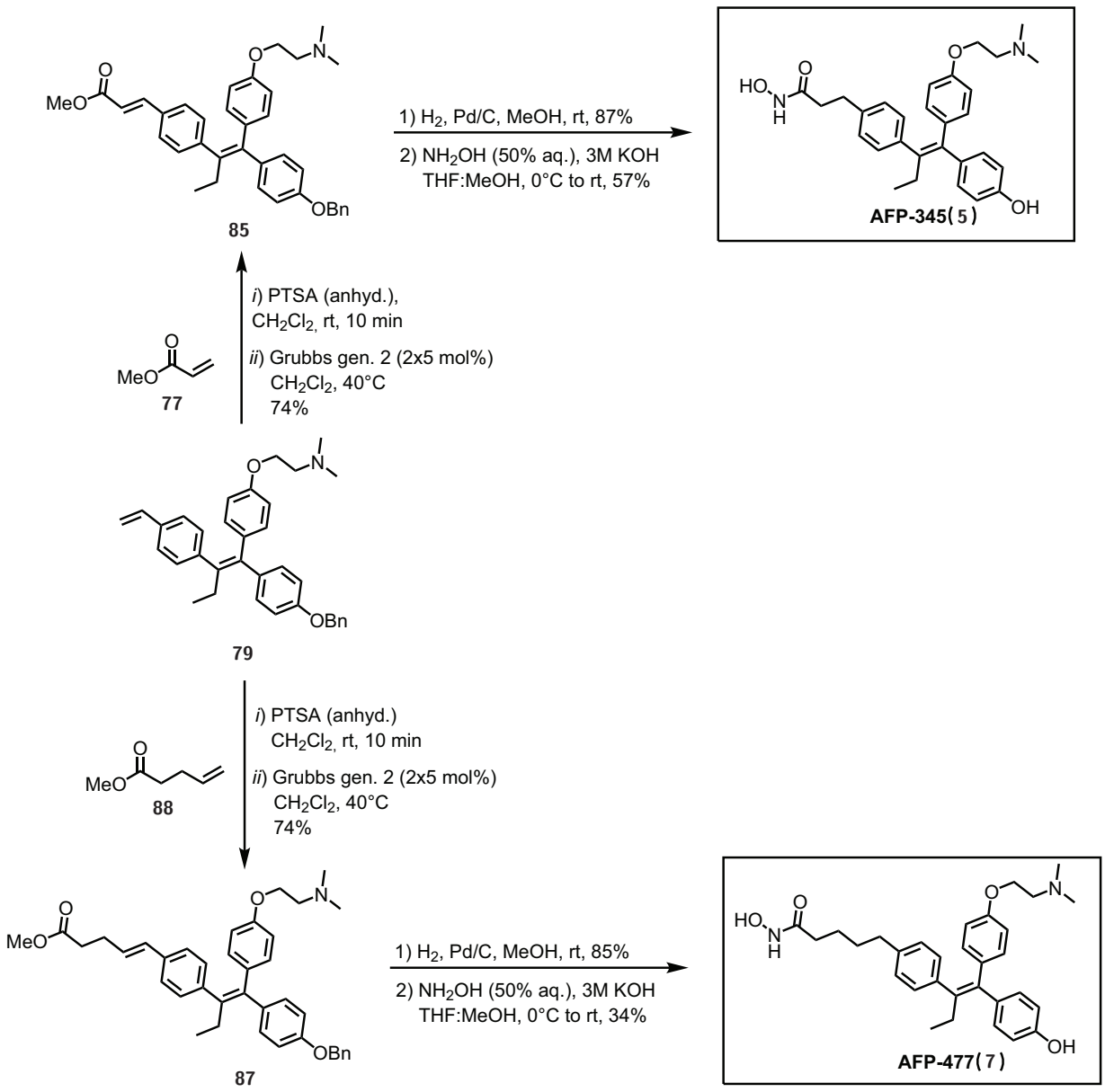

Scheme 20: Synthesis of final compounds AFP-345 (**5**) and AFP-477 (**7**).

Reduction of the styrenyl alkene was too rapid to intercept a deprotected intermediate that preserved the olefin functionality. Initially, we planned to remove the benzyl ether group using conditions that would leave the desired olefin untouched. Oxidation of the benzylic position to a benzoyl ester that would be susceptible to cleavage under basic conditions in the final synthetic step, or nucleophilic conditions alongside a Lewis acid, as has been described by Akiyama *et al.* were considered.[27] However, our lack of material at this stage required us to build up our stock once more, and instead allowed us to alter our protecting group strategy.

Fortunately, a preserved sample of McMurry product **12** was available and amenable to the newly realized late stage Suzuki/Grubbs sequence. Phenol **12** was triflated in 55% yield and then cleanly underwent Suzuki cross-coupling with **80** to give **89** in 89% yield (Scheme 21). Following the *in situ* protection and cross-metathesis sequence, the resulting intermediate was simultaneously deprotected and converted to hydroxamic acid **8** in 91% and 70% yields, respectively. The utility of the phenol **12** only extended to the synthesis of AFP-374 (**8**), and the sequence had to be revisited with a modified protecting group strategy in order to access the final carbon-linked hybrid AFP-458.

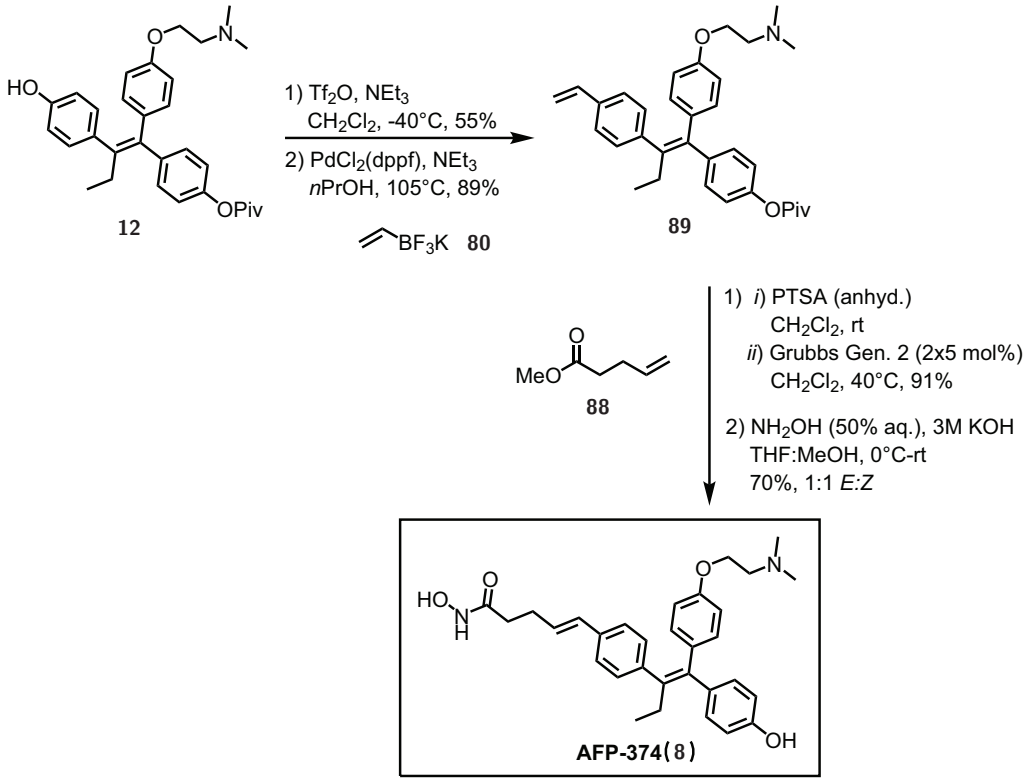

Scheme 21: Synthesis of final compound AFP-374 (**90**).

Para-methoxybenzyl bromide was chosen as a suitable replacement for the benzyl protecting group due to its structural similarity and susceptibility to non-reductive deprotection conditions. The synthesis commenced with a Sonogashira coupling of TMS acetylene and *p*-iodophenol followed by PMB protection of the phenol to yield terminal alkyne **91** in

51% yield over two steps (Scheme 22). Deprotection of TMS occurred spontaneously upon aqueous workup as a result of excess NaH that had formed aqueous NaOH. Organolithium addition of the lithiated **91** species to iodoethane produced internal alkyne **92** in 86% yield. Next, a 3-component coupling of **92** with **63** and **73** gave the protected scaffold in 21% yield which subsequently underwent a TBS deprotection to yield phenol **93** in 57% yield. The phenol was triflated and a relatively low yielding Suzuki coupling (54%) was carried out to give **94**. The low yield is presumed to be due to the instability of the PMB protected substrate under the given conditions, however, no byproducts could be identified to provide information regarding the unwanted reactivity. Nonetheless, with the PMB protected styrenyl intermediate **94** in hand, Grubbs cross-metathesis was carried out using the Woodward protocol to give conjugated methyl ester **95** in 65% yield. To our surprise, PTSA was also effective in removing the PMB group *in situ* leading to a fully deprotected and cross-metathesized product. Unfortunately, we were unable to produce the hydroxamic acid **6** directly from methyl ester **95**, likely due to the vinylogous phenolate that is generated under strongly basic conditions. The possibility of accessing the final carbon-linked hybrid from an activated carboxylic acid rather than a methyl ester was then considered.

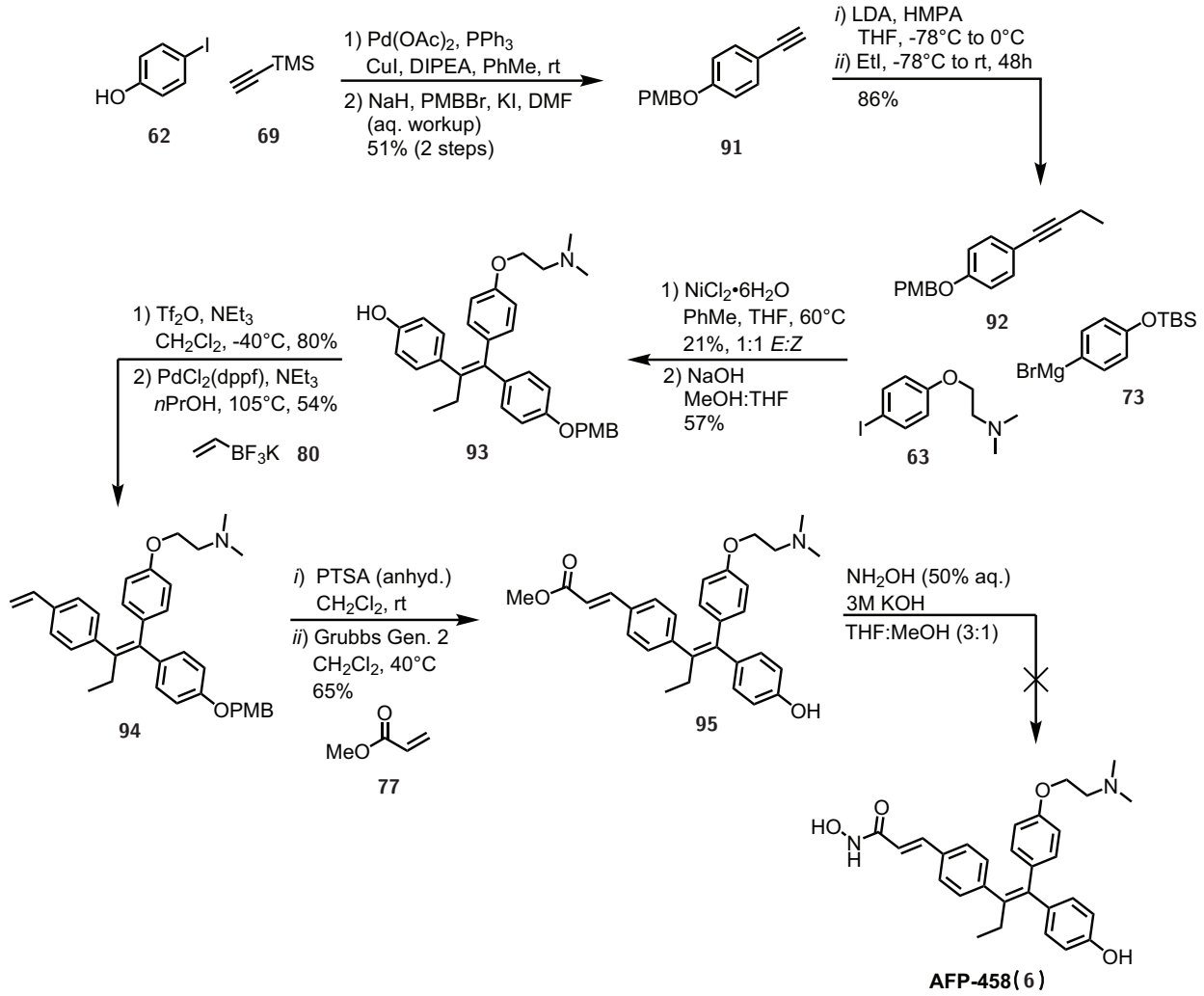

Scheme 22: Synthesis of final compound AFP-458 using modified protecting group strategy.

Initially, we considered an EDC coupling of hydroxylamine and a carboxylic acid derivative of our substrate to access the desired hybrid. With very limited examples of this reaction on similar substrates in literature and based on the fact that we had a limited quantity of methyl ester **95** in hand, we decided to first carry out the transformation on a model substrate. Bearing both a vinylogous phenol and an α,β-unsaturated carboxylic acid, *p*-coumaric acid was chosen to test EDC coupling conditions with hydroxylamine hydrochloride (Scheme 23). Unfortunately, under standard conditions, the reaction failed to provide any detectable hydroxamic acid product **96** and instead generated an insoluble precipitate that could not be identified.

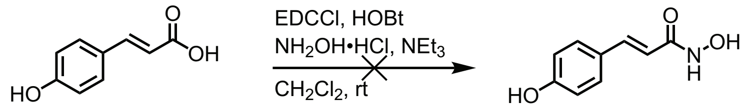

97 96

Scheme 23: EDC coupling on *p*-coumaric acid.

The failure of the EDC coupling led us to an alternate strategy based on a study from Ech-Chahad *et al.* who showed that hydroxamic acids could be generated from carboxylic acids in good yields and under mild conditions using propylphosphonic anhydride (T3P), a carboxylic acid activating reagent.[28] Briefly, formation of the mixed anhydride first occurs under mildly basic conditions and then the addition of a solution of hydroxylamine hydrochloride yields the desired hydroxamic acid (Scheme 24). The conditions outlined by Ech-Chahad *et al.* were applied to *p*-coumaric acid but failed due to the formation of a precipitate partway through the reaction (Table 3). A solvent screen was carried out in order minimize the precipitation of any intermediates and allow the reaction to proceed to completion. DMF was best suited for the task, and a 10% (v/v) solution of H_2O in DMF was used to fully dissolve the hydroxylamine hydrochloride prior to its addition to the activated anhydride. This protocol was capable of converting 50% of *p*-coumaric acid to hydroxamic acid **96**. In retrospect, two equivalents of T3P would have accounted for the nucleophilic phenol and may have led to improved yields. We then used the optimized conditions to access our final carbon-linked hybrid.

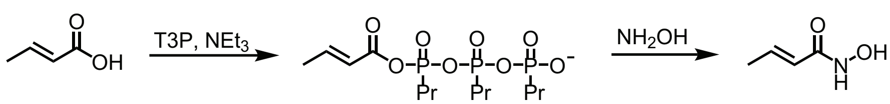

98 99 100

Scheme 24: General scheme of T3P activation of carboxylic acid with hydroxylamine to yield hydroxamic acids.

Table 3: T3P coupling solvent screen optimization.

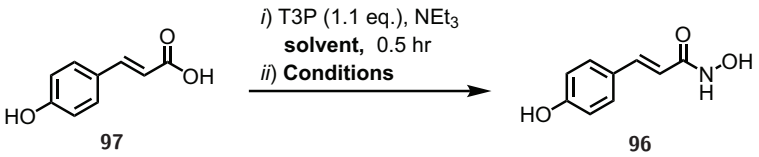

Entry	Solvent	Additive	$NH_2OH{\cdot}HCl$ (eq.)	Result
1	MeCN	-	2.0	No conversion
2	THF	-	2.0	No conversion
3	EtOAc	-	2.0	No conversion
4	DMF	-	2.0	No conversion
5	DMF	20% (v/v) H_2O	2.0	<50% conversion
6	**DMF**	**10% (v/v) H_2O**	**2.0**	**1:1 Product:SM**
7	DMF	10% (v/v) H_2O	3.0	No conversion

Methyl ester **95** was first hydrolyzed under basic aqueous conditions which resulted in significant decomposition, giving carboxylic acid **101** in 30% yield (Scheme 25). The optimized T3P protocol was then applied and successfully delivered hydroxamic acid **6** in low yields. Analysis of the crude product showed that roughly 50% conversion was achieved but difficulties in extracting the highly polar product led to diminished yields. Despite the low yielding final steps, hybrid AFP-458 (**6**) was obtained in acceptable quantities for biological evaluation.

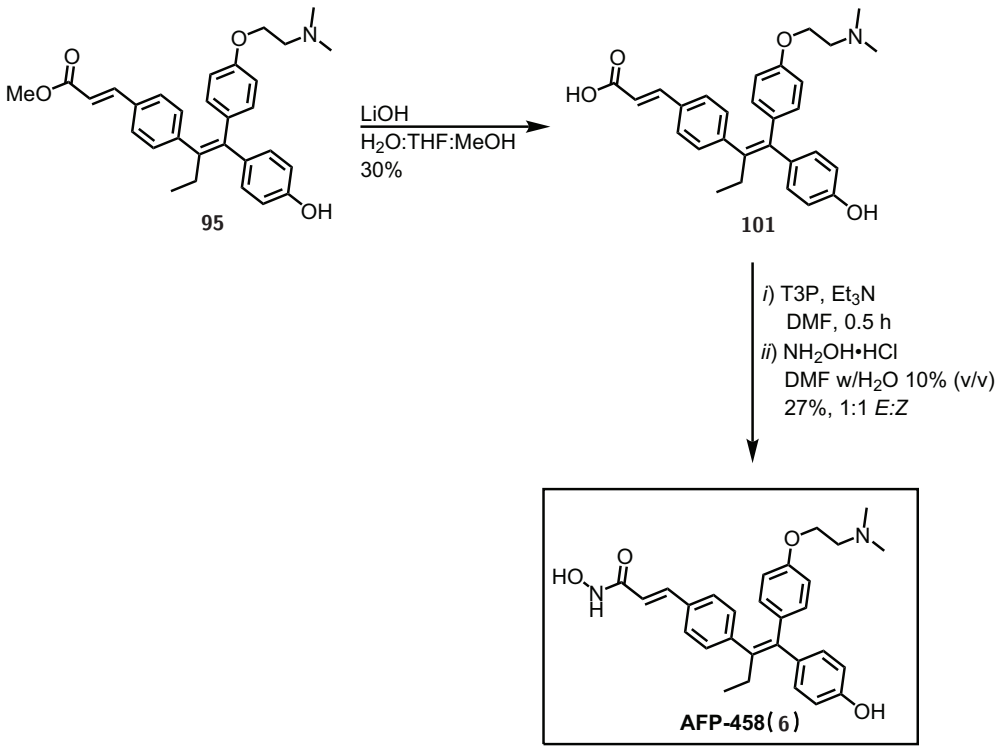

Scheme 25: Synthesis of carbon-linked hybrid AFP-458 (**6**) using T3P.

2.2.2 Synthesis of Oxygen-Linked B-Ring Substituted Hybrids

The synthetic route used to access the carbon-linked hybrids was directly applied to the oxygen-linked variants, with the exception of the late-stage Suzuki/Grubbs functionalization. Beginning with the phenol intermediate **74** generated from the 3-component coupling, the remaining hybrids were readily accessible.

Alkylation of phenol **74** was first attempted using K_2CO_3 in MeCN but there was no evidence of product formation (Scheme 26). Instead, NaH was used to fully generate the anion but no reactivity was observed in DMF, whereas the same conditions in THF led predominantly to N-alkylation and little no formation of the desired O-alkylation product **102**. Interestingly, the addition of NEt_3 to the reaction mixture mitigated N-alkylation and favoured the desired O-alkylated product **102** in 65% yield. Following the alkylation, benzyl ether deprotection and hydroxamic acid formation proceeded in 99% and 45% yields, respectively, to give **10** as a 1:1 mixture of *Z:E* isomers. The same sequence was applied to

the synthesis of the five carbon oxygen-linked variant, yielding **11** as a 1:1 mixture of *E:Z* isomers in similar yields.

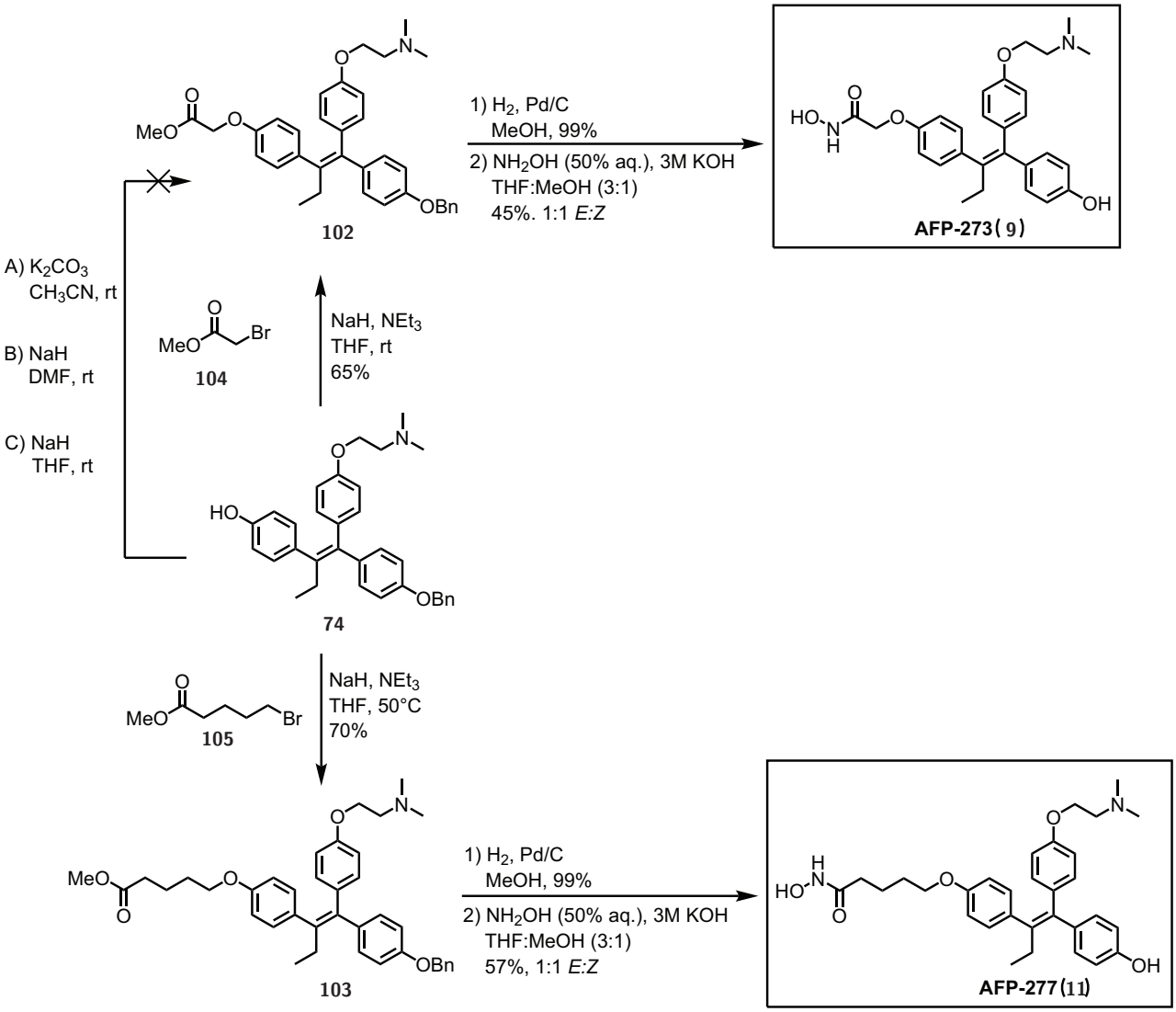

Scheme 26: Synthesis of oxygen-linked hybrids AFP-273 (**9**) and AFP-277 (**11**).

The shift in reactivity upon the addition of NEt_3 to the alkylation conditions may be explained by the formation of a highly electrophilic quaternary ammonium salt between NEt_3 and methyl bromoacetate. The N-alkylated species **74** would serve as an efficient electrophile for NEt_3 alkylation and both processes would be reversible, however alkylation of the phenolate via the $NEt_3R^+Br^-$ intermediate would be irreversible and net a thermodynamically stable product. Although many examples of quaternary ammonium salts as electrophiles

exist, this explanation fails to account for the inability of the strongly electrophilic β-oxy-N-alkylammonium intermediate to act as a suitable electrophile for phenolate alkylation.

Synthesis of the final oxygen-linked hybrid began with the alkylation of phenol **74** with TBS protected alkyl halide **106**. While this provided ether **107** poor yields (24%) limited material throughput (Scheme 27). An alternative approach appended the three carbon chain using monoprotected diol **108** with a Mitsunobu reaction followed by a TBS deprotection with TBAF to afford free alcohol **109** in 44% yield. Persistent tetraalkylammonium salts, either TBAF or byproducts of TBAF, were removed using DOWEX50WX8-400 resin and $CaCO_3$ mediated workup described by Kaburagi and Kishi.[29] Attempts at oxidizing the free alcohol were unsuccessful as PDC oxidation gave only complex mixtures of products and oxidation with DMP yielded an aldehyde that reverted to phenol **74** upon purification via an acid catalyzed β-hydroxy elimination.

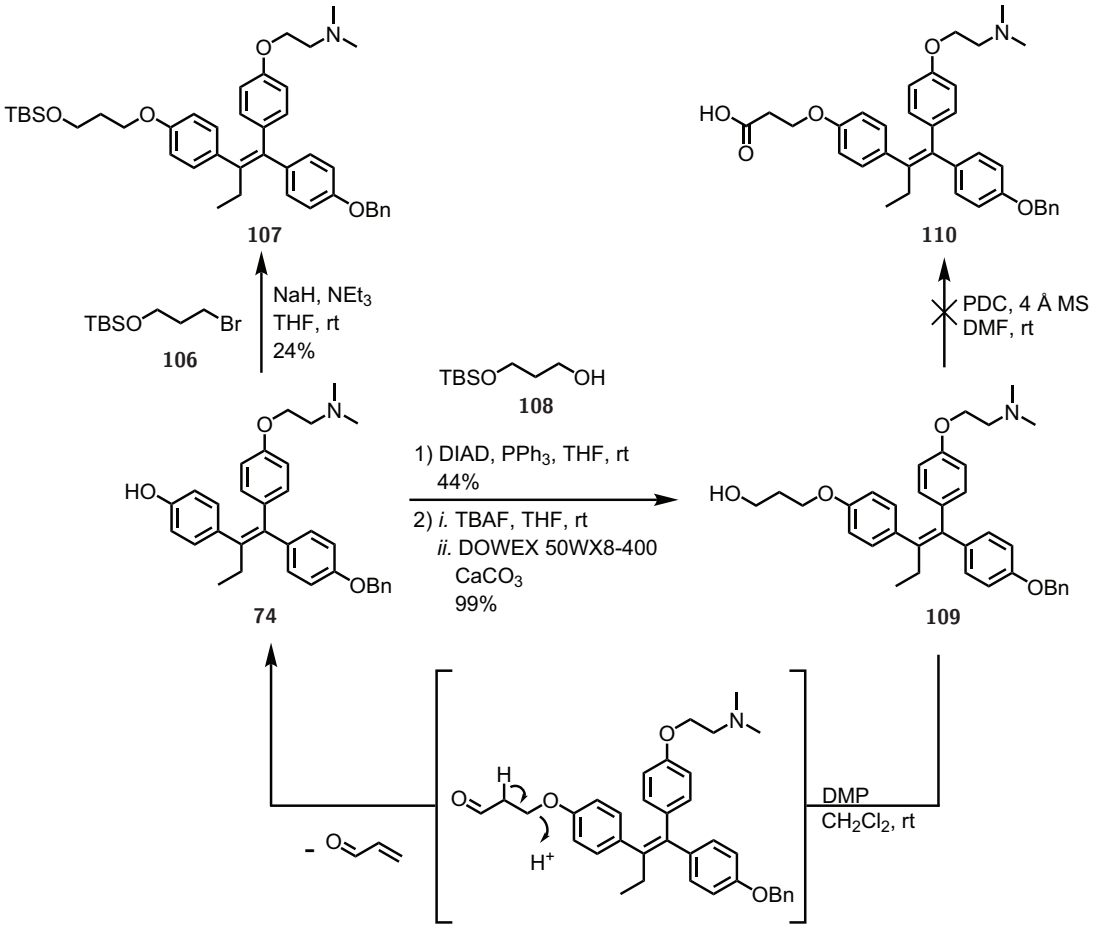

Scheme 27: Alkylation of **74** to access AFP-3CO-PHEN (**10**).

An alternate strategy was devised using a Mitsunobu reaction with a linker at the appropriate oxidation state to form **111** directly (Scheme 28). An acid catalyzed hydrolysis of 3-hydroxypropionitrile yielded the Mitsunobu coupling partner **112**. Unfortunately, the coupling failed to deliver the desired methyl ester **111**. Instead, elimination of the high energy oxonium intermediate **113** to methyl acrylate and triphenylphosphine oxide prevailed as the dominant reaction pathway.

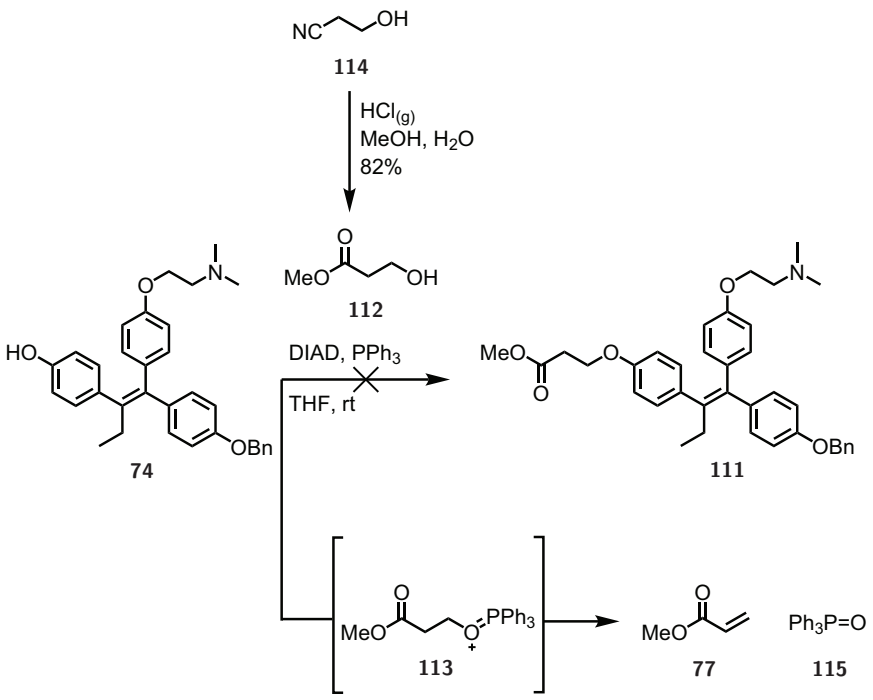

Scheme 28: β-hydroxy elimination hindered synthesis of AFP-3CO-PHEN (**10**).

The troublesome issue of β-hydroxy elimination had plagued both synthetic strategies in accessing the final oxygen-linked hybrid, and the strongly basic conditions that would be required to form the hydroxamic acid from methyl ester **111** would likely induce the same effect. As a result, we decided to purify each successfully synthesized hybrid by preparatory HPLC and then proceed with the biological testing of the desired isomers.

2.3 Biological Evaluation of SERM/HDACi Hybrids

2.3.1 Biological Evaluation Assays

Following the synthesis of hybrid SERM/HDACi molecules **5**, **6**, **7**, **8**, **10**, and **11**, the compounds were purified by preparatory HPLC to obtain the desired isomer. Despite considerable efforts, only compounds **5**, **6**, **8**, and **11** were successfully purified to give the desired *Z* isomers in >95% purity. Fluorogenic HDACi assays were conducted within the Gleason lab by the author following an assay methodology adapted for high throughput screening outlined by Schwienhorst *et al.* and modifications that outlined by Mazitschek *et al.* and

Olsen *et al.*[30–32] Additionally, samples of each compound were submitted to our collaborators at the Université de Montréal for cell-based BRET and luciferase transactivation assays in order to determine ER affinity and antagonism, respectively. Upon submission of this thesis, the ER assays have not yet been fully completed.

2.3.2 Fluorogenic HDACi Assay

The fluorogenic *in vitro* HDACi assay developed by Schweinhorst *et al.* involves a two-step enzymatic process (Figure 2.12).[30,33] In place of histone, the HDAC of interest is incubated with a peptide-derived substrate containing an ϵ-acylated lysine residue and 7-amino-4-methylcoumarin (AMC). Uninhibited HDAC deacetylates the ϵ-amino group of lysine to produces a substrate that can be recognized and cleaved by trypsin. Addition of trypsin to the assay following the incubation period leads to hydrolysis of the AMC-lysine amide bond within the substrate and the release of fluorescent AMC which is then measured using a standard 96-well plate reader (λ_{ex} = 390 nm and λ_{em} = 460 nm). The fluorescence is proportional to the amount of substrate that has been degraded by HDAC. In the context of inhibition, an IC_{50} can be derived from the attenuation of fluorescence brought on by inhibition of HDAC, where a potent inhibitor would lead to a significant reduction in fluorescence. SAHA was used as a positive control and to determine viability of the assay, and E2 was used as a negative control.

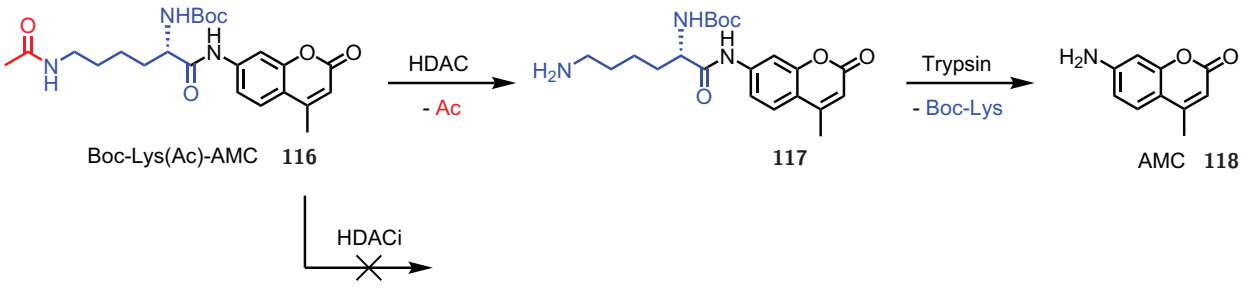

Figure 2.12: Two-stage enzymatic HDAC assay to measure HDAC inhibition.

The peptide substrate **116** originally used by Schweinhorst *et al.* was later modified by Mazitschek *et al.* in order to improve assay sensitivity during their investigation of the less

active class IIa HDACs[31] (Figure 2.13). The authors synthesized modified substrate **119** containing an Ac-Leu-Gly dipeptide in place of a Boc group and reported it to have a higher HDAC affinity. The higher affinity substrates lowered the amount of protein needed per well in each assay and was chosen for use by the Gleason group for the fluorogenic HDACi assays.

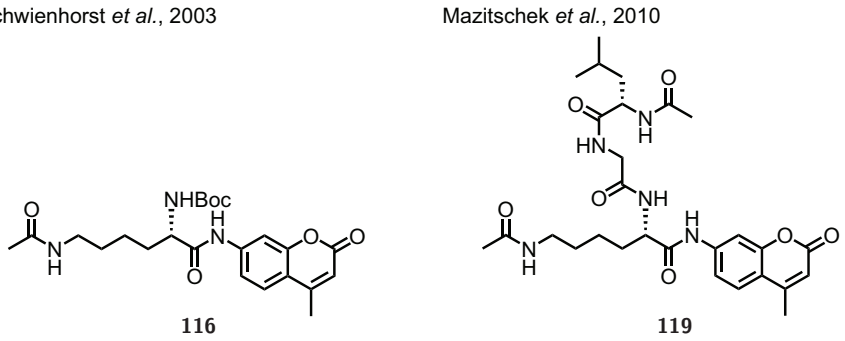

Figure 2.13: First and second generation pro-fluorescent HDAC substrates.[30,31]

2.3.3 ER Assays

The ER affinity of the hybrids would be examined using two cell-based assays that will be conducted in the Mader laboratory. ER affinity will be determined using a BRET assay whereas ER antagonism will be investigated using a luciferase transactivation assay. BRET is a naturally occurring phenomenon that is the result of non-radiative energy transfer between a donor-acceptor protein pair that are within <100 Å of each other.[34] The donor protein, derived from a luciferase, catalyzes the oxidation of a molecule of coelenterazine and which results in emission at 480 nm. The emissive light excites the proximal acceptor protein which then emits a second photon with a Stoke's shift greater than that of the original Stoke's shift of the donor protein. The detectable change in emission wavelength is thereby proximity-based and corresponds to the occurrence of a protein-protein interaction.[35] In this case, HEK293 cells were transfected with the donor-acceptor pair *Renilla* luciferase (RLucII) fused ERα and yellow fluorescent protein (YFP) fused SRC1 protein, respectively. SRC1 is a LXXLL motif containing a nuclear coactivator that is known to interact with ERα upon activation by agonists such as E2.[36] RLucII emits at 480 nm upon oxidation of a molecule of coelenterazine which results in the excitation of YFP and the subsequent emission at 530

nm.[37] The BRET[1] ratio is measured as the ratio of emitted light at 530 nm to 480 nm, which corresponds to the degree to which the protein-protein interaction is occurring. Using BRET, a dose response analysis of ER inhibition by the hybrid SERM/HDACis in the presence of E2 will be used to determine the IC_{50} values of each hybrid.

Cell-based luciferase transactivation assays will be the final component in determining whether the hybrids exhibit ER antagonism. In a reporter gene assay, a cell line is engineered to incorporate a reporter gene, which contains the genomic information for a reporter protein, downstream of a promoter gene.[38] The reporter protein luciferase is commonly used in transactivation assays; the oxidation of luciferins by luciferase is used as a means to generate a detectable signal in the form of fluorescence. Placement of the reporter gene downstream of a response element ensures that synthesis of the reporter protein is dependant on the activation of a protein-mediated transduction relay. Activation of the relay results in gene transcription and consequently the generation of fluorescence by luciferase-catalyzed oxidation of luciferin. T47DKBLuc cells will be transfected with an ERα vector, an ERE3-TATA-Luc reporter vector, and a cytomegalovirus (CMZ)-β-galactosidase vector which will serve as an internal control. Competitive and non-competitive transactivation assays involving the SERM/HDACi hybrids and E2 will be conducted to determine whether or not the hybrids exhibit antagonistic character. Potent antagonists will prevent activation of the ER in the absence or presence of E2 and will thereby attenuate fluorescence, while agonists will increase luciferase expression and fluorescence output.

2.4 Biological Results and Discussion

2.4.1 Fluorogenic HDACi Assay

The *Z* isomers of the four final compounds (**5**, **6**, **8**, and **11**) were evaluated against HDACs 3 and 6 to determine their IC_{50} and K_i values. SAHA and E2 were used as positive and negative controls, respectively, and eight hybrid inhibitor concentrations were used to generate a dose-response curve. Each assay was run twice using different assay substrate

concentrations in order to approximate K_i values using the Cheng-Prusoff equation.

Gratifyingly, each of the hybrid SERM/HDACi molecules exhibited single digit micromolar IC_{50} values and submicromolar K_i values. The dose-response curves are provided in Figure 2.14 and the IC_{50} and K_i values derived from the curves are provided in Table 4. In general, the results showed that HDACs 3 and 6 tolerated the bulky tetrasubstituted olefin scaffold of the hybrids, although this result is not surprising given the wide variety of capping groups that HDACis are known to possess.[39,40] The apparent selectivity the hybrids showed for HDAC 6 over HDAC 3 may be due to favourable π-stacking between Tyr and Phe residues on the surface of HDAC 6 and the triphenylethylene scaffold.[39] The short-chain hybrids AFP-458 (**6**) and AFP-345 (**5**) showed a 100-fold increase in affinity for HDAC 6 and have IC_{50} values of 0.37 µM and 0.38 µM, respectively. Compared to BMW-275 (**120**) which had an IC_{50} of 71.9 µM, the inclusion of two additional carbon atoms in the side chain led to a 100-fold increase in potency.[3] The significant difference in affinities between one-carbon and three-carbon side-chains can be rationalized by the narrow, hydrophobic tunnel of HDAC. Several instances of HDACi testing have shown that SAHA-like aliphatic side chains frequently surpass short-chain analogues with respect to binding affinity due to their increased ability to access the zinc containing catalytic core.[41] While the flexible side-chain of AFP-345 (**5**) outperformed the rigid, unsaturated analogue AFP-458 (**6**) at inhibiting HDAC 3, both analogues proved equally well at inhibiting HDAC 6. AFP-277 (**11**) showed relatively moderate HDAC 3 and 6 IC_{50} values, 1.83 µM and 0.64 µM, respectively, despite its six-atom side chain. AFP-477 (**7**) was the most potent of the series for both HDACs 3 and 6, with IC_{50} values of 0.69 µM and 0.25 µM.

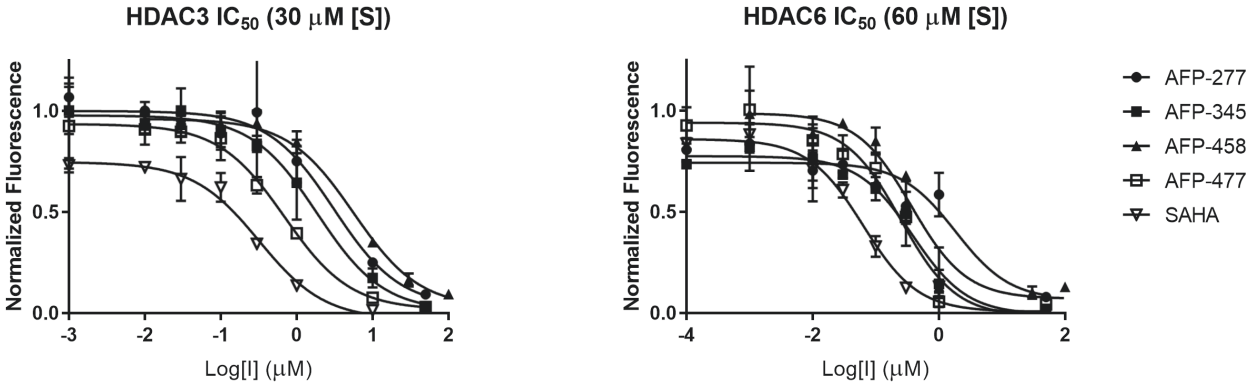

Figure 2.14: Dose response curves of HDACs 3 and 6 treated with hybrid SERM/HDACis.

Table 4: HDACs 3 and 6 fluorogenic HDACi assay results.

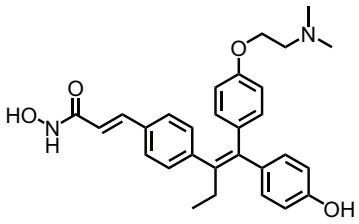

AFP-458 6

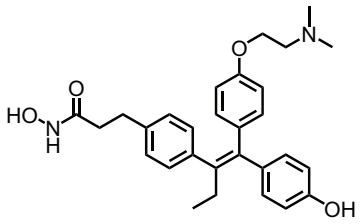

AFP-345 11

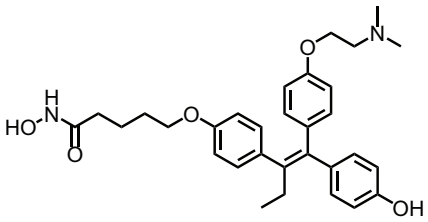

AFP-277 11

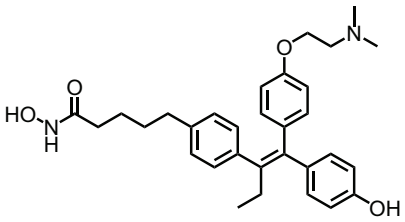

AFP-477 7

	HDAC 3		HDAC 6	
	IC_{50} (μM)	K_i (μM)	IC_{50} (μM)	K_i (μM)
AFP-458	5.64	1.61	0.37	0.13
AFP-345	1.87	0.53	0.38	0.13
AFP-277	3.1	0.88	1.83	0.64
AFP-477	0.69	0.20	0.25	0.086
SAHA	0.11	0.031	0.050	0.017

The five-fold difference in potency between AFP-477 (**7**) and AFP-277 (**11**) is likely attributed to a combination of the single atom difference in side-chain length and the atom connectivity of the side-chains to the hybrid core. The ether bridge of AFP-277 (**11**) may participate in a hydrogen bonding interaction at the ridge of the hydrophobic tunnel, stabilizing the molecule and decreasing the effective length of the HDACi side chain. The methylene linker of AFP-477 (**7**) is unable to form such hydrogen bonds and binding relies predominantly on hydrophobic interactions within the tunnel and chelation of the Zn^{2+} atom for stability. The lack of a polar functionality on the side chain of AFP-477 (**7**) thereby improves its ability to penetrate the hydrophobic tunnel, whereas the affinity of AFP-277 (**11**) is mitigated by such an interaction. An analogue of AFP-277 (**11**) that preserves the ether bridge and includes a six or seven carbon atom chain may benefit from the polar interaction while being long enough to fully occupy the hydrophobic tunnel.

A similar trend was observed by Benjamin Williams in his biological evaluation of the C-ring substituted hybrids.[3] C-ring substituted hybrids BMW-79b (**2**) and BMW-94a (**121**) both contained ether bridges between the aliphatic linker and scaffold and had a three-carbon difference in side chain length (Figure 2.15). BMW-94a (**121**) was twice as potent as BMW-79b (**2**), suggesting that the hydrogen bonding interaction persisted while the length increase granted BMW-94a greater tunnel penetration. The same trend was observed once more in the amide-linked hybrids BMW-255 (**122**), -185 (**123**), and -243 (**124**), where a longer aliphatic chain improved HDAC 6 affinity by a factor of 3 in the case of a two carbon length increase. While conclusions cannot be drawn from direct comparisons of the B- and A/C-ring substituted hybrids as they differ significantly in their structures, the trends lend insight into the design of future B-ring substituted analogues.

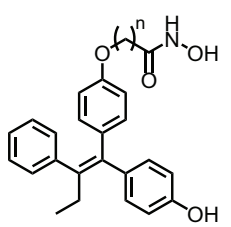
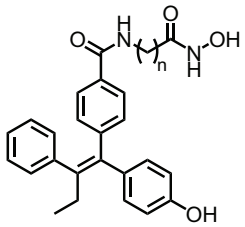

2	BMW-79b: n = 2	IC_{50} = 2.90 uM	**122**	BMW-225: n = 1	IC_{50} = 144 uM
121	BMW-94a: n = 5	IC_{50} = 1.07 uM	**123**	BMW-185: n = 4	IC_{50} = 0.99 uM
			124	BMW-243: n = 6	IC_{50} = 0.37 uM

Figure 2.15: Ether and amide bridged C-ring substituted analogues and their HDAC 6 affinities.

2.4.2 ER Assays

The antagonism profile of each hybrid was investigated using luciferase assays, and their affinity for the ER was determined using BRET experiments across a range of inhibitor concentrations. Throughout the experiments, endoxifen and 4-OHT were used as positive controls while E2 was used as the negative control and the competitive agonist. Two luciferase transactivation experiments were conducted using YFP-fused SRC1 protein and with YFP-fused receptor interacting domain (RID) protein. Substrate concentrations of E2 were 5 nM and 5 µM of an antiestrogen. The BRET assays were conducted using YFP-SRC1 and a 12-point inhibitor concentration range to generate a dose-response curve from the BRET[1] measurement.

Each of the hybrids showed antagonistic activity with respect to the ER in the absence and presence of E2 in both luciferase assays (Figure 2.16 blue bars). Hybrids AFP-277 (**11**), -345 (**5**), -458 (**6**) and -477 (**7**) exhibited very similar degrees of antagonism relative to both endoxifen and 4-OHT. In the presence of E2 (Figure 2.16 red bars), each of the hybrids maintained their antagonistic character but to a lesser extent than the positive controls with the exception of AFP-477 (**7**). AFP-477 (**7**) was remarkable in that its profile was comparable to 4-OHT in both the RID and SRC1-containing transactivation assays. The positive results from these assays strongly support the hypothesis that the ER is capable of facilitating the HDACi side chain while still being strongly affected by the antagonistic character of the SERM pharmacophore.

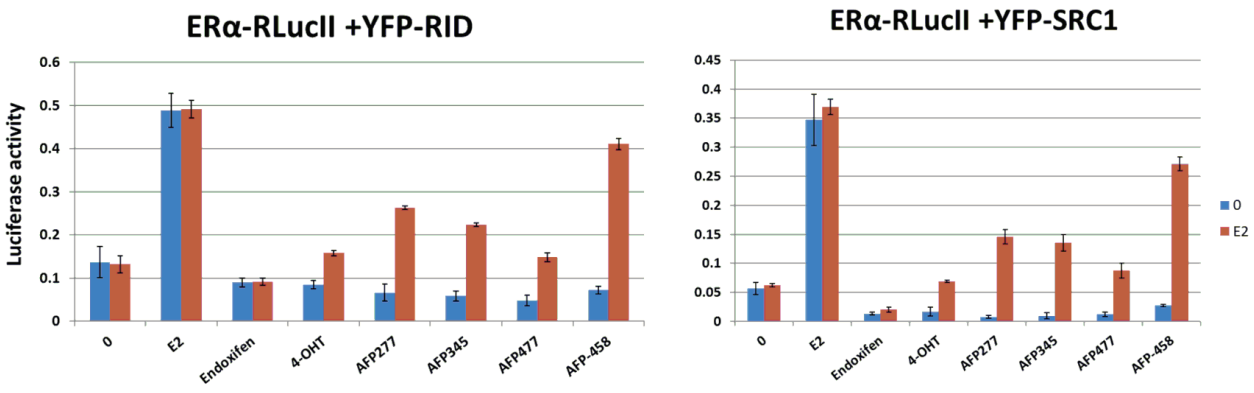

Figure 2.16: Luciferase transactivation assay results for each hybrid SERM/HDACi in the presence (red bars) and absence (blue bars) of E2.

BRET dose-response experiments were conducted in order to determine the IC_{50} values for each of the hybrids alongside 4-OHT (Figure 2.17). In general, the results of the BRET experiments correlated reasonably well with the luciferase transactivation assays. Each hybrid displayed an IC_{50} value in the submicromolar range, with the exception of AFP-345 (**5**) which had a moderate single digit IC_{50} of 1.94 µM. Hybrids AFP-277 (**11**) and -477 (**7**) displayed promising IC_{50} values of 0.802 µM and 0.818 µM, respectively, and were comparable to that of 4-OHT which had a measured IC_{50} value of 0.502 µM. While AFP-458 (**6**) displayed a surprisingly low IC_{50} value of 0.185 µM, this data contradicts that of the luciferase transactivation assay and of the docking scores initially determined during the virtual design phase of the project. AFP-458 (**6**) was unable to fully antagonize the ER in the presence of E2 while the remaining hybrids, each of which displayed lower ER affinities, were capable of antagonizing the ER to a much greater extent. The contradiction cannot fully be explained at this point, but follow-up investigations into hybrid **6** are unlikely due to its poor HDAC 3 inhibitory activity and the promising ER and HDACi activity of the other hybrids.

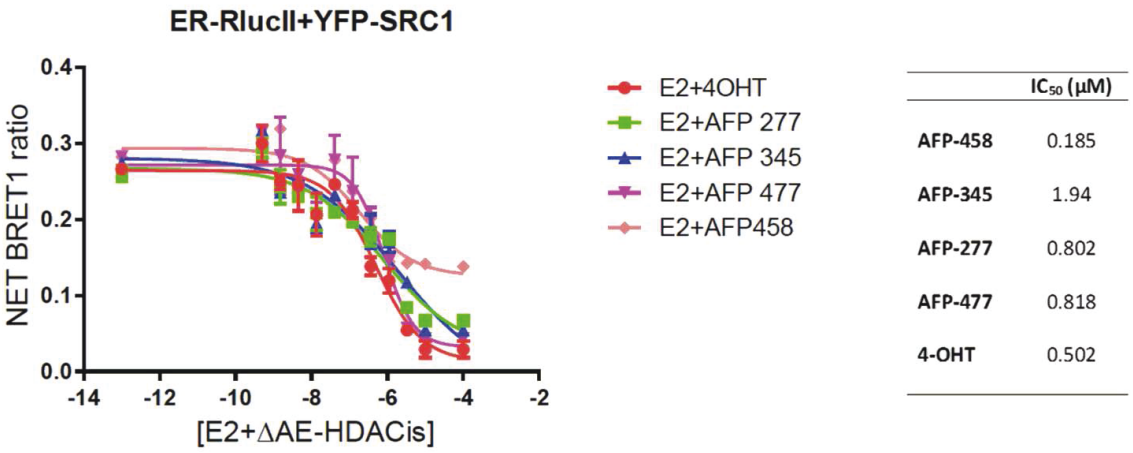

	IC_{50} (μM)
AFP-458	0.185
AFP-345	1.94
AFP-277	0.802
AFP-477	0.818
4-OHT	0.502

Figure 2.17: BRET[1] dose-response curves and the ER IC_{50} values for SERM/HDACi hybrids.

Four and seven day MCF-7 cell growth curves were constructed in order to determine whether the hybrids displayed antiproliferative effects compared to SAHA and 4-OHT (Figure 2.18). MCF-7 cells were cultured in alpha minimal essential medium (AMEM) supplemented with 5% fetal bovine serum (FBS) and then treated with the SERM/HDACi hybrids. Tamoxifen, 4-OHT, endoxifen, and SAHA were each used as positive controls throughout the experiments. While each hybrid showed comparable potency with respect to 4-OHT and endoxifen, AFP-477 (**7**) exhibited higher cytotoxicity relative to the positive controls over both four and seven days. Despite lower ER affinity and comparable antagonism compared to 4-OHT throughout the enzymatic BRET assays, AFP-477 (**7**) was highly competent in the *in vitro* cell assays.

The potent antiproliferative effects of AFP-477 against MCF-7 cells compared to 4-OHT and tamoxifen despite the 60 % difference in IC_{50} values (0.502 μM for 4-OHT and 0.818 for AFP-477) is suggestive of a functional dual inhibitor that is capable of acting on separate pathways of MCF-7 cells. A lower IC_{50} for the ER would translate to diminished antiproliferative effects when compared to 4-OHT if a compound with a single pharmacophore was considered. In this case, AFP-477 contains two functional pharmacophores, and exhibited submicromolar HDACi activity (0.69 μM for HDAC 3 and 0.25 μM for HDAC 6) which effectively led to a net overall increase in cancer cell cytotoxicity. This argument

is further strengthened by the cell growth curve data of hybrids AFP-458, -345, and -277. Although they did not exceed the positive control compounds, each hybrid exhibited modest antiproliferative effects comparable to those of the controls. In each case, the hybrids possessed lower ER affinity relative to 4-OHT, and lower affinities for HDACs 3 and 6 relative to AFP-477 (1.87 - 5.64 µM for HDAC 3 and 0.37 - 1.83 µM for HDAC 6) but the dual inhibitor character was apparent in their antiproliferative profile.

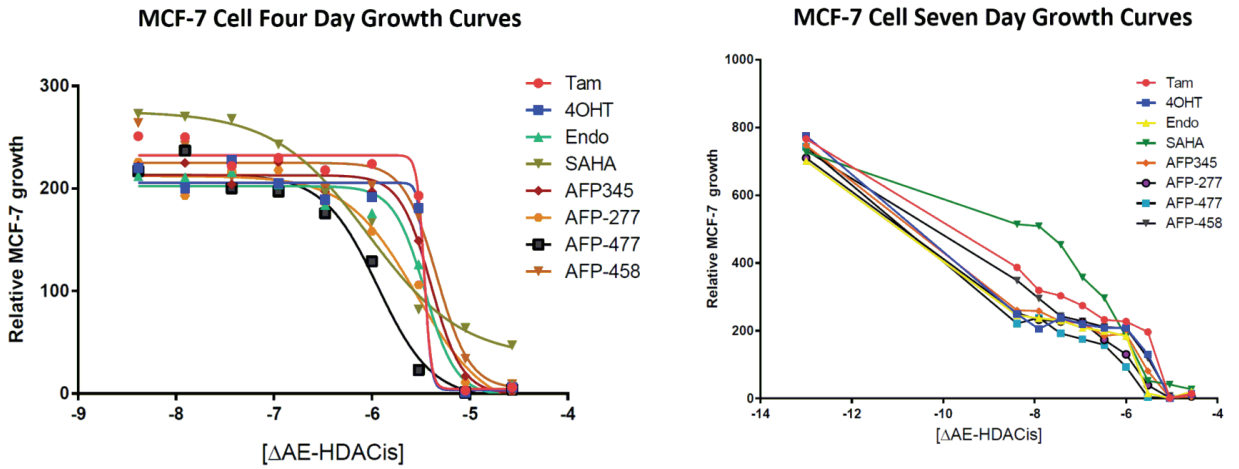

Figure 2.18: Four and seven day MCF-7 cell growth curves after treatment with positive controls and hybrid SERM/HDACis.

The antagonistic profile, ER affinity, and antiproliferative character of the SERM/HDACi hybrids towards MCF-7 breast cancer cells have been evaluated. Luciferase transactivation assays showed that each hybrid exhibited potent antagonistic activity toward the ER in the absence of E2. The antagonism profile of AFP-477 was similar to that of a potent antagonist 4-OHT. The IC_{50} values of each hybrid were submicromolar, with the exception of AFP-345, and similar to that of 4-OHT as determined by BRET[1] titration experiments. The positive results of the enzymatic assays extended to the four and seven day MCF-7 cell growth assays, in which each of the hybrids performed similarly to 4-OHT, tamoxifen, and endoxifen. Most notably, AFP-477 outperformed each of the positive controls over both four and seven days despite its lower ER affinity. Coupled with submicromolar HDAC inhibition values for both HDAC 3 and 6, the impressive antiproliferative potency of AFP-477 can be attributed to its dual-nature design and its ability to affect multiple proliferative pathways. These results

further strengthen the outlook of the hybrid SERM/HDACi project and showed that the ER binding pocket is capable of tolerating a second active pharmacophore built into an antiestrogen. The hybrid design principle indeed lead to a molecule of greater potency, AFP-477, than known drugs containing a single pharmacophores such as 4-OHT and endoxifen.

Summary and Conclusions

The development of effective and non-invasive therapies for breast cancer has progressed on several fronts throughout the century. SERMs have played a monumental role in the treatment of breast cancer and combination therapies involving other drug classes are gaining popularity due to their increased potency and ability to overcome endocrine resistance. Several projects within our group have focused specifically on the development of hybrid SERM/HDACi molecules that target two distinct proteins which have been strongly implicated in breast cancer.

The early stages of this project focused on developing a virtual library of B-ring substituted hybrid SERM/HDACi analogues using a 4-OHT scaffold. The general hybrid design was based on the combination of two distinct pharmacophores, the ER antagonist 4-OHT and the HDAC inhibitor SAHA. The basis for the investigation of B-ring substitution and its effects on the ER and HDAC were based on the findings of prior projects conducted by several former members of the Gleason lab. Using *FITTED*, the molecular docking software made available by the Moitessier lab, the binding affinity of the virtual hybrids for the ER were calculated based on a force-field scoring function and ranked according to their energy minimized poses within the binding cavity of an ER crystal structure. A series of seven B-ring substituted hybrids were selected for synthesis based on a combination of their docking results and their synthetic feasibility. Hybrids AFP-345 (**5**) and -458 (**6**) contained a three carbon side chain, the former being fully saturated and the later containing an olefin. AFP-477 (**7**) contained a saturated five carbon side chain and AFP-374 (**8**) contained a monounsaturated five carbon side chain. AFP-273 (**9**), -3CO-PHEN (**10**), and -277 (**11**) contained a two, three, and five carbon side chain, respectively, and were joined to the scaf-

fold via an ether bridge.

The initial synthetic strategy used to access the B-ring substituted hybrids utilized a McMurry cross-coupling as the key step to construct the tetrasubstituted olefin core. Unfortunately, an early stage *O*-alkylation of 4,4'-dihydroxybenzophenone was particularly low yielding and limited the material throughput required for the derivatization of late stage intermediates. Alternative strategies to access the McMurry precursor in larger quantities to increase material throughput were attempted but were ultimately unsuccessful. A second generation synthetic strategy using a one-pot nickel-catalyzed three-component coupling of an internal alkyne, aryl magnesium bromide, and an aryl iodide was then developed and successfully executed. The newly constructed scaffold then underwent a Suzuki cross-coupling and subsequent Grubbs' cross-metathesis sequence to eventually afford hybrids AFP-345 (**5**), AFP-458 (**6**), AFP-477 (**7**), and AFP-374 (**8**). The scaffold was also used to afford hybrids AFP-273 (**9**) and AFP-277 (**11**) by means of *O*-alkylation with the respective alkyl halide. AFP-3CO-PHEN (**10**) could not be accessed with the strategy due to issues arising from β-alkoxide elimination. Hybrids AFP-345 (**5**), AFP-458 (**6**), AFP-477 (**7**), and AFP-277 (**11**) were successfully purified by preparatory reverse phase HPLC to afford the active geometric isomers which were then evaluated for their biological activity.

Fluorogenic HDACi assays were conducted by the author within the Gleason lab using the purified hybrids. AFP-477 (**7**) proved to be the most potent inhibitor of HDACs 3 and 6 within the library with submicromolar IC_{50} values (0.69 µM for HDAC 3 and 0.25 µM for HDAC 6). The short chain hybrids AFP-458 (**6**) and AFP-345 (**5**) both showed submicromolar IC_{50} potencies for HDAC 6 (0.37 µM and 0.38 µM), and their HDAC 3 affinities were in the low micromolar range (5.64 µM and 1.87 µM). A comparison of AFP-277 (**11**), AFP-477 (**7**), and C-ring substituted hybrids from previous work suggest that a hydrogen bonding interaction at the surface of HDAC 6 can act to stabilize binding at the expense of a longer side chain length.

BRET, luciferase transactivation, and MCF-7 cell growth assays were conducted by the

Mader lab at the Université de Montréal using the hybrid molecules. AFP-477 had an antagonism profile comparable to that of 4-OHT based on luciferase transactivation assays and a high affinity for the ER (IC_{50} of 0.818 µM) as determined by BRET[1] dose-response experiments. AFP-277 and -345 showed moderate antagonism profiles and had IC_{50} values of 0.802 µM and 1.94 µM, respectively. AFP-458 had a poor antagonism profile but a surprisingly low IC_{50} value of 0.185 µM for the ER compared to that of 4-OHT (0.502 µM), prompting further investigation into its inhibitory profile. MCF-7 cell growth assays revealed AFP-477 as an excellent antiproliferative agent that was more potent than 4-OHT, tamoxifen, and endoxifen over both four and seven days. The contrast between the antiproliferative potency of hybrid AFP-477 and its lower affinity for each target compared to their respective gold standard inhibitors (i.e. SAHA and 4-OHT) support the notion of AFP-477 being a hybrid SERM/HDACi that is capable of eliciting a cooperative antiproliferative effect.

Further investigations into the B-ring substituted hybrids will be conducted by future students in the Gleason lab. Future goals can be put forward based on the the findings of this project: *i)* obtain an X-ray crystal structure of AFP-477 bound to the ER in order to confirm its binding mode and compare it to the binding modes of 4-OHT; *ii)* observe the effects of AFP-477 on a SERM resistant breast cancer cell line; *iii)* expand on the B-ring substituted library to include amide and *O*-linked analogues that contain longer side chains so as to affect greater HDAC potency and thereby greater MCF-7 antiproliferative potency; and *iv)* adapt the three-component coupling reaction to heterocyclic components in order to investigate the thiophenyl B-ring series that appeared promising based on docking results.

References

1. Sanchez, R. M. Design, synthesis and biological evaluation of novel antiestrogens. Ph.D. thesis, McGill University, 2013.
2. Lim, L. Effects Towards the Design and Synthesis of Small Molecule Inhibitors of the Estrogen Receptor. M.Sc. thesis, McGill University, 2011.
3. Williams, B. Design, synthesis and evaluation of selective estrogen receptor modulator/histone deacetylase inhibitor merged bifunctional ligands. M.Sc. thesis, McGill University, 2014.
4. Anstead, G. M.; Carlson, K. E.; Katzenellenbogen, J. A. *Steroids* **1997**, *62*, 268–303.
5. Brzozowski, A.; Pike, A.; Dauter, Z.; Hubbard, R.; Bonn, T.; Engstram, O.; Ohman, L.; Greene, G.; Gustafsson, J.; Carlquist, M. *Nature* **1997**, *389*, 753–758.
6. Lawandi, J.; Toumieux, S.; Seyer, V.; Campbell, P.; Thielges, S.; Juillerat-Jeanneret, L.; Moitessier, N. *J. Med. Chem.* **2009**, *52*, 6672–6684.
7. De Cesco, S.; Deslandes, S.; Therrien, E.; Levan, D.; Cueto, M.; Schmidt, R.; Cantin, L.-D.; Mittermaier, A.; Juillerat-Jeanneret, L.; Moitessier, N. *J. Med. Chem.* **2012**, *55*, 6306–6315.
8. Mariaule, G.; Cesco, S. D.; Airaghi, F.; Kurian, J.; Schiavini, P.; Rocheleau, S.; Huskić, I.; Auclair, K.; Mittermaier, A.; Moitessier, N. *J. Med. Chem.* **2016**, *59*, 4221–4234.
9. Moitessier, N.; Pottel, J.; Therrien, E.; Englebienne, P.; Liu, Z.; Tomberg, A.; Corbeil, C. R. *Acc. Chem. Res.* **2016**, *49*, 1646–1657.
10. Englebienne, P.; Moitessier, N. *J. Chem. Inf. Model.* **2009**, *49*, 2564–2571.
11. Shani, J.; Gazit, A.; Livshitz, T.; Biran, S. *J. Med. Chem.* **1985**, *28*, 1504–1511.
12. Coe, P. L.; Scriven, C. E. *J. Chem. Soc., Perkin Trans. 1* **1986**, 475.
13. McMurry, J. E. *Chem. Rev.* **1989**, *89*, 1513–1524.
14. Jordan, V. C.; Haldemann, B.; Allen, K. E. *Endocrinology* **1981**, *108*, 1353–1361.
15. Gauthier, S.; Mailhot, J.; Labrie, F. *J. Org. Chem.* **1996**, *61*, 3890–3893.
16. Detsi, A.; Koufaki, M.; Calogeropoulou, T. *J. Org. Chem.* **2002**, *67*, 4608–4611.
17. Yu, D. D.; Forman, B. M. *J Org. Chem.* **2003**, *68*, 9489–9491.
18. Zheng, L.; Wei, Q.; Zhou, B.; Yang, L.; Liu, Z.-L. *Anticancer Drugs* **2007**, *18*, 1039–1044.
19. Edwards, W. R.; Sibille, E. C. *J. Org. Chem.* **1963**, *28*, 674–679.
20. Kasturi, T. R.; Damodaran, K. M. *Can. J. Chem.* **1969**, *47*, 1529–1535.
21. Knochel, P.; Barl, N. M.; Werner, V.; Sämann, C. *Heterocycles* **2014**, *88*, 827.
22. Xue, F.; Zhao, J.; Hor, T. S. A.; Hayashi, T. *J. Am. Chem. Soc.* **2015**, *137*, 3189–3192.
23. Hesek, D.; Lee, M.; Noll, B. C.; Fisher, J. F.; Mobashery, S. *J. Org. Chem.* **2009**, *74*, 2567–2570.
24. Joshi-Pangu, A.; Wang, C.-Y.; Biscoe, M. R. *J. Am. Chem. Soc.* **2011**, *133*, 8478–8481.
25. Molander, G. A.; Rivero, M. R. *Org. Lett.* **2002**, *4*, 107–109.
26. Woodward, C. P.; Spiccia, N. D.; Jackson, W. R.; Robinson, A. J. *Chem. Commun.* **2011**, *47*, 779–781.
27. Akiyama, T.; Hirofuji, H.; Ozaki, S. *Tetrahedron Lett.* **1991**, *32*, 1321–1324.
28. Ech-Chahad, A.; Minassi, A.; Berton, L.; Appendino, G. *Tetrahedron Lett.* **2005**, *46*, 5113–5115.

29. Kaburagi, Y.; Kishi, Y. *Org. Lett.* **2007**, *9*, 723–726.
30. Wegener, D.; Wirsching, F.; Riester, D.; Schwienhorst, A. *Chem. Biol.* **2003**, *10*, 61–68.
31. Bradner, J. E.; West, N.; Grachan, M. L.; Greenberg, E. F.; Haggarty, S. J.; Warnow, T.; Mazitschek, R. *Nat. Chem. Biol.* **2010**, *6*, 238–243.
32. Villadsen, J. S.; Stephansen, H. M.; Maolanon, A. R.; Harris, P.; Olsen, C. A. *J. Med. Chem.* **2013**, *56*, 6512–6520.
33. Wegener, D.; Hildmann, C.; Riester, D.; Schwienhorst, A. *Anal. Biochem.* **2003**, *321*, 202–208.
34. Dacres, H.; Wang, J.; Dumancic, M. M.; Trowell, S. C. *Anal. Chem.* **2010**, *82*, 432–435.
35. Breton, B.; Sauvageau, É.; Zhou, J.; Bonin, H.; Gouill, C. L.; Bouvier, M. *Biophys. J.* **2010**, *99*, 4037–4046.
36. Kalkhoven, E.; Valentine, J.; Heery, D.; Parker, M. *EMBO J.* **1998**, *17*, 232–243.
37. Hamdan, F. F.; Percherancier, Y.; Breton, B.; Bouvier, M. *Current Protocols in Neuroscience*; John Wiley & Sons, Inc., 2001.
38. Naylor, L. H. *Biochem. Pharmacol.* **1999**, *58*, 749–757.
39. Bertrand, P. *Eur. J. Med. Chem.* **2010**, *45*, 2095–2116.
40. Falkenberg, K. J.; Johnstone, R. W. *Nat. Rev. Drug Discov.* **2014**, *13*, 673–691.
41. Yoshida, M.; Matsuyama, A.; Komatsu, Y.; Nishino, N. *Curr. Med. Chem.* **2003**, *10*, 2351–2358.

Chapter 3: Novel Substrates for the Organocatalytic Cope Rearrangement

3.1 The Cope Rearrangement

Sigmatropic rearrangements have been used extensively in organic synthesis and their scope and utility are being continuously developed. The Cope rearrangement is a [3,3]-sigmatropic shift that was first discovered by Cope and Hardy in 1940 when they observed the formal rearrangement of (1-methylpropenyl)allylcyanoacetate **125** to monoalkyl barbituic acid derivative **126** under high temperature conditions (Figure 3.1).[1] A catalytic variant of the Cope rearrangement was developed by Overman in the 1980s using $PdCl_2$, and later an enantioselective methodology was developed by Gagné *et al.* in 2012 using a chiral gold catalyst.[2–4] Interestingly, few accounts of Lewis acid or Brønstead acid catalyzed Cope rearrangements have been reported.[5–7] Gleason and Kaldre recently reported the first organocatalytic Cope rearrangement of 2-acyl-1,5-dienes using a novel 7-membered cyclic hydrazide carboxylate catalyst that promoted the reaction through reversible iminium ion formation (Figure 3.1).[8] The work focused on the rearrangement of 2-acyl-1,5-diene substrates in which imminium formation was possible due to the unique ability of the diazepane catalyst **127** to tolerate α-branched acyl substrates. This final section will discuss advancements in catalysis of the Cope rearrangement, and will present a project focusing on the synthesis of a novel 3-acyl-1,5-diene substrate that will be used in future projects to expand the substrate scope of the 7-membered ring catalyst developed within the Gleason group.

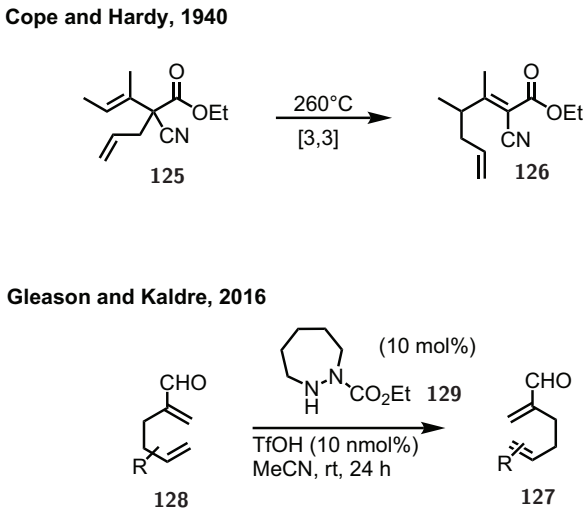

Figure 3.1: First observed thermal Cope rearrangement and the organocatalytic Cope.[1,8]

The concerted mechanism of the Cope rearrangement, put forth by Cope, was analogous to that of the Claisen rearrangement in that an allyl group undergoes an α,γ-shift. The same mode of reactivity was later observed by Berson and Jones in the oxy-Cope rearrangements of 1,5-dien-3-ols.[9] Evans and Golob later found that a 10^{10}-10^{17} rate acceleration of the oxy-Cope rearrangement could be achieved by forming the potassium alkoxide, suggesting that the highly electronegative group further weakened the adjacent carbon-carbon bond (Figure 3.2).[10–12] Even lower reaction temperatures could be achieved with the anionic oxy-Cope with the use of crown-ethers to maximize charge separation.[10,11] While the Cope rearrangement is driven by the thermodynamic stability of the resulting olefin, be it conjugated or more highly substituted, the oxy-Cope and anionic oxy-Cope are driven by the formation of a stable carbonyl or enolate.

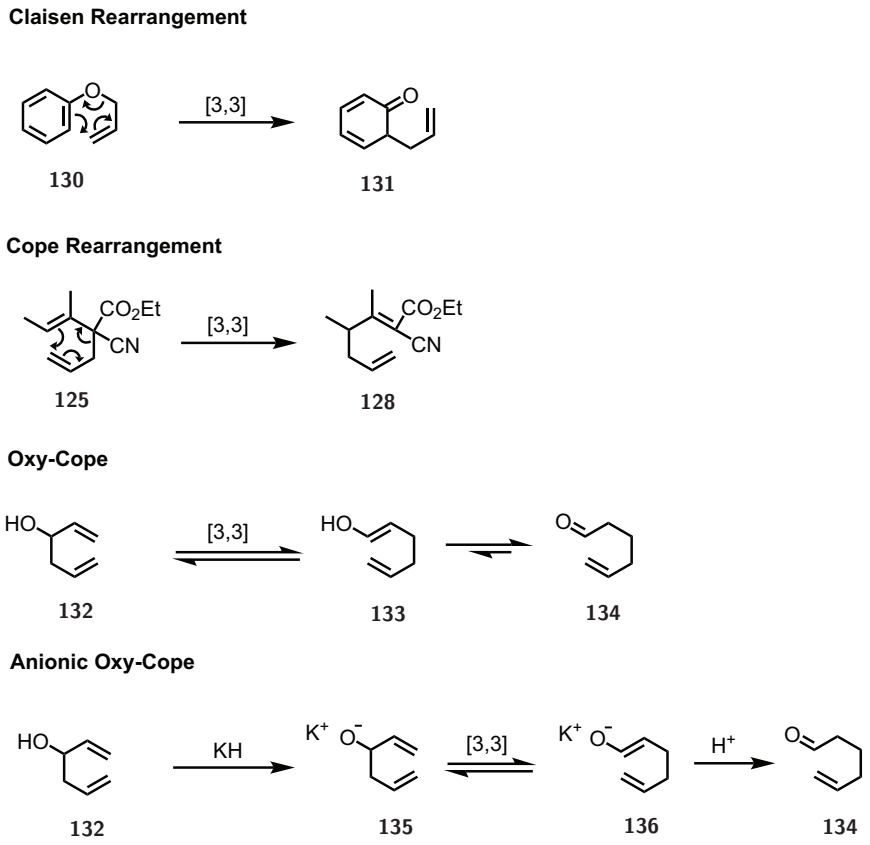

Figure 3.2: Oxy- and anionic oxy-Cope rearrangements of 1,5-dien-3-ol.[9,10]

The mechanism of the Cope rearrangement was the subject of debate and proved difficult to elucidate due to its concerted pericyclic nature and the absence of any detectable intermediates. Doering and Roth showed that the Cope rearrangement of *meso*- and *rac*-3,4-dimethylhexa-1,5-diene led to 99.7% *Z,E*-octa-2,6-diene and 9:1 *E,E-:Z,Z*-octa-2,6-diene, respectively (Figure 3.3). These results implied the rearrangement proceeded through a chair-like transition state whereas an energetically disfavoured boat-like transition ($\Delta\Delta G^{\ddagger}$ = 5.7 kcal/mol) state would have led to opposite outcomes.[13,14] Doering also envisioned three possible transition states consisting of either two independent allyl radicals, an aromatic transition state, or a diradical (Figure 3.3). However, Gajewski and Conrad later showed that the nature of the Cope transition state is highly dependent on the radical stabilizing nature of the substituents and can vary from case to case.[13,15] The Cope is generally accepted to proceed through a concerted, synchronous mechanism with a late transition state in which the substrate adopts the lowest energy conformation.

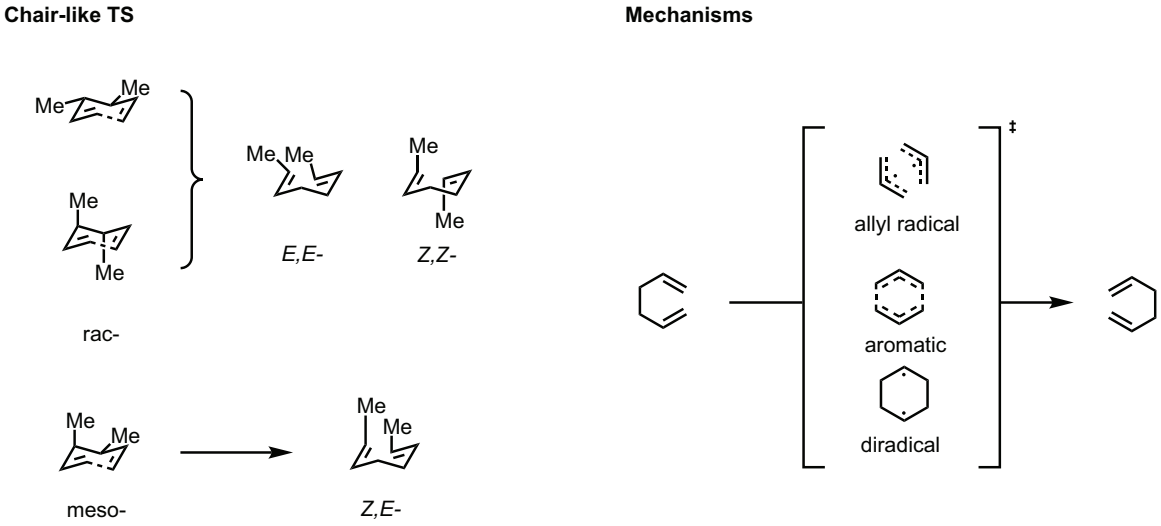

Figure 3.3: Chair-like transition state and allyl radical, aromatic, and diradical mechanisms.[13,14]

Like many pericyclic reactions, the Cope has seen extensive use in synthetic chemistry as a powerful stereospecific carbon-carbon bond forming reaction. In Wender's synthesis of a phorbol ester intermediate **137**, the Cope rearrangement of divinylcyclopropane **138** was strategically used to simultaneously construct a seven membered ring and selectively install a stereocenter at C4 through complementary C4-C8 stereocontrol. Additionally, the formation of enol intermediate **138** under basic conditions set the C4-C10 relative stereochemistry via hydrogen bonding prior to the Cope rearrangement to yield the fused 7,6 ring system of **137** as a single diastereomer.[16] The synthetic utility of the Cope rearrangement has been exemplified in a number of studies since its discovery. However, since the basic reaction typically requires high temperatures (150-200°C), it is poorly suited for thermally unstable substrates and has limited feasibility on industrial scales.[17,18]

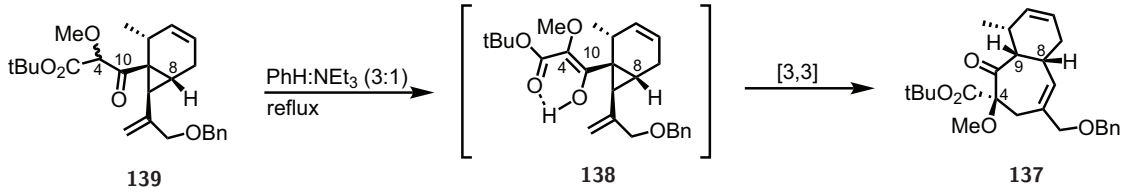

Figure 3.4: Cope rearrangement in Wender's synthesis of phorbol ester intermedate **137**.[16]

3.1.1 Catalytic Cope Rearrangement

Various transition metals have been investigated in efforts to catalyze the Cope rearrangement. Overman reported the first instance of a catalytic Cope rearrangement of acyclic 1,5-dienes using palladium dichloride.[2] In a later study, he found that the $PdCl_2$ catalyzed rearrangement of enantiopure (3*R*,5*E*)-2,3-dimethyl-3-phenyl-l,*S*-heptadiene (**140**) at room temperature to give *Z* and *E* isomers **141** and **142**, respectively, as a 7:3 mixture in 86% yield with complete transfer of chirality (Figure 3.5).[3] The preferential formation of the Z isomer suggests that the $PdCl_2$ catalyzed Cope proceeds through a chair-like transition state as it does in the thermal rearrangement. They proposed the diene **140** is first coordinated by $PdCl_2$ to give the alkene coordination complex **143**. Nucleophilic attack of the uncoordinated olefin onto the terminal carbon of the palladium-alkene adduct would then lead to the cationic intermediate **144**. Fragmentation to intermediate **145** would lead to the thermodynamically stable product **146** upon dissociation from $PdCl_2$. This mechanism invokes a stable chair-like transition state in which the bulky phenyl and palladium substituents are equatorial. The alternate chair-like transition state would lead to the *E* isomer product **147** and be less favoured due to the axial orientation of the phenyl group.[3]

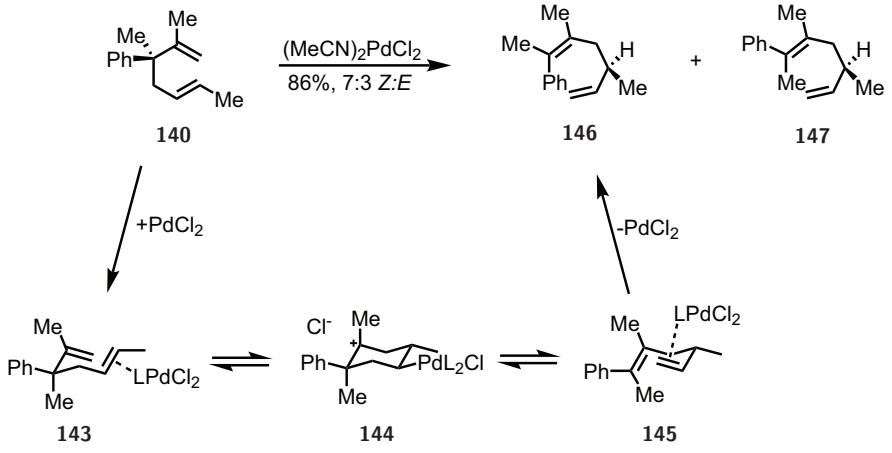

Figure 3.5: $PdCl_2$ catalyzed Cope rearrangement and mechanism proposed by Overman.[3]

Gagné *et al.* reported the first asymmetric catalytic Cope rearrangement of achiral dienes using a chiral $AuCl_2$ catalyst.[4] The group was able to achieve high yields and enan-

tioselectivity using catalytic (*S*)-3,5-xylyl-PHANEPHOS($AuCl_2$) on cyclopropyl hexadiene substrates (Figure 3.6). Although the driving force of the Cope typically relies on the formation of more highly substituted olefins, the work reported by Gagné is different in that the relief of ring strain upon forming an sp^3 from an sp^2 cyclopropyl carbon is favoured and leads to less substituted olefins. DFT calculations suggested that the Au-catalyzed Cope rearrangement occurs through a similar mechanism to that of Overman's Pd-catalyzed variant. Au^I first coordinates to the cyclopropyl-substituted alkene **148** to form a chiral complex and is followed by an intramolecular nucleophilic attack from the neighbouring olefin, forming carbocation intermediate **149**. Fragmentation of the intermediate yields the thermodynamically favoured rearrangement product **150** which can then dissociate from Au^I.[4]

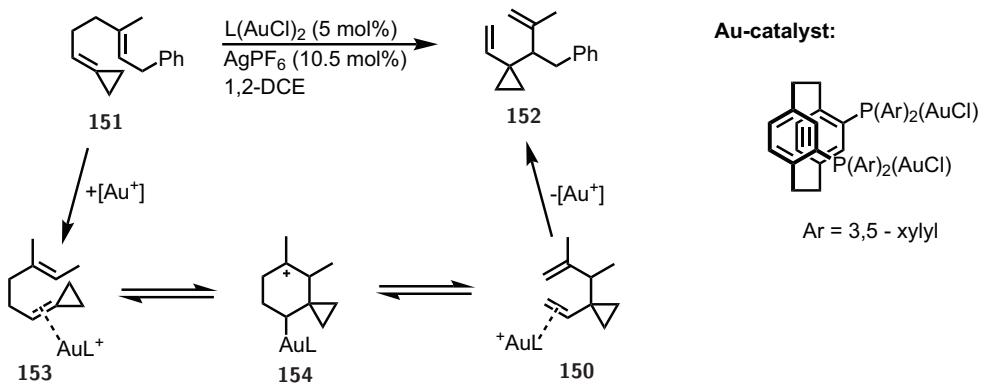

Figure 3.6: Gold catalyzed asymmetric Cope rearrangement and mechanism proposed by Felix *et al.*[4]

While transition metal catalysis of the rearrangement continue to be explored, reports of Lewis or Brønsted acid catalyzed Cope rearrangements are scarce. However, limited reports of acid catalyzed Cope rearrangements suggest metal-free catalysis of the reaction can be achieved. Yates and Eaton reported the rearrangement of oxo-dicyclopentadienes **155** using either H_2SO_4 or $AlCl_3$ and suggested that the driving force of the reaction is likely formation of a conjugated enone species (Figure 3.7).[5] Cookson *et al.* independently reported catalysis of the same rearrangement at elevated temperatures to enone **156**, and they noted that small amounts of $BF_3 \bullet Et_2O$ or HCl were capable of inducing the same rearrangement at room temperature.[6] Dauben and Chollet later reported a Cope rearrangement of 2-acyl-

1,5-diene **157** to the more stable trisubstituted enone **158** using either catalytic TFA or stoichiometric $BF_3 \bullet Et_2O$. In both cases, carbonyl activation was pivotal in accelerating the carbon-carbon bond breaking step. The aforementioned studies inspired the development of an organocatalytic Cope rearrangement of 2-acyl substituted dienes within the Gleason group through the use of LUMO-lowering catalysis.

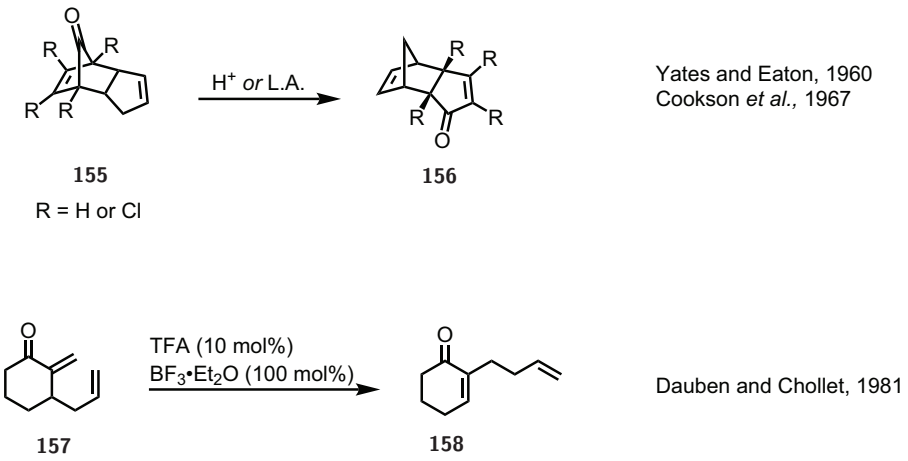

Figure 3.7: Brønsted and Lewis acid catalyzed Cope rearrangements.[5–7]

3.1.2 LUMO-Lowering Organocatalysts

LUMO-lowering catalysis is a concept that is ubiquitous in catalytic frameworks throughout organic synthesis. Lowering the energy gap between the LUMO of an electrophile and HOMO of a nucleophile to lower the activation energy and accelerate a reaction is commonly achieved by forming Lewis acid-base adducts between electrophiles (commonly carbonyls) and an external Lewis acid. The process is rendered catalytic when the Lewis acid is capable of dissociating from the product and forming additional reactive adducts. While Lewis acid catalysis is certainly a vast field, reagents are often sensitive to moisture or require inert atmospheric conditions.

Organocatalysts have become increasingly popular due to their inherent stability and low environmental impact, and significant advances have granted them widespread use. Imidazolidinone organocatalysts were introduced by MacMillan who reasoned that catalytic

LUMO-lowering could be achieved by reversible iminium ion formation. MacMillan initially showed that chiral imidazolidinone catalyst **159** was capable of forming iminium ions with α,β-unsaturated aldehydes such as cinnamaldehyde (Figure 3.8).[19] Under catalytic conditions, activated iminium ion **160** could then undergo Diels-Alder cycloaddition with cyclopentadiene at room temperature to give the bicyclic products in excellent yields (99%), enantiocontrol (93% *ee*) and with 1.3:1 *endo:exo* selectivity.[19] MacMillan later reported a second generation of catalysts that catalyzed enantioselective 1,3-dipolar cycloadditions, intramolecular Michael additions, Friedel-Crafts alkylations, α-chlorinations and α-fluorinations.[20–22] Despite the impressive range of reactivity that the imidazolidinone catalysts demonstrated, they were unable to form iminium ions with substrates that contained α-branching with high efficiency due to steric constraints.

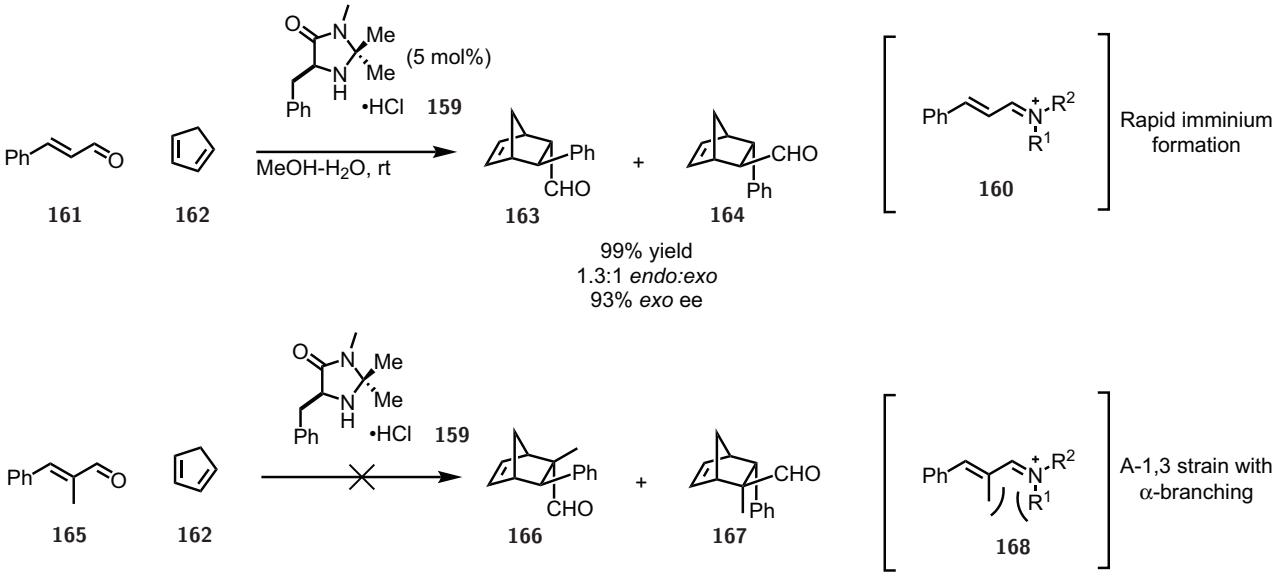

Figure 3.8: Iminium catalyzed Diels-Alder using MacMillans imidazolidinone catalyst **159**.[19]

The possibility of forming iminium ions from hindered enals to elicit LUMO-lowering catalysis of the Cope rearrangements was investigated within the Gleason group by Dainis Kaldre.[23] DFT calculations of 2-acyl-1,5-diene transition state energies supported the idea of LUMO-lowering via iminium ion formation. However, initial attempts to induce the rearrangement with cyclic secondary amines, including MacMillan's catalyst, proved unsuccessful

due to slow iminium ion formation.

The propensity of cyclic and acyclic *N*-acyl hydrazides to form iminium ions rapidly due to the α-effect has been investigated by Tomkinson and Ogilvie.[24,25] Their work inspired the design and synthesis of novel diazepane carboxylate organocatalyst **169** within the Gleason group that was capable of forming iminium ions with α-branched substrates such as in Figure 3.9. The ability is due to a combination of the improved nucleophilicity due to the α-effect, and reduced basicity of the amine which makes the protonaed catalyst a stronger acid, resulting in more efficient carbonyl protonation. The diazepane catalyst catalyzed the Cope rearrangement of 2-acyl-1,5-diene **170** in 83% using TfOH as a co-catalyst. The Cope rearrangement of a variety of other 2-acyl-1,5-dienes were also catalyzed by **170**.[8] The catalyst has also demonstrated its capability in catalyzing polyene cyclizations, Diels-Alder cycloadditions, and Michael additions. Currently, other aspects of reactivity and chiral variants of the diazepane catalyst are being investigated for their enantioinductive effects in these reactions.

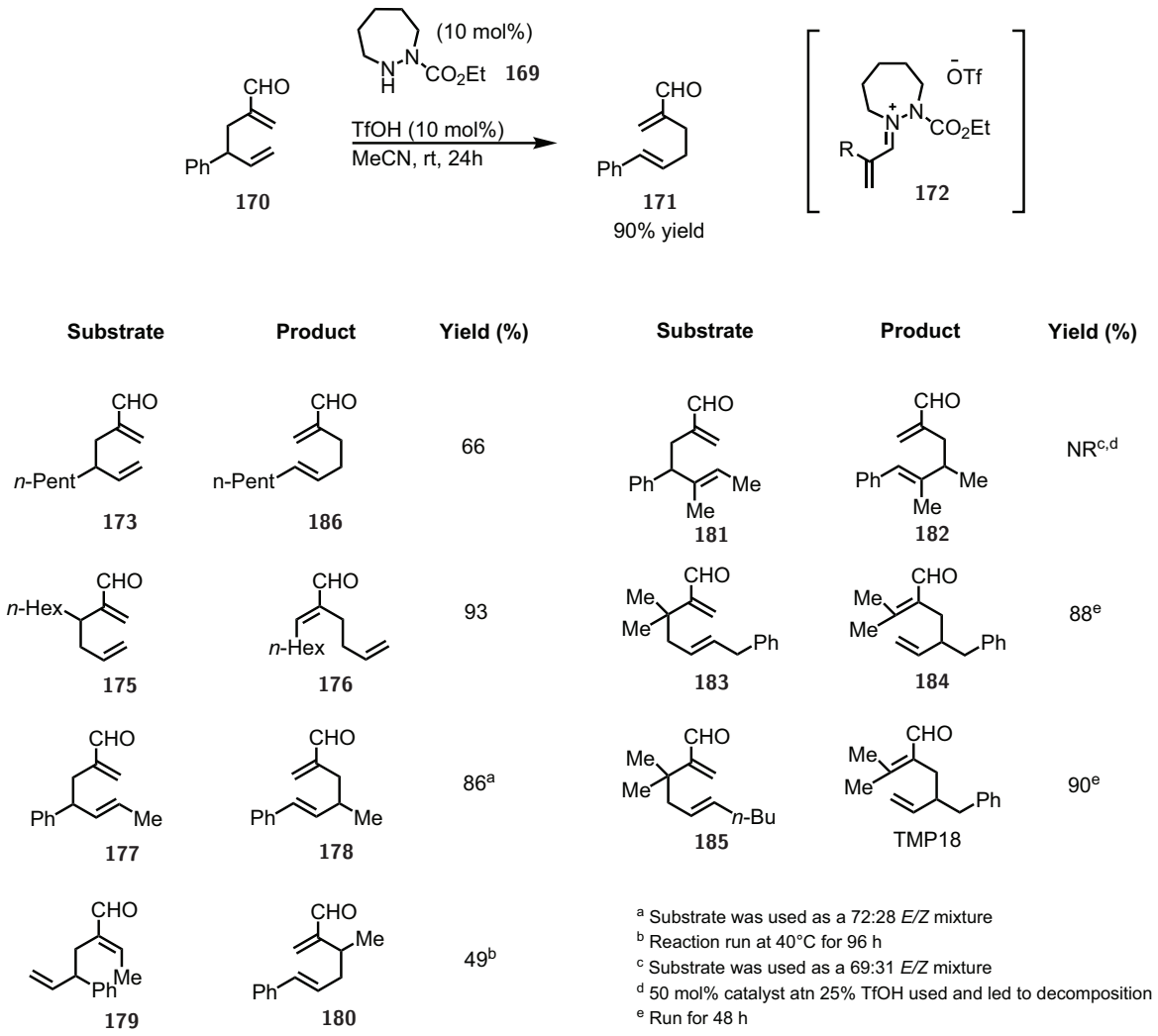

Figure 3.9: Organocatalytic Cope rearrangement using diazepane carboxylate **169** to form α-branched imminium ions and the substrate scope.[8,23]

3.2 3-acyl-1,5-diene Substrates for the Cope Rearrangement

To further expand the scope of the diazepane carboxylate catalyzed Cope rearrangement, we sought to explore 3-acyl-1,5-diene substrates. Very few instances of catalyzed 3-acyl-1,5-diene type substrates have been reported as substrates in the catalytic Cope rearrangement. However, Yates and Eaton and Cookson had described the Cope rearrangement of a cyclic 3-acyl substituted substrate (Figure 3.7).[5,6] Although the alkenes in such a substrate would not have the same LUMO lowering effects found in the 2-acyl series, DFT calculations (J. Gleason) suggested that iminium ion formation would still accelerate the

Cope.

Initially, we targeted aldehyde **187** as a potential substrate for the Cope rearrangement. The synthesis of (*E*)-2-allylpent-3-enal (**187**) began with a Wittig olefination of propionaldehyde to give α,β-unsaturated ester **188** in 54% yield. Unfortunately, initial attempts at deconjugative alkylation of methyl ester **189** led to the formation of an unidentified product, and the volatile intermediate **188** proved difficult to handle.

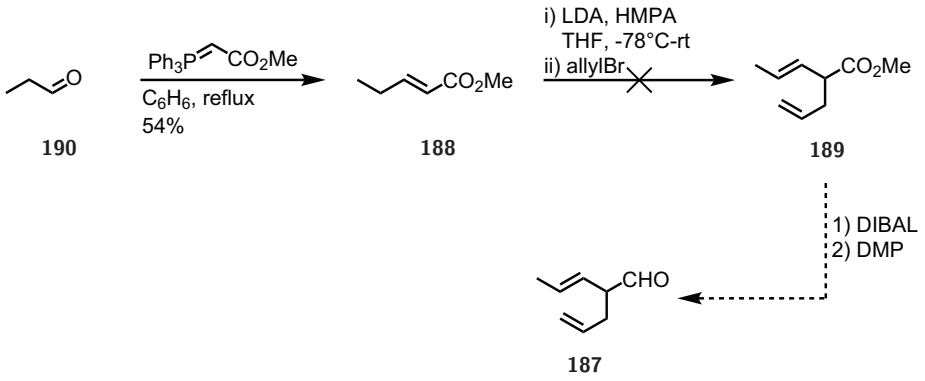

Scheme 29: Synthesis of 3-acyl-1,5-diene **187**.

The substrate was then redesigned to include an additional benzyl group in order to increase its boiling point and simplify its ease of handling. Dihydrocinnamaldehyde (**191**) underwent Wittig olefination to yield ethyl ester **192** in 43% yield which was then subjected to alkylation conditions using LDA (Scheme 30). Undesired conjugate addition of the bulky diisopropyl amide to the α,β-unsaturated system to give **193** occurred preferentially over the desired deprotonation/alkylation sequence with allyl bromide. Herrmann *et al.* had reported a solution to the problem of unwanted conjugate addition of LDA to ethyl crotonate by using a 1 M 1:1 LDA:HMPA suspension in THF.[26] Application of Herrmann's conditions proved successful and yielded alkylated ester **194** in 67% yield. The *Z*-isomer geometry was determined by proton coupling constant analysis. The synthesis concluded with DIBAL reduction of the ethyl ester **194** followed by DMP oxidation of the intermediate alcohol to the desired aldehyde **195** in 71% yield over two steps.

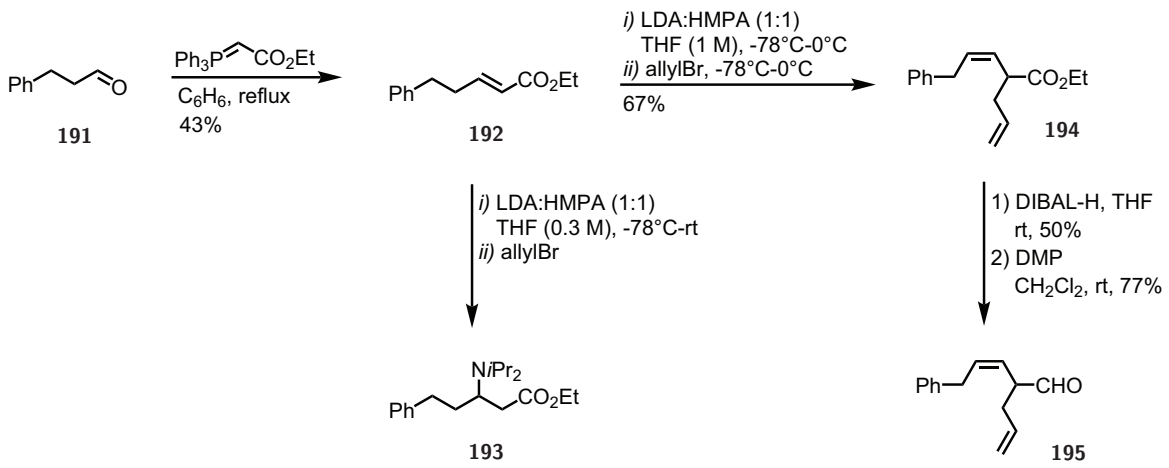

Scheme 30: Synthesis of 3-acyl-1,5-diene **195**.

With the 3-acyl-1,5-diene substrate **195** in hand, we attempted to employ organocatalytic conditions to affect a Cope rearrangement using a variety of primary and secondary amines, including MacMillan's imidazolidinone, and the diazepane carboxylate catalysts (Table 5). In all cases, the substrate isomerized to the α,β-unsaturated aldehyde **196**. The isomerization was shown to occur both under strictly acidic or basic conditions (Entries 5-7), and simple thermal conditions (60°C in CD_3CN) were unable to induce a Cope rearrangement. In order to eliminate the potential for isomerization to the α,β-unsaturated system, a modification of the substrate to include an α-quaternary center was devised.

Table 5: Catalytic conditions screening of 3-acyl-1,5-diene **195**.

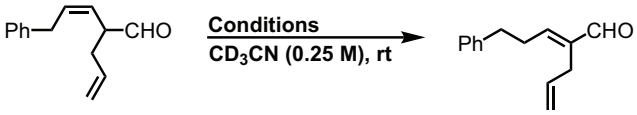

195 **196**

Entry	Catalyst (20 mol%)	Acid (18 mol%)
1	L-proline	HCl
2	pyrrolidine	HCl
3	MacMillan's catalyst	HCl
4	Achiral 7-membered ring (HCl salt)	HCl
5	pyrrolidine	-
6	L-proline	-
7	-	HCl

Allylated ethyl ester **194** underwent a second enolate alkylation with methyl iodide

to yield a deconjugated ethyl ester intermediate which was subsequetly reduced with LAH (16% yield over two steps). DMP oxidation of homoallylic alcohol **197** occurred smoothly to yield aldehyde **198** in 90% yield. Unfortunately, screening several catalytic conditions failed to induce conversion to the Cope product, and with only starting material observed in every case (Table 6). Thermal conditions (150°C in DMSO) also failed to induce a Cope rearrangement of the starting material (Entry 9).

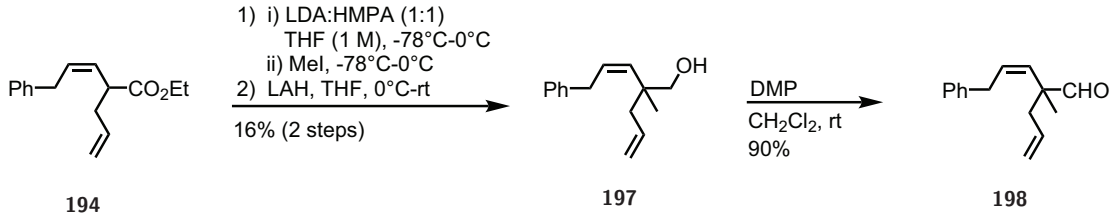

194 **197** **198**

Scheme 31: Synthesis of 3-acyl-1,5-diene **198**.

Table 6: Catalytic condition screening of 3-acyl-1,5-diene **198**.

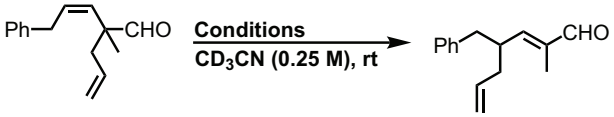

198 **199**

Entry	Solvent (0.25 M)	Catalyst (20 mol%)	Acid (18 mol%)	Temp. (°C)
1	CD_3CN	L-proline	HCl	22
2	CD_3CN	Pyrrolidine	HCl	22
3	CD_3CN	MacMillan's catalyst	HCl	22
4	CD_3CN	Achiral 7-membered ring (HCl salt)	HCl	22
5	CD_3CN	Pyrrolidine	HCl	22
6	CD_3CN	L-proline	HCl	22
7	CD_3CN	-	HCl	22
8	CD_3CN	-	-	60
9	DMSO-d_6	-	-	150

The apparent lack of reactivity exhibited by substrate **198** was unexpected by could be rationalized by an analysis of the expected chair-like transition state for the rearrangement of **198**. This suggested that a 1,3-diaxial interaction between the acyl/iminium and benzyl groups due to the Z-configuration of the internal olefin may have been significantly hindering the reaction (Figure 3.10). While an *E*-isomer would certainly have remedied the crowded transition state, control over the isomer geometry throughout the enolate alkylation would

have been nontrivial. Instead, the next substrate iteration (**200**) would include a benzyl group at its α-position rather than methyl. Placing benzyl at this position would eliminate the possibility of E or Z isomers as both olefins would be terminal, while maintaining the high molecular weight to prevent the troublesome handling of volatile intermediates.

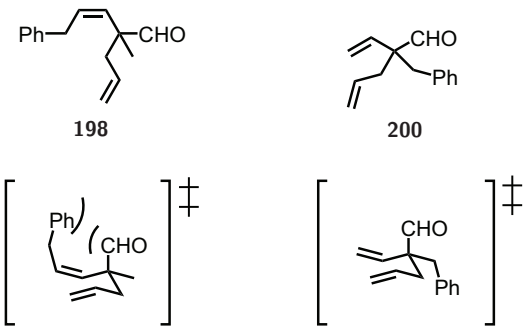

Figure 3.10: Chair-like transition states of **198** and **200**.

Synthesis of the new substrate began with a deconjugative enolate alkylation of ethyl crotonate with benzyl bromide. The alkylation led to the 1:2:1 formation of two monoalkylated isomers **201** and **202** and the dialkylated product **203** all of which were inseperable by flash chromatography (78% yield overall). Despite the mixture of products, the second alkylation with allyl bromide was conducted as both monoalkylated isomers would lead to the desired product while the dialkylated ester would be effectively inert under the strongly basic conditions. Alkylation with allyl bromide led to the convergent formation of the dialkylated ester and the recovery of the dibenzylated byproduct in 94% yield overall. However, the products remained inseparable. Reduction of both esters to their corresponding homoallylic alcohols **204** and **205** with LAH proceeded well (85% yield) but again failed to provide separable products. The order of steps was then altered in an attempt to try and produce separable intermediates.

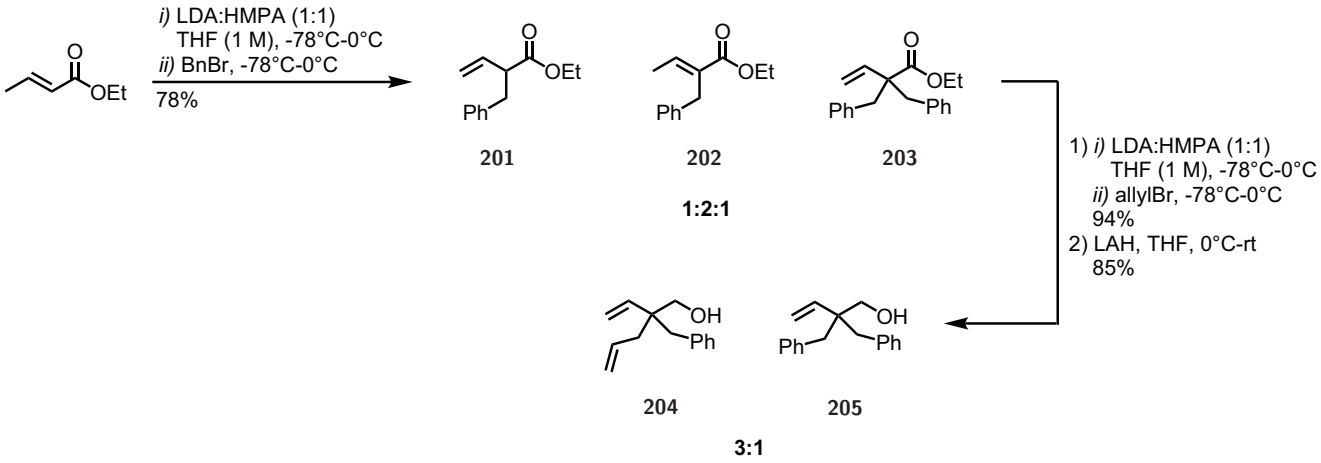

Scheme 32: Synthesis of inseparable homoallylic alcohols **204** and **205**.

Deconjugative alkylation of ethyl crotonate with allyl bromide proceeded well to yield a 2.5:1 mixture of mono- and diallylated products **206** and **207** in 66% yield. Extended reaction times led to the total conversion of the deconjugated product to **206** so as to simplify NMR analysis of the reaction. Subsequent alkylation with benzyl bromide occurred in 47% yield and was followed by LAH reduction and DMP oxidation to yield the 3,3-disubstituted aldehyde products in 97% and 40% yield, respectively. At this stage, the desired aldehyde **200** was successfully isolated by flash chromatography.

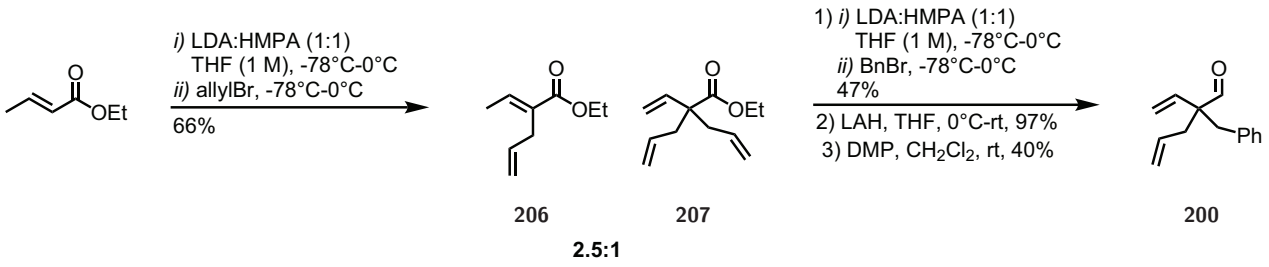

Scheme 33: Synthesis of 3-acyl-1,5-diene **200**.

Catalyst conditions were once again screened at both room temperature and at elevated temperatures, but each failed to induce the Cope rearrangement (Table 7). However, the thermal rearrangement to **208** in refluxing bromobenzene was successful indicating that the less hindered transition state was amenable to the Cope rearrangement. The geometry of the α,β-unsaturated olefin was not determined.

Table 7: Catalytic condition screening of 3-acyl-1,5-diene **198**.

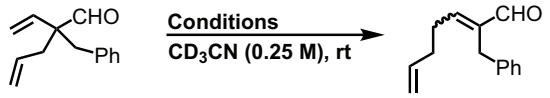

200 **208**

Entry	Solvent (0.25 M)	Catalyst (20 mol%)	Acid (18 mol%)	Temp. (°C)	Conversion (%)
1	CD_3CN	L-proline	HCl	22	-
2	CD_3CN	pyrrolidine	HCl	22	-
3	CD_3CN	MacMillan's catalyst	HCl	22	-
4	CD_3CN	Achiral 7-membered ring (HCl salt)	HCl	22	-
5	CD_3CN	L-proline	HCl	60	-
6	CD_3CN	pyrrolidine	HCl	60	-
7	CD_3CN	MacMillan's catalyst	HCl	60	-
8	CD_3CN	Achiral 7-membered ring (HCl salt)	HCl	60	-
9	CD_3CN	-	-	60	-
10	C_6H_5Br	-	-	160	100

Further investigation into the Cope rearrangement of 3-acyl-1,5-diene substrate **200** will require determining the minimal temperature at which approximately partial conversion can be achieved under thermal conditions. Employing catalytic conditions at the determined temperature is predicted to reveal whether the diazepane catalyst is capable of accelerating the rate of reaction for this class of substrates. This work will be continued by a student within the Gleason lab.

References

1. Cope, A. C.; Hardy, E. M. *J. Am. Chem. Soc.* **1940**, *62*, 441–444.
2. Overman, L. E.; Knoll, F. M. *J. Am. Chem. Soc.* **1980**, *102*, 865–867.
3. Overman, L. E.; Jacobsen, E. J. *J. Am. Chem. Soc.* **1982**, *104*, 7225–7231.
4. Felix, R. J.; Weber, D.; Gutierrez, O.; Tantillo, D. J.; Gagné, M. R. *Nat. Chem.* **2012**, *4*, 405–409.
5. Yates, P.; Eaton, P. *Tetrahedron Lett.* **1960**, *1*, 5–9.
6. Cookson, R. C.; Hudec, J.; Williams, R. O. *J. Chem. Soc., C* **1967**, 1382.
7. Dauben, W. G.; Chollet, A. *Tetrahedron Lett.* **1981**, *22*, 1583–1586.
8. Kaldre, D.; Gleason, J. L. *Angew. Chem. Int. Ed.* **2016**, *55*, 11557–11561.
9. Berson, J. A.; Jones, M. *J. Am. Chem. Soc.* **1964**, *86*, 5019–5020.
10. Evans, D. A.; Golob, A. M. *J. Am. Chem. Soc.* **1975**, *97*, 4765–4766.
11. Paquette, L. A. *Tetrahedron* **1997**, *53*, 13971–14020.
12. Baumann, H.; Chen, P. *Helv. Chim. Acta* **2001**, *84*, 124–140.
13. Doering, W. E.; Roth, W. *Tetrahedron* **1962**, *18*, 67–74.
14. Goldstein, M. J.; Benzon, M. S. *J. Am. Chem. Soc.* **1972**, *94*, 7147–7149.
15. Gajewski, J. J.; Conrad, N. D. *J. Am. Chem. Soc.* **1979**, *101*, 6693–6704.
16. Wender, P. A.; Brighty, K. *Tetrahedron Lett.* **1988**, *29*, 6741–6744.
17. Enders, D.; Knopp, M.; Schiffers, R. *Tetrahedron:-Asymmetr.* **1996**, *7*, 1847–1882.
18. Davies, H. M. *Tetrahedron* **1993**, *49*, 5203–5223.
19. Ahrendt, K. A.; Borths, C. J.; MacMillan, D. W. C. *J. Am. Chem. Soc.* **2000**, *122*, 4243–4244.
20. Wilson, R. M.; Jen, W. S.; MacMillan, D. W. C. *J. Am. Chem. Soc.* **2005**, *127*, 11616–11617.
21. Paras, N. A.; MacMillan, D. W. C. *J. Am. Chem. Soc.* **2001**, *123*, 4370–4371.
22. Fonseca, M. T. H.; List, B. *Angew. Chem. Int. Ed.* **2004**, *43*, 3958–3960.
23. Kaldre, D. Development of Hybrid Drugs for Cancer Treatment and Studies in Asymmetric Organocatalysis. Ph.D. thesis, McGill University, 2015.
24. Cavill, J. L.; Peters, J.-U.; Tomkinson, N. C. O. *Chem. Commun.* **2003**, 728–729.
25. Brazier, J. B.; Cavill, J. L.; Elliott, R. L.; Evans, G.; Gibbs, T. J.; Jones, I. L.; Platts, J. A.; Tomkinson, N. C. *Tetrahedron* **2009**, *65*, 9961–9966.
26. Herrmann, J.; Kieczykowski, G.; Schlessinger, R. *Tetrahedron Lett.* **1973**, *14*, 2433–2436.

Chapter 4: Experimental Procedures

4.1 HDAC Assay

Assay Materials

HDAC3-"NCoR1" complex (purity 90% by SDS-PAGE according to supplier; fusion protein of GST-tagged HDAC3 with the deacetylase activation domain (DAD) of NCoR1 (nuclear receptor corepressor)), HDAC6 (purity >90% by SDS-PAGE according to the supplier), The HDAC assay buffer consisted of 50 mM Tris-HCl, 137 mM NaCl, 2.7 mM KCl, 1 mM $MgCl_2$, and bovine serum albumin (0.5 mg/mL), pH was adjusted to 8 using 6 M NaOH and 1 M HCl as needed. Trypsin (25 mg/ml, from porcine pancreas, in 0.9% sodium chloride, from Sigma Aldrich). All inhibitors were purified (>95% purity at 254 nm) by reversed-phase preparative or semi-preparative HPLC. Stock solutions of inhibitors and substrate were obtained by dissolution in DMSO and addition of HDAC assay buffer to afford solutions containing 1.7% v/v DMSO. Serial dilution using HDAC buffer containing 1.7% v/v DMSO was used to obtain all requisite inhibitors and substrate solutions.

In vitro HDAC Assays

For inhibition of recombinant human HDAC3 and HDAC6, dose-response experiments with internal controls were performed in black low-binding Nunc 96-well microtiter plates. Dilution series (8 concentrations) were prepared in HDAC assay buffer with 1.7% v/v DMSO. The appropriate dilution of inhibitor (10 µL of 5 times the desired final concentration) was added to each well followed by HDAC assay buffer (25 µL) containing substrate [Ac-Leu-Gly-Lys(Ac)-AMC, 40 or 30 µM for HDAC 3 and 80 or 60 µM for HDAC 6]. Finally, a solution of the appropriate HDAC (15 µL) was added [HDAC3, 10 ng/well; HDAC 6, 60 ng/well] and the plate incubated at 37°C for 30 min with mechanical shaking (270 rpm). Then trypsin (50 µL, 0.4 mg/mL) was added and the assay developed for 30 min at room temperature with mechanical shaking (50 rpm). Fluorescence measurements were then taken on a Molecular Devices SpectraMax i3x plate reader with excitation at 360 nm (9 nm bandwidth) and detecting emission at 460 nm (15 nm bandwidth). Each assay was performed in triplicate

at two different substrate concentrations. Baseline fluorescence emission was accounted for using blanks, run in triplicate, containing substrate (25 µL), HDAC assay buffer (15 µL), HDAC assay buffer with 1.7% v/v DMSO (10 µL), and trypsin (50 µL). Fluorescence emission was normalized using controls, run in triplicate, containing substrate (25 µL), HDAC (15 µL), HDAC assay buffer with 1.7% v/v DMSO (10 µL), and trypsin (50 µL). The data were analyzed by nonlinear regression with GraphPad Prism to afford IC_{50} values from the dose-response experiments. K_i values were determined from the Cheng-Prusoff equation [$K_i = IC_{50}/(1+[S]/K_m)$] with the assumption of a standard fast-on-fast-off mechanism of inhibition.

4.2 Chemical Synthesis

Materials and Instruments

THF and diethyl ether were purified by distillation over Na metal and benzophenone under nitrogen atmosphere. Toluene and CH_2Cl_2 were purified by distillation over CaH_2 under an air atmosphere. Triethylamine and diisopropylamine were purified by distillation over CaH_2 under nitrogen atmosphere. DMF, methanol, pyridine, and diisopropylethylamine were gathered from solvent purification systems. All other commercial solvents and reagents were used as received from Sigma-Aldrich, Fisher Scientific, Chem Impex, Strem Chemicals, and Alfa Aesar unless otherwise specified. Normal-phase column chromatography was performed using SilioFlash®P60 Ultrapure silica (particle size: 40-63 µm, 230-400 mesh) obtained from Silicycle and was used as received. Reverse-phase column chromatography was performed using octadecyl-functionalized silica obtained from Sigma-Aldrich and was used as received. Preparatory High-Performance Liquid Chromatography (HPLC) was performed on an Atlantis®Prep T3 OBD™5µm, 9x50 mm column obtained from Waters Co. Analytical TLC was performed on glass-backed Ultrapure silica TLC plates (extra hard layer, 60 Å, thickness: 250 µm) obtained from Silicycle, visualized with a Spectroline UV254 lamp, and stained with acidic ceric ammonium molybdate solution, basic permanganate solution, acidic *p*-anisaldehyde solution, or acidic iron (III) chloride solution.

^1H and ^{13}C NMR, recorded at 400 MHz and 100 MHz, respectively, were performed on

a Varian Mercury 400 spectrometer. ^{1}H and ^{13}C NMR, recorded at 400 MHz and 100 MHz, respectively, were performed on a Bruker 400 spectrometer. ^{1}H and ^{13}C NMR, recorded at 500 MHz and 125 MHz, respectively, were performed on a Bruker 500 MHz spectrometer. Proton chemical shifts were internally referenced to the residual proton resonance in $CDCl_3$ (δ 7.26 ppm), CD_3OD (δ 3.31 ppm) and d_6-DMSO (δ 2.50 ppm). Carbon chemical shifts were internally referenced to the deuterated solvent signals in $CDCl_3$ (δ 77.2 ppm), CD_3OD (δ 49.0 ppm) and d_6-DMSO (δ 39.50 ppm). High-resolution mass spectrometry was performed by Dr. Nadim Saade and Dr. Alexander Wahba at the McGill University chemistry department mass spectrometry facilities using electrospray ionization and chemical ionization techniques.

General Procedure A: Hydroxamic acid formation from methyl esters:

A solution of methyl ester (1.0 eq.) dissolved in 5:1 THF:methanol was added to a flame dried round-bottom flask purged under argon and hydroxylamine (50% w/w in H_2O) was added to the solution. Cold 3M KOH (7.0 eq.) was added dropwise to the mixture at 0°C and the reaction was warmed to room temperature and stirred for 24 hours. The reaction was neutralized with 3M HCl solution, extracted with ethyl acetate (3x), dried over Na_2SO_4, filtered, and concentrated *in vacuo*. The crude mixture was purified by reverse phase column chromatography using a 10%-100% methanol:H_2O elution gradient. Concentration of the purified fractions *in vacuo* followed by lyophilization of residual H_2O overnight yielded the purified products.

General Procedure B: Preparation of (4-((tert-butyldimethylsilyl)oxy)phenyl)-magnesium bromide:

To a flame-dried three-necked round-bottom flask equipped with a condenser, Mg turnings (1.2 eq) were added and flame-dried under vacuum. Once cooled to room temperature, the turnings were suspended in THF and a single crystal of I_2 was added. The brown suspension was quickly heated to reflux with a heat gun and then left to stir while returning to room temperature. Once the suspension of Mg became grey and turbid, (4-bromophenoxy)(tert-butyl)dimethylsilane (1.0 eq.) was dissolved in THF, in a separate dry flask, and cannulated into the reaction vessel. The reaction was heated to reflux and stirred for 6-14 hours. The

green/brown solution was then cooled to room temperature and stirring was ceased. Concentration of the Grignard was determined by titration of 300µL Grignard with 1.0 M *s*BuOH solution using 1,10-phenanthroline as an indicator.

General Procedure C: Grubbs olefin metatheses:

To a flame-dried round bottom flask equipped with a condenser, starting material was added and dissolved in 1 mL CH_2Cl_2 and anhydrous PTSA was added. The mixture was stirred for 10 minutes or until all PTSA had dissolved and the solvent was then removed *in vacuo*. The solids were redissolved in CH_2Cl_2 and a solution of alkene in CH_2Cl_2 was added via cannula. Catalyst, as a solution in CH_2Cl_2 was added to the solution of olefins via cannula and the reaction was heated to 40°C for 24 hours. An additional 5 mol% of catalyst was added at room temperature and the reaction was stirred for an additional 24 hours. Cooled to room temperature and quenched with 3 mL saturated $NaHCO_3$ solution, extracted with 3x 5 mL CH_2Cl_2, dried over Na_2SO_4, filtered, and concentrated. Purified by silica gel column chromatography using a 0%-8% MeOH:CH_2Cl_2 gradient.

General Procedure D: Benzyl group deprotections and olefin hydrogenations:

To a dry flask, starting material was added and dissolved in MeOH. A pipette-tip full of 10% Pd/C was added and the suspension was stirred. An atmosphere of H_2 was established using a balloon and a vent to purge the flask of all air, the balloon was refilled with H_2 and the vent was removed and the flask was sealed. The reaction was stirred for 24 hours upon which is was filtered through celite and concentrated directly.

General Procedure E: Organocatalytic Cope rearrangement screening procedure:

Stock solutions of catalyst, HCl, and starting material were prepared in CD_3CN. The stock solutions of starting material contained mesitylene such that the reaction concentration of mesitylene was 0.083 mM. The total reaction volumes were 500 µL and the final substrate concentrations were 0.25 M. The components were added in the following order from their respective stock solutions: 0.025 mmol of catalyst, 0.023 mol% of HCl, CD_3CN, and then 0.125 mmol of starting material. The reactions were stirred at the defined temperatures for

24 hours and then transferred directly to NMR tubes for analysis.

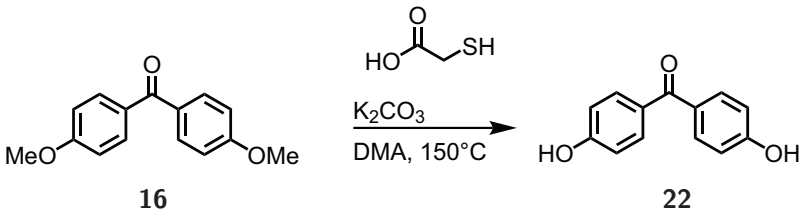

Synthesis of 4,4'-dihydroxybenzophenone (22):

4,4'-dimethoxybenzophenone (2.0 g, 8.3 mmol, 1.0 eq.) was added to a flame dried round-bottom flask and dissolved in dry CH_2Cl_2 (80 mL). The flask was then equipped with an oven dried addition funnel and cooled to -15°C. The addition funnel was charged with BBr_3 (1.0 M solution in CH_2Cl_2 (82.6 mL, 82.6 mmol, 10 eq.) which was then added dropwise to the reaction. The reaction was brought to room temperature and stirred for 48 hours. The reaction was quenched with 3:1 CH_2Cl_2:*i*PrOH (150 mL) delivered via addition funnel over 1 hour. The clear yellow solution turned opaque. The solution was then extracted with 3x200 mL EtOAc, the combined organic phases were dried over $MgSO_4$, filtered, and concentrated *in vacuo* to an orange solid. Purification by silica gel column chromatography using a 20%-70% EtOAc:hexanes solvent gradient delivered the product as a beige solid (1.63 g, 7.6 mmol) in 92% yield. The spectroscopic data is in agreement with that reported in the literature.[1]

Alternate synthesis of 4,4'-dihydroxybenzophenone (22):

4,4'-dimethoxybenzophenone (10.0 g, 41.3 mmol, 1.0 eq.) was added to a flame dried round-bottom flask equipped with a condenser and dissolved in DMA (100 mL). K_2CO_3 (68.0 g, 492 mmol, 12 eq.) was added followed by 3-mercaptopropionic acid (28.8 mL, 330 mmol, 8 eq.) to give a clear purple solution. Upon heating to 150°C, the reaction turned white and opaque and was left to stir for 18 hours. The reaction was cooled to 0°C, H_2O was added (250 mL) followed by 37% HCl added dropwise. The reaction was warmed to room temperature while stirring vigorously until bubbling ceased. The solution was then extracted with 3x200 mL EtOAc which was then washed with 3x100 mL saturated $NaHCO_3$

solution followed by 3x100 mL saturated NaCl solution. The organic layer was dried over Na_2SO_4, filtered, and concentrated *in vacuo* to a beige solid. The product was recrystallized from H_2O and isolated as a beige solid (8.1 g, 37.8 mmol) in 92% yield.

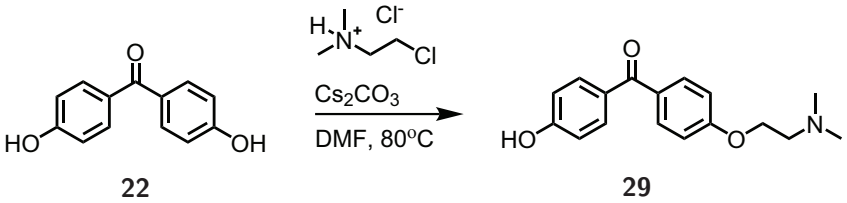

22 **29**

Synthesis of (4-(2-(dimethylamino)ethoxy)phenyl)(4-hydroxyphenyl)methanone (29):

22 (3.3 g, 15.0 mmol, 1.0 eq.) was added to a flame dried round-bottom flask equipped with a condenser, followed by the addition of Cs_2CO_3 (19.9 g, 61.0 mmol, 4.0 eq.). The solids were dissolved in DMF (60 mL) and heated to 90°C while stirring vigorously and then to 160°C for 1 hour. The reaction was cooled and 2-chloro-*N,N*-dimethylethylamine hydrochloride (2.38 g, 16.5 mmol, 1.1 eq.)was added portionwise and the reaction was heated to 90°C for 4 hours. The reaction was then coled, diluted with H_2O (350 mL) and extracted with 3x200 mL EtOAc. The organic fraction were combined and washed with 3x200 mL 1:1 brine:H_2O, dried over Na_2SO_4, filtered and concentrated to a dark orange oil. Purification by silica gel column chromatography using a 5%-20% MeOH:CH_2Cl_2 gradient gave the product as a light brown solid (1.39 g, 4.9 mmol) in 33% yield. The spectroscopic data is in agreement with that reported in the literature.[2]

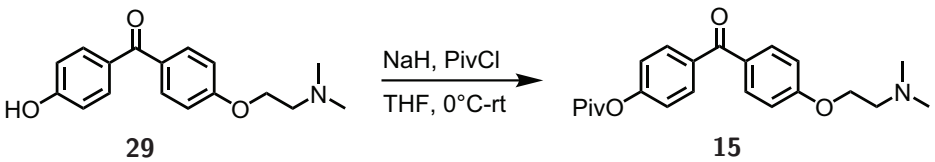

29 **15**

Synthesis of 4-(4-(2-(dimethylamino)ethoxy)benzoyl)phenyl pivalate (15):

29 (1.68 g, 5.90 mmol, 1.0 eq.) was added to a flame dried round-bottom flask and dissolved in THF (59 mL). NaH (60% suspension in mineral oil) (944 mg, 23.6 mmol, 4.0 eq.)

was added directly to the solution and the colour changed from translucent orange to bright yellow and opaque. The reaction was cooled to 0°C and stirred for 10 minutes, followed by the dropwise addition of pivaloyl chloride (1.10 mL, 8.84 mmol, 1.5 eq.). The reaction was then warmed to room temperature and stirred for 2 hours. The reaction was quenched with 50 mL H_2O and extracted with 3x50 mL EtOAc. The organic layer was dried over Na_2SO_4, filtered, and concentrated to a pale yellow solid. Purification by silica gel column chromatography using a 2%-15% MeOH:CH_2Cl_2 gradient gave the product as a white solid (1.67 g, 4.52 mmol) in 77% yield. ^{1}H NMR (400 MHz, $CDCl_3$) δ 7.86 – 7.78 (m, 4H), 7.23 – 7.16 (m, 2H), 7.04 – 6.97 (m, 2H), 4.17 (t, J = 5.7 Hz, 2H), 2.79 (t, J = 5.7 Hz, 2H), 2.37 (s, 6H). ^{13}C NMR (126 MHz, $CDCl_3$) δ 194.43, 176.69, 162.54, 154.01, 135.56, 132.45, 131.28, 130.13, 121.36, 114.15, 66.32, 58.15, 45.96, 39.22, 27.11. HRMS calculated for $C_{22}H_{28}NO_4$ (M+H)=370.2001, found m/z=370.2013.

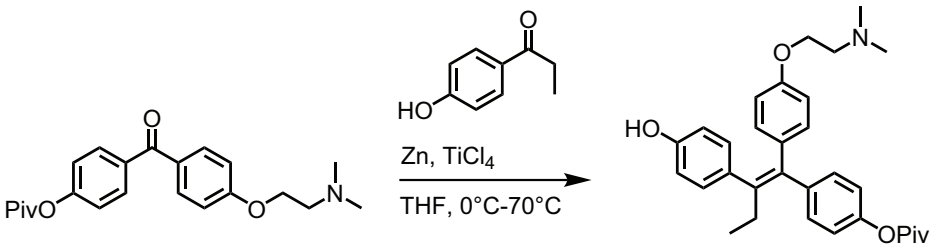

15 **12**

Synthesis of (E)-4-(1-(4-(2-(dimethylamino)ethoxy)phenyl)-2-(4-hydroxyphenyl)-but-1-en-1-yl)phenyl pivalate (12):

Zn (300 mesh) (2.1 g, 32.2 mmol, 8.0 eq.) was added to a flame dried, three-necked round-bottom flask equipped with a condenser and suspended in THF (12 mL). The suspension was cooled to 0°C and neat $TiCl_4$ was slowly added to the stirred suspension. The suspension was then heated to reflux and stirred for 3 hours. The black slurry was cooled again to 0°C and a solution of **15** (1.49 g, 4.0 mmol, 1.0 eq.) and 4-hydroxypropiophenone (1.82 g, 12.1 mmol, 3.0 eq) dissolved in THF (20 mL) was cannulated into the reaction vessel. The reaction was heated to reflux and stirred for 3 hours, then cooled to 0°C and slowly quenched with 10% K_2CO_3 (50 mL). The reaction was then vacuum filtered over filter paper, and the filtrate was extracted with 3x50 mL EtOAc. The organic fraction was

dried over Na_2SO_4, filtered, and concentrated to a green foam. Purification by silica gel column chromatography using an 8%-16% MeOH:CH_2Cl_2 gradient gave the product as a beige foam (534 mg, 1.1 mmol) in 27% yield as a 7:1 *E:Z* mixture of isomers. ^{1}H NMR (400 MHz, CD_3OD_4) δ 7.24 (d, J = 8.6 Hz, 2H), 7.05 (d, J = 8.6 Hz, 2H), 6.95 (d, J = 8.6 Hz, 3H), 6.81 (d, J = 8.8 Hz, 2H), 6.62 (dd, J = 13.2, 8.7 Hz, 4H), 4.01 (t, J = 5.4 Hz, 2H), 2.76 (t, J = 5.4 Hz, 2H), 2.46 (q, J = 7.3 Hz, 2H), 2.35 (s, 6H), 1.38 (s, 9H), 0.94 (t, J = 7.4 Hz, 3H). ^{13}C NMR (126 MHz, CD_3OD) δ 177.32, 177.19, 157.49, 156.61, 155.57, 155.50, 149.72, 148.80, 142.08, 141.61, 141.56, 141.25, 136.73, 136.66, 136.27, 135.96, 133.03, 132.92, 131.67, 131.46, 131.28, 131.21, 131.00, 130.54, 130.50, 130.37, 130.33, 130.22, 130.15, 129.25, 129.13, 120.86, 120.58, 120.50, 119.97, 114.68, 114.49, 114.40, 113.92, 113.77, 113.75, 113.16, 64.97, 64.70, 57.65, 57.57, 44.34, 44.27, 44.25, 38.71, 28.41, 26.15, 26.11, 26.09, 12.64.

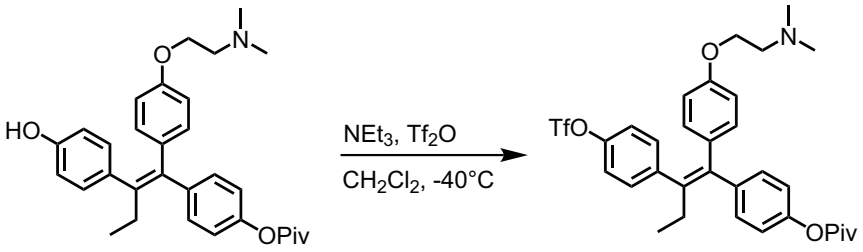

12 **25**

Synthesis of (E)-4-(1-(4-(2-(dimethylamino)ethoxy)phenyl)-2-(4-(((trifluoromethyl)sulfonyl)oxy)phenyl)but-1-en-1-yl)phenyl pivalate (25):

12 (146 mg, 0.30 mmol, 1.0 eq.) was added to a flame-dried round-bottom flask purged with argon and dissolved in CH_2Cl_2 (6.0 mL). The solution was cooled to -40°C and freshly distilled NEt_3 (63.0 µL, 0.45 mmol, 1.5 eq.) was added and the reaction was stirred for 15 minutes. Tf_2O (76.0 µL, 0.45 mmol, 1.5 eq.) was slowly added and the reaction was stirred for 1.5 hours. The reaction was quenched with 5.0 mL H_2O, extracted with 3x10 mL CH_2Cl_2, the organic layer was dried over Na_2SO_4, filtered, and concentrated to a yellow oil. Purification by silica gel column chromatography using a 5%-15% MeOH:CH_2Cl_2 solvent gradient gave the product as a yellow oil (173 mg, 0.28 mmol) in 93% yield as a 1:1 *E:Z* mixture of isomers. ^{1}H NMR (400 MHz, CD_3OD) δ 7.27 – 7.03 (m, 10H), 6.92 (d, J = 8.7 Hz, 2H), 6.84 (d, J = 8.7 Hz, 1H), 6.74 (dd, J = 8.7, 6.7 Hz, 3H), 6.59 (d, J = 8.8 Hz, 2H),

4.11 (t, J = 5.8 Hz, 2H), 3.96 (t, J = 5.8 Hz, 2H), 2.73 (d, J = 35.5 Hz, 4H), 2.51 (dq, J = 14.9, 7.5 Hz, 4H), 2.35 (d, J = 23.2 Hz, 12H), 1.39 (s, 9H), 1.32 (s, 9H), 1.01 – 0.89 (m, 4H). ^{13}C NMR (126 MHz, CD_3OD) δ 177.35, 157.12, 153.28, 150.01, 147.92, 143.25, 140.47, 140.08, 139.13, 134.85, 131.58, 131.46, 130.03, 120.90, 120.50, 113.94, 113.32, 64.70, 57.48, 44.18, 38.56, 28.17, 26.01, 12.32.

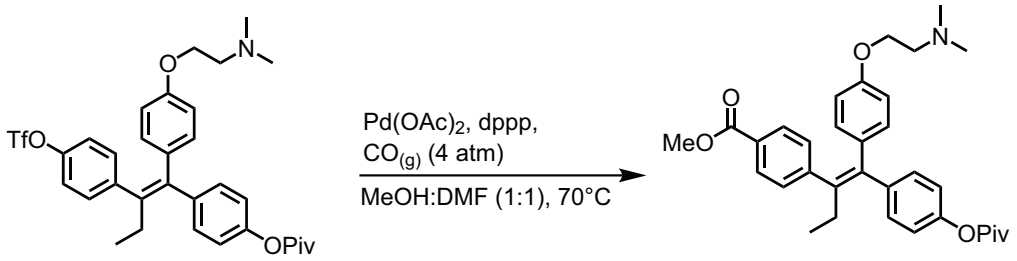

25 **40**

Synthesis of methyl (E)-4-(1-(4-(2-(dimethylamino)ethoxy)phenyl)-1-(4-(pivaloyloxy) phenyl)but-1-en-2-yl)benzoate (40):

25 (178 mg, 0.29 mmol, 1.0 eq.) was dissolved in DMF (7.25) (obtained from SPS) and added to a flame-dried Schlenk bomb. Freshly distilled Et_3N (121 µL, 0.87 mmol, 3.0 eq.) was added followed by $Pd(OAc)_2$ (27 mg, 0.12 mmol, 40 mol%) and dppp (36 mg, 0.09 mmol, 30 mol%) dissolved in dry MeOH (7.25 mL) via cannula. The flask was backfilled with argon 3 times and then charged with 4 atm CO_2 and heated to 70°C for 24 hours. The reaction was cooled to room temperature and the CO_2 was vented. Diluted with 35 mL H_2O, extracted wtih 3x 50 mL EtOAc and then washed with 3x 50 mL 1:1 brine:H_2O. The organic later was dried over Na_2SO_4, filtered, and concentrated to a dark orange oil. Purification by silica gel column chromatography using a 2.5%-4% MeOH:CH_2Cl_2 solvent gradient gave the product as an orange oil (98 mg, 0.19 mmol) in 64% yield. ^{1}H NMR (400 MHz, CD_3OD) δ 7.87 – 7.76 (m, 2H), 7.33 – 7.19 (m, 4H), 7.14 – 7.02 (m, 2H), 6.79 (dd, J = 8.6, 2.0 Hz, 2H), 6.68 – 6.56 (m, 2H), 3.95 (q, J = 3.6 Hz, 2H), 3.85 (d, J = 1.8 Hz, 3H), 2.78 – 2.66 (m, 2H), 2.62 – 2.45 (m, 2H), 2.31 (d, J = 2.0 Hz, 6H), 1.37 (d, J = 1.9 Hz, 8H), 0.93 (td, J = 7.4, 1.9 Hz, 3H). ^{13}C NMR (126 MHz, CD_3OD) δ 177.28, 167.05, 157.02, 149.08, 147.79, 140.96, 140.60, 138.92, 135.10, 131.57, 131.01, 129.74, 128.79, 127.65, 120.91, 113.31, 64.64,

57.48, 51.02, 44.19, 38.73, 28.11, 26.01, 12.38.

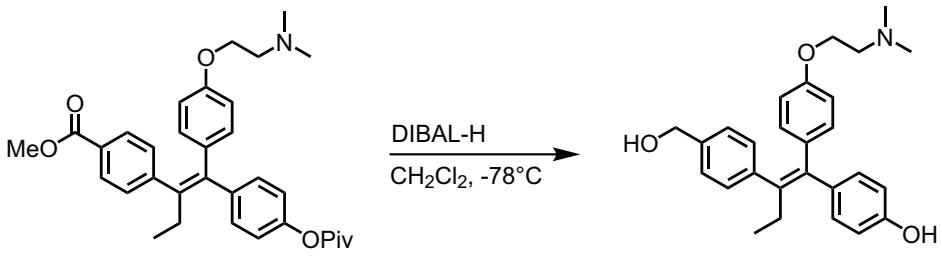

40 **41**

Synthesis of (Z)-4-(1-(4-(2-(dimethylamino)ethoxy)phenyl)-2-(4-(hydroxymethyl)phenyl)but-1-en-1-yl)phenol (41):

40 (31 mg, 0.06 mmol, 1.0 eq.) was added to a flame dried round-bottom flask purged under argon and dissolved in CH_2Cl_2 (1.5 mL). The solution was cooled to -78°C and stirred for 10 minutes before the dropwise addition of DIBAL-H (1 M in PhMe) (175 µL, 0.26 mmol, 4.4 eq.). TLC indicated a small amount of starting material remained after 2 hours, an addition of DIBAL-H (11 µL, 0.06 mmol, 1.1 eq.) was used to push the reaction to completion. After a total of 2.5 hours, TLC indicated complete consumption of starting material and the reaction was quenched with 4 mL MeOH and warmed to 0°C in an ice bath. Saturated Rochelle's salt solution was added and the biphasic mixture was stirred overnight to clear up. The organic layer was washed with 3x 5 mL of saturated Rochelle's salt solution, dried over Na_2SO_4, filtered, and concentrated *in vacuo* to an orange oil. Purification by silica gel column chromatography using a 2%-20% MeOH:CH_2Cl_2 solvent gradient gave the product as a yellow oil (15 mg, 0.03 mmol) in 49% yield. ^{1}H NMR (400 MHz, CD_3OD) δ 7.22 – 7.07 (m, 7H), 7.03 (d, J = 8.6 Hz, 2H), 6.79 (dd, J = 11.8, 8.6 Hz, 4H), 6.61 (d, J = 8.8 Hz, 2H), 4.54 (d, J = 3.9 Hz, 3H), 4.22 (t, J = 5.2 Hz, 1H), 4.06 (t, J = 5.2 Hz, 2H), 3.06 (s, 1H), 2.97 (d, J = 5.5 Hz, 2H), 2.64 – 2.40 (m, 12H), 0.92 (t, J = 7.5 Hz, 6H).

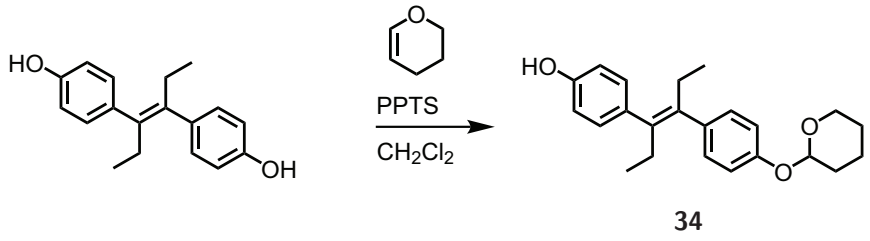

34

Synthesis of (E)-4-(4-(4-((tetrahydro-2H-pyran-2-yl)oxy)phenyl)hex-3-en-3-yl)phenol (34):

Diethylstilbestrol (**37** (281 mg, 1.04 mmol, 1.0 eq.) was added to a flame dried round bottom flask and dissolved in CH_2Cl_2 (0.1 mL) followed by the addition of PPTS (27 mg, 0.104 mmol, 0.1 eq.) and dihydropyran (289 µL, 3.16 mmol, 3.0 eq.). The reaction was stirred at room temperature for 12 hours upon which is became yellow and clear. The reaction mixture was then quenched with saturated NaCl solution and diluted with Et_2O and H_2O. The organic fraction was set aside and the aqueous was extracted with 3x10mL (EtOAc), dried over Na_2SO_4, filtered, and concentrated. Crude was purified by silica gel column chromatography using a 15-25% EtOAc:hexanes gradient to give the product as a white solid (140 mg, 0.40 mmol) in 45% yield.

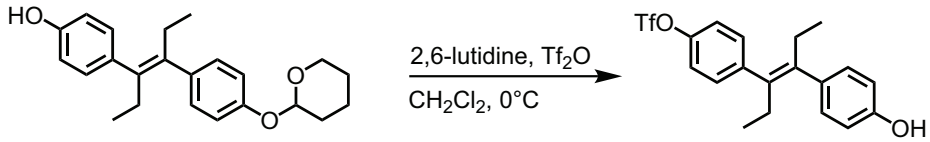

34 **35**

Synthesis of (E)-4-(4-(4-hydroxyphenyl)hex-3-en-3-yl)phenyl trifluoromethanesulfonate (35):

To a flame dried round bottom flask, **209** (283 mg, 0.803 mmol, 1.0 eq.) and 2,6-lutidine (122 µL, 1.04 mmol, 1.3 eq.) were added to CH_2Cl_2 (8 mL) and left to stir at 0°C for 10 minutes. Tf_2O (176 µL, 1.04 mmol, 1.3 eq.) was then added dropwise and the reaction was stirred for 2 hours at 0°C upon which is was quenched with saturated $NaHCO_3$ and diluted with EtOAc and H_2O. The organic layer was set aside and the aqueous was washed with 3x10 mL EtOAc. Organic fractions were dried over Na_2SO_4, filtered, and concentrated to a brown oil. Purification by silica gel column chromatography using a 20-30% EtOAc:hexanes

gradient yielded the product **35** (203 mg, 0.51 mmol) in 63% yield. ^{1}H NMR (400 MHz, CD_3OD) δ 7.82 (t, J = 7.8 Hz, 1H), 7.40 (dd, J = 15.1, 1.6 Hz, 4H), 7.27 (d, J = 7.8 Hz, 2H), 7.04 (d, J = 8.5 Hz, 2H), 6.82 (d, J = 8.5 Hz, 2H), 2.20 (p, J = 7.3 Hz, 2H), 2.11 (q, J = 7.5 Hz, 2H), 1.02 – 0.87 (m, 2H), 0.79 (td, J = 7.4, 1.0 Hz, 6H).

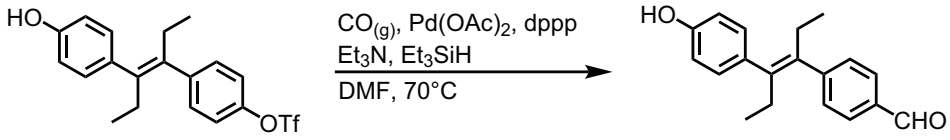

35 **36**

Synthesis of (E)-4-(4-(4-hydroxyphenyl)hex-3-en-3-yl)benzaldehyde (36):

To a flame dried round bottom flask purged with argon, **35** (50 mg, 0.32 mmol, 1.0 eq.), $Pd(OAc)_2$ (7.2 mg, 0.03 mmol, 0.1 eq.), and dppp (13.2 mg, 0.03 mmol, 0.1 eq.) were dissolved in DMF (1.5 mL) and the solution was sparged with argon for 5 minutes. The mixture was then heated to 70°C and a $CO_{(g)}$ atmosphere was established with a balloon upon which the reaction turned black. Et_3N (532 µL, 3.2 mmol 10 eq.) was then added and Et_3SiH (104 µL, 0.65 mmol, 2.0 eq.) dissolved in 0.5 mL DMF was then added dropqise over 2 hours via syringe pump. After 4 hours, TLC indicated complete consumption of starting material. The reaction was diluted with EtOAc and washed with 3x5 mL H_2O, and the organic was dried over Na_2SO_4, filtered, and concentrated. Crude was not purified.

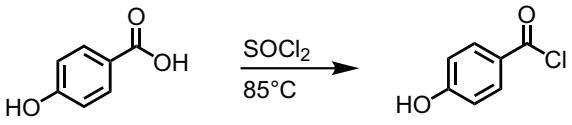

42

Synthesis of 4-hydroxybenzoyl chloride (42):

To a flame dried round bottom flask equipped with a condenser, **47** (2.28 g, 16.5 mmol, 1.5 eq.) was added and dissolved in $SOCl_2$ (46 mL, 0.64 mmol, 58 eq.) and refluxed for 1 hour. $SOCl_2$ was then removed under reduced pressured and the crude acyl chloride was used in the next step without further purification.

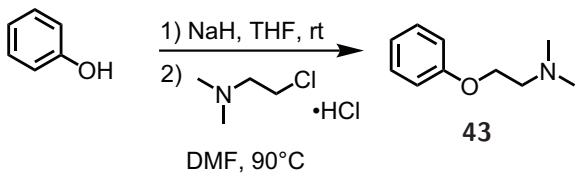

43

Synthesis of N,N-dimethyl-2-phenoxyethan-1-amine (43):

Phenol (500 mg, 5.3 mmol, 1.0 eq.) was added to a flame dried round bottom flask and dissolved in THF (13 mL). NaH (60% suspension in mineral oil) (636 mg, 15.9 mmol, 3.0 eq.) was added and the reaction was stirred for 30 minutes upon which the solvent was removed under reduced pressure. The solids were redissolved in DMF (12 mL) and **24** was added. The reaction was heated to 90°C and stirred for 1 hour upon which is was cooled to room temperature and quenched with 60 mL H_2O. The solution was extracted with 3x35 mL EtOAc, the organic fractions were combined and dried over Na_2SO_4, filtered, and concentrated to a pale yellow liquid. Used in the next reaction without any further purification. The spectroscopic data of the product is in agreement with that reported in the literature.[3]

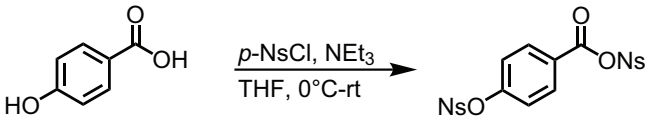

48

Synthesis of 4-nitrobenzenesulfonic 4-(((4-nitrophenyl)sulfonyl)oxy)benzoic anhydride (48):

To a flame dried round bottom flask, **47** (250 mg, 1.81 mmol, 1.0 eq.) was added and dissolved in THF (18 mL). Freshly distilled NEt_3 (757 µL, 5.43 mmol, 3.0 eq.) was added and the reaction was stirred for 10 minutes upon which it was cooled to 0°C and *p*-nitrobenzenesulfonyl chloride (882 mg, 3.98 mmol, 2.2 eq.) was added and the reaction was warmed to room temperature and stirred for 1.5 hours. TLC indicated complete consumption of starting material, product was not isolated and was used in the subsequent reaction without further purification. ^{1}H NMR (400 MHz, $CDCl_3$) δ 8.44 (d, J = 8.6 Hz, 2H), 8.26 (d, J = 8.5 Hz, 4H), 8.08 (d, J = 8.5 Hz, 4H), 7.23 (d, J = 8.7 Hz, 2H).

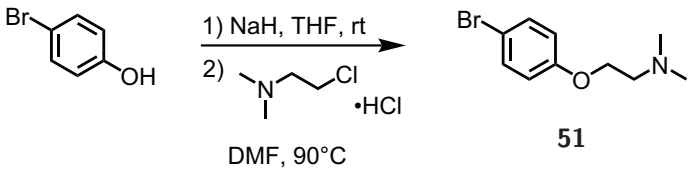

Synthesis of 2-(4-bromophenoxy)-N,N-dimethylethan-1-amine (51):

NaH (60% dispersion in mineral oil) (833 mg, 34.7 mmol, 3.0 eq.) was added to a flame dried round bottom flask and washed with 3x5 mL hexanes and then dried under vacuum. The dry NaH was then dissolved in THF (23 mL) and the suspension was cooled to 0°C upon which bromophenol was added in two portions. The reaction was warmed to room temperature and stirred for 30 minutes. After removing the THF under reduced pressure, the solids were redissolved in DMF (23 mL) and **24** (2.5 g, 17.3 mmol, 1.5 eq.) was added. The reaction was heated to 90°C and stirred for 1 hour. After cooling to room temperature, the reaction was slowly quenched with 100 mL H_2O and extracted with 3x30 mL EtOAc. The EtOAc fraction was then washed with 3x100 mL brine:H_2O (1:1), dried over Na_2SO_4, filtered, and concentrated to a light orange oil. Purification by silica gel column chromatography using a 5-15% MeOH:CH_2Cl_2 gradient gave the product as a light orange liquid (2.83 g, 11.6 mmol) in quantitative yield. The spectroscopic data of the product is in agreement with that reported in the literature.[4]

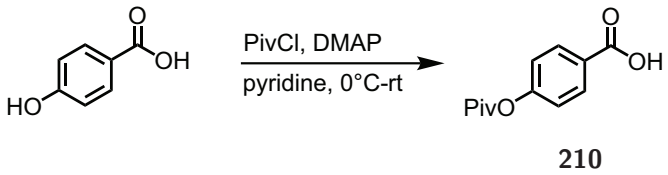

Synthesis of 4-(pivaloyloxy)benzoic acid (210):

To a flame dried round bottom flask, **47** was added and dissolved in pyridine (2.5 mL) and cooled to 0°C. DMAP (66.3 mg, 0.54 mmol, 0.3 eq.) was added and the reaction was stirred for 5 minutes before PivCl (670 µL, 5.43 mmol, 3.0 eq.) was added upon which the solution turned white. The reaction was warmed to room temperature and stirred for 2 hours, then diluted with 5 mL H_2O at 0°C. The mixture was extracted with 3x4 mL CH_2Cl_2 and the organic was washed with 4x13 mL H_2SO_4 (2M) followed by 10 mL brine. The organic

fraction was then dired over Na_2SO_4, filtered, and concentrated to a white solid. Purification by silica gel column chromatography using a 20-70% EtOAc:hexanes gradient. Product was isolated as a white solid (305 mg, 1.29 mmol) in 71% yield. The spectroscopic data of the product is in agreement with that reported in the literature.[5]

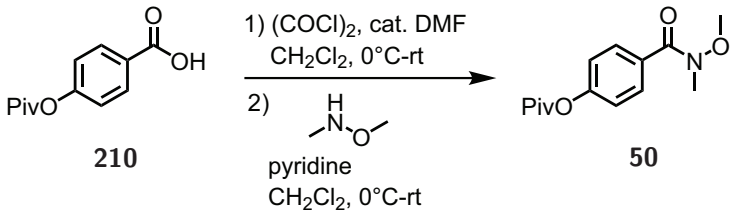

Synthesis of 4-(methoxy(methyl)carbamoyl)phenyl pivalate (50):

To a flame dried round bottom flask, **210** (905 mg, 4.08 mmol, 1.0 eq.) was added and dissolved in CH_2Cl_2 (10 mL) and cooled to 0°C. Oxalyl chloride (537 µL, 6.12 mmol, 1.5 eq.) was added followed by a catalytic amount of DMF (ca. 30 µL) and the reaction was warmed to toom temperature and stirred for 2 hours. The reaction was then cooled to 0°C and *N,O*-dimethylhydroxylamine (438 mg, 4.49 mmol, 1.1 eq.) was added followed by pyridine (723 µL, 8.98 mmol, 2.2 eq.) which turned the reaction opaque. The reaction was the stirred overnight and then diluted with 10 mL Et_2O and washed with 20 mL brine. The organic was dried over Na_2SO_4, filtered, and concentrated to a pale yellow oil. Purification by silica gel column chromatography using a 15-70% EtOAc:hexanes gradient gave the product as a clear oil (271 mg, 1.02 mmol) in 25% yield. ^{1}H NMR (400 MHz, $CDCl_3$) δ 7.73 – 7.63 (m, 2H), 7.09 – 7.00 (m, 2H), 3.47 (s, 3H), 3.28 (s, 3H), 1.30 (s, 9H).

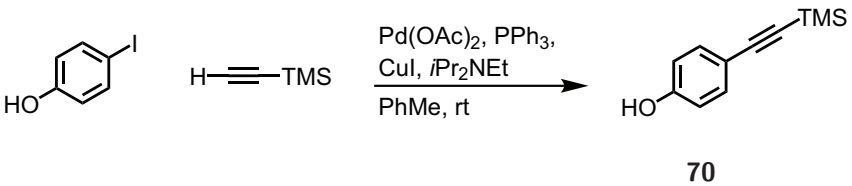

Synthesis of 4-((trimethylsilyl)ethynyl)phenol (70):

$Pd(OAc)_2$ (91 mg, 0.41 mmol, 3 mol%) and recrystallized PPh_3 (535 mg, 2.04 mmol, 15 mol%) were added to a flame-dried round-bottom flask and dissolved in CH_2Cl_2 (9 mL) and

stirred for 1 hour. The bright yellow solution was concentrated *in vacuo* and the yellow solids were redissolved in PhMe (27 mL). 4-iodophenol (10.3 g, 46.91 mmol, 1.0 eq.), CuI (893.2 mg, 4.69 mmol, 10 mol%), N,N-diisopropylethylamine (obtained from SPS) (8.17 mL, 46.91 mmol, 1.0 eq.) and TMS acetylene (6.63 mL, 46.91 mmol, 1.0 eq.) were added, in that order, to the flask at room temperature. The reaction gradually turned black and was left to stir for 24 hours. Once TLC indicated complete consumption of starting material, the reaction was concentrated directly *in vacuo* and purified by silica gel column chromatography using a 0%-12% EtOAc:hexanes solvent gradient. The product was isolated as a dark orange liquid (10.3 g, 54.12 mmol), yield reported in two steps. The spectroscopic data of the product is in agreement with that reported in the literature.[6]

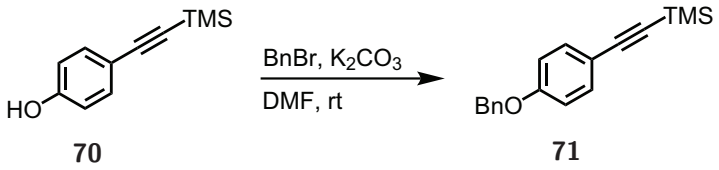

70 **71**

Synthesis of ((4-(benzyloxy)phenyl)ethynyl)trimethylsilane (71):

70 (10.3 g, 54.12 mmol, 1.0 eq.) was added to a flame-dried round-bottom flask and dissolved in DMF (135 mL) .K_2CO_3 (22.4 g, 162.4 mmol, 3.0 eq.) was added followed by benzylbromide (19.3 mL, 162.4 mmol, 3.0 eq.) which had been passed through a plug of basic alumina prior to use. The reaction was stirred overnight, diluted with 250 mL H_2O, and extracted with 3x 150 mL EtOAc. The organic layers were then combined and washed with 3x 200 mL 1:1 brine:H_2O. The organic was dried over $MgSO_4$, filtered, and concentrated to a dark orange oil. Purification by silica gel column chromatography using a 0%-3% EtOAc solvent gradient gave the product as a yellow liquid (10.1 g, 36.0 mmol) in 77% yield over two steps. The spectroscopic data of the product is in agreement with that reported in the literature.[7]

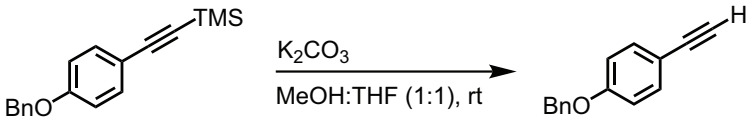

71 **72**

Synthesis of 1-(benzyloxy)-4-ethynylbenzene (72):

STARTING MATERIAL (10.1 g, 36.0 mmol, 1.0 eq.) was added to a round-bottom flask and dissolved in 1:1 MeOH:THF (100 mL). K_2CO_3 (99.5 g, 720 mmol, 20 eq.) was added and the reaction was stirred overnight. The cream coloured reaction was then quenched with 50 mL H_2O and the volatile solvents were removed *in vacuo*. The aqueous was extracted with 3x 100 mL Et_2O which was then washed with 3x 50 mL brine. The organic was dried over $MgSO_4$, filtered, and concetrated to an orange liquid. The product was recrystallized from CH_2Cl_2 and isolated as long, shiny yellow crystals (5.57 g, 26.75 mmol) in 74% yield. The spectroscopic data of the product is in agreement with that reported in the literature.[7]

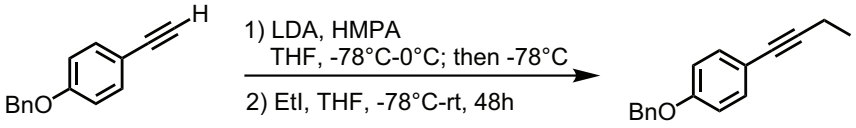

72 **66**

Synthesis of 1-(benzyloxy)-4-(but-1-yn-1-yl)benzene (66):

THF (62 mL) was added to a flame-dried round-bottom flask followed by freshly distilled *i*$PrNH_2$ (4.87 mL, 34.78 mmol, 1.3 eq.). The solution was cooled to -78°C and stirred for 15 minutes. *n*BuLi (1.83 M solution in hexanes) (17.5 mL, 32.09 mmol, 1.2 eq.) was then slowly added and the pale yellow solution was stirred for 15 minutes. In a separated, flame-dried round-bottom flask, STARTING MATERIAL (5.57 g, 26.75 mmol, 1.0 eq.) was dissolved in THF (27 mL) and slowly added to the -78°C solution of LDA via cannula. The reaction quickly turned brown and was stirred for 30 minutes and HMPA (1.86 mL, 10.7 mmol, 40 mol%) was added. The reaction was stirred for 15 minutes at -78°C, warmed to 0°C and stirred for 20 minutes, then cooled to -78°C and stirred for 15 minutes. Iodoethane (6.45 mL, 80.25 mmol, 3.0 eq.) was passed through a plug of basic alumina and slowly added to the reaction mixture. The reaction was stirred for 48 hours while slowly warming

to room temperature. TLC indicated full conversion of starting material and the reaction was quenched with 10 mL of saturated NH_4Cl solution and diluted with 25 mL H_2O. The THF was removed *in vacuo* and the aqueous was extracted with 3x 75 mL Et_2O. The organic layers were combined, washed with 100 mL brine, dried over $MgSO_4$, filtered, and concentrated to a yellow liquid. Purification by silica gel column chromatography using a 0%-2% EtOAc:hexanes solvent gradient yielded the product as a waxy, light yellow solid (5.87 g, 25.68 mmol) in 93% yield. ^{1}H NMR (400 MHz, $CDCl_3$) δ 7.52 – 7.33 (m, 7H), 6.92 (d, J = 8.9 Hz, 2H), 5.08 (s, 2H), 2.44 (q, J = 7.5 Hz, 2H), 1.27 (t, J = 7.5 Hz, 3H). HRMS calc. for $C_{17}H_{16}NaO$ (M + Na)+: 259.1093. Found: 259.1088.

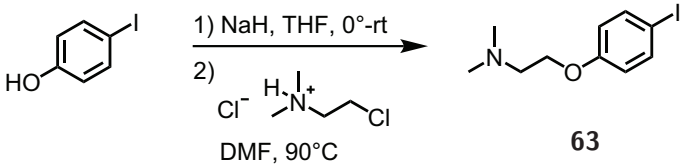

63

Synthesis of 2-(4-iodophenoxy)-N,N-dimethylethan-1-amine (63):

NaH (60% dispersion in mineral oil) (5.45 g, 136.36 mmol, 3.0 eq.) was added to a flame-dried round-bottom flask and suspended in THF (91 mL). The suspension was cooled to 0°C and 4-iodophenol (10.0 g, 45.5 mmol, 1.0 eq.) was slowly added. The reaction was warmed to room temperature and stirred for 30 minutes until all bubbling ceased. THF was removed *in vacuo* and the solids were redissolved in DMF (91 mL) and the solution was cooled to 0°C. N,N-dimethylaminoethyl chloride (9.83 g, 68.25 mmol, 1.5 eq.) was then added portion-wise and the reaction was warmed to 90°C and stirred overnight. TLC showed complete consumption of starting material and the reaction was cooled to room temperature and quenched with 250 mL H_2O. The mixture was extracted with 3x100 mL EtOAc, the organic was then washed with 3x 100 mL 1:1 brine:H_2O, dried over Na_2SO_4, filtered, and concentrated to an orange oil. Purification by silica gel column chromatography using a 5%-6.5% MeOH:CH_2Cl_2 solvent gradient gave the product as an orange oil that became turbid (13.1 g, 45.05) in 99% yield. The spectroscopic data of the product is in agreement with that reported in the literature.[8]

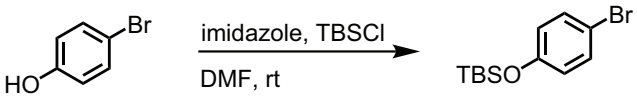

68

Synthesis of (4-bromophenoxy)(tert-butyl)dimethylsilane (68):

4-Bromophenol (15 g, 86.7 mmol, 1.0 eq.) was added to a flame-dried round-bottom flask and dissolved in DMF (116 mL). The solution was cooled to 0°C and imidazole (14.2 g, 208.1 mmol, 2.4 eq.) was added followed by TBSCl (15.67 g, 104.0 mmol, 1.2 eq). The reaction was warmed to room temperature and stirred overnight. TLC indicated complete conversion of starting material and the reaction was diluted with 250 mL H_2O and extracted with 3x 150 mL EtOAc which was then washed with 3x 100 mL 1:1 brine:H_2O. The organic was dried over $MgSO_4$, filtered, and concentrated to a yellow/orange oil. Purification by silica gel column chromatography using hexanes as the eluent afforded the product as a clear, viscous oil (24.5 g, 85.8 mmol) in 99% yield. The spectroscopic data of the product is in agreement with that reported in the literature.[9]

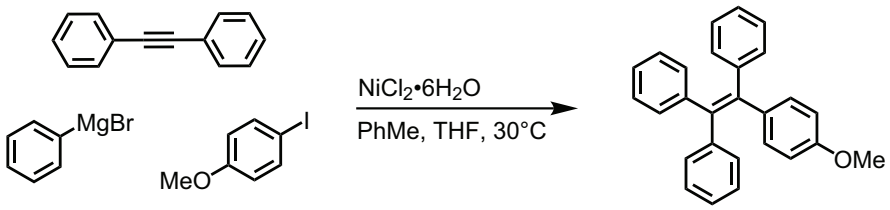

59

Synthesis of (2-(4-methoxyphenyl)ethene-1,1,2-triyl)tribenzene (59):

p-iodoanisole (393 mg, 1.7 mmol, 1.2 eq), diphenylacetylene (250 mg, 1.4 mmol, 1.0 eq.) and $NiCl_2 \cdot 6\,H_2O$ (3.3 mg, 0.014 mmol, 1 mol%) were added to a dry round-bottom flask and dissolved in PhMe (6 mL). Phenyl magnesium bromide (3 M solution in THF) (561 µL, 1.68 mmol, 1.2 eq.) was then slowly added to the stirring solution. The reaction was heated to 30°C and stirred overnight. TLC indicated complete consumption of starting material, the reaction was then quenched with 1 mL H_2O and filtered through a plug of silica and eluted with EtOAc. The filtrate was concentrated to an orange oil and then purified by silica gel column chromatography using a 0%-10% EtOAc:hexanes solvent gradient. The product

was isolated as a bright yellow foam (307 mg, 0.80 mmol) in 60% yield. The spectroscopic data of the product is in agreement with that reported in the literature.[10]

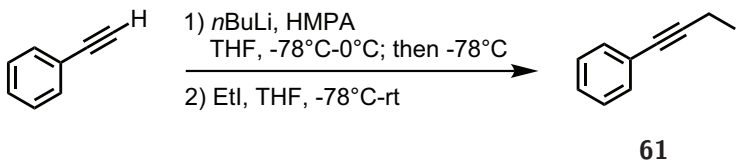

61

Synthesis of but-1-yn-1-ylbenzene (61):

Phenylacetylene 3.0 g, 29.4 mol, 1.0 eq. was added to a flame-dried round-bottom flask and dissolved in THF (100 mL), the solution was cooled to -78°C and stirred for 15 minutes. *n*BuLi (1.99 M solution) (17.7 mL, 35.2 mmol, 1.2 eq.) was slowly added and reaction was left to stir for 30 minutes. HMPA (1.1 mL, 8.82 mmol, 30 mol%) was added and reaction was stirred for 20 minutes at -78°C, warmed to 0°C and stirred for 30 minutes, and then cooled to -78°C and stirred for 20 minutes. Iodoethane (5.0 mL, 48.5 mmol, 1.6 eq.) was passed through a plug of basic alumina and then slowly added to the reaction. The reaction stirred overnight while slowly coming to room temperature. The reaction was then quenched with 10 mL saturated NH_4Cl solution and diluted with 10 mL H_2O. THF was removed *in vacuo* and the aqueous was extracted with 3x 50 mL Et_2O, dried over $MgSO_4$, filtered, and concentrated to a dark yellow oil. Purification by silica gel column chromatography using a 0%-8% EtOAc:hexanes solvent gradient gave the product as a bright yellow liquid (1.72 g, 13.2 mmol) in 45% yield. The spectroscopic data of the product is in agreement with that reported in the literature.[11]

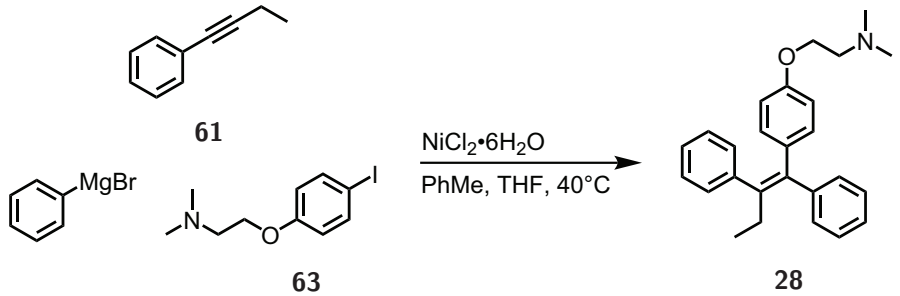

61 **63** **28**

Synthesis of (Z)-2-(4-(1,2-diphenylbut-1-en-1-yl)phenoxy)-N,N-dimethylethan-1-

amine (28):

61 (250 mg, 1.9 mmol, 1.0 eq.), **63** (671 mg, 2.3 mmol, 1.2 eq.) and $NiCl_2 \cdot 6\,H_2O$ (4.5 mg, 0.019 mmol, 1 mol%) were added to a flame-dried round-bottom flask and dissolved in PhMe (7.7 mL). Phenyl magnesium bromide (3 M solution in THF) (767 µL, 2.3 mmol, 1.2 eq.) was slowly added and the reaction was heated to 40°C and stirred for 19 hours. After cooling to room temperature, the reaction was quenched with 1 mL H_2O, filtered through a silica plug and eluted with EtOAc, and concentrated to a brown oil. Purification by silica gel column chromatography using a 3%-12% MeOH:CH_2Cl_2 solvent gradient gave the product as a brown/orange oil (166 mg, 0.44 mmol) in 23% yield as the pure *Z* isomer. The spectroscopic data of the product is in agreement with that reported in the literature.[10]

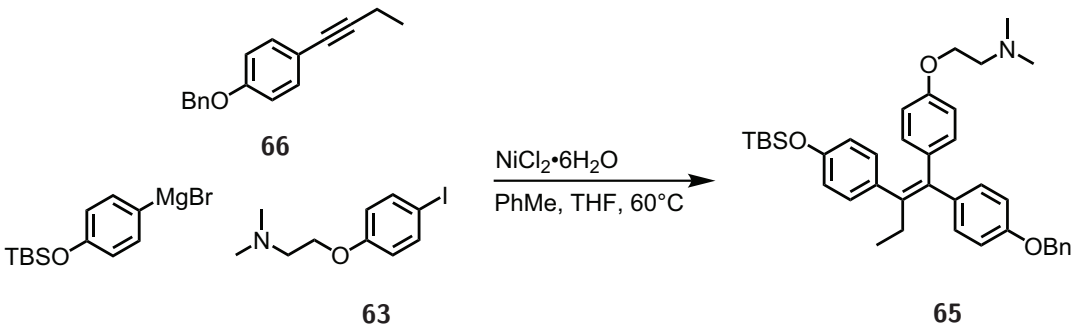

Synthesis of (Z)-2-(4-(1-(4-(benzyloxy)phenyl)-2-(4-((tert-butyldimethylsilyl)oxy)phenyl)but-1-en-1-yl)phenoxy)-N,N-dimethylethan-1-amine (65):

66 (1.0 g, 4.23 mmol, 1.0 eq.), **63** (1.48 g, 5.08 mmol, 1.2 eq.), and $NiCl_2 \cdot 6\,H_2O$ (10.1 mg, 0.042 mmol, 1 mol%) were added to a flame-dried round-bottom flask and dissolved in PhMe (17 mL). (4-((tert-butyldimethylsilyl)oxy)phenyl)magnesium bromide (0.80 M solution in THF) (6.35 mL, 5.08 mmol, 1.2 eq.) was prepared according to General Procedure B and slowly added to the solution. The reaction was then heated to 50°C and stirred for 24 hours. TLC indicated complete consumption of starting material and the reaction was quenched with 1 mL H_2O and filtered through a silica plug using EtOAc as an eluent. Purification by silica gel column chromatography using a 1%-9% MeOH:CH_2Cl_2 solvent gradient gave the product as a brown oil (786 mg, 1.31 mmol) in 31% yield as the pure *Z* isomer. ^{1}H NMR (400 MHz, $CDCl_3$) δ 7.52 – 7.47 (m, 2H), 7.46 – 7.40 (m, 3H), 7.39 – 7.34 (m, 1H),

7.19 (d, J = 8.7 Hz, 2H), 6.99 (d, J = 8.6 Hz, 4H), 6.80 (d, J = 8.7 Hz, 2H), 6.69 (d, J = 8.5 Hz, 2H), 6.60 (d, J = 8.8 Hz, 2H), 5.11 (s, 2H), 3.99 (t, J = 5.8 Hz, 2H), 2.71 (t, J = 5.8 Hz, 2H), 2.50 (q, J = 7.3 Hz, 2H), 2.35 (s, 7H), 1.01 (s, 15H), 0.21 (s, 6H). ^{13}C NMR (126 MHz, $CDCl_3$) δ 157.50, 156.61, 153.78, 140.74, 137.28, 137.14, 136.77, 136.13, 135.59, 131.96, 130.70, 130.67, 128.60, 127.98, 127.60, 119.60, 114.34, 113.32, 70.05, 65.63, 58.28, 45.85, 28.93, 25.80, 25.77, 18.29, 13.74, -4.36. HRMS calc. for $C_{39}H_{50}NO_3Si$ (M + H)+: 608.3554. Found: 608.3567.

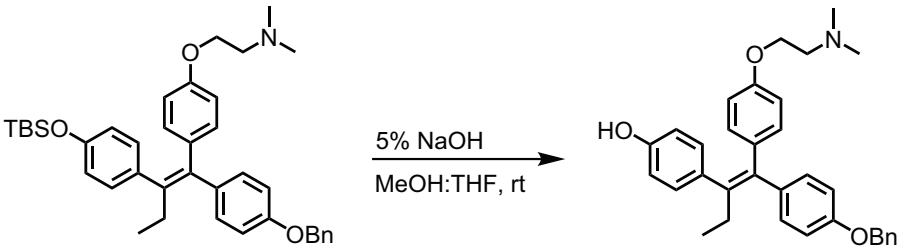

65 **74**

Synthesis of (Z)-4-(1-(4-(benzyloxy)phenyl)-1-(4-(2-(dimethylamino)ethoxy)phenyl)but-1-en-2-yl)phenol (74):

65 (875 mg, 1.44 mmol, 1.0 eq.) was added to a round-bottom flask and dissolved in MeOH (14 mL). Crushed NaOH (570 mg, 14.25 mmol, 10 eq.) was added and the reaction was stirred overnight at room temperature. TLC indicated complete conversion of starting material and the reaction was then quenched with 5 mL H_2O, MeOH was removed *in vacuo* and the aqueous was extracted with 3x 15 mL EtOAc, dried over Na_2SO_4, filtered, and concentrated to a brown oil. Purification by silica gel column chromatography using a 0%-8% MeOH:CH_2Cl_2 solvent gradient gave the product as a brown oil that tended to foam (557 mg, 1.13 mmol) in 78% yield as a 1:1 mixture of *E:Z* isomers. ^{1}H NMR (400 MHz, $CDCl_3$) δ 7.48 (d, J = 7.3 Hz, 2H), 7.44 – 7.27 (m, 3H), 7.18 – 7.09 (m, 2H), 7.03 – 6.89 (m, 4H), 6.79 (dd, J = 9.0, 2.4 Hz, 2H), 6.66 – 6.56 (m, 4H), 5.11 (s, 2H), 4.02 (t, J = 5.4 Hz, 2H), 2.79 (s, 2H), 2.51 – 2.39 (q, 2H), 2.37 (s, 6H), 0.93 (t, J = 7.4 Hz, 3H). ^{13}C NMR (126 MHz, $CDCl_3$) δ 157.47, 157.25, 156.65, 156.28, 154.33, 153.99, 140.76, 140.61, 137.12, 137.09, 136.79, 136.70, 136.42, 136.32, 134.67, 134.30, 131.96, 131.94, 130.91, 130.86, 130.63, 130.58, 128.58, 128.52, 128.49, 127.96, 127.86, 127.58, 127.55, 115.01, 114.93, 114.32, 114.06, 113.66, 113.36, 70.04,

69.84, 65.50, 64.96, 58.15, 57.97, 45.66, 45.43, 28.94, 28.90, 13.71, 13.69. HRMS calc. for $C_{33}H_{36}NO_3$ (M + H)+: 494.2690. Found: 494.2699.

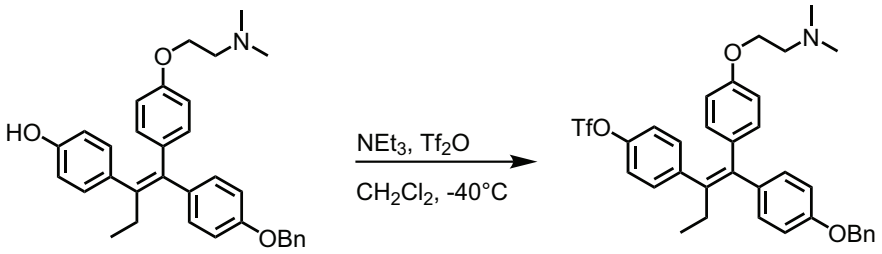

74 75

Synthesis of (Z)-4-(1-(4-(benzyloxy)phenyl)-1-(4-(2-(dimethylamino)ethoxy)phenyl)but-1-en-2-yl)phenyl trifluoromethanesulfonate (75):

To a flame-dried round-bottom flask, **74** (700 mg, 1.42 mmol, 1.0 eq) was added and dissolved in CH_2Cl_2, followed by the addition of freshly distilled NEt_3 (297 µL, 2.13 mmol, 1.5 eq.). The reaction was cooled to -40°C and stirred for 10 minutes before the dropwise addition of freshly distilled Tf_2O (238 µL, 1.42 mmol, 1.0 eq.). The reaction was stirred for 1 hour, TLC indicated full conversion of starting material and the reaction was quenched with 200 µL ethylenediamine, followed by 30 mL H_2O. After warming to room temperature, the reaction was extracted with 3x 25 mL CH_2Cl_2, dried over Na_2SO_4, filtered, and concentrated to a foamy yellow oil. Purification by silica gel column chromatography using a 0%-8% solvent gradient gave the product as a yellow oil (737 mg, 1.18 mmol) in 83% yield as a 1:1 mixture of *E:Z* isomers. ^{1}H NMR (400 MHz, $CDCl_3$) δ 7.54 – 7.31 (m, 12H), 7.24 – 7.12 (m, 6H), 7.09 (dd, J = 8.8, 1.8 Hz, 4H), 6.99 (d, J = 8.7 Hz, 2H), 6.92 (d, J = 8.7 Hz, 2H), 6.79 – 6.67 (m, 4H), 6.65 (d, J = 8.8 Hz, 2H), 6.59 (d, J = 8.8 Hz, 2H), 5.10 (s, 2H), 4.95 (s, 2H), 4.11 (t, J = 5.8 Hz, 2H), 3.96 (t, J = 5.8 Hz, 2H), 2.77 (t, J = 5.7 Hz, 2H), 2.68 (t, J = 5.8 Hz, 2H), 2.52 (dq, J = 7.9, 4.0 Hz, 3H), 2.38 (s, 7H), 2.32 (s, 6H), 1.01 – 0.88 (t, 6H). ^{13}C NMR (126 MHz, $CDCl_3$) δ 157.80, 157.11, 147.57, 143.36, 139.52, 136.93, 135.85, 131.94, 131.89, 131.44, 130.51, 130.45, 128.60, 128.51, 128.01, 127.92, 127.56, 127.51, 120.69, 114.42, 114.16, 113.85, 113.56, 70.06, 69.88, 65.98, 65.77, 58.37, 58.27, 45.95, 45.89, 28.81, 13.59.

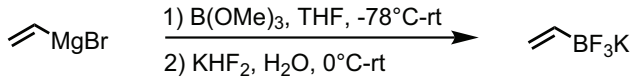

80

Synthesis of Potassium vinyltrifluoroborate (80):

To a flame-dried round bottom flask, trimethylborate (1.61 mL, 14.4 mmol, 1.2 eq.) was added followed by THF (15 mL) and the solution was cooled to -78°C. Vinyl magnesium bromide (1.0 M solution in THF) (12 mL, 12.0 mmol, 1.0 eq) was added using an addition funnel and the thick suspension as stirred for 20 minutes, then warmed to room temperature and stirred for 1 hour. After cooling to 0°C, KHF_2 (4.49 g, 60 mmol, 5.0 eq.) was added followed by 7 mL H_2O over 30 minutes using an addition funnel. The reaction was stirred for 20 minutes at room temperature and then concentrated *in vacuo* and lyophilized overnight. The resulting solids were dissolved in acetone, filtered, and the filtrate was concentrated. The white solids were then dissolved in minimal hot acetone and the product was precipitated by the addition of Et_2O. Vacuum filtration afford the product as a dull solid (756 mg, 5.64 mmol) in 47% yield. The spectroscopic data of the product is in agreement with that reported in the literature.[12]

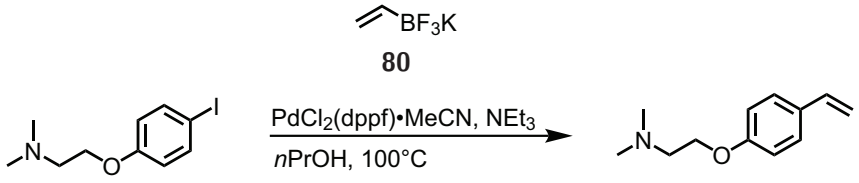

63 **83**

Synthesis of N,N-dimethyl-2-(4-vinylphenoxy)ethan-1-amine (83):

To a flame-dried round bottom flask equipped with a condenser, **63** (200 mg, 0.69 mmol, 1.0 eq.) was added and dissolved in *n*PrOH (14 mL). To the solution, **80** (110 mg, 0.82 mmol, 1.2 eq.), $PdCl_2$(dppf) (25 mg, 0.035 mmol, 5 mol%) and freshly distilled NEt_3 (96 µL, 0.69 mmol, 1.0 eq.) were added and the reaction was heated to 100°C and stirred for 24 hours. Once complete, it was cooled to room temperature and quenched with 5 mL H_2O, extracted with 3x 15 mL EtoAc which was then dried over Na_2SO_4, filtered, and concetrated to a dark brown oil. Purification by silica gel column chromatography using a 2%

MeOH:CH_2Cl_2 solvent system ave the product as a dark brown oil (95 mg, 0.50 mmol) in 72% yield. ^{1}H NMR (400 MHz, $CDCl_3$) δ 7.58 (d, J = 8.9 Hz, 2H), 6.72 (d, J = 9.0 Hz, 2H), 4.26 (t, J = 5.2 Hz, 2H), 3.15 – 3.09 (m, 2H), 2.64 (s, 6H).

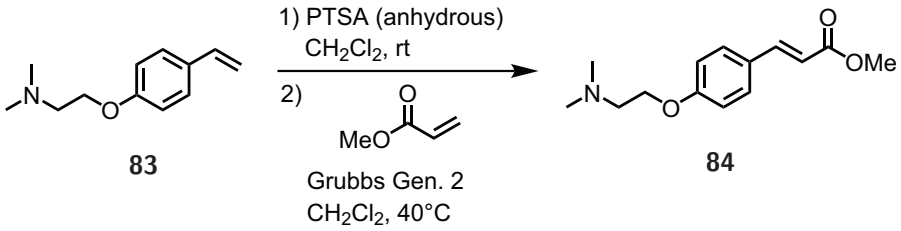

83 **84**

Synthesis of methyl (E)-3-(4-(2-(dimethylamino)ethoxy)phenyl)acrylate (84):

Prepared according to General Procedure C using **83** (60 mg, 0.31 mmol, 1.0 eq.), anhydrous PTSA (59 mg, 0.34 mmol, 1.1 eq.), methyl acrylate (285 µL, 3.14 mmol, 10 eq.) and Grubbs gen. 2 catalyst (13 mg, 0.016 mmol, 5 mol%). The product was not purified, crude isolated as a dark brown residue. ^{1}H NMR (400 MHz, $CDCl_3$) δ 7.35 (d, J = 8.7 Hz, 2H), 6.90 (d, J = 8.8 Hz, 2H), 6.67 (dd, J = 17.7, 11.0 Hz, 1H), 5.62 (dd, J = 17.6, 1.0 Hz, 1H), 5.14 (dd, J = 10.9, 0.9 Hz, 1H), 4.13 (t, J = 5.7 Hz, 2H), 2.83 (t, J = 5.7 Hz, 2H), 2.42 (s, 6H).

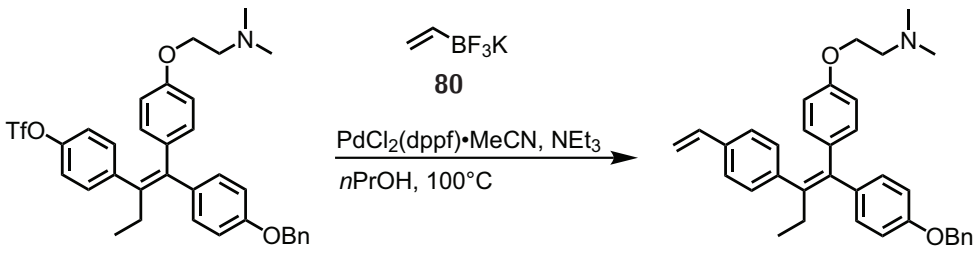

75 **79**

Synthesis of (Z)-2-(4-(1-(4-(benzyloxy)phenyl)-2-(4-vinylphenyl)but-1-en-1-yl)phenoxy)-N,N-dimethylethan-1-amine (79):

To a flame-dried flask equipped with a condenser, **75** (380 mg, 0.61 mmol, 1.0 eq.), **80** (97.8 mg, 0.73, 1.2 eq.), and $PdCl_2$(dppf) (22.3 mg, 0.031 mmol, 5 mol%) were added and dissolved in *n*PrOH (12 mL). Freshly distilled NEt_3 (85 µL, 0.61 mmol, 1.0 eq) was then added and the reaction was heated to 100°C and stirred for 24 hours. After cooling to room

temperature, the reaction was quenched with 5 mL H_2O, extracted with 3x15 mL EtOAc, dried over Na_2SO_4, filtered, and concentrated to a dark yellow oil. Purification by silica gel column chromatography using a 0%-8% MeOH:CH_2Cl_2 solvent gradient gave the product as a yellow oil (250 mg, 0.50 mmol) in 81% yield as a 1:1 mixture of *E:Z* isomers. ^{1}H NMR (400 MHz, $CDCl_3$) δ 7.52 – 7.45 (m, 2H), 7.45 – 7.29 (m, 10H), 7.27 – 7.22 (m, 3H), 7.18 (dd, J = 8.6, 6.2 Hz, 4H), 7.11 (dd, J = 8.3, 3.5 Hz, 3H), 6.99 (d, J = 8.7 Hz, 2H), 6.93 (d, J = 8.7 Hz, 2H), 6.83 (dd, J = 8.9, 7.1 Hz, 3H), 6.67 (d, J = 8.8 Hz, 3H), 6.61 (d, J = 8.8 Hz, 2H), 5.72 (ddd, J = 17.6, 3.0, 1.0 Hz, 2H), 5.22 (ddd, J = 10.8, 2.6, 1.0 Hz, 2H), 5.11 (s, 2H), 4.96 (s, 2H), 4.13 (t, J = 5.8 Hz, 2H), 3.98 (t, J = 5.8 Hz, 2H), 2.80 (t, J = 5.7 Hz, 2H), 2.71 (t, J = 5.7 Hz, 2H), 2.52 (qd, J = 7.4, 3.6 Hz, 4H), 2.37 (d, J = 30.1 Hz, 12H), 0.97 (td, J = 7.5, 1.4 Hz, 6H). ^{13}C NMR (126 MHz, $CDCl_{3)}$ δ 157.61, 157.56, 156.84, 156.80, 142.35, 142.33, 140.68, 140.66, 138.04, 137.11, 137.07, 136.75, 136.73, 136.60, 136.40, 136.09, 135.91, 135.09, 132.00, 131.95, 131.93, 131.73, 130.64, 130.59, 130.55, 130.41, 129.90, 129.86, 128.60, 128.52, 128.49, 128.31, 127.98, 127.87, 127.59, 127.56, 127.47, 127.39, 126.15, 126.11, 125.82, 125.80, 125.75, 115.38, 114.93, 114.36, 114.11, 114.04, 113.73, 113.46, 113.40, 113.01, 70.06, 69.83, 65.89, 65.66, 58.38, 58.31, 45.93, 45.90, 45.88, 28.91, 28.88, 13.72, 13.70. HRMS calc. for $C_{35}H_{38}NO_2$ (M + H)+: 504.2897. Found: 504.2906.

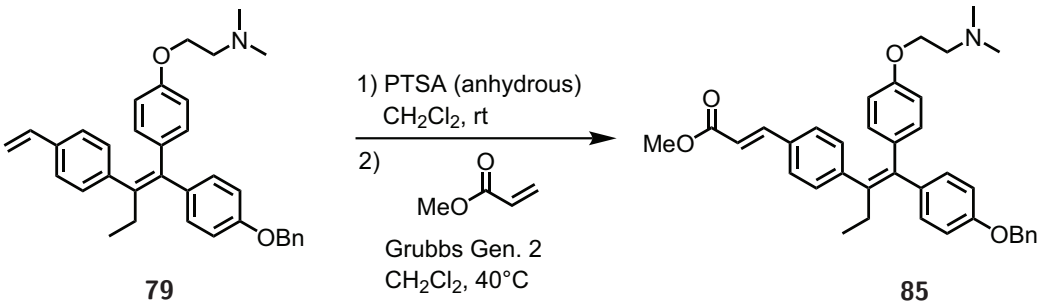

79 **85**

Synthesis of methyl (E)-3-(4-((Z)-1-(4-(benzyloxy)phenyl)-1-(4-(2-(dimethylamino)ethoxy)phenyl)but-1-en-2-yl)phenyl)acrylate (85):

Prepared according to General Procedure C using **79** (155 mg, 0.31 mmol, 1.0 eq.), anhydrous PTSA (58 mg, 0.34 mmol, 1.1 eq.), methyl acrylate (281 µL, 3.1 mmol, 10 eq.), and Grubbs gen. 2 catalyst (13.2 mg, 0.02 mmol, 5 mol%). The product was isolated as a dark brown/green oil (123 mg, 0.22 mmol) in 71% yield as a 1:1 mixture of *E:Z* isomers. ^{1}H

NMR (400 MHz, $CDCl_3$) δ 7.65 (dd, J = 16.0, 3.0 Hz, 2H), 7.51 – 7.45 (m, 2H), 7.45 – 7.29 (m, 12H), 7.22 – 7.13 (m, 6H), 6.98 (d, J = 8.7 Hz, 2H), 6.92 (d, J = 8.7 Hz, 2H), 6.79 (dd, J = 8.7, 5.8 Hz, 3H), 6.66 (d, J = 8.8 Hz, 2H), 6.59 (d, J = 8.8 Hz, 2H), 6.39 (dd, J = 16.0, 2.3 Hz, 2H), 5.10 (s, 2H), 4.95 (s, 2H), 4.12 (t, J = 5.8 Hz, 2H), 3.97 (t, J = 5.7 Hz, 2H), 3.82 (s, 6H), 2.80 (t, J = 5.7 Hz, 2H), 2.70 (t, J = 5.7 Hz, 2H), 2.53 (qd, J = 7.4, 3.6 Hz, 4H), 2.40 (s, 6H), 2.34 (s, 6H), 0.96 (td, J = 7.4, 1.1 Hz, 6H). ^{13}C NMR (126 MHz, $CDCl_{3)}$ δ 167.59, 157.72, 157.67, 157.01, 156.98, 145.35, 144.77, 140.20, 138.91, 137.04, 136.98, 136.26, 136.07, 135.76, 135.59, 132.01, 131.96, 131.93, 130.60, 130.55, 130.28, 128.59, 128.49, 127.99, 127.89, 127.77, 127.72, 127.57, 127.55, 127.52, 116.87, 114.38, 114.12, 113.79, 113.51, 70.05, 69.83, 65.88, 65.66, 58.34, 58.26, 51.63, 45.90, 45.86, 28.77, 13.68. HRMS calc. for $C_{37}H_{40}NO_4$ (M + H)+: 562.2952. Found: 562.2965.

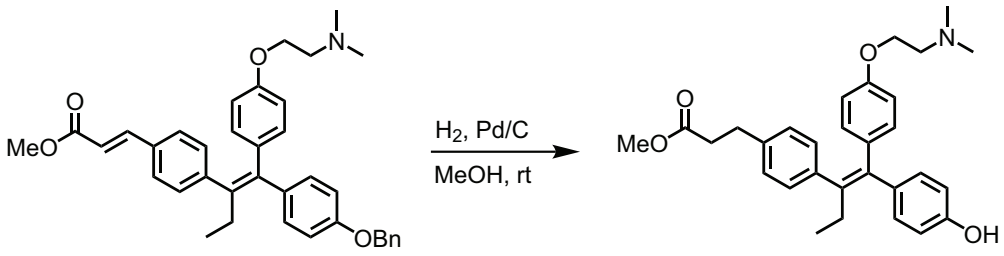

85 **211**

Synthesis of methyl (Z)-3-(4-(1-(4-(2-(dimethylamino)ethoxy)phenyl)-1-(4-hydroxyphenyl)but-1-en-2-yl)phenyl)propanoate (211):

To a dry flask, **85** (123 mg, 0.22 mmol, 1.0 eq.) was added and dissolved in MeOH (4 mL) and a pipette tip full of 10% Pd/C was added. A balloon was used to establish an H_2 atmosphere and the reaction was stirred for 24 hours. H_2 was vented and the suspension was filtered through a column of celite and concentrated to a pale yellow oil (90 mg, 0.19 mmol) that did not require purification in 87% yield as a 1:1 mixture of *E:Z* isomers. ^1H NMR (500 MHz, $CDCl_3$) δ 7.09 (d, J = 8.6 Hz, 2H), 7.07 – 6.92 (m, 10H), 6.80 (d, J = 7.9 Hz, 3H), 6.75 – 6.61 (m, 6H), 6.47 (d, J = 8.2 Hz, 2H), 6.39 – 6.32 (m, 2H), 4.10 (t, J = 5.6 Hz, 2H), 3.94 (t, J = 5.6 Hz, 2H), 3.67 (d, J = 4.0 Hz, 6H), 2.93 – 2.86 (m, 4H), 2.84 (t, J = 5.5 Hz, 2H), 2.75 (t, J = 5.6 Hz, 2H), 2.61 (td, J = 7.9, 5.5 Hz, 4H), 2.48 (dd, J

= 11.1, 7.4 Hz, 6H), 2.41 (s, 6H), 2.36 (s, 6H), 0.93 (td, J = 7.4, 4.3 Hz, 6H). ^{13}C NMR (126 MHz, $CDCl_3$) δ 173.62, 173.59, 157.21, 156.41, 155.83, 154.83, 140.76, 140.74, 140.23, 140.10, 138.05, 138.04, 137.80, 137.78, 136.70, 136.15, 135.10, 134.82, 132.05, 131.90, 130.63, 130.51, 129.85, 129.82, 127.69, 127.66, 115.41, 114.72, 113.81, 113.05, 64.86, 64.52, 58.13, 58.09, 53.46, 51.60, 51.59, 45.60, 45.37, 45.28, 35.71, 35.70, 30.65, 30.55, 30.36, 29.03, 28.91, 28.89, 27.04, 27.01, 26.93, 26.89, 26.59, 26.49, 26.41, 26.32, 25.33, 13.76, 13.71. HRMS calc. for $C_{30}H_{36}NO_4$ (M + H)+: 474.2639. Found: 474.2636.

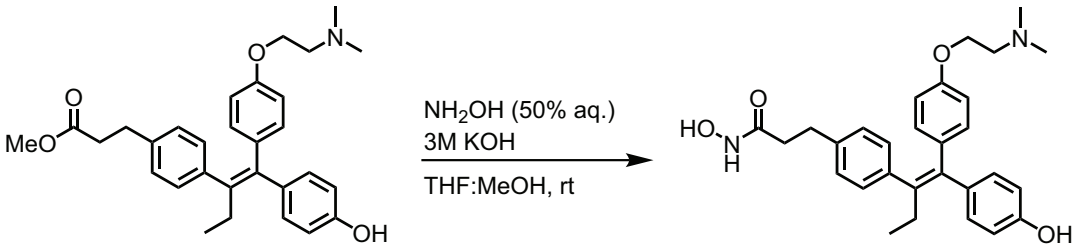

211 **5**

Synthesis of (Z)-3-(4-(1-(4-(2-(dimethylamino)ethoxy)phenyl)-1-(4-hydroxyphenyl)but-1-en-2-yl)phenyl)-N-hydroxypropanamide (5):

Prepared according to General Procedure A using methyl ester **211** (90 mg, 0.19 mmol, 1.0 eq.), NH_2OH (50% w/w in H_2O) (5.82 mL, 95.01 mmol, 500 eq.), and 3 M KOH (443 µL, 1.33 mmol, 7.0 eq.). Neutralized with 3 M HCl and concentrated to a white/yellow residue. Purification by reverse phase C18 column chromatography using a 10%-100% MeOH:H_2O solvent gradient yielded the product as a white solid (51 mg, 0.11 mmol) in 57% yield as a 1:1 mixture of *E:Z* isomers. ^{1}H NMR (500 MHz, $CDCl_3$) δ 8.57 (s, 3H), 7.02 (d, J = 8.5 Hz, 6H), 6.84 – 6.71 (m, 4H), 6.60 (d, J = 8.8 Hz, 2H), 4.02 (t, J = 5.4 Hz, 2H), 2.86 (t, J = 7.7 Hz, 2H), 2.80 (t, J = 5.4 Hz, 2H), 2.52 – 2.44 (m, 3H), 2.39 (s, 6H), 0.91 (t, J = 7.4 Hz, 3H). HRMS calc. for $C_{29}H_{35}N_2O_4$ (M + H)+: 475.2591. Found: 475.2594.

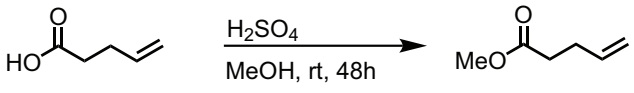

212

Synthesis of methyl pent-4-enoate (212):

To a dry round bottom flask equipped with a condenser, pent-4-enoic acid (5.0 g, 50 mmol, 1.0 eq.) and dissolved in MeOH (10 mL). Catalytic concentrated H_2SO_4 (5 drops) was added and the reaction was heated to reflux and stirred overnight. Once cooled, 5 mL H_2O were added and the product separated to the top phase. The organic phase was pipetted off and filtered through a plug of Na_2SO_4. Product isolated as a clear, colourless liquid (3.9 g, 34.5 mmol) in 69% yield. The spectroscopic data of the product is in agreement with that reported in the literature.[13]

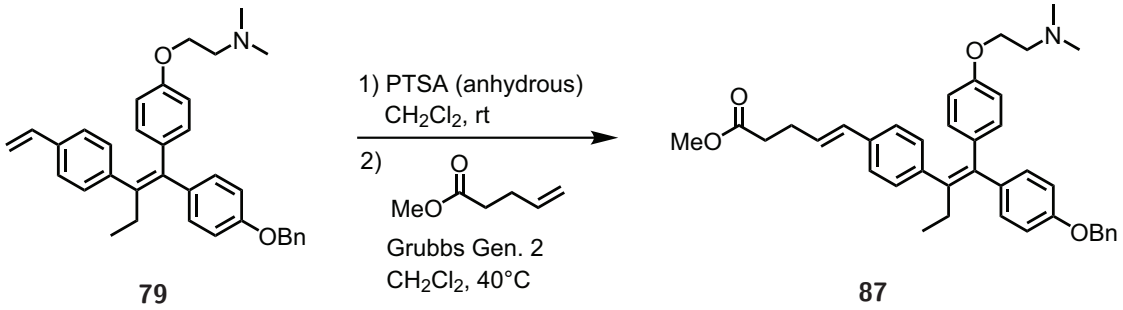

79 **87**

Synthesis of methyl (E)-5-(4-((Z)-1-(4-(benzyloxy)phenyl)-1-(4-(2-(dimethylamino)ethoxy)phenyl)but-1-en-2-yl)phenyl)pent-4-enoate (213):

Prepared according to General Procedure C using **87** (148 mg, 0.29 mmol, 1.0 eq.), anhydrous PTSA (56 mg, 0.32 mmol, 1.1 eq.), methyl pentenoate (336 mg, 2.9 mmol, 10 eq.), and Grubbs gen. 2 catalyst (12.5 mg, 0.015 mmol, 5 mol%). The product was isolated as a dark brown/green oil (129 mg, 0.22 mmol) in 74% yield as a 1:1 mixture of *E:Z* isomers. ^{1}H NMR (500 MHz, $CDCl_3$) δ 7.48 (d, J = 7.0 Hz, 2H), 7.46 – 7.30 (m, 9H), 7.24 – 7.10 (m, 7H), 7.06 (td, J = 6.0, 3.1 Hz, 4H), 6.97 (d, J = 8.6 Hz, 3H), 6.91 (d, J = 8.6 Hz, 2H), 6.80 (ddd, J = 8.0, 6.4, 1.6 Hz, 4H), 6.71 – 6.62 (m, 2H), 6.59 (d, J = 8.7 Hz, 2H), 5.09 (s, 2H), 4.95 (s, 1H), 4.12 (t, J = 5.8 Hz, 2H), 3.97 (t, J = 6.0 Hz, 2H), 3.74 (s, 2H), 3.71 (s, 3H), 3.29 – 3.22 (m, 1H), 2.78 (s, 2H), 2.69 (s, 2H), 2.51 (td, J = 9.4, 8.7, 3.8 Hz, 6H), 2.39 (s,

6H), 2.33 (s, 6H), 2.00 – 1.79 (m, 6H), 1.45 (t, J = 10.4 Hz, 2H), 0.94 (t, J = 7.3 Hz, 6H). ^{13}C NMR (126 MHz, $CDCl_{3)}$ δ 131.97, 131.92, 130.62, 130.56, 129.90, 128.58, 128.47, 127.97, 127.64, 127.57, 127.54, 126.10, 125.63, 120.78, 119.16, 114.33, 114.08, 113.70, 113.43, 70.04, 69.81, 53.42, 51.62, 45.90, 27.01, 26.91, 26.39, 26.18, 13.67. HRMS calc. for $C_{39}H_{44}NO_4$ (M + H)+: 590.3265. Found: 590.3260.

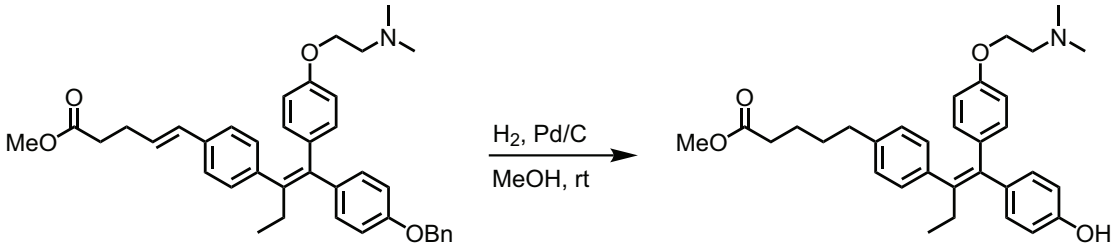

87 **214**

Synthesis of methyl (Z)-5-(4-(1-(4-(2-(dimethylamino)ethoxy)phenyl)-1-(4-hydroxyphenyl)but-1-en-2-yl)phenyl)pentanoate (214):

Prepared according to General Procedure D using **87** (127 mg, 0.22 mmol, 1.0 eq.). The product was isolated as a pale yellow oil (94 mg, 0.19 mmol) that did not require purification in 85% yield as a 1:1 mixture of *E:Z* isomers. ^{1}H NMR (500 MHz, $CDCl_3$) δ 7.21 – 7.03 (m, 5H), 7.03 – 6.89 (m, 7H), 6.79 (dd, J = 10.8, 8.5 Hz, 4H), 6.75 – 6.60 (m, 4H), 6.53 – 6.43 (m, 2H), 6.43 – 6.34 (m, 1H), 4.10 (td, J = 5.7, 1.8 Hz, 2H), 3.94 (t, J = 5.6 Hz, 2H), 3.69 (s, 4H), 2.85 – 2.76 (m, 2H), 2.72 (t, J = 5.6 Hz, 2H), 2.62 – 2.43 (m, 6H), 2.43 – 2.36 (m, 5H), 2.35 – 2.24 (m, 4H), 2.00 – 1.80 (m, 6H), 1.71 – 1.53 (m, 5H), 1.44 (t, J = 9.4 Hz, 3H), 1.02 – 0.83 (m, 6H). ^{13}C NMR (126 MHz, $CDCl_{3)}$ δ 140.80, 140.60, 132.08, 131.89, 130.70, 130.57, 130.54, 129.71, 129.71, 129.63, 127.89, 127.81, 127.81, 127.81, 126.31, 115.23, 114.44, 113.89, 113.88, 113.06, 58.29, 53.42, 51.64, 51.49, 45.67, 45.48, 35.50, 35.02, 34.24, 33.97, 33.36, 30.67, 26.95, 26.86, 26.31, 26.28, 26.12, 24.57, 13.73, 13.72, 13.72. HRMS calc. for $C_{32}H_{40}NO_4$ (M + H)+: 502.2952. Found: 502.2948.

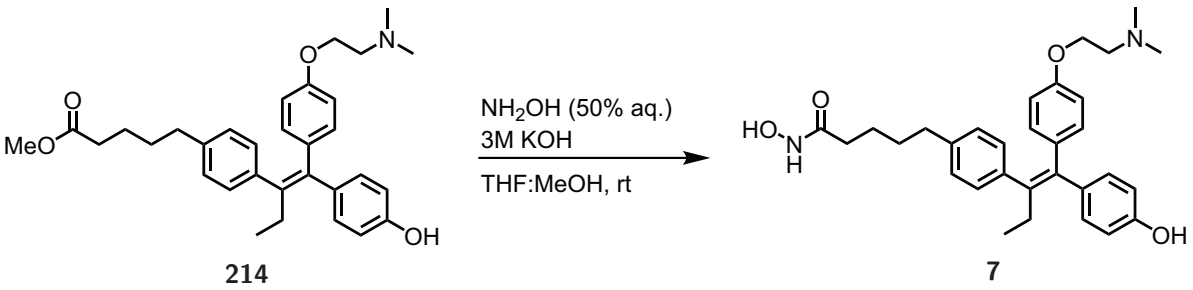

214 7

Synthesis of (Z)-5-(4-(1-(4-(2-(dimethylamino)ethoxy)phenyl)-1-(4-hydroxyphenyl)but-1-en-2-yl)phenyl)-N-hydroxypentanamide (7):

Prepared according to General Procedure A using methyl ester **214** (93 mg, 0.19 mmol, 1.0 eq.), NH_2OH (50% w/w in H_2O) (5.7 mL, 92.7 mmol, 500 eq.), and 3 M KOH (443 µL, 1.33 mmol, 7.0 eq.). Neutralized with 3 M HCl and concentrated to a white/yellow residue. Purification by reverse phase C18 column chromatography using a 10%-100% MeOH:H_2O solvent gradient yielded the product as a white solid (33 mg, 0.06 mmol) in 34% yield as a 1:1 mixture of *E:Z* isomers. ^{1}H NMR (500 MHz, $CDCl_3$) δ 7.07 – 6.94 (m, 6H), 6.83 – 6.73 (m, 4H), 6.62 (d, J = 8.4 Hz, 2H), 4.15 (s, 2H), 3.28 (s, 2H), 2.76 (s, 6H), 2.58 (t, J = 6.8 Hz, 2H), 2.49 (q, J = 7.4 Hz, 2H), 2.10 (d, J = 7.5 Hz, 2H), 1.70 – 1.47 (m, 5H), 0.94 (t, J = 7.4 Hz, 4H). HRMS calc. for $C_{31}H_{39}N_2O_4$ (M + H)+: 503.2904. Found: 503.2912.

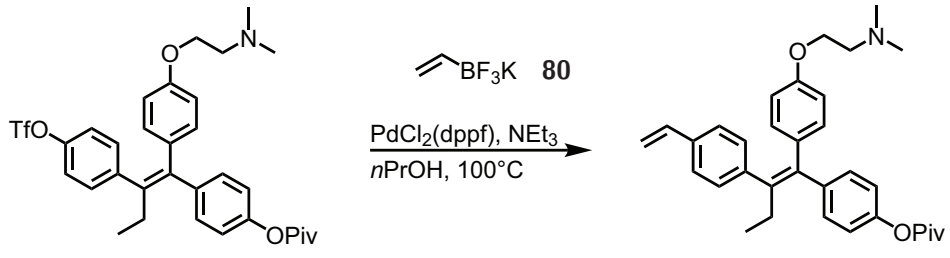

25 89

Synthesis of (E)-4-(1-(4-(2-(dimethylamino)ethoxy)phenyl)-2-(4-vinylphenyl)but-1-en-1-yl)phenyl pivalate (89):

To a flame dried round bottom flask equipped with a reflux condenser, **25** (220 mg, 0.36 mmol, 1.0 eq.), potassium vinyltrifluoroborate (**80**) (57 mg, 0.43 mmol, 1.2 eq.), and $PdCl_2$(dppf) (13 mg, 0.02 mmol, 5 mol%) were added and dissolved in nPrOH (7 mL). NEt_3 (50 µL, 0.36 mmol, 1.0 eq.) was then added and the reaction was heated to 100°C and stirred

for 20 h. The reaction was then cooled to room temperature, quenched with 5 mL H_2O and extracted with 3x10 mL EtOAc. The organic was dried over Na_2SO_4, filtered, and concentrated to a dark orange oil. The crude was purified by silica gel column chromatography using a 0-10% MeOH:CH_2Cl_2 gradient and the product was isolated as an orange solid (158 mg, 0.32 mmol) in 89% yield.

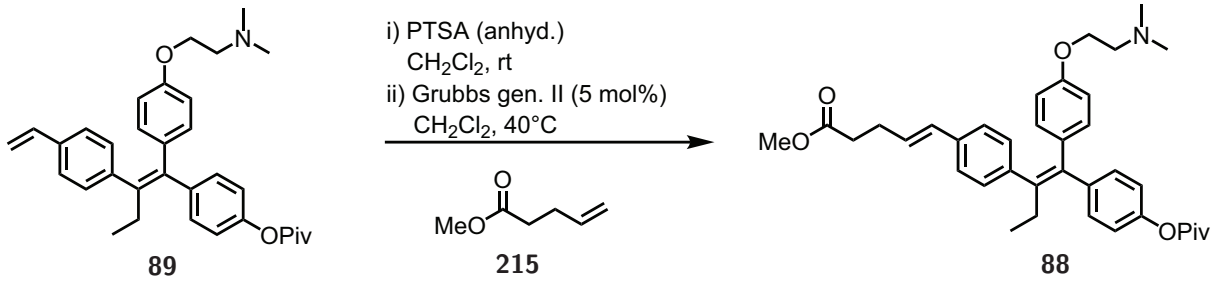

Synthesis of methyl (E)-5-(4-((E)-1-(4-(2-(dimethylamino)ethoxy)phenyl)-1-(4-(pivaloyloxy)phenyl)but-1-en-2-yl)phenyl)pent-4-enoate (215):

Prepared according to General Procedure C using **89** (158 mg, 0.32 mmol, 1.0 eq.), anhydrous PTSA (60 mg, 0.35 mmol, 1.1 eq.), methyl pentenoate (365 mg, 3.2 mmol, 10 eq.), and Grubbs gen. 2 catalyst (14 mg, 0.016 mmol, 5 mol%). The product was isolated as a dark brown/green oil (170 mg, 0.29 mmol) in 91% yield as a 1:1 mixture of *E:Z* isomers. ^{1}H NMR (500 MHz, $CDCl_3$) δ 7.27 – 7.22 (m, 3H), 7.22 – 7.12 (m, 7H), 7.06 (dtt, J = 8.6, 4.3, 2.0 Hz, 6H), 6.93 – 6.86 (m, 5H), 6.81 – 6.76 (m, 2H), 6.76 – 6.71 (m, 2H), 6.62 – 6.55 (m, 2H), 6.40 – 6.34 (m, 2H), 6.20 – 6.13 (m, 2H), 4.11 (t, J = 5.7 Hz, 2H), 3.97 (t, J = 5.6 Hz, 2H), 3.72 (dd, J = 10.9, 1.0 Hz, 6H), 2.78 (d, J = 5.8 Hz, 2H), 2.70 (s, 2H), 2.50 (dtd, J = 14.9, 7.0, 3.4 Hz, 4H), 2.38 (d, J = 12.4 Hz, 6H), 2.33 (s, 6H), 1.39 (s, 9H), 1.31 (s, 9H), 0.97 – 0.89 (m, 6H). ^{13}C NMR (126 MHz, $CDCl_{3)}$ δ 177.08, 176.90, 173.42, 157.60, 156.83, 149.71, 148.91, 141.75, 141.30, 141.26, 141.20, 141.18, 140.69, 137.54, 137.46, 135.99, 135.42, 135.11, 135.02, 133.37, 131.92, 131.73, 131.42, 131.20, 130.80, 130.63, 130.40, 130.35, 130.31, 129.89, 129.86, 129.84, 127.81, 127.77, 125.96, 125.92, 125.71, 125.67, 121.06, 120.92, 120.34, 120.32, 114.15, 113.50, 65.87, 58.31, 58.25, 51.91, 51.60, 45.88, 45.86, 39.10, 38.99, 38.28, 33.84, 33.82, 28.95, 28.82, 28.27, 27.15, 27.11, 27.09, 27.03, 13.60. HRMS calc. for $C_{37}H_{46}NO_5$ (M + H)+: 584.3370. Found: 584.3395.

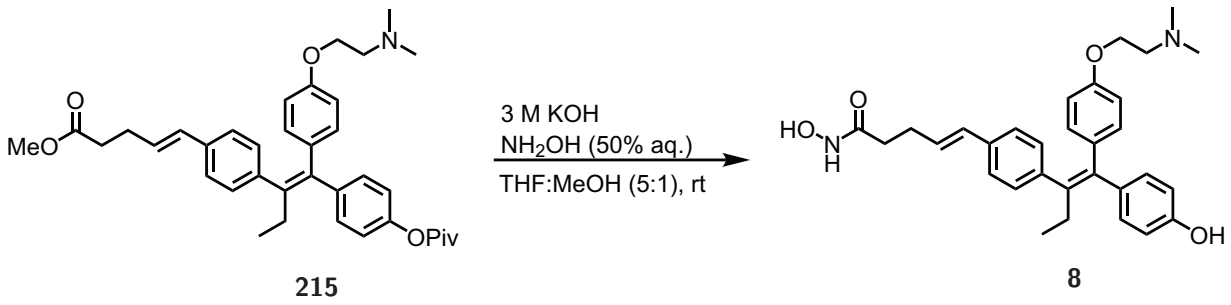

215 **8**

Synthesis of (E)-5-(4-((Z)-1-(4-(2-(dimethylamino)ethoxy)phenyl)-1-(4-hydroxyphenyl)but-1-en-2-yl)phenyl)-N-hydroxypent-4-enamide (8):

Prepared according to General Procedure A using methyl ester **215** (169 mg, 0.29 mmol, 1.0 eq.), NH_2OH (50% w/w in H_2O) (8.9 mL, 145 mmol, 500 eq.), and 3 M KOH (677 µL, 2.03 mmol, 7.0 eq.). Neutralized with 3 M HCl and concentrated to a white/yellow residue. Purification by reverse phase C18 column chromatography using a 10%-100% MeOH:H_2O solvent gradient yielded the product as a white solid (101 mg, 0.20 mmol) in 70% yield as a 1:1 mixture of *E:Z* isomers. ^{1}H NMR (400 MHz, CD_3OD) δ 7.25 – 7.09 (m, 6H), 7.09 – 6.98 (m, 6H), 6.95 (d, J = 8.6 Hz, 2H), 6.82 – 6.73 (m, 4H), 6.70 – 6.65 (m, 2H), 6.60 (d, J = 8.7 Hz, 3H), 6.43 (d, J = 8.7 Hz, 2H), 6.38 (s, 1H), 6.26 – 6.12 (m, 3H), 4.16 (t, J = 5.4 Hz, 6H), 4.00 (t, J = 5.4 Hz, 2H), 2.85 (t, J = 5.5 Hz, 6H), 2.75 (t, J = 5.4 Hz, 2H), 2.49 (dd, J = 10.7, 7.5 Hz, 7H), 2.41 (s, 6H), 2.35 (s, 6H), 2.26 (t, J = 7.4 Hz, 3H), 0.93 (t, J = 7.4 Hz, 6H). ^{13}C NMR (126 MHz, CD_3OD) δ 170.76, 157.45, 156.65, 155.94, 155.10, 141.68, 141.64, 140.31, 140.08, 138.43, 138.38, 136.62, 136.29, 135.10, 134.93, 134.64, 134.62, 131.72, 131.29, 131.22, 130.81, 130.79, 130.28, 130.25, 130.04, 129.78, 129.76, 129.70, 129.68, 127.37, 127.34, 125.48, 125.31, 125.24, 114.56, 113.88, 113.81, 113.07, 65.05, 64.78, 57.68, 57.59, 44.39, 44.33, 35.01, 34.53, 32.35, 28.65, 28.38, 28.33, 26.45, 26.36, 25.87, 25.85, 25.78, 12.74, 12.71. HRMS calc. for $C_{31}H_{37}N_2O_4$ (M + H)+: 501.2748. Found: 501.2769.

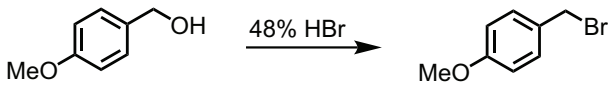

216

Synthesis of 1-(bromomethyl)-4-methoxybenzene (216):

p-methoxybenzyl alcohol (7.2 mL, 57.9 mmol, 1.0 eq.) was added to a dry flask followed by 48% HBr (16 mL) and the mixture was stirred for 20 minutes. The mixture was then diluted with 20 mL Et_2O and washed with 3x20 mL saturated $NaHCO_3$ solution, 3x20 mL H_2O, and then with 2x30 mL brine. The organic was dried over $MgSO_4$, filtered, and concentrated to a clear oil that was not purified. The spectroscopic data of the product is in agreement with that reported in the literature[14]

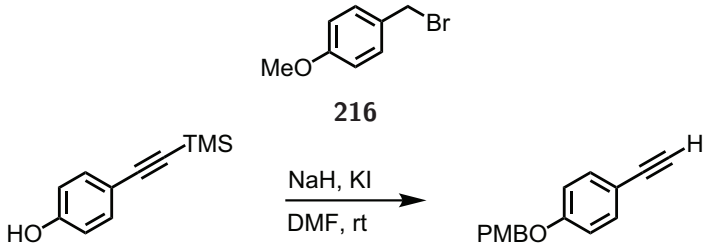

Synthesis of 1-ethynyl-4-((4-methoxybenzyl)oxy)benzene (91):

To a flame-dried round bottom flask, **70** (4.18 g, 21.94 mmol, 1.0 eq.) was added and dissolved in DMF (55 mL). NaH (60% dispersion in mineral oil) (1.75 g, 43.9 mmol, 2.0 eq) and KI (364 mg, 2.19 mmol, 10 mol%) were added and the mixture was stirred for 10 minutes. **216** (4.31 mL, 30.7 mmol, 1.4 eq.) was then added and the reaction was stirred overnight. TLC indicated complete consumption of starting material, the reaction was quenched with 200 mL H_2O, extracted with 3x 100 mL EtOAc which was then washed with 3x100 mL 1:1 brine:H_2O. The organic was dried over Na_2SO_4, filtered, and concentrated to a dark brown/orange oil. Purification by silica gel column chromatography using a 45% PhMe in hexanes solvent system gave the product as a yellow solid (2.75 g, 11.6 mmol) in 51% yield over 2 steps. ^{1}H NMR (500 MHz, $CDCl_3$) δ 7.45 (d, J = 8.8 Hz, 2H), 7.37 (d, J = 8.7 Hz, 2H), 6.94 (dd, J = 8.8, 6.9 Hz, 4H), 5.02 (s, 2H), 3.84 (s, 3H), 3.02 (s, 1H). ^{13}C NMR (126

MHz, $CDCl_3$) δ 159.57, 159.19, 133.59, 129.23, 128.53, 114.86, 114.34, 114.07, 83.66, 75.80, 69.84, 55.32.

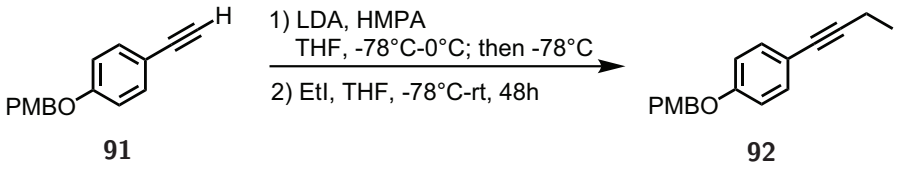

91 **92**

Synthesis of 1-(but-1-yn-1-yl)-4-((4-methoxybenzyl)oxy)benzene (92):

To a flame-dried round bottom flask containing THF (26 mL) cooled to -78°C, freshly distilled iPr_2NH (2.26 mL, 16.16 mmol, 1.4 eq) was added followed by *n*BuLi (2.09 M solution, 7.18 mL, 15.00 mmol, 1.3 eq.) and the mixture was stirred for 15 minutes. In a separate dry flask, **92** (2.75 g, 11.54 mmol, 1.0 eq.) was added and dissolved in THF (6.5 mL) and the solution was cannulated into the -78°C LDA solution and stirred for 30 minutes. HMPA (804 µL, 4.62 mmol, 40 mol%) was then added, the reaction was stirred for 15 minutes, warmed to 0°C and stirred for 20 minutes, then cooled again to -78°C and stirred for 15 minutes. Iodoethane (2.8 mL, 34.62 mmol, 3.0 eq.) was passed through a plug of basic alumina and then added to the reaction flask. The mixture was stirred for 48 hours while slowly warming to room temperature. Quenched with 5 mL saturated NH_4Cl solution and diluted with 10 mL H_2O. THF was removed *in vacuo* and the aqueous was extracted with 3x50 mL Et_2O, dried over $MgSO_4$, filtered, and concentrated to a yellow oil. Purification by silica gel column chromatography using a 0%-12% EtOAc:hexanes gradient gave the product as an off-white solid (2.64 g, 9.92 mmol) in 86% yield. ^{1}H NMR (400 MHz, $CDCl_3$) δ 7.36 (dd, J = 8.7, 7.8 Hz, 4H), 6.92 (dd, J = 16.1, 8.8 Hz, 4H), 5.00 (s, 2H), 3.84 (s, 3H), 2.43 (q, J = 7.5 Hz, 2H), 1.25 (t, J = 7.5 Hz, 3H). ^{13}C NMR (126 MHz, $CDCl_3$) δ 159.51, 158.26, 132.84, 129.23, 128.76, 116.38, 114.76, 114.03, 90.10, 79.57, 69.81, 55.32, 14.04, 13.10.

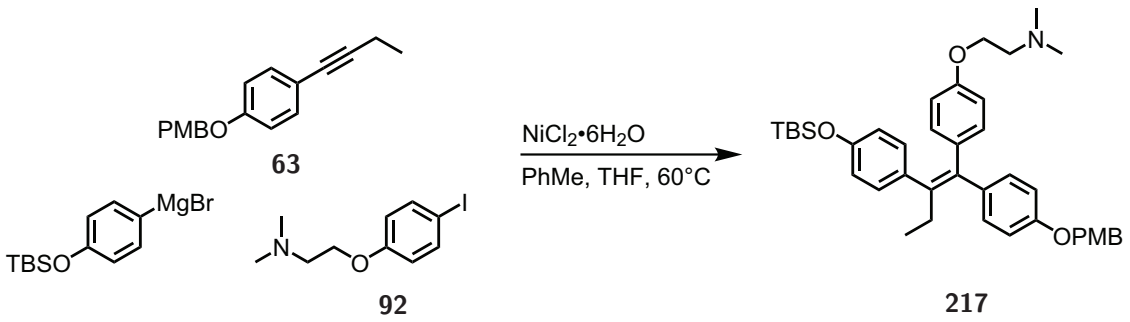

Synthesis of (Z)-2-(4-(2-(4-((tert-butyldimethylsilyl)oxy)phenyl)-1-(4-((4-methoxybenzyl)oxy)phenyl)but-1-en-1-yl)phenoxy)-N,N-dimethylethan-1-amine (217):

To a flame-dried round bottom flask, **92** (1.0 g, 3.75 mmol, 1.0 eq.), **63** (1.31 g, 4.51 mmol, 1.2 eq.), and $NiCl_2 \cdot 6\,H_2O$ (8.9 mg, 0.038 mmol, 1 mol%) were added to a flame-dried round-bottom flask and dissolved in PhMe (13 mL). (4-((tert-butyldimethylsilyl)oxy)phenyl)-magnesium bromide (0.76 M solution in THF) (5.93 mL, 4.51 mmol, 1.2 eq.) was prepared according to General Procedure B and slowly added to the solution. The reaction was then heated to 60°C and stirred for 24 hours. TLC indicated complete consumption of starting material and the reaction was quenched with 1 mL H_2O and filtered through a silica plug using EtOAc and then 8% MeOH:CH_2Cl_2 as an eluent. Purification by silica gel column chromatography using a 1%-9% MeOH:CH_2Cl_2 solvent gradient gave the product as a brown oil (492 mg, 0.79 mmol) in 21% yield as the pure *Z* isomer. ^{1}H NMR (400 MHz, $CDCl_3$) δ 7.41 (d, J = 8.7 Hz, 2H), 7.18 (d, J = 8.7 Hz, 2H), 7.03 – 6.92 (m, 6H), 6.80 (d, J = 8.8 Hz, 2H), 6.69 (d, J = 8.5 Hz, 2H), 6.59 (d, J = 8.8 Hz, 2H), 5.03 (s, 2H), 3.98 (t, J = 5.8 Hz, 2H), 3.85 (s, 3H), 2.70 (t, J = 5.8 Hz, 2H), 2.50 (q, J = 7.4 Hz, 2H), 2.34 (s, 6H), 1.01 (s, 9H), 0.21 (s, 6H). ^{13}C NMR (126 MHz, $CDCl_{3)}$ δ 159.49, 157.61, 155.57, 153.82, 141.11, 137.13, 137.07, 136.47, 135.49, 132.10, 130.73, 130.62, 129.36, 129.32, 129.14, 129.12, 119.68, 114.43, 114.08, 114.05, 114.02, 113.48, 69.82, 63.35, 57.14, 55.35, 55.33, 44.57, 29.00, 25.87, 25.84, 25.83, 25.81, 18.30, 13.75, -4.29. HRMS calc. for $C_{40}H_{52}NO_4Si$ (M + H)+: 638.3660. Found: 638.3661.

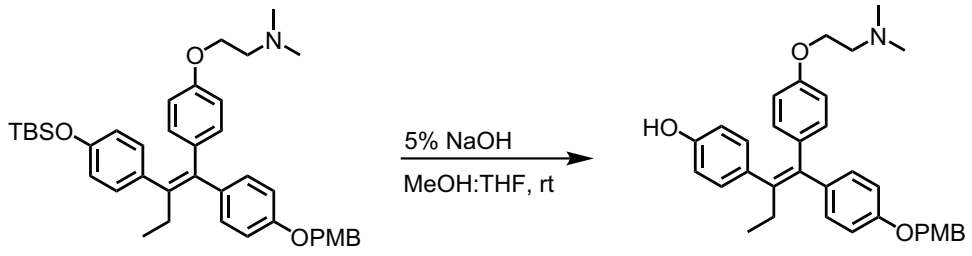

217 **93**

Synthesis of (Z)-4-(1-(4-(2-(dimethylamino)ethoxy)phenyl)-1-(4-((4-methoxybenzyl)oxy)phenyl)but-1-en-2-yl)phenol (93):

To a flame dried round bottom flask, **93** (492 mg, 0.77 mmol, 1.0 eq.) was added and dissolved in MeOH (5 mL). Crushed NaOH (139 mg, 3.47 mmol, 4.5 eq.) was added and the reaction was stirred overnight at room temperature. TLC indicated complete conversion of starting material and the reaction was then quenched with 5 mL H_2O, MeOH was removed *in vacuo* and the aqueous was extracted with 3x 15 mL EtOAc, dried over Na_2SO_4, filtered, and concentrated to a brown oil. Purification by silica gel column chromatography using a 0%-8% MeOH:CH_2Cl_2 solvent gradient gave the product as a brown oil that tended to foam (233 mg, 0.44 mmol) in 57% yield as a 1:1 mixture of *E:Z* isomers. ^{1}H NMR (400 MHz, $CDCl_3$) δ 7.37 (dd, J = 39.5, 8.4 Hz, 6H), 7.20 (t, J = 8.4 Hz, 4H), 7.09 – 6.79 (m, 14H), 6.68 (t, J = 9.1 Hz, 6H), 6.55 (d, J = 8.3 Hz, 2H), 5.02 (s, 2H), 4.86 (s, 2H), 4.19 (s, 2H), 4.03 (s, 2H), 3.83 (d, J = 13.2 Hz, 6H), 2.92 (d, J = 29.6 Hz, 4H), 2.48 (d, J = 20.9 Hz, 12H), 1.00 (s, 6H). ^{13}C NMR (101 MHz, $CDCl_{3)}$ δ 159.49, 159.39, 157.55, 157.00, 156.67, 156.05, 155.09, 155.03, 141.02, 140.90, 137.04, 136.96, 136.80, 136.76, 136.40, 133.82, 133.74, 132.05, 130.90, 130.70, 130.47, 129.41, 129.39, 129.25, 129.18, 115.34, 114.40, 114.12, 114.08, 113.99, 113.86, 113.75, 113.43, 69.84, 69.65, 64.86, 64.36, 57.82, 57.64, 55.37, 55.34, 55.30, 45.29, 45.22, 45.07, 29.05, 13.87.

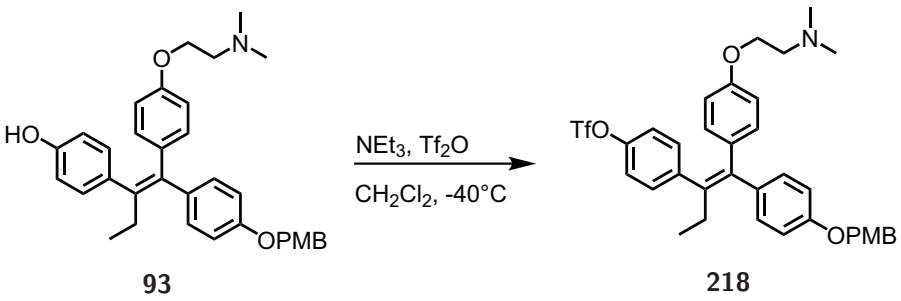

93 **218**

Synthesis of (Z)-4-(1-(4-(2-(dimethylamino)ethoxy)phenyl)-1-(4-((4-methoxybenzyl)oxy)phenyl)but-1-en-2-yl)phenyl trifluoromethanesulfonate (218):

To a flame-dried round-bottom flask, **93** (233 mg, 0.44 mmol, 1.0 eq) was added and dissolved in CH_2Cl_2 (8.8 mL), followed by the addition of freshly distilled NEt_3 (92 µL, 0.66 mmol, 1.5 eq.). The reaction was cooled to -40°C and stirred for 10 minutes before the dropwise addition of freshly distilled Tf_2O (124 µL, 0.44 mmol, 1.0 eq.). The reaction was stirred for 1 hour, TLC indicated full conversion of starting material and the reaction was quenched with 200 µL ethylenediamine, followed by 10 mL H_2O. After warming to room temperature, the reaction was extracted with 3x 10 mL CH_2Cl_2, dried over Na_2SO_4, filtered, and concentrated to a yellow oil. Purification by silica gel column chromatography using a 0%-8% solvent gradient gave the product as a pale yellow oil that tended to foam (232 mg, 0.35 mmol) in 80% yield as a 1:1 mixture of *E:Z* isomers. ^{1}H NMR (500 MHz, $CDCl_3$) δ 7.40 (d, J = 8.7 Hz, 3H), 7.31 (d, J = 8.7 Hz, 2H), 7.17 (ddd, J = 18.0, 8.7, 3.9 Hz, 6H), 7.09 (dd, J = 8.8, 4.3 Hz, 4H), 7.01 – 6.89 (m, 8H), 6.74 (dd, J = 8.8, 4.0 Hz, 4H), 6.64 (d, J = 8.8 Hz, 2H), 6.59 (d, J = 8.8 Hz, 2H), 5.02 (s, 2H), 4.87 (s, 2H), 4.12 (s, 2H), 3.97 (s, 2H), 3.88 – 3.81 (m, 6H), 2.78 (t, J = 5.7 Hz, 2H), 2.69 (t, J = 5.7 Hz, 2H), 2.52 (qd, J = 7.4, 3.9 Hz, 4H), 2.38 (s, 6H), 2.33 (s, 6H), 1.00 – 0.92 (m, 6H). ^{13}C NMR (101 MHz, $CDCl_{3)}$ δ 159.56, 159.50, 157.95, 157.77, 157.26, 157.07, 147.64, 143.45, 139.62, 139.60, 139.14, 139.11, 135.78, 135.73, 135.30, 135.24, 131.99, 131.53, 130.53, 129.31, 129.26, 129.22, 129.08, 129.05, 128.99, 120.72, 120.40, 117.21, 114.48, 114.25, 114.04, 113.98, 113.94, 113.91, 113.64, 69.80, 69.64, 65.73, 65.51, 58.24, 58.13, 55.22, 55.19, 53.51, 45.74, 45.67, 28.85, 28.82, 13.60. HRMS calc. for $C_{35}H_{37}NO_6F_3S$ (M + H)+: 656.2299. Found: 656.2282.

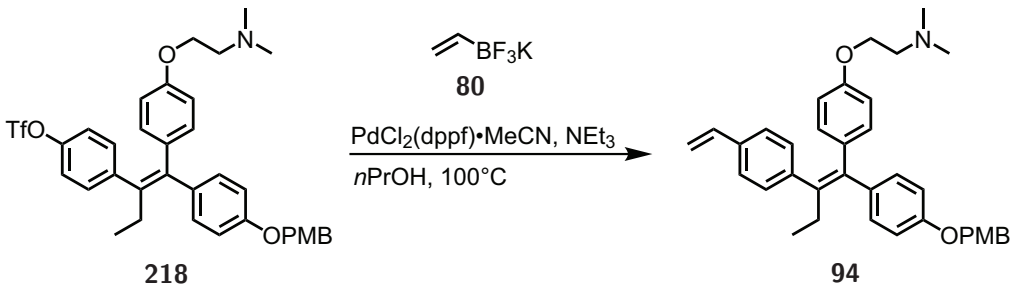

Synthesis of (Z)-2-(4-(1-(4-((4-methoxybenzyl)oxy)phenyl)-2-(4-vinylphenyl)but-1-en-1-yl)phenoxy)-N,N-dimethylethan-1-amine (94):

To a flame-dried flask equipped with a condenser, **218** (232 mg, 0.35 mmol, 1.0 eq.), **80** (57 mg, 0.42, 1.2 eq.), and $PdCl_2$(dppf) (12.8 mg, 0.015 mmol, 5 mol%) were added and dissolved in *n*PrOH (7 mL). Freshly distilled NEt_3 (49 µL, 0.35 mmol, 1.0 eq) was then added and the reaction was heated to 100°C and stirred for 24 hours. After cooling to room temperature, the reaction was quenched with 5 mL H_2O, extracted with 3x15 mL EtOAc, dried over Na_2SO_4, filtered, and concentrated to a brown oil. Purification by silica gel column chromatography using a 0%-8% MeOH:CH_2Cl_2 solvent gradient gave the product as a dark brown oil (100 mg, 0.19 mmol) in 54% yield as a 1:1 mixture of *E:Z* isomers. ^{1}H NMR (400 MHz, $CDCl_3$) δ 7.46 – 7.36 (m, 5H), 7.36 – 7.31 (m, 3H), 7.27 (dd, J = 8.2, 3.4 Hz, 6H), 7.23 – 7.16 (m, 5H), 7.12 (dd, J = 8.1, 3.8 Hz, 5H), 7.05 – 6.89 (m, 13H), 6.84 (dt, J = 9.4, 2.4 Hz, 6H), 6.73 – 6.56 (m, 8H), 5.73 (dd, J = 17.6, 2.9 Hz, 2H), 5.27 – 5.18 (m, 2H), 5.03 (s, 4H), 4.88 (s, 2H), 4.16 (t, J = 5.5 Hz, 2H), 4.01 (t, J = 5.6 Hz, 3H), 3.83 (d, J = 10.7 Hz, 10H), 2.89 (t, J = 5.5 Hz, 2H), 2.80 (t, J = 5.6 Hz, 3H), 2.61 – 2.35 (m, 22H), 0.98 (t, J = 7.4 Hz, 9H). ^{13}C NMR (101 MHz, $CDCl_{3)}$ δ 159.51, 159.42, 157.69, 157.39, 156.92, 156.60, 142.36, 142.34, 140.71, 140.68, 138.05, 136.75, 136.73, 136.59, 136.46, 136.12, 135.97, 135.11, 132.00, 130.63, 129.92, 129.34, 129.31, 129.13, 129.11, 125.84, 114.38, 114.14, 114.05, 114.05, 114.01, 113.97, 113.94, 113.76, 113.49, 113.06, 69.82, 69.60, 65.49, 65.21, 58.20, 58.12, 55.32, 55.29, 53.48, 45.71, 45.65, 28.93, 28.91, 13.74. HRMS calc. for $C_{36}H_{40}NO_3$ (M + H)+: 534.3003. Found: 534.2995.

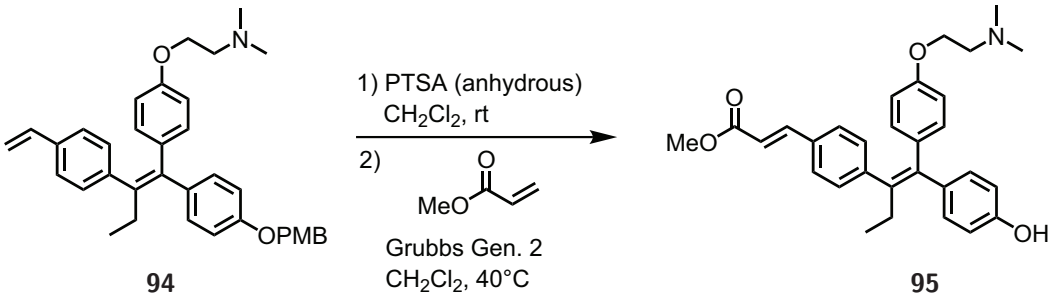

Synthesis of methyl (E)-3-(4-((Z)-1-(4-(2-(dimethylamino)ethoxy)phenyl)-1-(4-hydroxyphenyl)but-1-en-2-yl)phenyl)acrylate (95):

Prepared according to General Procedure C using **94** (100 mg, 0.19 mmol, 1.0 eq), anhydrous PTSA (36 mg, 0.21 mmol, 1.1 eq.), methyl acrylate (172 µL, 1.9 mmol, 10 eq.), and Grubbs gen. 2 catalyst (8.1 mg, 0.009 mmol, 5 mol%). The product was isolated as a dark brown/green oil (40 mg, 0.09 mmol) in 45% yield as a 1:1 mixture of *E:Z* isomers. ^{1}H NMR (500 MHz, $CDCl_3$) δ 7.72 – 7.55 (m, 2H), 7.38 – 7.23 (m, 4H), 7.20 – 6.99 (m, 8H), 6.99 – 6.90 (m, 1H), 6.90 – 6.76 (m, 5H), 6.76 – 6.63 (m, 6H), 6.60 – 6.54 (m, 1H), 6.54 – 6.40 (m, 2H), 6.37 (ddd, J = 12.2, 6.9, 3.2 Hz, 3H), 4.11 (q, J = 5.9 Hz, 2H), 4.01 – 3.87 (m, 2H), 3.87 – 3.78 (m, 6H), 3.74 (d, J = 12.6 Hz, 6H), 2.93 – 2.81 (m, 2H), 2.77 (t, J = 5.5 Hz, 2H), 2.57 – 2.47 (m, 4H), 2.44 (s, 6H), 2.38 (s, 6H), 0.93 (tq, J = 5.8, 3.1, 2.3 Hz, 6H). ^{13}C NMR (126 MHz, $CDCl_3$) δ 167.77, 167.74, 167.71, 157.78, 157.60, 157.30, 157.28, 156.59, 156.13, 155.30, 153.75, 153.04, 145.86, 145.64, 145.03, 144.95, 144.93, 139.68, 139.64, 139.49, 139.38, 139.31, 139.28, 139.26, 136.45, 136.35, 135.91, 135.01, 134.94, 134.71, 134.65, 134.33, 133.66, 132.96, 132.40, 132.10, 132.05, 132.00, 131.74, 131.72, 131.66, 131.63, 130.59, 130.53, 130.46, 130.39, 130.33, 130.31, 130.08, 130.05, 129.88, 129.79, 129.70, 129.59, 129.54, 128.56, 127.80, 127.77, 127.42, 126.61, 116.69, 116.67, 116.65, 116.64, 115.47, 115.45, 115.11, 114.88, 113.92, 113.87, 113.78, 113.63, 113.60, 113.25, 113.21, 64.95, 64.72, 64.35, 58.00, 57.93, 55.25, 55.15, 51.66, 50.63, 45.35, 45.26, 45.14, 35.29, 35.24, 28.88, 28.82, 28.73, 28.70, 21.05, 17.78, 13.75, 13.73, 13.71, 13.63. HRMS calc. for $C_{30}H_{34}NO_4$ (M + H)+: 472.2482. Found: 472.2501.

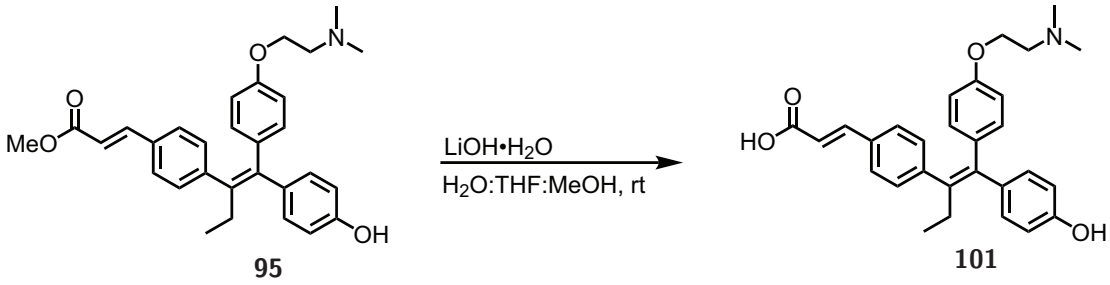

95 101

Synthesis of (E)-3-(4-((Z)-1-(4-(2-(dimethylamino)ethoxy)phenyl)-1-(4-hydroxyphenyl)but-1-en-2-yl)phenyl)acrylic acid (101):

Ester **95** was added to a round bottom flask and dissolved in MeOH (400 µL), THF (400 µL), and H_2O (800 µL). LiOHĹH_2O (63 mg, 1.48 mmol, 10 eq.) was then added and the reaction was stirred at room temperature for 24 hours. The reaction was then quenched with saturated NH_4Cl solution and extracted with 3x5 mL EtOAc. The organic was dried over Na_2SO_4, filtered, and concentrated to a green residue. Purification by reverse phase C18 silica gel column chromatography using a 10-100% MeCN:H_2O gradient gave the product **101** as a yellow/green residue (40 mg, 0.09 mmol) in 60% yield. ^{1}H NMR (500 MHz, $CDCl_3$) δ 7.36 (ddd, J = 15.7, 13.1, 2.2 Hz, 2H), 7.28 (ddd, J = 12.7, 8.4, 2.2 Hz, 4H), 7.09 (ddd, J = 22.5, 8.4, 3.9 Hz, 6H), 7.02 – 6.88 (m, 5H), 6.76 (ddd, J = 15.2, 8.8, 2.3 Hz, 5H), 6.68 – 6.53 (m, 5H), 6.39 (dt, J = 12.7, 6.3 Hz, 4H), 5.43 – 5.26 (m, 2H), 4.27 (d, J = 5.2 Hz, 2H), 4.10 (d, J = 4.7 Hz, 2H), 3.25 (s, 2H), 2.76 (d, J = 24.9 Hz, 12H), 2.53 – 2.34 (m, 4H), 0.88 (qd, J = 7.5, 2.2 Hz, 6H). ^{13}C NMR (126 MHz, $CDCl_{3)}$ δ 160.75, 160.03, 159.95, 159.28, 148.11, 144.95, 144.68, 144.35, 143.94, 142.81, 142.78, 141.05, 140.80, 138.53, 138.21, 137.12, 137.06, 135.84, 135.77, 135.66, 135.63, 134.42, 134.32, 134.15, 134.13, 133.96, 133.93, 130.90, 130.87, 118.50, 117.92, 117.89, 117.88, 117.18, 66.79, 66.32, 60.56, 60.43, 53.63, 53.55, 46.94, 46.78, 32.25, 32.18, 16.62, 16.57, 16.54. HRMS calc. for $C_{37}H_{40}NO_5$ (M + H)+: 578.2901. Found: 578.2894.

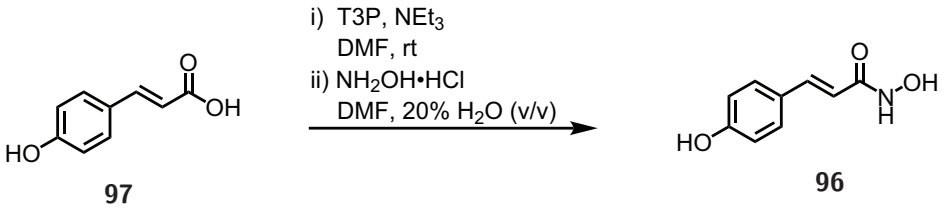

Synthesis of (E)-N-hydroxy-3-(4-hydroxyphenyl)acrylamide (96):

T3P (50 wt.% in EtOAc) (214 µL, 0.36 mmol, 1.2 eq.) was added to a vial containing DMF (850 µL) and NEt_3 (170 µL, 1.22 mmol, 4.0 eq.) was added followed by **97** and the reaction was stirred at room temperature for 30 minutes. A separate vial of hydroxylamine hydrochloride (42 mg, 0.60 mmol, 2.0 eq.) dissolved in DMF (500 µL) and H_2O (150 µL) was prepared and added via pipette to the reaction vessel and the resulting mixture was stirred for 24 hours at room temperature. The reaction was quenched with 4 mL H_2O and washed with 3x5 mL EtOAc. The organic was dried over Na_2SO_4, filtered, and concentrated. The crude was not purified. ^{1}H NMR (400 MHz, CD_3OD) δ 7.36 7.51 (d, J = 15.3 Hz, 1H), 7.42 (d, J = 8.2 Hz, 2H), 6.81 (d, J = 8.0 Hz, 2H), 6.30 (d, J = 15.7 Hz, 1H).

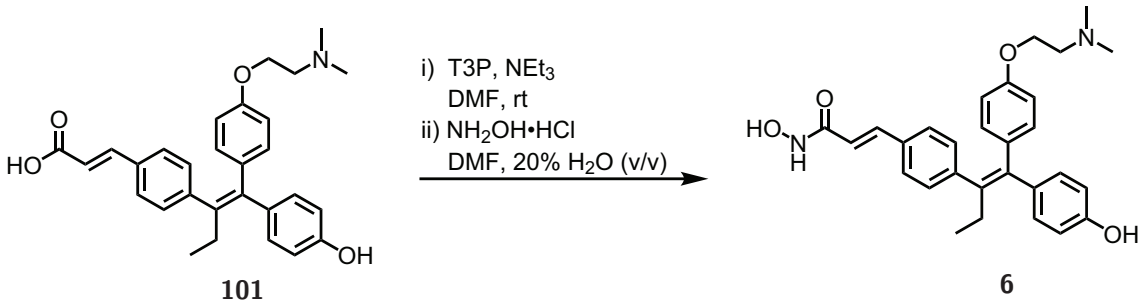

Synthesis of (E)-3-(4-((Z)-1-(4-(2-(dimethylamino)ethoxy)phenyl)-1-(4-hydroxyphenyl)but-1-en-2-yl)phenyl)-N-hydroxyacrylamide (6):

T3P (50 wt.% in EtOAc) (35 µL, 0.06 mmol, 1.2 eq.) was added to a vial containing DMF (300 µL) and NEt_3 (33 µL, 0.24 mmol, 4.0 eq.) was added followed by **101** (22 mg, 0.05 mmol, 1.0 eq.) dissolved in DMF (100 µL) and the reaction was stirred at room temperature for 30 minutes. A separate vial of hydroxylamine hydrochloride (6.7 mg, 0.1 mmol, 2.0 eq.) dissolved in DMF (100 µL) and H_2O (50 µL) was prepared and added via pipette to the reaction vessel and the resulting mixture was stirred for 24 hours at room

temperature. The reaction was quenched with 4 mL H_2O and washed with 3x5 mL EtOAc. The organic was dried over Na_2SO_4, filtered, and concentrated to a light green residue. The crude was purified by reverse phase C18 silica gel column chromatography using a 10-100% MeCN:H_2O gradient to yield the product as a green oil (6 mg, 0.012 mmol) in 27% yield. ^{1}H NMR (500 MHz, CD_3OD) δ 7.50 (d, J = 15.9 Hz, 1H), 7.36 (d, J = 8.1 Hz, 2H), 7.16 (d, J = 7.9 Hz, 2H), 7.04 (d, J = 8.3 Hz, 2H), 6.81 (dd, J = 19.9, 8.3 Hz, 4H), 6.66 (d, J = 8.5 Hz, 2H), 6.40 (d, J = 15.7 Hz, 1H), 4.10 (s, 2H), 2.70 – 2.48 (m, 8H), 0.94 (q, J = 6.3, 5.2 Hz, 6H). ^{13}C NMR (101 MHz, CD_3OD) δ 157.55, 156.81, 156.07, 155.32, 140.01, 139.74, 139.24, 134.64, 134.35, 131.69, 130.21, 130.16, 126.96, 116.21, 114.48, 113.85, 113.80, 113.11, 64.90, 64.61, 57.63, 57.52, 44.23, 44.16, 28.14, 12.55, 12.53. HRMS calc. for $C_{29}H_{33}N_2O_4$ (M + H)+: 473.2435. Found: 473.2436.

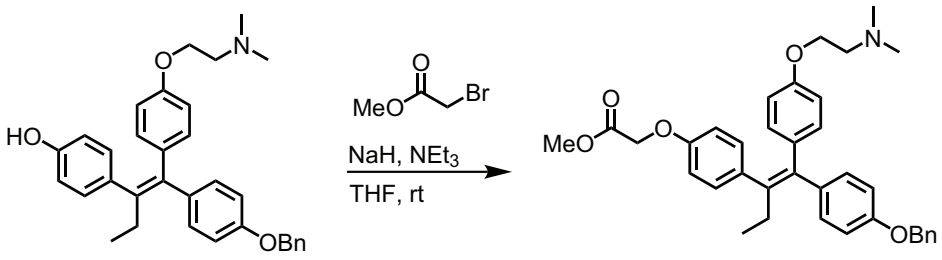

74 **102**

Synthesis of methyl (Z)-2-(4-(1-(4-(benzyloxy)phenyl)-1-(4-(2-(dimethylamino)-ethoxy)phenyl)but-1-en-2-yl)phenoxy)acetate (102):

74 (223 mg, 0.45 mmol, 1.0 eq.) was added to a flame-dried round-bottom flask and dissolved in THF (2.3 mL). NaH (60% dispersion in mineral oil) (21.6 mg, 0.54 mmol, 1.2 eq.) was added and the reaction was stirred for 5 minutes. Freshly distilled NEt_3 (75 µL, 0.54 mmol, 1.2 eq.) was added followed by methyl bromoacetate (51 µL, 0.54 mmol, 1.2 eq.), which had been passed through a plug of basic alumina prior to the addition, which immediately turned the reaction to a cream colour. The reaction was heated to 50°C and stirred overnight. TLC indicated full conversion of starting material and the reaction was cooled to room temperature and quenched with 15 mL H_2O and extracted with 3x 5 mL EtOAc. The organic layer was dried over Na_2SO_4, filtered, and concentrated to a light brown solid. Purification by silica gel column chromatography using a 6%-6.5% MeOH:CH_2Cl_2 solvent

gradient gave the product as a light brown oil (72 mg, 0.13 mmol) in 29% yield as a 1:1 mixture of *E:Z* isomers. ^{1}H NMR (500 MHz, $CDCl_3$) δ 7.48 (d, J = 6.9 Hz, 3H), 7.45 – 7.30 (m, 11H), 7.21 – 7.13 (m, 4H), 7.06 (dd, J = 8.8, 3.1 Hz, 4H), 6.98 (d, J = 8.7 Hz, 3H), 6.92 (d, J = 8.7 Hz, 3H), 6.79 (dd, J = 8.6, 5.6 Hz, 4H), 6.77 – 6.70 (m, 5H), 6.66 (d, J = 8.8 Hz, 2H), 6.59 (d, J = 8.8 Hz, 2H), 5.09 (s, 2H), 4.95 (s, 1H), 4.61 (s, 4H), 4.14 (t, J = 5.8 Hz, 2H), 4.00 (t, J = 5.7 Hz, 2H), 3.83 (s, 7H), 2.81 (t, J = 5.6 Hz, 2H), 2.74 (t, J = 5.7 Hz, 3H), 2.53 – 2.44 (m, 3H), 2.41 (s, 7H), 2.37 (s, 7H), 0.95 (t, J = 7.4 Hz, 6H). ^{13}C NMR (126 MHz, $CDCl_3$ δ 169.46, 157.54, 157.43, 156.71, 156.59, 155.98, 140.31, 137.66, 137.11, 137.09, 136.64, 136.06, 136.03, 136.02, 131.96, 131.92, 130.86, 130.60, 130.56, 128.59, 128.55, 128.53, 128.49, 127.97, 127.87, 127.57, 127.55, 114.35, 114.10, 114.05, 113.69, 113.42, 70.04, 69.83, 65.77, 65.50, 65.45, 65.42, 58.28, 58.21, 53.44, 52.20, 45.85, 45.82, 45.76, 28.92, 28.90, 13.71. HRMS calc. for $C_{28}H_{33}N_2O_5$ (M + H)+: 477.2384. Found: 477.2387.

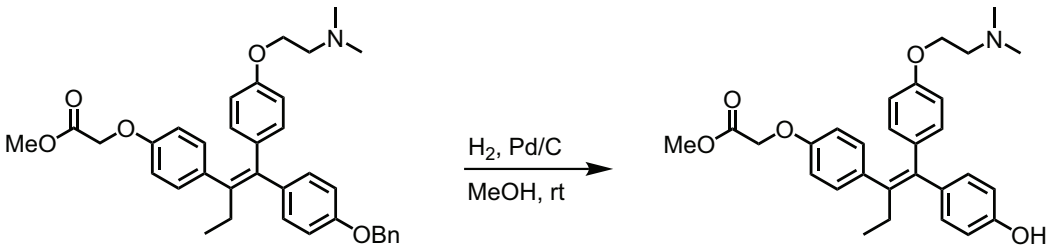

102 **219**

Synthesis of methyl (Z)-2-(4-(1-(4-(2-(dimethylamino)ethoxy)phenyl)-1-(4-hydroxyphenyl)but-1-en-2-yl)phenoxy)acetate (220):

Prepared according to General Procedure D using **102** (71.6 mg, 0.13 mmol, 1.0 eq.). The product was isolated as a pink oil (65 mg, 0.13 mmol) and was used without any further purification. ^{1}H NMR (500 MHz, $CDCl_3$) δ 7.18 (dd, J = 22.1, 8.4 Hz, 5H), 7.00 (dd, J = 8.5, 5.0 Hz, 6H), 6.96 – 6.84 (m, 6H), 6.84 – 6.61 (m, 15H), 6.50 (t, J = 9.2 Hz, 8H), 4.05 (t, J = 5.7 Hz, 3H), 3.98 – 3.88 (m, 4H), 3.79 (s, 6H), 3.20 – 3.08 (m, 2H), 2.79 (td, J = 5.7, 2.1 Hz, 2H), 2.71 (t, J = 5.7 Hz, 2H), 2.57 – 2.44 (m, 3H), 2.35 (d, J = 25.2 Hz, 13H), 0.64 (td, J = 7.2, 2.1 Hz, 6H). ^{13}C NMR (126 MHz, $CDCl_{3)}$ δ 169.68, 169.65, 156.86, 156.20, 155.69, 154.75, 153.96, 137.20, 137.02, 136.93, 136.00, 135.86, 130.86, 130.66, 130.45, 129.48, 129.09, 129.07, 129.03, 128.95, 128.91, 128.88, 115.59, 115.05, 114.51, 114.46, 114.14, 114.09, 113.90,

65.47, 65.39, 65.32, 65.06, 58.09, 58.03, 56.82, 56.77, 52.23, 52.19, 51.44, 51.38, 45.54, 45.53, 45.48, 30.93, 27.78, 27.74, 12.04, 12.03.

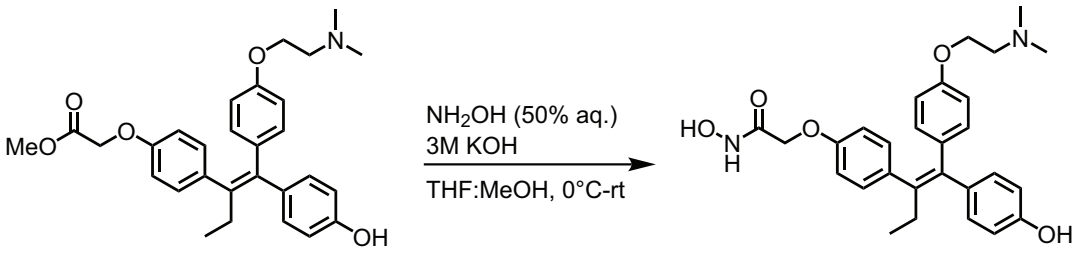

219 **10**

Synthesis of (Z)-2-(4-(1-(4-(2-(dimethylamino)ethoxy)phenyl)-1-(4-hydroxyphenyl)but-1-en-2-yl)phenoxy)-N-hydroxyacetamide (10):

Prepared according to General Procedure A using methyl ester **219** (65 mg, 0.14 mmol, 1.0 eq.), NH_2OH (50% w/w in H_2O) (4.21 mL, 68.65 mmol, 500 eq.), and 3 M KOH (326 µL, 0.98 mmol, 7.0 eq.). Neutralized with 3 M HCl and concentrated to a white/yellow residue. Purification by reverse phase C18 column chromatography using a 10%-100% MeOH:H_2O solvent gradient yielded the product as a white solid (30 mg, 0.06 mmol) in 45% yield as a 1:1 mixture of *E:Z* isomers. ^{1}H NMR (400 MHz, CD_3OD) δ 7.16 (d, J = 8.6 Hz, 2H), 7.07 (d, J = 8.2 Hz, 2H), 7.00 (d, J = 8.7 Hz, 2H), 6.82 (d, J = 8.6 Hz, 2H), 6.72 – 6.62 (m, 2H), 6.43 (d, J = 8.6 Hz, 2H), 4.51 (s, 2H), 4.31 (t, J = 5.1 Hz, 2H), 2.80 (s, 6H), 2.45 (q, J = 7.4 Hz, 2H), 0.92 (t, J = 7.4 Hz, 3H). HRMS calc. for $C_{28}H_{33}N_2O_5$ (M + H)+: 477.2384. Found: 477.2383.

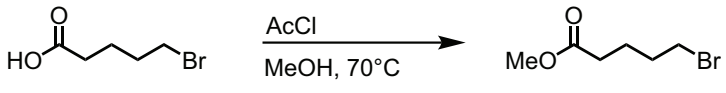

221

Synthesis of methyl 5-bromopentanoate (221):

To a flame-dried round bottom flask equipped with a condenser, 5-bromopentenoic acid was added and dissolved in MeOH (10 mL). Catalytic AcCl (5 drops) was added and the reaction was brought to reflux for 48 hours. After cooling to room temperature, the reaction

was quenched with 5 mL saturated $NaHCO_3$ solution and MeOH was removed *in vacuo*. The aqueous was extracted with 3x 15 mL EtOAc which was then combined and washed with 3x 15 mL brine, dried over $MgSO_4$, filtered, and concentrated to a pale orange liquid (913 mg, 4.69 mmol) in 85% yield that required no further purification. The spectroscopic data of the product is in agreement with that reported in the literature.[15]

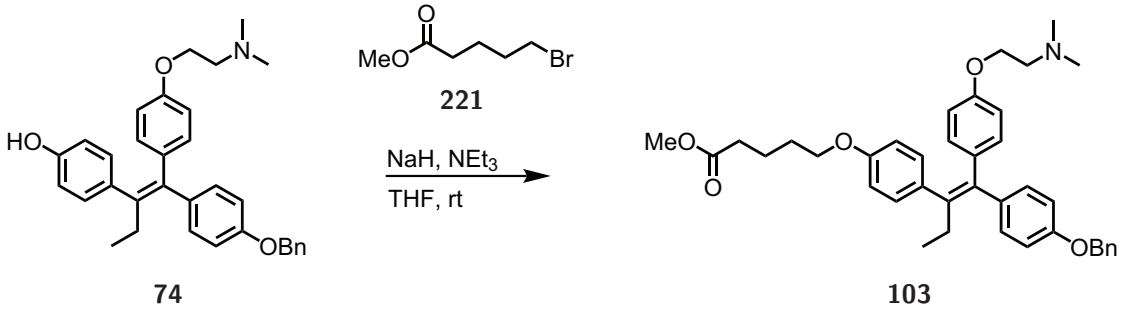

Synthesis of methyl (Z)-5-(4-(1-(4-(benzyloxy)phenyl)-1-(4-(2-(dimethylamino)ethoxy)phenyl)but-1-en-2-yl)phenoxy)pentanoate (103):

To a flame-dried round-bottom flask, **74** (244 mg, 0.52 mmol, 1.0 eq.) and dissolved in THF (3 mL). NaH (60% dispersion in mineral oil) (25 mg, 0.62 mmol, 1.2 eq.) was added followed by freshly distilled NEt_3 (87 µL, 0.62 mmol, 1.2 eq) and **221** (112 µL, 0.78 mmol, 1.5 eq.) which was first passed through a plug of basic alumina. The reaction was heated to 50°C and stirred for 50 hours, then cooled to room temperature and quenched with 5 mL H_2O. THF was removed *in vacuo* and the aqueous was extracted with 3x 10 mL EtOAc, dried over Na_2SO_4, filtered, and concentrated to a brown residue. Purification by silicia gel column chromatography using a 6.5% MeOH:CH_2Cl_2 solvent system gave the product as an orange oil (117 mg, 0.19 mmol) in 37% yield as a 1:1 mixture of *E:Z* isomers. ^{1}H NMR (500 MHz, $CDCl_3$) δ 7.56 – 7.25 (m, 12H), 7.18 (dd, J = 8.5, 5.2 Hz, 3H), 7.05 (dd, J = 8.6, 4.0 Hz, 3H), 6.98 (d, J = 8.7 Hz, 2H), 6.92 (d, J = 8.6 Hz, 2H), 6.82 (dd, J = 8.7, 6.4 Hz, 4H), 6.73 (d, J = 3.4 Hz, 2H), 6.72 – 6.65 (m, 3H), 6.61 (d, J = 8.7 Hz, 2H), 5.09 (s, 2H), 4.96 (s, 2H), 4.14 (t, J = 5.8 Hz, 2H), 4.00 (t, J = 5.7 Hz, 2H), 3.94 (t, J = 5.6 Hz, 3H), 2.82 (t, J = 5.6 Hz, 2H), 2.74 (t, J = 5.6 Hz, 2H), 2.49 (dd, J = 7.4, 3.8 Hz, 3H), 2.42 (d, J = 4.7 Hz, 9H), 2.37 (s, 6H), 1.94 – 1.76 (m, 8H), 1.01 – 0.89 (m, 6H). ^{13}C NMR (126 MHz, CD_3OD) δ

173.88, 157.51, 157.38, 157.14, 156.66, 156.53, 140.59, 137.28, 137.14, 136.83, 136.70, 136.36, 136.26, 134.73, 134.70, 131.99, 131.94, 131.92, 130.74, 130.70, 130.63, 130.60, 130.55, 130.40, 128.59, 128.55, 128.52, 128.49, 128.45, 127.97, 127.90, 127.86, 127.58, 127.54, 127.51, 127.47, 127.40, 114.35, 114.14, 114.10, 114.04, 113.93, 113.86, 113.85, 113.82, 113.79, 113.76, 113.70, 113.43, 113.37, 113.31, 70.04, 69.82, 67.20, 67.17, 65.73, 65.50, 60.30, 58.26, 58.20, 53.46, 51.53, 45.83, 45.82, 45.80, 45.78, 45.74, 45.72, 34.03, 33.75, 33.71, 30.92, 28.98, 28.95, 28.79, 28.77, 21.72, 14.30, 13.75, 13.74. HRMS calc. for $C_{39}H_{46}NO_5$ (M + H)+: 608.3370. Found: 608.3382.

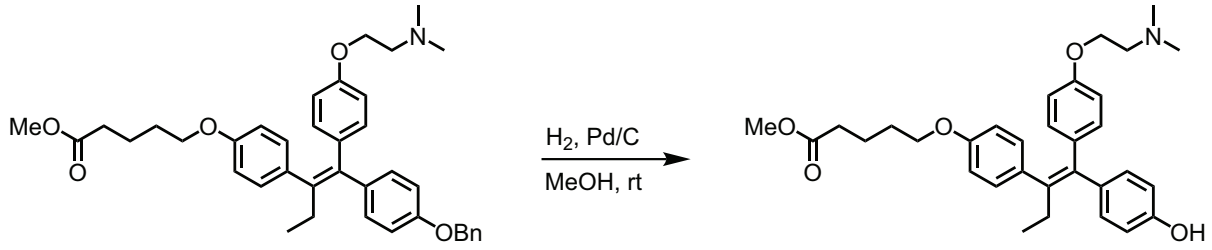

103 **222**

Synthesis of methyl (Z)-5-(4-(1-(4-(2-(dimethylamino)ethoxy)phenyl)-1-(4-hydroxyphenyl)but-1-en-2-yl)phenoxy)pentanoate (222):

Prepared according to General Procedure D using **103** (82 mg, 0.13 mmol, 1.0 eq.). The product was isolated as a bright yellow oil (71 mg, 0.13 mmol) in quantitative yield as a 1:1 mixture of *E:Z* isomers and used without further purification. ^{1}H NMR (400 MHz, CD_3OD) δ 7.13 (d, J = 8.7 Hz, 1H), 7.07 – 6.98 (m, 3H), 6.94 (d, J = 8.7 Hz, 2H), 6.84 – 6.64 (m, 5H), 6.61 (d, J = 8.9 Hz, 1H), 6.44 (d, J = 8.7 Hz, 1H), 4.16 (dd, J = 5.9, 4.9 Hz, 2H), 4.05 – 3.84 (m, 3H), 2.88 (q, J = 5.2 Hz, 1H), 2.80 (t, J = 5.5 Hz, 1H), 2.53 – 2.34 (m, 10H), 1.79 (ddt, J = 6.8, 4.6, 2.9 Hz, 5H), 0.98 – 0.88 (m, 6H). ^{13}C NMR (126 MHz, $CDCl_3$) δ 174.18, 174.16, 174.11, 174.11, 157.12, 156.99, 156.29, 155.48, 154.45, 140.10, 140.02, 137.52, 136.86, 136.35, 135.52, 135.26, 134.92, 132.09, 132.05, 131.92, 130.76, 130.74, 130.68, 130.63, 130.52, 115.33, 115.19, 114.68, 114.57, 114.04, 113.89, 113.85, 113.84, 113.15, 67.19, 67.16, 65.89, 64.87, 64.52, 58.06, 58.03, 53.45, 51.62, 51.60, 45.35, 45.32, 45.25, 33.78, 33.76, 33.73, 28.98, 28.90, 28.85, 28.77, 28.75, 28.73, 21.70, 21.69, 15.24, 14.26, 13.77, 13.75, 13.73. HRMS

calc. for $C_{32}H_{40}NO_5$ (M + H)+: 518.2901. Found: 518.2909.

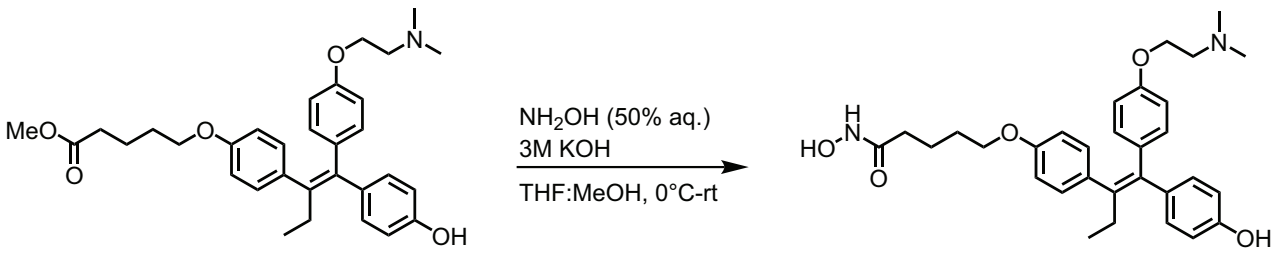

222 **11**

Synthesis of (Z)-5-(4-(1-(4-(2-(dimethylamino)ethoxy)phenyl)-1-(4-hydroxyphenyl)but-1-en-2-yl)phenoxy)-N-hydroxypentanamide (11):

Prepared according to General Procedure A using methyl ester **222** (70 mg, 0.14 mmol, 1.0 eq.), NH_2OH (50% w/w in H_2O) (4.15 mL, 68 mmol, 500 eq.), and 3 M KOH (326 µL, 0.98 mmol, 7.0 eq.). Neutralized with 3 M HCl and concentrated to a white/yellow solid. Purification by reverse phase C18 column chromatography using a 10%-100% MeOH:H_2O solvent gradient yielded the product as an off white solid (41 mg, 0.06 mmol) in 57% yield as a 1:1 mixture of *E:Z* isomers. ^{1}H NMR (400 MHz, CD_3OD) δ 7.01 (dd, J = 7.9, 4.5 Hz, 5H), 6.86 – 6.75 (m, 5H), 6.68 (dd, J = 25.8, 8.3 Hz, 6H), 4.11 (s, 2H), 3.94 (s, 2H), 3.22 – 3.05 (m, 3H), 2.65 (d, J = 13.3 Hz, 7H), 2.54 – 2.39 (m, 4H), 1.79 (s, 6H), 0.92 (td, J = 7.4, 3.1 Hz, 3H). ^{13}C NMR (101 MHz, CD3OD) δ 157.34, 156.85, 154.91, 140.16, 137.63, 137.39, 134.78, 134.64, 131.72, 131.59, 130.47, 130.30, 130.15, 128.62, 114.45, 113.85, 113.75, 113.53, 113.07, 63.41, 57.02, 43.38, 28.31, 12.58. HRMS calc. for $C_{31}H_{39}N_2O_5$ (M + H)+: 519.2853. Found: 519.2858.

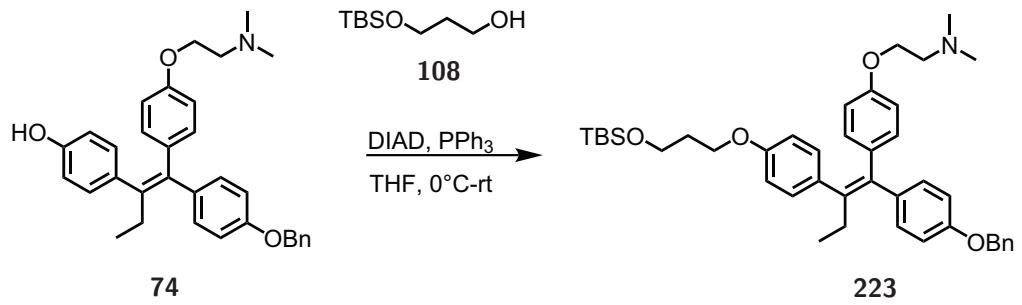

Synthesis of (Z)-2-(4-(1-(4-(benzyloxy)phenyl)-2-(4-(3-((tert-butyldimethylsilyl-)oxy)propoxy)phenyl)but-1-en-1-yl)phenoxy)-N,N-dimethylethan-1-amine (223):

To a flame dried round bottom flask, **223** (340 mg, 0.69 mmol, 1.0 eq), PPh_3 (217 mg, 0.83 mmol, 1.2 eq.), and **108** (158 mg, 0.83 mmol, 1.2 eq.) were added and dissolved in THF (6 mL) .The solution was cooled to 0°C, DIAD (163 µL, 0.83 mmol, 1.2 eq.) was slowly added and the solution was warmed back to room temperature and stirred overnight. TLC indicated complete conversion and the reaction was concentrated and purified directly by silica gel column chromatography using a 0%-4% MeOH:CH_2Cl_2 solvent system, giving the product as a yellow oil (201 mg, 0.30 mmol) in 44% yield as a 1:1 mixture of *E:Z* isomers ^{1}H NMR (400 MHz, $CDCl_3$)) δ 7.54 – 7.32 (m, 8H), 7.20 – 7.11 (m, 2H), 7.03 (dd, J = 8.7, 3.1 Hz, 2H), 6.97 (dd, J = 8.8, 2.3 Hz, 2H), 6.91 (d, J = 8.6 Hz, 2H), 6.84 – 6.77 (m, 2H), 6.77 – 6.70 (m, 2H), 6.70 – 6.62 (m, 2H), 6.59 (d, J = 8.7 Hz, 1H), 5.09 (s, 1H), 4.95 (s, 1H), 4.20 – 4.11 (m, 1H), 4.02 (ddt, J = 10.1, 7.3, 3.9 Hz, 3H), 3.82 (t, J = 5.9 Hz, 2H), 2.85 (d, J = 5.6 Hz, 1H), 2.77 (t, J = 5.7 Hz, 1H), 2.53 – 2.34 (m, 9H), 2.06 – 1.94 (m, 3H), 0.91 (d, J = 0.9 Hz, 15H), 0.07 (s, 6H).

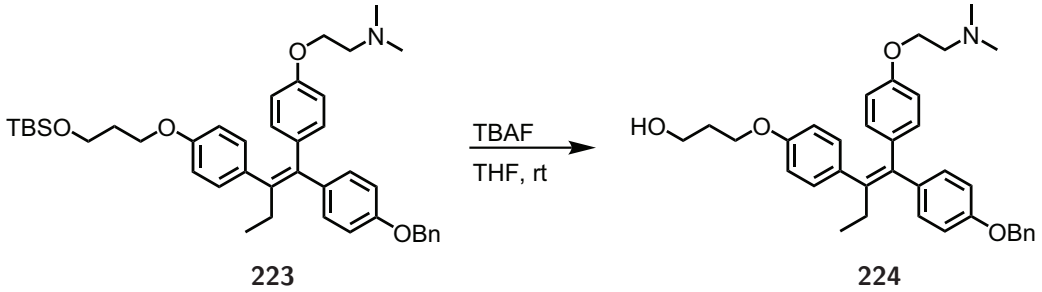

Synthesis of (Z)-3-(4-(1-(4-(benzyloxy)phenyl)-1-(4-(2-(dimethylamino)ethoxy)-phenyl)but-1-en-2-yl)phenoxy)propan-1-ol (224):

To a flame dried round bottom flask, **224** (201 mg, 0.30 mmol, 1.0 eq) was added and dissolved in THF (3 mL). TBAF (600 µL, 0.6 mmol, 2.0 eq) was added and the reaction was stirred for 2 hours at room temperature. TLC indicated complete consumption of product, DOWEX 50WX8-400 resin was added (excess) followed by excess solid $CaCO_3$ and the suspension was stirred for 2.5 hours, filtered, and contrated. The residue was dissolved in EtOAc and washed with saturated $NaHCO_3$ solution, then washed with 3x 5 mL brine, dried over Na_2SO_4, filtered, and concentrated to an orange oil (170 mg, 0.30 mmol). Product isolated in quantitative yield and did not require any further purification.

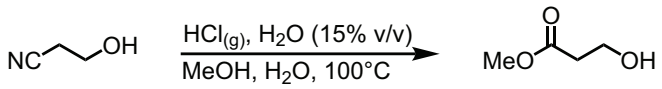

225 **112**

Synthesis of methyl 3-hydroxypropanoate (112):

MeOH (20 mL) and H_2O (3 mL) were added to a round bottom flask and the vessel was sealed and backfilled with argon three times. The mass of the flask was recorded and HCl gas was then bubbled through the solution for approximately 5 minutes, or until roughly 11 g of HCl (0.3 mol, 2.1 eq.) was added. The pale green solution was then cooled to 0°C and **225** (9.6 mL, 0.14 mol, 1.0 eq.) was slowly added, a reflux condenser was equipped, and the reaction was warmed to room temperature upon which it sustained reflux itself for approximately 10 minutes. An oil bath was then used to reflux the reaction for 2 hours upon which it was cooled to room temperature and stired for an additional 2 hours. Solid $NaHCO_3$ (7.85 g, 0.09 mol, 0.7 eq.) was then added portionwise and the mixture was stirred, filtered, and concentrated to a pale yellow oil that was dried under vacuum overnight. The crude product (11.9, 0.11 mol) was obtained in 82% yield and was not purified. The spectroscopic data of the product is in agreement with that reported in the literature.[16]

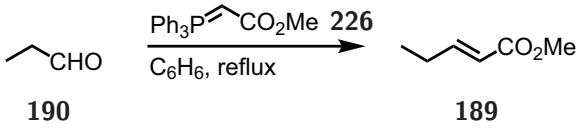

190 **189**

Synthesis of methyl (E)-pent-2-enoate (189):

To a dry round bottom flask equipped with a reflux condenser, propionaldehyde (**190**) (316 mg, 5.44 mmol, 1.0 eq.) was added and dissolved in benzene (6 mL). Ylide **226** (2.0 g, 5.98 mmol, 1.1 eq.) was then added and the reaction was heated to reflux and stirred for 2 hours. The reaction was the concentrated to an off-white solid and purified directly by silica gel column chromatography using pure hexanes to give the product as a colourless oil (296 mg, 2.94 mmol) in 54% yield. The spectroscopic data of the product is in agreement with that reported in the literature.[17]

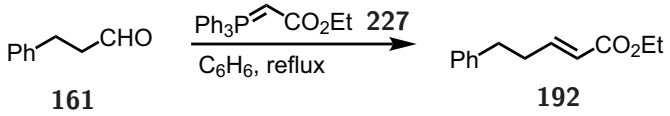

161 **192**

Synthesis of ethyl (E)-5-phenylpent-2-enoate (192):

To a dry round bottom flask equipped with a reflux condenser, dihydrocinnamaldehyde (**161**) (8.02 g, 59.8 mmol, 1.0 eq.) was added and dissolved in benzene (80 mL). Ylide **227** (25 g, 71.8 mmol, 1.2 eq.) was then added and the reaction was heated to reflux and stirred for 2 hours. The reaction was then concentrated to an off-white solid and purified directly by silica gel column chromatography using pure hexanes to give the product as a colourless oil (5.3 g, 25.7 mmol) in 43% yield. 7.37 – 7.27 (m, 2H), 7.27 – 7.16 (m, 3H), 5.87 – 5.69 (m, 2H), 5.59 – 5.49 (m, 1H), 5.19 – 5.03 (m, 2H), 4.18 (q, J = 7.3 Hz, 2H), 3.63 – 3.36 (m, 3H), 2.64 – 2.47 (m, 2H), 2.35 (dtt, J = 14.1, 7.0, 1.4 Hz, 1H), 1.28 (t, J = 7.1 Hz, 4H). ^{13}C NMR (126 MHz, $CDCl_3$) δ 173.53, 135.02, 131.15, 128.47, 128.42, 127.76, 126.09, 117.04, 60.63, 44.03, 36.95, 33.91, 33.89, 14.27, 14.25.

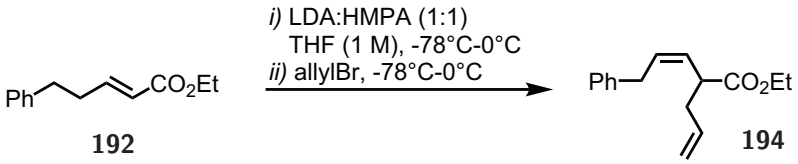

Synthesis of ethyl (Z)-2-allyl-5-phenylpent-3-enoate (194):

To a flame dried round bottom flask containing THF (1.13 mL), iPr_2NH (346 µL, 2.45 mmol, 1.0 eq.) was added and the solution was cooled to -78°C, nBuLi (2.4 M in hexanes) (970 µL, 2.33 mmol, 0.95 eq.) was slowly added and the reaction was then warmed to 0°C and stirred for 15 minutes. The solution was then cooled to -78 °C and HMPA (470 µL, 2.70 mmol, 1.1 eq.) was added dropwise and the resulting suspension was stirred for 30 minutes and α,β-unsaturated ester **192** (500 mg, 2.45 mmol, 1.0 eq.) was added dropwise using positive pressure cannulation from a dry flask. The resulting yellow solution was stirred for 10 minutes before the dropwise addition of allyl bromide (254 µL, 2.94 mmol, 1.2 eq.) (neutralized with basic alumina prior to use). The reaction was stirred for 10 minutes at -78°C then for 1 hour at 0°C. The reaction was then quenched with 3 mL saturated NH_4Cl solution, diluted with 3 mL H_2O and extracted with 3x5 mL Et_2O. The organic was dried over Mg_2SO_4, filtered, and concentrated to a yellow oil. Purification by silica gel column chromatography using a 0-2% EtOAc:hexanes gradient gave the product as a colourless oil (400 mg, 1.64 mmol) in 67% yield. ^{1}H NMR (400 MHz, $CDCl_3$) δ 7.34 (ddd, J = 7.7, 6.5, 1.8 Hz, 2H), 7.25 (d, J = 7.3 Hz, 3H), 5.94 – 5.77 (m, 2H), 5.39 – 5.29 (m, 1H), 5.18 – 5.03 (m, 2H), 3.67 (ddd, J = 10.6, 7.4, 5.6 Hz, 1H), 3.51 (dtd, J = 7.5, 5.2, 4.5, 2.5 Hz, 3H), 2.94 – 2.81 (m, 1H), 2.29 (dddt, J = 13.1, 7.1, 5.6, 1.3 Hz, 1H), 2.20 – 2.08 (m, 1H), 1.74 (dd, J = 7.5, 4.2 Hz, 1H).

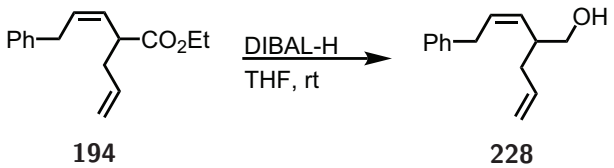

Synthesis of (Z)-2-allyl-5-phenylpent-3-en-1-ol (228):

Ester **194** (2.1 g, 8.59 mmol, 1.0 eq.) was added to a dry round bottom flask and dissolved in THF (20 mL) then cooled to 0°C. DIBAL-H (1.52 M) (14.14 mL, 21.5 mmol,

2.5 eq.) was slowly added and the reaction was stirred for 2 hours. The reaction was then quenched with 20 mL MeOH and 30 mL of saturated Rochelle's salt solution, and stirred overnight until the emulsion cleared. The clear solution was the extracted with 3x30 mL Et_2O and then washed sequentially with 10 mL Rochelle's salt solution, H_2O, then brine and the organic was dried over Mg_2SO_4, filtered, and concentrated to a clear liquid. Purification by silica gel column chromatography using a 10-20% EtOAc:hexanes gradient gave the product as a colourless liquid (847 mg, 4.18 mmol) in 49% yield. ^{1}H NMR (500 MHz, $CDCl_3$) δ 9.60 (d, J = 2.0 Hz, 1H), 7.33 (dd, J = 8.2, 6.9 Hz, 2H), 7.29 – 7.18 (m, 3H), 5.96 (dtd, J = 10.7, 7.5, 1.2 Hz, 1H), 5.81 (ddt, J = 17.1, 10.2, 6.9 Hz, 1H), 5.44 – 5.37 (m, 1H), 5.19 – 5.08 (m, 2H), 3.57 – 3.42 (m, 3H), 2.66 – 2.58 (m, 1H), 2.40 – 2.30 (m, 1H). ^{13}C NMR (126 MHz, $CDCl_3$) δ 200.33, 139.82, 134.59, 133.82, 128.60, 128.54, 128.35, 126.27, 124.61, 117.39, 51.09, 34.17, 33.62.

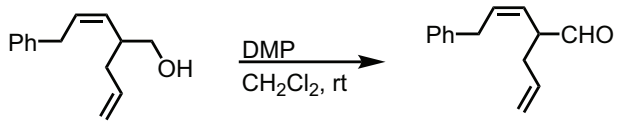

228 **187**

Synthesis of (Z)-2-allyl-5-phenylpent-3-enal (187):

Alcohol **228** (847 mg, 4.23 mmol, 1.0 eq.) was added to a round bottom flask and dissolved in CH_2Cl_2 (42 mL) followed by the addition of DMP (2.15 g, 5.07 mmol, 1.2 eq.). Full conversion was indicated by TLC after 20 minutes and the reaction was quenched with 5 mL saturated $Na_2S_2O_4$ solution and stirred for 1 hour. The resulting mixture was then extracted with 3x20 mL CH_2Cl_2 and the organic was washed sequentially with 20 mL saturated $NaHCO_3$ solution, H_2O, then brine. The organic was dried over Na_2SO_4, filtered, and concentrated to a pale yellow oil that contained a white precipitate. Purification by silica gel column chromatography using a 10-15% EtOAc:hexanes gradient gave the product as a pale yellow oil (654 mg, 3.27 mmol) in 77% yield. ^{1}H NMR (400 MHz, $CDCl_3$) δ ^{13}C NMR (126 MHz, $CDCl_3$) δ 200.33, 139.82, 134.59, 133.82, 128.60, 128.54, 128.35, 126.27, 124.61, 117.39, 51.09, 34.17, 33.62.

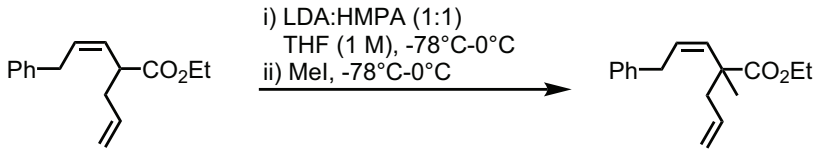

194 **229**

Synthesis of ethyl (Z)-2-allyl-2-methyl-5-phenylpent-3-enoate (229):

To a flame dried round bottom flask containing THF (7.2 mL), iPr_2NH (3.19 mL, 22.6 mmol, 1.3 eq.) was added and the solution was cooled to -78°C, nBuLi (2.4 M in hexanes) (8.71 mL, 20.9 mmol, 1.2 eq.) was slowly added and the reaction was then warmed to 0°C and stirred for 15 minutes. The solution was then cooled to -78 °C and HMPA (3.9 mL, 22.6 mmol, 1.3 eq.) was added dropwise and the resulting suspension was stirred for 30 minutes and α,β-unsaturated ester **194** (4.25 mg, 17.4 mmol, 1.0 eq.) was added dropwise using positive pressure cannulation from a dry flask. The resulting yellow solution was stirred for 10 minutes before the dropwise addition of methyl iodide (1.62 mL, 26.1 mmol, 1.5 eq.) (neutralized with basic alumina prior to use). The reaction was stirred for 10 minutes at -78°C then for 1 hour at 0°C. The reaction was then quenched with 10 mL saturated NH_4Cl solution, diluted with 10 mL H_2O and extracted with 3x50 mL Et_2O. The organic was dried over Mg_2SO_4, filtered, and concentrated to a yellow oil. Purification by silica gel column chromatography using a 0-10% Et_2O:hexanes gradient gave the product as a pale yellow oil (1.96 g, 7.7 mmol) in 44% yield. ^{1}H NMR (400 MHz, $CDCl_3$) δ 7.36 – 7.26 (m, 2H), 7.26 – 7.16 (m, 2H), 5.89 – 5.40 (m, 3H), 5.20 – 5.03 (m, 2H), 4.24 – 4.06 (m, 2H), 3.46 – 3.35 (m, 1H), 2.67 – 2.27 (m, 3H), 1.41 (s, 2H), 1.26 (t, J = 7.1 Hz, 3H).

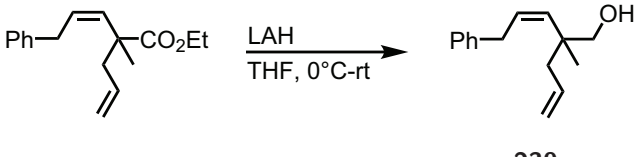

229 **230**

Synthesis of ethyl (Z)-2-allyl-2-methyl-5-phenylpent-3-enoate (230):

Ester **229** (1.96 g, 7.59 mmol, 1.0 eq.) was added to a flame dried round bottom flask, dissolved in THF (80 mL), and cooled to 0°C while stirring for 10 minutes. LAH (1.01 g,

26.gg mmol, 3.5 eq.) was very slowly added to the stirred solution and the reaction was warmed to room temperature and stirred for 2 hours. The reaction was then cooled to 0°C and 1 mL H_2O was slowly added, followed by the slow addition of 1 mL 15% NaOH solution. H_2O was added (3 mL) and the reaction was warmed to room temperature and stirred for 20 minutes. $MgSO_4$ was added and the reaction was stirred for an additional 15 minutes and then filtered over celite into a round bottom flask upon which is was concentrated to a colourless oil. The crude was purified by silica gel column chromatography using a 10-30% EtOAc:hexanes gradient to give the product as a colourless oil (611 mg, 2.82 mmol) in 37% yield. ^{1}H NMR (500 MHz, $CDCl_3$) δ 7.37 – 7.30 (m, 2H), 7.27 – 7.17 (m, 3H), 5.89 (ddt, J = 17.4, 10.2, 7.3 Hz, 1H), 5.66 (dt, J = 12.1, 7.6 Hz, 1H), 5.37 (dt, J = 12.1, 1.9 Hz, 1H), 5.18 – 5.05 (m, 2H), 3.62 – 3.50 (m, 4H), 2.35 (ddt, J = 13.7, 7.1, 1.3 Hz, 1H), 2.25 (ddt, J = 13.8, 7.5, 1.2 Hz, 1H), 1.25 (s, 3H). ^{13}C NMR (126 MHz, $CDCl_3$) δ 140.86, 134.91, 134.47, 131.07, 128.54, 128.45, 128.27, 126.06, 117.55, 70.72, 43.43, 42.10, 34.94, 31.60, 22.96, 22.67, 14.14.

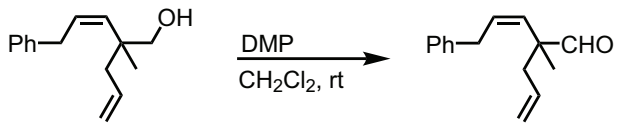

197 **198**

Synthesis of ethyl (Z)-2-allyl-2-methyl-5-phenylpent-3-enal (198):

Alcohol **197** (611 mg, 2.82 mmol, 1.0 eq.) was added to a round bottom flask and dissolved in CH_2Cl_2 (10 mL) followed by the addition of DMP (1.44 g, 3.4 mmol, 1.2 eq.). Full conversion was indicated by TLC after 20 minutes and the reaction was quenched with 5 mL saturated $Na_2S_2O_4$ solution and stirred for 1 hour. The resulting mixture was then extracted with 3x10 mL CH_2Cl_2 and the organic was washed sequentially with 20 mL saturated $NaHCO_3$ solution, H_2O, then brine. The organic was dried over Na_2SO_4, filtered, and concentrated to a pale yellow oil that contained a white precipitate. Purification by silica gel column chromatography using a 10-15% EtOAc:hexanes gradient gave the product as a pale yellow oil (544 mg, 2.54 mmol) in 90% yield. ^{1}H NMR (500 MHz, $CDCl_3$) δ 9.62 (s, 1H), 7.34 – 7.27 (m, 2H), 7.26 – 7.13 (m, 3H), 5.85 – 5.74 (m, 2H), 5.49 – 5.42 (m, 1H),

5.19 – 5.10 (m, 2H), 3.34 (d, J = 7.7 Hz, 2H), 2.52 – 2.40 (m, 2H), 1.30 (s, 3H). ^{13}C NMR (126 MHz, $CDCl_3$) δ 202.90, 139.79, 133.29, 132.88, 130.53, 128.56, 128.50, 128.20, 126.23, 118.87, 50.94, 41.43, 34.77, 31.61, 22.67, 20.62, 14.14.

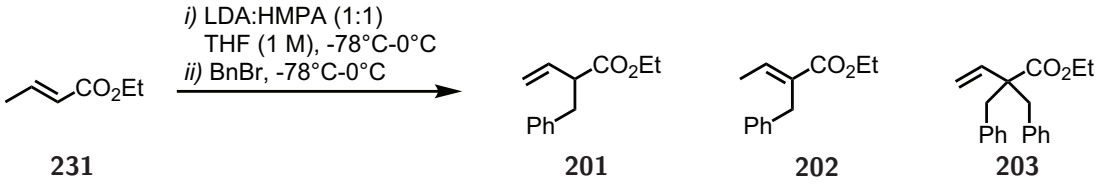

231 **201** **202** **203**

Synthesis of ethyl 2-benzylbut-3-enoate (201), and ethyl (E)-2-benzylbut-2-enoate (202):

To a flame dried round bottom flask containing THF (18 mL), iPr_2NH (8.04 mL, 56.95 mmol, 1.3 eq.) was added and the solution was cooled to -78°C, nBuLi (2.4 M in hexanes) (21.9 mL, 52.6 mmol, 1.2 eq.) was slowly added and the reaction was then warmed to 0°C and stirred for 15 minutes. The solution was then cooled to -78 °C and HMPA (9.91 mL, 56.95 mmol, 1.3 eq.) was added dropwise and the resulting suspension was stirred for 30 minutes and α,β-unsaturated ester **231** (5.45 mL, 43.81 mmol, 1.0 eq.) was added dropwise using positive pressure cannulation from a dry flask. The resulting yellow solution was stirred for 10 minutes before the dropwise addition of benzyl bromide (7.82 mL, 65.72 mmol, 1.5 eq.) (neutralized with basic alumina prior to use). The reaction was stirred for 10 minutes at -78°C then for 1 hour at 0°C. The reaction was then quenched with 10 mL saturated NH_4Cl solution, diluted with 20 mL H_2O and extracted with 3x50 mL Et_2O. The organic was dried over Mg_2SO_4, filtered, and concentrated to a yellow oil. Purification by silica gel column chromatography using a 0-10% Et_2O:hexanes gradient gave the product as a pale yellow oil (7.0 g, 34.27 mmol) in 78% yield. ^{1}H NMR (500 MHz, $CDCl_3$) δ 7.33 – 7.14 (m, 27H), 7.10 – 7.03 (m, 2H), 6.09 (dd, J = 17.9, 11.1 Hz, 1H), 5.90 (ddd, J = 17.1, 10.3, 8.3 Hz, 1H), 5.33 (dd, J = 11.2, 0.8 Hz, 1H), 5.23 (dd, J = 17.9, 0.8 Hz, 1H), 5.17 – 5.08 (m, 3H), 4.17 (q, J = 7.1 Hz, 4H), 4.11 (dq, J = 10.4, 7.1 Hz, 5H), 3.73 (s, 4H), 3.39 – 3.31 (m, 1H), 3.25 (d, J = 13.8 Hz, 2H), 3.15 – 3.05 (m, 3H), 2.88 (dd, J = 13.6, 7.2 Hz, 1H), 1.93 (d, J = 7.2 Hz, 6H), 1.26 (t, J = 7.1 Hz, 7H), 1.18 (dt, J = 18.3, 7.1 Hz, 7H). ^{13}C NMR (126 MHz, $CDCl_3$) δ 174.22, 173.34, 167.58, 139.80, 139.31, 138.68, 138.48, 137.26, 135.51,

132.24, 130.36, 129.07, 128.31, 128.29, 128.28, 127.86, 126.43, 126.39, 125.92, 117.52, 115.67, 60.74, 60.62, 60.48, 54.38, 52.08, 43.84, 38.47, 32.04, 14.69, 14.20, 14.12, 13.99. HRMS calc. for $C_{13}H_{17}O_2$ (M + H)+: 205.1223. Found: 205.1224. HRMS calc. for $C_{11}H_{11}O$ (M + H)+: 159.0804. Found:159.0805.

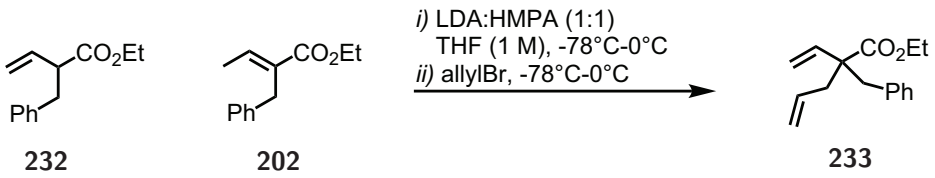

Synthesis of ethyl 2-benzyl-2-vinylpent-4-enoate (233):

To a flame dried round bottom flask containing THF (14 mL), iPr_2NH (6.29 mL, 44.55 mmol, 1.3 eq.) was added and the solution was cooled to -78°C, nBuLi (2.4 M in hexanes) (17.13 mL, 41.12 mmol, 1.2 eq.) was slowly added and the reaction was then warmed to 0°C and stirred for 15 minutes. The solution was then cooled to -78 °C and HMPA (7.75 mL, 44.55 mmol, 1.3 eq.) was added dropwise and the resulting suspension was stirred for 30 minutes and the mixture of esters **232** and **202** (7.0 g, 34.27 mmol, 1.0 eq.) was added dropwise using positive pressure cannulation from a dry flask. The resulting yellow solution was stirred for 10 minutes before the dropwise addition of allyl bromide (4.45 mL, 51.41 mmol, 1.5 eq.) (neutralized with basic alumina prior to use). The reaction was stirred for 10 minutes at -78°C then for 1 hour at 0°C. The reaction was then quenched with 10 mL saturated NH_4Cl solution, diluted with 20 mL H_2O and extracted with 3x50 mL Et_2O. The organic was dried over Mg_2SO_4, filtered, and concentrated to a yellow oil. Purification by silica gel column chromatography using a 0-10% Et_2O:hexanes gradient gave the product as a pale yellow oil (7.9 g, 32.33 mmol) in 73% yield. ^{1}H NMR (500 MHz, $CDCl_3$) δ 7.33 – 7.12 (m, 29H), 6.11 (dd, J = 17.9, 11.1 Hz, 1H), 6.02 (dd, J = 17.8, 11.0 Hz, 3H), 5.90 – 5.77 (m, 4H), 5.37 – 5.10 (m, 16H), 4.18 (q, J = 7.1 Hz, 7H), 4.11 (q, J = 7.2 Hz, 2H), 3.30 – 3.03 (m, 11H), 2.61 – 2.49 (m, 7H), 1.27 (t, J = 7.2 Hz, 11H), 1.18 (t, J = 7.1 Hz, 4H). ^{13}C NMR (126 MHz, $CDCl_3$) δ 174.24, 139.39, 139.34, 137.28, 137.06, 134.02, 130.43, 130.37, 127.89, 127.87, 126.51, 126.44, 118.20, 115.67, 115.22, 60.77, 60.74, 53.29, 43.86, 42.96, 39.37, 31.63, 22.70, 14.18, 14.16, 14.00. HRMS calc. for $C_{16}H_{21}O$ (M + H)+: 245.1536. Found: 245.1539.

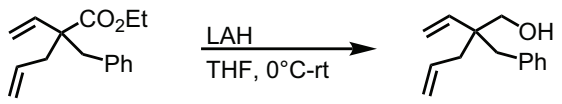

233 **204**

Synthesis of 2-benzyl-2-vinylpent-4-en-1-ol (204):

Ester **233** (7.9 g, 32.35 mmol, 1.0 eq.) was added to a flame dried round bottom flask, dissolved in THF (250 mL), and cooled to 0°C while stirring for 15 minutes. LAH (4.3 g, 113.2 mmol, 3.5 eq.) was very slowly added to the stirred solution and the reaction was warmed to room temperature and stirred for 2 hours. The reaction was then cooled to 0°C and 4 mL H_2O was slowly added, followed by the slow addition of 4 mL 15% NaOH solution. H_2O was added (16 mL) and the reaction was warmed to room temperature and stirred for 20 minutes. $MgSO_4$ was added and the reaction was stirred for an additional 15 minutes and then filtered over celite into a round bottom flask upon which is was concentrated to a pale yellow oil. The desired product could not be separated from the dibenzylated impurity by silica gel column chromatography.

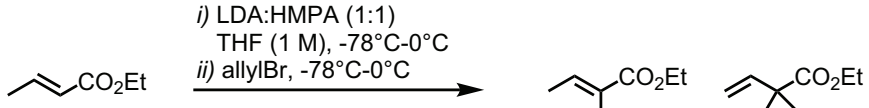

231 **206** **207**

Synthesis of ethyl (E)-2-ethylidenepent-4-enoate (206) and ethyl 2-allyl-2-vinylpent-4-enoate (207):

To a flame dried round bottom flask containing THF (9 mL), iPr_2NH (4.0 mL, 28.5 mmol, 1.3 eq.) was added and the solution was cooled to -78°C, nBuLi (2.4 M in hexanes) (10.9 mL, 26.3 mmol, 1.2 eq.) was slowly added and the reaction was then warmed to 0°C and stirred for 15 minutes. The solution was then cooled to -78 °C and HMPA (4.95 mL, 28.5 mmol, 1.3 eq.) was added dropwise and the resulting suspension was stirred for 30 minutes and ethyl crotonate (**231**) (2.5 g, 21.9 mmol, 1.0 eq.) was added dropwise using positive pressure cannulation from a dry flask. The resulting yellow solution was stirred

for 10 minutes before the dropwise addition of allyl bromide (2.46 mL, 28.5 mmol, 1.5 eq.) (neutralized with basic alumina prior to use). The reaction was stirred for 10 minutes at -78°C then for 1 hour at 0°C. The reaction was then quenched with 10 mL saturated NH_4Cl solution, diluted with 20 mL H_2O and extracted with 3x50 mL Et_2O. The organic was dried over Mg_2SO_4, filtered, and concentrated to a yellow oil. Purification by silica gel column chromatography using a 0-10% Et_2O:hexanes gradient gave the product as a pale yellow oil (2.23 g, 14.5 mmol) in 66% yield. ^{1}H NMR (500 MHz, $CDCl_3$) δ 6.96 (q, J = 7.1 Hz, 2H), 5.97 (dd, J = 17.7, 10.9 Hz, 1H), 5.83 (ddt, J = 17.3, 10.1, 6.0 Hz, 2H), 5.72 (ddt, J = 17.5, 10.4, 7.3 Hz, 2H), 5.27 – 4.94 (m, 10H), 4.18 (dq, J = 19.1, 7.1 Hz, 6H), 3.10 (dd, J = 6.1, 1.7 Hz, 4H), 2.57 – 2.44 (m, 3H), 1.82 (d, J = 7.1 Hz, 6H), 1.36 – 1.22 (m, 25H). ^{13}C NMR (126 MHz, $CDCl_3$) δ 174.22, 167.45, 139.33, 138.32, 135.19, 133.57, 130.93, 118.16, 115.04, 114.92, 60.70, 60.39, 51.78, 39.60, 34.66, 34.52, 31.59, 30.48, 26.91, 25.27, 22.65, 20.67, 14.24, 14.21, 14.15, 14.10. HRMS calc. for $C_9H_{13}O_2$ (M + H)+: 153.0921. Found: 153.0914.

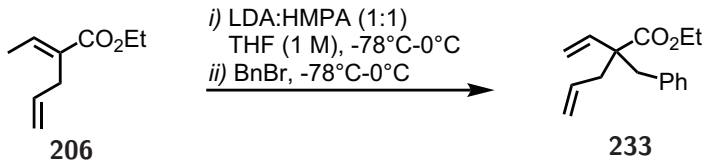

Synthesis of ethyl 2-benzyl-2-vinylpent-4-enoate (233):

To a flame dried round bottom flask containing THF (6 mL), iPr_2NH (2.65 mL, 18.8 mmol, 1.3 eq.) was added and the solution was cooled to -78°C, nBuLi (2.4 M in hexanes) (7.2 mL, 17.4 mmol, 1.2 eq.) was slowly added and the reaction was then warmed to 0°C and stirred for 15 minutes. The solution was then cooled to -78 °C and HMPA (3.27 mL, 18.8 mmol, 1.3 eq.) was added dropwise and the resulting suspension was stirred for 30 minutes and ester **206** (2.23 g, 14.5 mmol, 1.0 eq.) was added dropwise using positive pressure cannulation from a dry flask. The resulting yellow solution was stirred for 10 minutes before the dropwise addition of benzyl bromide (2.2 mL, 18.8 mmol, 1.5 eq.) (neutralized with basic alumina prior to use). The reaction was stirred for 10 minutes at -78°C then for 1 hour at 0°C. The reaction was then quenched with 10 mL saturated NH_4Cl solution, diluted with 20 mL H_2O and extracted with 3x50 mL Et_2O. The organic was dried over Mg_2SO_4, filtered,

and concentrated to a yellow oil. Purification by silica gel column chromatography using a 0-10% Et_2O:hexanes gradient gave the product as a pale yellow oil (1.65 g, 6.8 mmol) in 47% yield. ^{1}H NMR (500 MHz, $CDCl_3$) δ 7.31 – 7.20 (m, 6H), 7.20 – 7.13 (m, 4H), 6.06 – 5.93 (m, 2H), 5.88 – 5.68 (m, 3H), 5.31 – 5.07 (m, 10H), 4.17 (q, J = 7.1 Hz, 5H), 3.12 – 3.00 (m, 4H), 2.61 – 2.45 (m, 5H), 1.26 (t, J = 7.1 Hz, 7H). ^{13}C NMR (126 MHz, $CDCl_3$) δ 174.25, 139.37, 137.05, 134.00, 133.60, 130.42, 127.88, 126.50, 118.21, 118.20, 115.22, 60.77, 53.28, 42.93, 39.62, 39.35, 14.17.

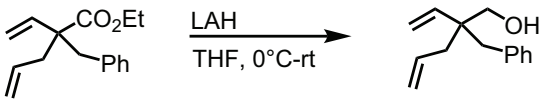

233 **204**

Synthesis of 2-benzyl-2-vinylpent-4-en-1-ol (204):

Ester **233** (1.65 g, 6.75 mmol, 1.0 eq.) was added to a flame dried round bottom flask, dissolved in THF (60 mL), and cooled to 0°C while stirring for 15 minutes. LAH (898 g, 23.6 mmol, 3.5 eq.) was very slowly added to the stirred solution and the reaction was warmed to room temperature and stirred for 2 hours. The reaction was then cooled to 0°C and 1 mL H_2O was slowly added, followed by the slow addition of 1 mL 15% NaOH solution. H_2O was added (3 mL) and the reaction was warmed to room temperature and stirred for 20 minutes. $MgSO_4$ was added and the reaction was stirred for an additional 15 minutes and then filtered over celite into a round bottom flask upon which is was concentrated to a pale yellow oil. The reaction was purified by silica gel column chromatography to give the product as a pale yellow oil (1.32 g, 6.55 mmol) in 97% yield. ^{1}H NMR (500 MHz, $CDCl_3$) δ 7.34 – 7.20 (m, 10H), 5.97 – 5.72 (m, 5H), 5.26 (dd, J = 11.1, 1.0 Hz, 2H), 5.21 – 4.99 (m, 7H), 3.54 – 3.39 (m, 5H), 2.81 (d, J = 13.2 Hz, 2H), 2.72 (d, J = 13.3 Hz, 2H), 2.28 – 2.09 (m, 5H), 1.47 (t, J = 6.3 Hz, 2H). ^{13}C NMR (126 MHz, $CDCl_3$) δ 142.52, 137.62, 134.60, 134.25, 130.77, 127.86, 126.18, 117.87, 117.79, 115.17, 65.83, 45.68, 40.37, 38.49.

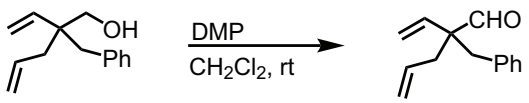

204 **200**

Synthesis of 2-benzyl-2-vinylpent-4-enal (200):

Alcohol **204** (1.32 mg, 6.52 mmol, 1.0 eq.) was added to a round bottom flask and dissolved in CH_2Cl_2 (30 mL) followed by the addition of DMP (3.32 g, 7.82 mmol, 1.2 eq.). Full conversion was indicated by TLC after 20 minutes and the reaction was quenched with 15 mL saturated $Na_2S_2O_4$ solution and stirred for 1 hour. The resulting mixture was then extracted with 3x20 mL CH_2Cl_2 and the organic was washed sequentially with 30 mL saturated $NaHCO_3$ solution, H_2O, then brine. The organic was dried over Na_2SO_4, filtered, and concentrated to a pale yellow oil that contained a white precipitate. Purification by silica gel column chromatography using CH_2Cl_2 gave the pure product as a pale yellow oil (324 mg, 2.61 mmol) in 40% yield. ^{1}H NMR (500 MHz, $CDCl_3$) δ 9.58 (s, 1H), 7.33 – 7.19 (m, 3H), 7.19 – 7.10 (m, 2H), 5.87 – 5.74 (m, 2H), 5.39 (d, J = 10.9 Hz, 1H), 5.22 – 5.09 (m, 3H), 3.01 (q, J = 13.9 Hz, 2H), 2.42 (dddt, J = 7.3, 4.8, 2.8, 1.5 Hz, 2H). ^{13}C NMR (126 MHz, $CDCl_3$) δ 202.56, 137.30, 136.33, 132.98, 130.44, 128.13, 126.63, 118.98, 118.12, 56.49, 39.63, 36.89.

References

1. Magano, J.; Chen, M. H.; Clark, J. D.; Nussbaumer, T. *J. Org. Chem* **2006**, *71*, 7103–7105.
2. Pal, A.; Ganguly, A.; Ghosh, A.; Yousuf, M.; Rathore, B.; Banerjee, R.; Adhikari, S. *ChemMedChem* **2014**, *9*, 727–732.
3. Campbell, L. J.; Borges, L. F.; Heldrich, F. J. *Bioorg. Med. Chem. Lett.* **1994**, *4*, 2627–2630.
4. Zhou, C.; Larock, R. C. *J. Org. Chem.* **2005**, *70*, 3765–3777, PMID: 15876060.
5. Safi, R.; Rodriguez, F.; Hilal, G.; Diab-Assaf, M.; Diab, Y.; El-Sabban, M.; Najjar, F.; Delfourne, E. *Chem. Biol. Drug Des.* **2015**, *87*, 382–397.
6. Xu, C.; Du, W.; Zeng, Y.; Dai, B.; Guo, H. *Org. Lett.* **2014**, *16*, 948–951.
7. Yuan, H.; Bi, K.; Chang, W.; Yue, R.; Li, B.; Ye, J.; Sun, Q.; Jin, H.; Shan, L.; Zhang, W. *Tetrahedron* **2014**, *70*, 9084–9092.
8. Percivalle, C.; Sissi, C.; Greco, M. L.; Musetti, C.; Mariani, A.; Artese, A.; Costa, G.; Perrore, M. L.; Alcaro, S.; Freccero, M. *Org. Biomol. Chem.* **2014**, *12*, 3744–3754.
9. Shrestha, T.; Bossmann, S.; Troyer, D. *Synthesis* **2014**, *46*, 646–652.
10. Xue, F.; Zhao, J.; Hor, T. S. A.; Hayashi, T. *J. Am. Chem. Soc.* **2015**, *137*, 3189–3192.
11. Ting, C.-M.; Hsu, Y.-L.; Liu, R.-S. *Chem. Commun.* **2012**, *48*, 6577.
12. Molander, G. A.; Rivero, M. R. *Org. Lett.* **2002**, *4*, 107–109.
13. Lambert, J. D.; Rice, J. E.; Hong, J.; Hou, Z.; Yang, C. S. *Bioorg. Med. Chem. Lett.* **2005**, *15*, 873–876.
14. O'Rourke, N. F.; Micalizio, G. C. *Org. Lett.* **2016**, *18*, 1250–1253.
15. Voliani, V.; Signore, G.; Vittorio, O.; Faraci, P.; Luin, S.; Peréz-Prieto, J.; Beltram, F. *J. Mater. Chem. B* **2013**, *1*, 4225.
16. Butler, C. R. *et al. J. Med. Chem.* **2015**, *58*, 2678–2702.
17. Yoshida, M.; Otaka, H.; Doi, T. *Eur. J. Org. Chem.* **2014**, *2014*, 6010–6016.